DYNAMIC ANALYSIS OF LAMINATED COMPOSITE PLATE INTERACTING WITH FLUID

Thesis submitted by

PRITHWISH SAHA

DOCTOR OF PHILOSOPHY IN ENGINEERING

DEAPRTMENT OF CIVIL ENGINEERING

FACULTY COUNCIL OF ENGINEERING & TECHNOLOGY

JADAVPUR UNIVERSITY

KOLKATA-700032, INDIA

2024

INDEX NO.: 285/18/E

1. **Title of the Thesis:**

   DYNAMIC ANALYSIS OF LAMINATED COMPOSITE PLATE INTERACTING WITH FLUID

2. Name, Designation and Institutions of the Supervisor:

   Prof. (Dr.) Kalyan Kumar Mandal
   Associate Professor,
   Department of Civil Engineering
   Jadavpur University,
   Kolkata-700032, India.

3. **List of Journal Paper Publications:**
   i. Prithwish Saha and Kalyan Kumar Mandal (2020) *Transient responses of laminated composite plates.* Asian Journal of Civil Engineering 22: 137-157. Publisher – Springer.
   ii. Prithwish Saha and Kalyan Kumar Mandal (2021) *A study on earthquake-induced vibration on laminated composite plates using finite element method.* Natural Hazards 106: 2251-2277. Publisher – Springer.
   iii. Prithwish Saha and Kalyan Kumar Mandal (2023) *Study on free vibration response of a liquid retaining composite structure considering fluid-wall interaction.* Innovative Infrastructure Solutions 8(238): 3-14. Publisher – Springer.
4. **List of International Conference Paper Publications:**
   i. Prithwish Saha and Kalyan Kumar Mandal (2024) *A study on free vibration analysis of composite tank considering fluid-wall interaction.* Presented in 2nd International Conference on Mechanical Engineering, organised by Jadavpur University, Kolkata.
   ii. Prithwish Saha and Kalyan Kumar Mandal (2017) *Dynamic analysis of laminated composite plates using Finite Element Method.* Presented in 7th International Conference on Theoretical, Applied, Computational and Experimental Mechanics (ICTACEM), organised by IIT-Kharagpur, India.

STATEMENT OF ORIGINALITY

I, Prithwish Saha, registered on 28.05.2018 do hereby declare that this thesis entitled "**Dynamic Analysis of Laminated Composite Plate Interacting with Fluid**" contains literature survey and original research work done by the undersigned candidate as part of Doctoral studies.

All information in this thesis have been obtained and presented in accordance with existing academic rules and ethical conduct. I declare that, as required by these rules and conduct, I have fully cited and referred all materials and results that are not original to this work.

I also declare that I have checked this thesis as per the "Policy on Anti Plagiarism, Jadavpur University, 2019", and the level of similarity as checked by iThenticate software is 3%.

Signature of Candidate: Prithwish Saha

Date: 12.08.2024

Certified by Supervisor:

(Signature with date, seal)

1. Kalyan Kr. Mandal
12/08/2024

Associate Professor
Department of Civil Engineering
Jadavpur University
Kolkata-700 032

CERTIFICATE FROM THE SUPERVISOR

This is to certify that the thesis entitled "**Dynamic Analysis of Laminated Composite Plate Interacting with Fluid**" submitted by **Shri Prithwish Saha**, who got his name registered on 28.05.2018 for the award of Ph. D. (Engineering) degree of Jadavpur University is absolutely based upon his own work under the supervision of **Prof. (Dr.) Kalyan Kumar Mandal**, Associate Professor, Department of Civil Engineering, Jadavpur University and that neither his thesis nor any part of the thesis has been submitted for any degree/diploma or any other academic award anywhere before.

Kalyan Kr. Mandal
12/08/2024

Signature of the Supervisor and date with Office Seal

Associate Professor
Department of Civil Engineering
Jadavpur University
Kolkata-700 032

ACKNOWLEDGEMENTS

I feel proud to express my profound and heartfelt gratitude to my research supervisor Prof. (Dr.) Kalyan Kumar Mandal, without whose constant source of inspiration throughout my study, I would not be able to complete this thesis. I am grateful to him for his valuable guidance, encouragement and continuous support throughout my research work.

I would like to offer thanks to the Head of the Department, Civil Engineering Department, Jadavpur University, for the valuable suggestions time to time during my research.

I would also like to express thanks to Prof. (Dr.) Tapas Sadhu (HOD, Civil Engineering Department, Heritage Institute of Technology) and my colleagues at the Civil Engineering Department, Heritage Institute of Technology for their constant support during this tenure. I would also mention the management of Heritage Institute of Technology for providing me necessary supports for the timely completion of the thesis.

I am extremely thankful to my friends and students, who are engaged in research at various premium institutes round the globe for their continuous support during the time of my research.

My deepest gratitude goes to my respected parents, without whose blessings, it would not be possible for me to maintain the same dedication throughout this tenure. I would also like to mention the support received from my lovely wife Sudeshna, who helped me in all possible way to stay focused towards my research journey. Last but not the least, I must mention the names of my daughters Ahana and Aviva, the greatest motivation for timely completion of the research.

Finally, I bow down before the Almighty who had made everything possible.

Prithwish Saha 12/8/24

Place: Jadavpur University

Prithwish Saha

Abstract

Fluid retaining structures such as tanks should be designed considering dynamic loading such that it can effectively sustain ground excitations. These structures are the source of the basic needs of common people. Hence malfunction of such structures has direct adverse effect on society. Large liquid retaining structures are the source of huge mass and failure of the same under earthquake can be catastrophic. Side walls of such structures are generally made of concrete or steel which is another source of huge mass and which leads to worsen the situation. Composite materials having high strength with low seismic weight contributes less in seismic excitations. Stiffness of such materials can also be modified with simple modification of fiber orientation. Hence the designer has the freedom to use the material as per requirement. Hence in the present study composite material is used for the construction of side walls of the tank. This will effectively reduce the overall response of the tank under dynamic loading. The side walls are modeled as two dimensional isoparamentric plate elements with eight nodes per element. First order shear deformation theory is considered for the formation of strain terms of the thin plate. Displacement is considered as the nodal variable following Lagrangian approach.

Fluid is considered to be compressible and inviscid. It is modelled as twenty node three dimensional brick elements. The effect of sloshing is considered in the present study. One opposite sides of tank are considered to have composite plates as side walls where the rest two sides are considered to be rigid. The tank is always considered to be filled with liquid.

In case of a fluid retaining structure, the structure or the fluid does not behave as a separate entity at the interface. Rather they behave in a coupled way. Hence, in the present study direct coupling method is employed to couple the composite plate and adjacent fluid within the tanks. A MATLAB code has been generated for the numerical simulation of this composite-fluid coupled systems.

The present study starts with the free and forced vibration of uncoupled side walls with parametric variations. The fundamental frequency increases with increment of ply angle up to 45˚. Central displacement of the side walls is higher for symmetric laminations. Effect of

various boundary conditions are studied and simply supported edge shows highest displacement values. Stress contour for two, four and six layered plate is also presented. The response of the same is studied under Koyna ground motion also.

The coupled structure is then studied for free and forced vibration. Displacement time history at the middle of the side walls is studied considering variations in ply orientations, boundary conditions and tank geometry. It is clear from the present study that coupled frequency of the system increases up to wall height to length ratio 0.5, then it becomes constant. Central displacement of the side walls is higher for anti-symmetric lamination for the coupled system which is in contrast with the uncoupled one. Comparative study of central displacement of left and right tank (both cross and angle ply laminations) wall is presented. It is found that initially both the wall responded in the same manner but as time progresses there is a phase difference between the two plates. Time history response of normal stress, inplane shear stress and transverse shear stress at side walls are also obtained and presented. Contour plot at different layers under various loading conditions are plotted using Origin software and presented. The response of the same is studied under El-Centro ground motion also.

Keywords: *Composite plates; 3-D finite element method; Transient response; Stress contour plot; Koyna earthquake; El-Centro earthquake; Fluid-structure interaction; Direct coupling*.

CONTENTS

LIST OF FIGURES

LIST OF TABLES

LIST OF SYMBOLS

h	Thickness of the plate
a	Width of the plate
b	Height of the plate
ξ, η	Local coordinate axis of finite element
N_i	Shape function
u,v and w	Displacement along three orthogonal directions
α and β	Rotations about two axes
z	distance of a particular fiber layer from the middle layer
ε_x^0 , ε_y^0 and ε_s^0	Normal strain along three orthogonal directions
γ_x , γ_y and γ_s	Shear strain along three orthogonal directions
γ_{xz} and γ_{yz}	Transverse shear strain
$[B]$	Strain-displacement relationship matrix
$[J]$	Jacobian matrix
E	Young's modulus
v	Poisson's ratio
$[Q_{ij}]$	Elasticity matrix
σ	Stress
ε	Strain
G_{ij}	Shear modulus
N_X , N_Y	Normal forces per unit length
N_S	Inplane shear force per unit length
M_X, M_Y	Bending moment per unit length
M_S	Twisting moment per unit length
$[D]$	Constitutive relationship matrix
$[M_e]$	Mass matrix
m	Mass per unit area
ρ	Mass density
I	Moment of inertia
U	Potential energy

V	Kinetic energy
Q	Applied load
F	Total energy in the element
$[K]$	Element stiffness matrix
ω	Fundamental frequency
$\{\varphi\}$	Mode shape
$\bar{\sigma}_i$ *i=1 to 8*	Stresses at the node points
$\bar{\sigma}_{ig}$ *i=1 to 4*	Stresses at Gauss points
$\acute{\sigma}_j$ *j=1 to 8*	Stresses at node points
B and γ	Coefficient of Newmark's integration method
T_{ij}	Total stress of fluid
δ_{ij}	Kronecker delta
u_i	Velocity of fluid
p	Hydrostatic pressure
μ_b	Coefficient of bulk viscosity
B_i	Body force
$\boldsymbol{\alpha}$	Acoustic velocity of the wave in the fluid domain
H	Height of fluid element
L	Length of the fluid element
B	Width of the fluid element
ρ_f	Fluid density
a'	Horizontal ground acceleration
N_r	Shape function for the reservoir domain
Ω	Reservoir domain
∇^2	Three-dimensional Laplacian operator
$\boldsymbol{\Gamma}$	Surface of the fluid domain
n	Normal to the boundary surface of the fluid
$[M_l]$	Mass matrix of the left wall of the coupled system
$[K_l]$	Stiffness matrix of the left wall of the coupled system
$[Q_l]$	Coupling matrix between left wall and fluid

F_{dl}	Force vector on left wall
$[M_r]$	Mass matrix of the right wall of the coupled system
$[K_r]$	Stiffness matrix of the right wall of the coupled system
$[Q_r]$	Coupling matrix between right wall and fluid
F_{dr}	Force vector on right wall
N_s	Shape function of the structure
N_f	Shape function of the fluid

CHAPTER 1

INTRODUCTION

1.1 GENERAL

Liquid retaining structures such as water tank plays a vital role in everyday life of common people. Water supply being the prime source of life must remain uninterrupted under any circumstances. As per the latest seismic code of India, the country has become more prone to earthquake excitations. Effect of ground motion directly depends upon the mass of the structure itself. Large amount of mass contributes to higher seismic force and the structure become more vulnerable. Failure of such huge structure is always devastating and must be avoided. Hence a thorough and careful analysis of such huge liquid retaining structures is necessary. Dynamic response of such structures, being carried out by researchers round the globe, mainly using concrete or steel as the construction unit of the structure. Concrete having high unit weight contributes more to the seismic force. Steel on the other hand does not give freedom to the designer to model as per the site-specific requirement. It was always felt by the practicing engineers to have a material as the construction unit of such structure, which can effectively reduce the seismic weight without compromising the strength and there is also a gap in research on this area. Composite being high strength/stiffness to weight ratio, it is being used as the side walls of the structure in the present study to mitigate this gap. Dynamic performance of the overall system is studied using composite plates as side walls.

Composites having property of high strength to weight ratio are very popular among researchers since long back. This is particularly important for the weight sensitive branches of engineering. Moreover, due to the flexibility of the designing criteria by altering the lamination scheme, it became very popular as the construction unit of different structures. Free and forced vibration, bending, buckling even failure of composites all aspects are explored by the researchers. Still the use of composites is limited only in individual structures. It is not used as the construction unit of any liquid retaining structure, where there is a provision of interaction between fluid and structure, which in turn modifies the independent response of fluid or structure. Hence in the present study graphite-epoxy composite is used as side wall of a tank and the coupling response of the two is studied.

Fluid in the present study is considered as compressible and inviscid in nature. Three-dimensional finite element method is used to model the fluid domain following Eulerian approach using twenty node brick elements having pressure as the only nodal variable. The tank is always considered to be totally filled with liquid during all the analysis.

Structure and fluid at the interface do not behave as two separate entities, rather they behave as a coupled entity. Hence their study needs to be carried out in a coupled way. Direct coupling method has certain advantages over indirect coupling, hence direct coupling method is employed in the present study to prepare the numerical model of the coupled composite-fluid tank structure in MATLAB. Fluid-structure interaction is an important aspect of research which on composites is very limited as far as practical liquid retaining structures are considered. Dynamic analysis of such coupled structure is performed in the present study using transient load as well as ground motion and corresponding displacement and stresses are reported. Stress contour at different ply layers are also reported under different boundary conditions.

1.2 OBJECTIVE OF WORK

Dynamic response of composite plate-fluid coupled system is the prime objective of the present study of a liquid retaining structure using finite element method by preparing a numerical model in MATLAB environment.

1.3 SCOPE OF WORK

The scopes of the present work are as follows:

- Finite element modelling of 3D tank with composite plates as side walls and fluid as compressible and inviscid using direct coupling method.
- Numerical modelling and simulation of the coupled system in MATLAB environment.
- Study of free and force vibration response of the uncoupled composite plate modelled as thin 2D plate using first order shear deformation theory.
- Application of Koyna ground motion on composite plate and study the displacement and stress response.
- Study of free vibration as well as forced vibration of the fluid-structure coupled system under transient loading.

- Application of El-Centro ground motion on the coupled system to study the corresponding response.
- Formation and study of stress contour plots at different ply layers using Origin-Pro software.

1.4 ORGANIZATION OF THESIS

The total research work is presented in five chapters.

In **Chapter 1**, a brief introduction on the present research work is stated. Objective and scope of present research is also mentioned in this chapter. The organization of the thesis is presented at the end.

In **Chapter 2**, an extensive review on existing literature on present research work is furnished. The chapter is further subdivided into the major research topics related to the present work. A critical discussion is framed based upon the work already done by previous researchers. Identification of gap and research goal is shown at the end of this chapter.

In **Chapter 3**, mathematical formulation of the present problem is provided. The chapter is subdivided based upon the formulation of composite plate, fluid and coupling separately.

In **Chapter 4**, numerical results, solution of benchmark problem and graphs and tables supporting the numerical problems with parametric variations are presented. In the first section (section 4.2), the analysis of uncoupled composite plate is presented. In second section (section 4.3) response of coupled system is furnished. A discussion on each result is also provided in subsequent sections.

In **Chapter 5**, summary of the present research is presented. Major conclusions obtained from present work is given in bulleted form. Suggestions for the probable extension of present research work is also furnished at the end of the chapter.

A list of relevant references is provided at the end of the thesis.

CHAPTER 2

LITERATURE REVIEW

2.1 GENERAL

In order to study the effect of dynamic response of composite plate and fluid-structure interaction problem a detailed review of literature is required, which is is very difficult to accommodate in a single chapter, due to its vastness. Still an effort is made to provide an elaborate review on vibration response of composite plate starting from the very primitive studies to the modern-day latest material and theories being applied. The fluid-structure interaction effect on dynamic response is presented separately in the second half of this review section. The review mainly focuses the amount of work previously been done directly related to the present study along with the recent contribution from the researchers.

2.2 REVIEW ON COMPOSITE PLATES

Composites have excellent strength/stiffness to weight ratio for which they are being used as the construction material for many important structures. Composites are much lighter in weight for same volume of other conventional constructional materials. This is particularly important for the liquid retaining structures carrying huge mass of fluid and exposed to high seismic zones. The maximum displacement and stresses get modified due to lower seismic weight. Reduced displacement and stresses will lead to more economical design. Interaction between the two materials play significant role. Hence the study on the behaviour of composite materials and the effect of interaction is of utmost importance. A detailed study on composites were carried out following the books published by Jones (2018), Reddy (2004) and Mukhopadhyay (2005).

2.2.1 FREE VIBRATION RESPONSE OF COMPOSITE PLATES

Analysis of vibration response of composite plate was studied by Reddy (1979) incorporating the effect of transverse shear. Author has considered shear deformation theory for plates proposed by Yang-Norris-Stavsky. Fundamental frequency of composite plate is calculated with varying mesh size, number of layers, ply-angle and geometry of the plate.

Reddy and Khedir (1989) analysed and presented a comparative study of all the plate theories to obtain buckling and free vibration response.

Shankara and Iyengar (1996) developed a finite element model to analysis a free vibration problem using a FSDT and HSDT both. Authors presented the results for rectangular, antisymmetric, angle-ply laminated using first order and higher order deformation theories. Parametric variation of ply orientations and properties of the materials were presented.

Free and forced vibration response under step loading was performed by Sinha et al. (1999). A nine node Lagrangian element was considered to model the folded plate using finite element method. Authors considered FSDT for strain-displacement model and a shear correction factor of 5/6 was assumed. Natural frequencies were studied for the folded plate with varying crank angle, ply angle and stacking sequence.

Free vibration and buckling of angle-ply composite plates were analysed by Matsunaga (2001) under inplane stresses. Authors had taken into account the effects of shear deformation, in the study. Authors have investigated the effect of variation in thickness of the ply layers as well as effect of rotatory inertia.

White et al. (2002) applied the theoretical model developed by them to analyse CFRP laminated plate and shell structures in terms of mode shapes and resonance frequencies. Authors investigated free dynamic response of rectangular laminated plates considering geometric non-linearity.

Geometrically nonlinear free vibration analysis of composite plate was carried out by Bennouna et al. (2003). Fundamental nonlinear mode shapes, amplitude dependent resonant frequency and flexural stress distribution were presented. Linear and nonlinear analysis for various aspect ratio and vibration amplitude were reported.

Setoodeh and Karami (2003) analyzed composite plates with elastic restrained edges for free vibration and buckling. A three-dimensional elasticity approach was used for the solution of vibration and buckling of plates. Various plate geometries with variation in plate edge elastic stiffness was modelled and analysed.

Davi and Milazzo (2003) analysed a composite plate using a mesh free approach, called displacement boundary method. Authors calculated free vibration response of anisotropic plates for validation of the formulation. It was also concluded by the authors that the model derived by them in the present study is better that the finite element method, finite difference method and boundary element problems.

The effect of stiffener in free vibration of composite plate, was carried out by Prusty and Ray (2004). Authors used eight node isoparametric elements to model the plates and three node isoparametric curved beam element to formulate the stiffeners.

Haddad et al. (2004) studied free vibration of composite plates using finite difference method considering various boundary conditions. Shear deformation and rotary inertia were varied and corresponding effects on natural frequency of laminated composite plates were studied. Authors also investigated the effect of span-to-depth ratio, aspect ratio, angle and cross-ply lamination and lamination sequence.

Jorge et al. (2005) used FSDT and multiquadric radial basis function (MQRBF) for the prediction of free vibration frequency of composite plates. Cross and angle ply laminations are used for square and skewed plates and frequency responses were reported. The capability and efficiency of the MQRBF method for Eigen value problems were also demonstrated by authors.

Ong et al. (2006) studied natural frequencies of FGM materials considering Von-Karman theory to account for nonlinearity. Authors presented the dynamic effects of plate under thermal loading. Boundary conditions and material properties were varied to study the effect.

Sheikh et al. (2006) studied the vibration and buckling characteristics of sandwich plates with imperfections to different degrees. A refined plate theory was used. Authors used finite element method to model the plate.

Undamped free vibration analysis of rectangular plate was carried out by Pandit et al. (2007) using nine node isoparametric plate element. Authors presented frequency response of laminated composite plates with cut-outs and distributed mass all over the plate. It was observed that the frequency of the plate can be modified by the position of the distributed mass (such as

machines) in such a manner that the frequency of the vibrating machine remains far apart from that of the plate. It effectively resists chance of resonance in the plate structure.

Free vibration of functionally graded curved panel was carried out by Pradyumna and Bandyopadhyay (2008) using higher order shear deformation theory to effectively remove the shear correction factors. A realistic parabolic strain distribution was assumed through the thickness of the shell element. Fundamental frequency of various FG plates was studied and corresponding values for HSDT and FSDT were reported.

Han et al. (2008) studied static as well as free vibration analyses of composite plates. A mesh-free approach was considered. using a linearly conforming radial point interpolation method. Authors used FSDT with proper correction for shear locking such that the formulation can handle thin and thick plates efficiently.

Kari et al. (2008) used a third order shear deformation theory (TSDT) to formulate a laminated composite plate and studied free vibration response with distributed patch mass present in the plate. Angle ply and cross ply lamination was used for the plate and the free vibration response was presented for FSDT, CLPT and TSDT.

Malekzadeh (2009) studied the three-dimensional free vibration analysis of thick plates. Functionally graded material was used. The material properties were varied in the thickness direction of the plate and the corresponding effects on natural frequencies were reported. Authors considered simply supported as well as elastic foundation for the analysis of the plates.

Watkins et al. (2010) presented an experimental investigation on free vibration response of isotropic plates. Impulse load was applied. The plate was modelled as point supported. Results were obtained using COMSOL software. The frequency values obtained using the software were compared with the Rayleigh-Ritz method. Mode shapes of the plates were also reported.

Thinh and Quoc (2010) presented free vibration of composite plates. Various types of stiffeners were used. Authors used a 9-node isoparametric element to model the plate. Authors considered degrees of freedom per node as 9 and 5 respectively for the plate and beam element. A 3 -node isoparametric beam element was used to model the stiffener element.

Delaminated as well as healthy structure was analyzed by Kumar et al. (2014) for free mode vibration using Mixed Interpolation Tensorial Component, nine node quadrilateral (MITC9) elements. The results were compared with the available experimental. Three-dimensional finite was used for simulation. and the three-dimensional finite element simulations. First three frequencies were considered in which the effect of delamination was considered.

Nonlinear free vibration analysis of point supported laminated composite skewed plate was studied by Naghsh and Azhari (2015). Geometric non linearity based upon Von-Karman's assumptions and element free Galerkin method were implemented. Authors studied free vibration response of skewed plate for large amplitude. Authors considered four types of point support conditions, various amplitude ratios, skew angles, aspect rations and fibre orientations for analysis purpose and corresponding results were reported.

Serdoun and Cherif (2016) studied thick composite plate modelled using Reddy's higher order theory. Free vibration of the plate is presented. The shear stress is considered zero value at the top and bottom surface following the shear deformation theory. Hence shear correction factor is not required. In spite of the attractive theory, due to difficulties associated with satisfaction of C^1 continuity, author modified and developed a new C^1-HSDT p-element with eight degrees of freedom, which could be efficiently used to model the plate in finite element analysis. Natural frequencies of thick composite plates were reported by authors.

Free vibration on conical panels was studied by Civalek (2017). Functionally graded material was used as the basic construction unit of the plates. Love's shell theory was used to medel the paneks and FSDT was used to model the plates. Geometric parameters and boundary conditions were varied to study the response. The effect of grid number on vibration is also reported.

Study on delaminated composite plate for free vibration response is carried out by Mahato et al. (2017). Authors have used FSDT to formulate the strain terms. The modeling is prepared using finite element method. The study was made on simply supported and cantilevers type boundary condition to obtain the vibration response of the plate. Analytical and computational approach was employed to calculate the displacements at different positions of the plate.

Ebrahimi and Dabbagh (2018) analysed a multi-scale hybrid composite (carbon fiber-epoxy and carbon nanotube-Epoxy) beam using higher-order beam model. An elastic substrate as used as base for the beam and the equation of motion was derived using energy principle. Finally, the same was solved using Galerkin's method to obtain the fundamental frequency.

Mandal et al. (2019) investigated vibration response of laminated plates with arbitrary and multiple cut-outs. Authors studied experimentally as well as numerically the modification of vibration response of the plate with varying size, position and number of cut-outs of the plate.

Free vibration analysis of composite plate was studied by Vidal et al. (2019) using separation of variable method which is more computational cost effective than the conventional layer wise model.

Sinha et al. (2021) studied free vibration response of laminated composite plates with cut-outs. Experimental as well as numerical model were analyzed. Effect of position of cut out on frequency was studied, this helps in designing the laminated plate.

Free vibration response of three-layer composite plate with crack in the inner layer was studied by Tho et al. (2023). Finite element was used to model the plate. It was reported by the authors that in certain cases, increment in crack length does not modify the frequency response. Hence frequency response does not always give an indication of composite plate failure.

Madenci et al. (2020) studied buckling and free vibration response of pultruded glass fiber reinforced polymer (GFRP) using FSDT. Authors carried out experimental, numerical and analytical study up to failure of the plate. An exhaustive study on damage analysis with special focus on experimental results was presented.

Free vibration analysis of functionally graded material (FGM) was studied by Abdelbaki (2022). The study was carried out on FGM plates with uneven thickness and resting on elastic foundation. Geometry and material properties were varied along with different support conditions and corresponding variation in first three natural frequencies were noted.

Free vibration of beam made of functionally graded material (Graphene platelets reinforced composite) in partial contact with liquid was presented by WU et al. (2022). Influence of graphene platelets on the free vibration response of the beam was studied by varying the distribution pattern, weight fraction and dimension of the beam along with geometry and boundary conditions. Fluid parameters such as density and depth were also varied to observe the modification in free vibration response.

2.2.2 FORCED VIBRATION RESPONSE OF COMPOSITE PLATES

Rajamani and Prabhakaran (1977) have presented the forced vibration response of square, simply supported plate with cut-outs. Analytical solution to the forced vibration natural frequencies was reported by the authors. The effect of cut-outs on the natural frequency of the plate was elaborately discussed.

Geometrically nonlinear forced vibration study was performed by Reddy (1983) on composite plates. The transient analysis of plate was carried out by the author considering the transverse shear strain, rotary inertia and Von-Karman strains to account for the non-linearity. Author also studied the effect of thickness of the plate, various boundary conditions on vibration response. Different types of loadings were applied and corresponding change in vibration is reported.

Kant et al. (1988) studied dynamic response of composite plates using a higher order shear deformation element developed by the authors. They have calculated and presented the stresses and deflections of plates under various boundary conditions and loadings.

Balamurugan and Narayanan (2001) studied the vibration control performance of piezolaminated plate and shell structures. The piezolaminated plate was modelled by considering thin PZT piezoceramic layers embedded on top and bottom surfaces which were considered as sensors.

Huang et al. (2004) presented an analytical way for the examination of nonlinear dynamic responses of a composite plate. Short fibers were laid in each layer. Elastic modulus of each lamina

was obtained using Mori–Tanaka mean field theory. Authors have used Mindlin shear deformation theory. The non-linearity was introduced using Von-Karman kinematics.

Lim et al. (2004) investigated the dynamic response of laminated composite plates. The plates consist of piezoelectric sensors. Authors used EFG method to investigate the plate problem. FSDT were used to formulate the displacement field. Most suitable position of the sensors was also reported by studying the effect of dynamic response of the plate in terms of changing the fiber stacking sequence and sensor positions.

Moy et al. (2004) reported the transient response of layered sandwich plates using Reddy's higher-order theory which shows parabolic variation of the transverse shear stresses. Authors used Newmark'sdirect integration technique to solve the governing equilibrium equations. Parametric variations are made and its effect on transient response is observed and reported.

Oh et al. (2005) analysed the dynamic response of delaminated composite plate. Authors have used higher order zigzag theory. Finite element method was used and each element consists of four nodes. A prediction of delamination from changed frequency and mode shapes are reported.

Onkar and Yadav (2005) studied random vibration of a simply supported laminated composite plate. Authors considered as a random process for the material properties and also the excitations. The random response was observed and reported. The effect of lamina thickness and geometric variations are also studied in depth by the authors.

Lee and Han (2006) investigated the forced vibration natural frequencies of isotropic and composite laminated plates subjected to arbitrary loading. Authors used assumed natural strain method to overcome membrane and shear locking phenomena.

The numerical solution of an initially stressed laminate plate was carried out using two different plate theories by Chen (2007). Authors studied the nonlinear vibration behaviour of laminated plate. The authors concluded that discrepancies in the displacement fields is the indication of nonlinear vibration due to the transverse shear strain, normal strain and initial stress state.

Han et al. (2008) performed a nonlinear analysis on plates and shells. Lagrangian shell element was used with FSDT. Assumed natural strain method was used to overcome the shear locking effect.

Nonlinear vibration due to flexure is studied on composite plates by Singha and Daripa (2009). Harmonic loading was considered in the present study. The nonlinear stiffness matrix was formulated using Von-Karman's assumptions. Authors also carried out time history analysis to explain the steady state and unsteady nature of the vibration. The loading and boundary conditions were also varied and corresponding effects are reported.

The dynamic analysis of composite plates was investigated by Ghafoori and Asghari (2010) under moving mass.. Authors used finite element method and FSDT for the formulation of strain values. They applied stationary as well as adaptive mesh techniques to avoid off-nodal position of moving mass. Numerical results were presented by authors based upon parametric variations. Dynamic response is greatly modified by the stacking sequence of the ply layers and also by the moving mass.

Thinh and Ngoc (2010) studied the vibration characteristics of a glass fibre/polyester composite plate in which piezoelectric actuator was used. FSDT were used for the displacement formulation. Authors considered the mass and stiffness of piezoelectric layer in their model. A negative velocity feedback control algorithm was used to control the transient response of the structure.

Non-linear forced vibration characteristics of nano beams were presented by Ansari (2014). Third order shear deformation theory with Gurtin-Murdoch elasticity theory was used along with third order shear deformation theory.

Khan and Patel (2014) investigated the nonlinear forced vibration characteristics of laminated composite plates. FSDT is considered along with Von-Karman theory to formulate the nonlinearity in finite element method. A detailed study was made to understand the effect aspect ratio, thickness ratio and other parameters.

Hirwani et al. (2016) studied internal debonding considering geometric nonlinearity. Higher order shear deformation theory was used to model the damaged composite plate and the dynamic properties of delaminated plate were studied using finite element method.

Fang et al. (2017) proposed an analytical wave propagation model to study the forced vibration response of the composite plates. Authors calculated the steady state forced vibration of built-up plate's structure using the finite element method. The relationship between the specific damping capacity of wave mode and that of modal mode was explained in details.

Meftah and Youzera (2017) analysed nonlinear forced vibration of sandwich beam with viscoelastic core layer. Authors considered the refined higher-order zig-zag theory to account for normal, transverse and shear deformations in the core layer. The frequency response were reported with different material and geometric properties.

Arumugam and Rajamohan (2017) studied free and forced vibration of composite plates. The plate was tapered in the thickness direction. The plate formulation was based upon CLPT. Authors used finite element method to study the plate problem. Numerical results were also presented for the tapered plate, considering the variation of taper model, rotational speed, length and location of delamination.

Arani et al. (2019) have studied free and forced vibration analysis of cylindrical panels. Functionally graded materials were used as the construction unit of the panels. The effect of variation in distribution, orientation and volume fraction of CNT on vibration is thoroughly studied.

Draoui et al. (2019) studied vibration of carbon nanotube reinforced sandwitch plates analytically. Carbon nanotubes were varied in position for core and face sheets. Parametric variation on aspect ratio, volume fraction, reinforcement type, plate thickness and corresponding response on bending and vibration characteristics were studied. Authors found that face sheet reinforced with CNT gives better resistance in deflection compared to its counterpart.

Free and forced vibration response of composite plates having curvilinear fiber with piezoelectric layers was studied by Sharma et al. (2022). The response of the plate was studied

under delaminated condition of the fiber. Fiber delamination leads to modification in stiffness at particular layers. Hence modification in dynamic response of such plate under fiber delamination was studied in this article.

2.2.3 FAILURE STUDY ON COMPOSITE PLATES

Reddy and Pandey (1987) presented first-ply failure of composite plates considering FSDT. It was observed by the authors that all the failure theories give comparable results for in-plane loading. In case of transverse loading, maximum strain and Tsai-Hill criteria gives different results than the rest.

Vibration characteristics of delaminated plate was also very important and studied by Parhi et al. (2001). Delamination under hygrothermal condition was studied and observed that dynamic displacement and stress is modified by concentration of moisture.

An excellent review paper was presented by Murugesan and Rajamohan (2017) on the progressive ply failure of composites. Extensive compilation of work done by various researchers on convention failure theories such as Tsai-Wu failure criterion, Maximum stress criterion, Tsai-Hill failure criterion, Hoffman failure criterion, Maximum Strain Failure Criterion is covered by the authors. Moreover they also reported other newer failure theories such as Puck's failure criterion, Hashin–Rotem failure, Hashin's failure criterion, Hoffman and Hashin failure criteria. Lee's failure criterion and many and their extent of work done.

2.2.4 EFFECT OF GROUND MOTION ON THE STRUCTURE/FLUID

A finite element study on concrete gravity dams under earthquake force was presented by Chopra and Chakrabarti (1972). A predictive study on the response of gravity dams and developed stresses due to different earthquake excitation was reported. Authors concluded that "A gravity dam having a typical section of height and concrete strength similar to that at Koyna dam would be expected to suffer comparable damage during an earthquake similar to the Koyna earthquake." Authors also concluded that earthquake similar to Koyna earthquake with intense short periods are relatively more severe to structures having short time periods.

Dynamic analysis of gravity dam considering non-linearity of water, i.e. allowing cavitation was presented by Zienkiewicz et al. (1983). Effect of cavitation on earthquake and blast loading was thoroughly studied by the authors.

Haroun and Tayel (1985) studied the effect of vertical and horizontal component of earthquake excitation on steel tank. Elephant foot bulge failure of the tank is mainly due to horizontal component of the motion. Authors concluded that vertical component of the seismic excitation is especially important for concrete tanks which is more susceptible to hoop stress.

Bayraktar et al. (2010) studied the variation of response in a gravity dam due to the effect of different reservoir length. Folsom dam was numerically modeled and far- and near-fault ground motions of 1989 Loma Prieta earthquake ground motion was used to study the displacement and stress response of the dam.

Free vibration and time history analysis of elevated conical tank is studied by Moslemi et al. (2011) considering El Centro ground motion using finite element method. various mode shapes under convective wave pressure were presented. Authors considered fluid-structure interaction to study the response of the tank under ground motion.

Dynamic analysis of perforated steel plates was carried out by Bhowmick et al. (2014) under seismic excitation. Perforation leads to decrease in mass contribution towards seismic load, hence the behaviour of the same is studied for El Centro ground motion. It was reported that bending moment and shear values developed were less than solid plate.

Performance analysis of steel silo under Van earthquake is studied by Uckan et al. (2014). Similar silos were studied for non-linear analysis at the same zone and corresponding results were reported.

The effect of ground motion has significant effect on aged concrete dam and was studied by Mandal and Maity (2016). The response was studied on the dam-water coupled structure. Authors observed that convective nonlinearity increases the hydrodynamic pressure to a great extent.

Ground supported cylindrical tank made of composite materials were studied by Kormanikova and Kotrasova (2018). Microscopic analysis of the composite element under hydrodynamic impulsive and convective pressure from the fluid was carried out.

Non-linear study of concrete nuclear power plant was studied by Huang et al. (2018) under ground motion. Post seismic increment of pressure in the structure is also studied. Time dependant parameter such as the effect of creep, shrinkage of the material is also studied.

Nikkhakian et al. (2020) carried out a 3D finite element investigation on a concrete gravity dam considering geometric as well as material nonlinearity. Ground acceleration recorded during Kern County earthquake was used as external excitation.

Sadeghi and Moradloo (2020) studied the behaviour of damaged concrete gravity dam under the aftershock loading of Koyna and Manjil earthquake. Authors modelled cracked dam and they studied nonlinear analysis of the cracked dam model for future earthquake energies.

The crack propagation in concrete gravity dam under seismic excitation was studied by Ghallab (2020). Koyna dam model is generated and crack propagation was verified using Koyna ground motion history.

2.3 REVIEW ON FLUID

Jae Kwan Kim et al. (1998) studied the vibration response of rectangular water tank under vertical and horizontal seismic excitation by Rayleigh-Ritz method. Variation of pressure along vertical and horizontal direction was reported. It was reported by the authors that sensitivity of the side walls is dependent upon the length to height ratio.

The effect of wall flexibility on hydrodynamic pressures for rectangular tanks were analysed by Chen and Kianoush (2004). Dynamic time history analysis of shallow, medium and tall tanks was conducted for Low, moderate and high earthquake zones. Sequential analysis were used hence process of approximation of the hydrodynamic pressures by added mass is not required. It was reported by the authors that lumped mass model is not sufficient to represent the behavior

of liquid storage tanks and the hydrodynamic load was highly dependent on the input of ground motion.

The effect of hydrostatic pressure and self-weight on seismic parameters and response of cylindrical tanks made of steel of different height to diameter ratio using FE modelling was studied by Juan C. Virella et al. (2005). It was found that the pre-stress had its influence on fundamental periods and mode shapes of tank regardless of *H/D* ratio and the pre-stress was strongly influenced by the shell slenderness (tank radius/thickness).

Experimental investigation on the behavior of small scale rectangular water tanks during dynamic loading with water sloshing using a shake table was carried out by Jure Radnic et al. (2008). It was found that hydrodynamic pressures and hydrodynamic forces on the side tank walls were increased due to increase of stiffness of side tank walls.

Algreane et al. (2011) modified the adding of impulsive mass using LUSAS FEA 14.1, to elevated tank instead of Westergaard approach, by examining six rectangular and six circular models of elevated tanks by three-dimensional finite elements method, based on vibration dynamic analysis to obtain the time of impulsive mass at every case. Method of adding impulsive mass to the walls of tank in case of circular and rectangular shapes did not affect significantly the dynamic analysis of elevated tanks.

A finite element method was presented by Hosseini and Farshadmanesh (2011) to simplify the response calculations for rectangular tanks with parametric variations. Authors used neural network for the formation of easy relationships between the highest frequency and amplitude of the base excitations in the tank during the sloshing. It was found that sloshing effect can be reduced by the position and spacing of the baffle walls.

Time history analysis of 900 cubic meter capacity elevated reinforced concrete water tank using mechanical and finite-element modelling technique is presented by S. Bozorgmehrnia et al. (2013). Authors reported that maximum displacement occurred in the support system joint with the container. It was observed that maximum response not always occurs with the tank full condition.

Time history analysis of an elevated 900 m^3 water tank constructed with moment resisting frame was performed using Housner two-mass models by Ranjbar et al. (2013). The maximum displacement occurred in the support system at the joint with the container.

Wakchaure and Sonal (2014) studied sloshing effect in an elevated water tank using Finite Element Method. It was found that the critical response totally dependent upon the specific seismic characteristics and earthquake records. Elevated water tank having different compartments effectively reduce the sloshing effect of the tank.

M. Yazdanian et al. (2016) analysed rectangular concrete tanks using finite element method under static, modal, response-spectrum and time-history analysis. It was reported by the authors that all responses obtained from the time history analysis were more than other methods of analysis. Maximum displacement was achieved at the highest part of the tank due to the wave height.

Dudhatra and Desani (2016) performed a parametric study on ground supported rectangular concrete tank considering different length to depth ratio. The earthquake analysis was carried out considering impulsive mass and convective mass separately as suggested by GSDMA guidelines.

The distribution of pressure on the rectangular and trapezoidal storage tanks' perimeters due to sloshing phenomenon using Laplace equation and finite element method was investigated by Hassan Saghi (2016) using a numerical code. Authors showed that the free surface fluctuation in the trapezoidal storage tanks are maximum. On the other hand, horizontal and the vertical force applied on the tank perimeter in the trapezoidal tanks were considerably less in comparison with the rectangular one.

Rectangular water tank of different lengths against horizontal harmonic excitation using finite element method was analysed by Mandal and Maity (2016) considering nonlinear convective acceleration in Navier–Stokes equations and tank walls as rigid. Water domain was modelled by eight node isoparametric elements. The results showed that the convective nonlinearity increased the hydrodynamic pressure to a great extent when the excitation frequency was equal to or lower than the fundamental frequency of the water. Pressure increment is higher for narrow tank.

The sloshing behaviour of fluid under harmonic excitation for various tank lengths was investigated using finite element analysis in Eulerian approach by Mandal and Maity (2016). The hydrodynamic pressure along the wall was found to be increased with the decrease of length of the tank. Greater value of sloshed displacement were responsible for greater hydrodynamic pressure on the tank wall for lower length of the tank.

Ali and Telang (2017) studied dynamic analysis of elevated water tanks supported on RC framed structure by using STAAD Pro V8i SS6 software to compare the seismic analysis parameters with different capacities of storage tanks using IS 1893:2014. Highest nodal displacement and lowest nodal displacement were found at the wall of water tank when tank was full.

Rectangular ground supported liquid storage tanks with and without baffle walls were studied by Ashwini Dalvi et al. (2017) under seismic excitation using IS 1893 Part-2. It was found that time period and base shear were reduced with introduction of number of baffle walls. The sloshing height reduced by introduction of additional number of baffle walls when the Seismic forces were acting perpendicular to baffle wall direction.

Aregawi and Kassahun (2017) investigated an idealized reinforced concrete rectangular water tank supported on ground under seismic excitation. Authors have used linear three-dimensional finite element analysis and SAP2000 software to obtain the tank response. It was shown that, there was increment in the moment and displacement of each hydrostatic and hydrodynamic analysis with a reduced aspect ratio (tank height to length ratio).

Seismic behaviour of ground rested water tank with change in geometry was analysed by Kalane and Pophali (2018). It was observed that maximum displacement occurred for fixed support rectangular tank and minimum for hinged circular tank.

Experimental study on the effect of sloshing of liquid was carried out by Kotrasova and Kormanikova (2018) in partially and fully filled ground supported cylindrical container subjected to external excitation horizontal harmonic motion. The resulting highest slosh heights for various excitation frequencies and amplitudes were compared with the fluid natural frequencies. With the

increase and decrease of water height in tank, the impulsive and convective hydrodynamic effect increased respectively.

Hemalatha and Rao (2018) using STAAD Pro studied the response of supporting structure as well as rectangular tank boundaries to impulsive and convective pressure as a spring model. Provision of free board reduced pressure on tank boundaries and base shear. The base moment in full storage condition were greater compared to empty tank.

The sloshing phenomenon in a rectangular water tank was investigated experimentally by Chia-Ren Chu et al. (2018). Bottom mounted baffles were used in the laboratory for the experiments. Volume of fluid method was used to solve the kinematic motion of water surface. It was concluded that multiple baffles performs better than a single baffle.

Nonlinear sloshing in rectangular Liquefied gas (LNG) tanks under forced excitation using Boundary Element Method is carried out by Dongya Zhao et al. (2018). A numerical code was developed with the support of potential flow theory to analyse the sloshing effect. Sloshing properties in rectangular tank under were investigated. Authors reported that the sloshing under horizontal and rotational excitations shared similar properties.

Aruna Rawat et al. (2019) studied three-dimensional ground-supported tanks filled with water, subjected to ground motion using coupled acoustic-structural (CAS) and coupled Eulerian-Lagrangian (CEL) approaches. It was found that hydrodynamic pressure distribution does not depend upon the non-linearity of the sloshing wave displacement.

Effects of baffles on the seismic behaviour of concrete cylindrical tanks were carried out by Hossein Hajimehrabi (2019). Authors considered three different lengths of tank and nine different ground motions. Authors have shown that baffles reduce chances of overflow to a great extent. With the use of baffles, it increases the hoop force as it acts like stiffener in the tank.

Hejazi and Mohammadi (2019) studied the effect of sloshing in partially filled rectangular tanks subjected to ground motions. Nonlinear numerical simulations for practical tanks were performed under different horizontal and vertical ground excitations. Results showed that vertical

displacement at the free surface depends on the first fundamental period of sloshing behavior and peak ground acceleration.

The combined effect of base-isolator system and vertical baffle on the performance of a three-dimensional (3D) rectangular liquid storage container, under ground motion assuming the fluid to be irrotational, inviscid, and incompressible was analysed by M. R. Shekari et al. (2019) numerically. A boundary element technique was initially prepared to treat the spectral problem of the motion of the liquid using the zoning method. Highest base shear was achieved by time-dependent analysis of the counselled baffled non-isolated slender tank and a decrease to almost 9% and 13% respectively were found in the shallow tank compared to the unbaffled tank result. With the increase in baffle height, closer to the still water level, the slosh amplitude became more suppressed, as the baffle creates a blocking effect, which was responsible for extra energy and viscosity dissipation.

2.4 REVIEW ON FLUID-STRUCTURE INTERACTION

Liu (1981) studied non-linear dynamic analysis of liquid storage tanks, in terms of dynamics and buckling of it using finite element technique. Fluid-structure interaction was considered to study the modification in response of dynamic and buckling behaviours of the storage tank. Sloshing in a tank with different geometry and buckling of the same are reported in this paper.

A quasi-Eulerian technique for the analysis of transients loading in a fluid with pressurized bubble was developed by Belytschko et al. (1982). Both two and three dimensional finite element was used. The novelty of this paper lies in the fact that the authors have formatted such a way that the meshing can move independent of the material. Hence it can treat the fluid-structure interaction better.

Olson and Bathe (1983) studied the fluid structure interaction frequencies using displacement based finite element formulation. The fluid was considered to be inviscid, compressible. The study was confined for small displacement fluid motions.

Transient response due to fluid structure interaction is studied by Olson and Bathe (1985) using finite element method. Authors have considered velocity potentials as the nodal variable in fluid, hydrostatic pressure variable measured at one node in each fluid region and the displacement variable at each node in the solid. This formulation proposed by the authors provides an excellent alternative to the displacement based finite element formulation techniques.

Finite element solution of incompressible fluid-structure vibration problems was studied by Bermudez et al. (1997). Authors solved an Eigen solution of the vibrations of a coupled fluid-structure system. The fluid was incompressible and the structure was elastic and the analysis was carried out in absence of external forces. Displacement based finite element formulation is used for both solid and fluid.

Gong and Lam (1998) studied the effect of underwater explosive shock load on composite submersible hull considering fluid-structure interaction. Composite and steel hull under underwater shock was also studied and reported by authors.

Maity and Bhattacharyya (1999) presented a time domain analysis for the modelling of an infinite fluid domain using a truncation boundary condition. Their study includes the radiation effects and the same can be implemented in the finite element formulation. Authors modelled an equation along the truncated boundary in order to get the effect of an unbounded fluid domain within the dam-reservoir interface. Authors presented the equation of motion of fluid in terms of pressure alone where the fluid was considered as compressible, inviscid and irrotational.

Pal et al. (1999) considered composite conical tank filled with liquid for their study. Finite element method was used by the authors to study the dynamic effect of oscillating fluid inside the composite tank.

Fluid-structure interaction in form of fluid flow through pipes was investigated by Bathe et al. (1999) using finite element solver ADINA.

Interaction between fluid and rigid body in terms of a cylinder presented in the flowing fluid is studied by Mendes and Branco (1999).

Arbitrary Lagrangian approach (ALE) was used to model fluid-structure interaction by Souli et al. (2000). ALE can handle mesh geometry independent of material geometry. This is advantageous in the modelling of fluid part near the interaction region. Application of ALE can control the distorted fluid mesh efficiently.

Liang et al. (2001) analysed the free vibration response of a linearly elastic, homogeneous and isotropic cantilever plate, submerged in fluid using the added mass formulation. Natural frequency of the plate, vibrating in fluid was obtained by the authors analytically and compared with finite element code in ABAQUS.

Pal et al. (2001) carried out a 3D finite element analysis for numerical simulation on the sloshing response of liquid filled cylindrical rigid base container assuming the contained fluid was incompressible and inviscid, resulting in an irrotational flow field. An experimental study on the sloshing response of liquid filled container was carried out by authors. The sloshing effect was calculated using Newmark's time integration scheme. The fluid was modeled using finite element method assuming fluid velocity potential as the only nodal unknown. Two different element types were introduced to discretize the three dimensional fluid domain, based upon the tank geometry. The result obtained from numerical solution was compared with experimental value obtained by the authors themselves to judge the accuracy.

Vibration response of coupled system of fluid bounded by cylindrical plates were analysed by Jeong (2003). The problem was analysed by analytical method and compared the result with finite element technique.

An energy based finite element analysis formulation was used by Zhang et al. (2003) for analysis of high-frequency vibration of thin elastic plates, in contact with fluid of high density. Very dense fluid loading on plate was studied and the frequency response was reported by the authors in this paper and the results were validated with statistical energy analysis (SEA) and finite element method.

Geometrically nonlinear free and forced vibration of circular cylindrical shell panels were studied by Amabili and Paidoussis (2003). The study was performed considering effect of fluid-structure interaction and without considering the effect. Frequency of shells and panels were

studied in contact with dense fluid (liquid), vacuum and light fluids (gases). Stability of circular cylindrical shells and panels coupled with flowing fluid was also studied by the authors.

Fluid-structure interaction with some parametric variation considering the fluid to be inviscid and compressible was presented by Maity and Bhattacharyya (2003). Dynamic response of the coupled fluid-structure system was studied under ramp acceleration. Thickness of the structure, modulus of elasticity of the structure, effect of water level in the structure was varied.

Design optimization study was carried out by Craig et al. (2003) for a fuel tank under the effect of sloshing and impact. The interaction between fluid and structure was considered in terms of sloshing and impact. Impact load on tank wall due to sloshing was considered first then the effects of both are optimized for the design of the tank.

Effect of impact between water tank and ground was studied by Anghileri et al. (2005). Sloshing effect of tank after accident of a helicopter was extremely important criteria as it causes death of cabin crews. Fluid structure interaction was considered during the formulation of numerical model and the results are validated with experimental data.

3-D finite element analysis of fluid-structure interaction considering geometric non-linearity was presented by Teixeira and Awruch (2005). Finite element method was employed to model the problem. Pressure generated on plates and displacement is studied under supersonic inviscid flow and due to flow of wind.

The effect of fluid-structure interaction between the lock gate of a rigid dam and the reservoir was studied by Pani and Bhattacharyya (2007). The dynamic pressure of the lock gate was studied for both compressible and incompressible fluids. Effect of fluid compressibility, applied excitation frequency, aspect ratio and thickness of the gate on dynamic pressure was investigated.

Natural frequency of a rectangular plate was studied by Kerboua et al. (2008) coupled with fluid. Natural frequency of steel rectangular and square plate was presented by the authors, totally submerged in water. The variation in dynamic response of plate due to change in fluid height was also investigated and reported by the authors. Floating plate and plate immersed in water vertically

was studied and variation in fundamental frequency with change in position of water level is reported.

Dynamic analysis of a rectangular tank was performed by Mitra and Sinhamahapatra (2008) considering the effect of coupling between the plate and fluid. Pressure based Galerkin approach was employed in order to limit the number of unknowns per nodes.

The interaction between shock wave and the structure was studied by Gong and Andreopoulos (2009) by a moving mesh algorithm and finite element method. Authors implemented a fully coupled approach which is capable of accounting for the mutual interaction. An Eulerian solver was used for the compressible fluid formulation and Lagrangian solver was used for finite element formulation of the solid structure by the authors.

LeBlanc and Shukla (2010) used conical shock tube for their study on composite materials. The study deals with the response of underwater shock wave on the composites. The behaviour of composite material, their delamination location and pattern, fibre damage and breakage locations were studied experimentally as well as using finite element method in this paper.

A review on numerical approach of fluid-structure interaction was presented by Rebouillat and Liksonov (2010). Authors focused mainly on the different research articles where sloshing effect of liquid is predominant. Sloshing model in naval, aerospace and other areas were also studied in depth.

The fluid-structure interaction at the wind turbine blades made of composite materials was studied by Bazilevs et al. (2010). Numerical simulation was performed at realistic wind velocity and rotor speed conditions. Residual-based variational formulation was used to model the air flow and Kirchhoff-Love shell theory was used to model the structure.

Ma and Mahfuz (2012) analysed the fluid-structure interaction effect on composite ship hull using finite element technique. Authors prepared the composite hull using finite element method and the fluid domain with wave motion was generated by ANSYS CFX.

Chang (2013) presented a study on vibration characteristics of a rectangular plate which is in contact with fluid. The plate was transversely isotropic and made of smart composites (magneto-electro-elastic material) which were capable to convert mechanical energy to magnetic or electrical energies or vice-versa.

Vibration of composite cantilever beam was investigated by Gordis et al. (2013) under the influence of fluid-structure interaction. Multiple experiments with varying boundary condition and material properties were conducted. The natural frequency was reduced significantly due to the added mass of the liquid for the coupled system.

You and Inaba (2013) studied analytically and experimentally the effect of FSI in composite pipe. Impact load was applied and corresponding wave speeds were recorded.

Motley et al. (2013) studied the free vibration response of steel and composite cantilever plate considering the effect of added mass, material anisotropy, partially submerged in liquid. Authors observed that the effect of added mass on composite plate in reduction of natural frequency is more compared to plate in vacuum.

Free vibration analysis of rectangular composite plate in contact with fluid was studied by Khorshid and Farhadi (2013). Analytical solution was carried out considering various shear deformation theories. Natural frequencies of the tank fluid system were presented with various lamination scheme and geometric properties.

Composite plates were more prone to damage than metallic plates under impact loads. Change in contact force history and dynamic response of composite plates in contact with water was studied by Abrate (2014) under impact loading. Portion of immersion of the plate in water was varied and corresponding frequency response was reported. Author ~~has~~ also varied the nature of projectile (impactor) to study their influence on the plate vibration.

Vibration and buckling analysis of elliptical composite plate was studied by Ghaheri et al. (2014) using variational approach to obtain the governing equations and solved by Ritz method. The vibration and buckling response were studied for symmetric angle ply laminated plates with varying boundary conditions under in plane edge load resting on elastic foundation.

A fluid-structure interaction model was prepared by Tran et al. (2014) to study the effect of interaction between water and composite plate. The plate response was reported due to an underwater impulse loading.

Schiffer and Tagarielli (2014) constructed a finite element model of clamped composite circular plate and the dynamic response was observed by applying under water shock wave load.

Talookolaei and Lasemi-Imani (2015) studied the dynamic response of delaminated beam interacting partially with fluids. Authors prepared the fluid-structure response of composite beam and extended their study towards delaminated beam.

Underwater shock wave loading on composite curved plate was studied by LeBlanc and Shukla (2015). The effect of curvature of the plate on deformation and fluid-structure interaction was the main objective of study in this paper.

Fluid-structure interaction of liquid retaining tank was carried out by Zou and Wang (2015). The sloshing effect of the tank under horizontal excitation was modified due to variations in bulkhead bending stress and filling ratios. These variations were studied in detail by the authors.

Direct coupling method was used to analyse the response of a water tank under ground motion using finite element method by Mandal and Maity (2015).

Liao and Ma (2016) presented a study on dynamic response of elastic thin plate. The plate on which the study was carried out, placed at the bottom of a tank rectangular in shape. Authors considered the coupling between the plate and fluid and variation of resonating frequency, mode shapes of the plate were studied considering the effect of viscous as well as inviscid fluid filled in the tank.

The variation in natural frequencies by changing boundary conditions, dimension of fluid and tank, fluid depth and fluid density was studied thoroughly. An experimental study on the effect of ice equivalent object with composite plate in motion is studied by Kwon et al. (2016). Authors obtained the density of sea water; sea ice and similar real-life simulation was made in the laboratory in a tank.

Fluid-structure interaction (FSI) for wind or earthquake load was studied by Zhu and Scott (2016) using finite element method.

Experimentally using shake table, the interaction between the sloshing fluid and the structure was studied by V. S. Sanapala et al. (2019). At different locations on the walls of the tank, a flow visualization was reported. The variation in free surface and measurement of dynamic pressure at same locations was also studied. Higher hydrodynamic pressures were observed near the liquid free surface compared to those measured near the tank base.

An analytical solution of functionally graded circular plate coupled with fluid to study the vibration characteristics was presented by Yousefzadeh et al. (2017). The variation in natural frequencies by changing boundary conditions, dimension of fluid and tank, fluid depth and fluid density was studied thoroughly.

Canales and Mantari (2017) presented a free vibration study of thick laminated plate, in contact with fluid. The properties of the fluid considered by the authors for evaluation are inviscid and incompressible in nature. The influence of fibre orientations on the natural frequencies and on the plate and fluid domain geometry were discussed.

The vibration study was carried out on a rectangular plate with various dimensions and material properties by Ghadirian et al. (2017). Authors studied experimentally the response of the plate by acoustic and modal method by clamping the plate at the side of a steel fluid container.

Sandwich plates with crushable foam cores used in marine structures were analysed due to the application of blast loading by Fatt and Sirivolu (2017). Authors studied the effect of blast load on composite plates both in air as well as under water using finite element solver ABAQUS.

The effect of the position of a rigid block placed at the bottom of a water tank was studied by Adhikary and Mandal (2018). Free and forced vibration study carried out and the developed hydrodynamic pressure on the tank walls was reported considering the effect of fluid structure interaction. The modification of frequency values due to various position, height, size and distance of the block from tank surface was studied by the authors. The variation in fundamental frequency with block height and excitation frequency was also reported.

Huang et al. (2018) studied experimentally the effect of underwater impulse loading on composite laminates. They carried out several non-destructive tests on the plate to study the failure modes. It was observed by the authors that delamination and fibre failure occur a way advance of local failure. Increment in thickness does not enhance in blast resistance of the composite plate, as authors concluded that the failure modes are inconsistent along the thickness of the plate.

The vibration characteristics of a plate either partial or fully submerged in fluid was studied by Soni et al. (2018). The uniqueness of the study is, authors carried out the study on cracked plate. A nonlinear study was performed using Berger's formulation. The plate was modeled using classical plate theory. Bending hardening/softening phenomenon was presented in terms of frequency response. Authors showed the modification of frequency parameters due to the presence of crack in the plate, fluid density, depth of immersion and fluid depth.

Free vibration and time history response of a composite conical tank was performed by Elansary and Damatty (2018). The tank was made of steel outer core and concrete inner core. A case study was also presented considering four different seismic excitation frequencies on a conical tank situated at Mexico and corresponding variation in results was also presented.

Bendahmane et al. (2019) investigated the free vibration effect on variable stiffness composite laminates. The fibre angle at each layer of the composite was varied along with the depth of submersion in the fluid. Higher order shear deformation theory was used to model the plate and the fluid was modelled by using Bernoulli's equation and velocity potential function. In the formulation, authors incorporated the fluid as an added mass. The effect of fibre orientation angle, depth of submersion and boundary conditions on natural frequency was studied. It was concluded by the authors that natural frequency of the plate drops significantly due to the fluid-structure interaction, which lead to instability of the structure.

Alavi and Eipakchi (2019) studied analytically the vibration properties of viscoelastic functionally graded material (VFGM) considering FSDT. Authors developed an analytical solution using perturbation technique by separating the shear and bulk behaviors of the viscoelastic structure.

Xue et al. (2019) studied the free vibration of porous (both along thickness as well as in plane direction) plate with central hole. FSDT was used to formulate the displacement field and non-uniform rational B-spline function was used for the generation of the geometry. Variation in frequency parameters due to alteration of shape of the plate and direction as well as number of porosities was presented.

Hydrodynamic pressure generated at various points on the tank is studied. Fluid-structure interaction inside the fuel tank of helicopter under impact load was assessed by Kim and Kim (2019). The impact load considered here was due to the impact by birds when the helicopter was in operation. The fuel tank was made of composite materials. Hence the failure criteria for composite fuel tank were also considered. Authors concluded that curved geometry of the fuel tank provides negative impact during strike along with the amount of fuel present inside it.

The dynamic response of ceramic matrix composite (CMC) plate was studied by Han et al. (2020). The analysis was carried out considering the damage modes of CMC including matrix cracking and debonding. Impulse and harmonic loading was applied on the simulated model to study the nonlinear dynamic response. A detailed fluid structure interaction between CMC plate and in-compressible fluid was presented by the authors.

Nitti et al. (2020) developed a computational framework to study the FSI problem of thin shells on incompressible flow. Isogeometric analysis was coupled with finite difference method to solve FSI problems by the authors. Several case studies were carried out on engineering and biological objects to study the flow dynamics.

Dynamic analysis of composite pipeline was studied by Oke and Khulief (2020) considering both the conditions, when the pipe was liquid filled or empty. Along with healthy composite pipes, authors also studied the dynamic response of the pipe, with internal surface degradation/discontinuity, both in transverse or longitudinal directions in presence of flowing fluid.

Palmer and smith (2021) reported a numerical simulation of full Navier-Stokes equation for a nonlinear fluid-structure interaction and compared with analytical results. Authors used asymptotic theory for the formulation of nonlinearity and provided a comparative study on FSI

problem at moderate Reynolds number. The gap between a thin structure and wall was varied along with the inclination. The wall inertia was also varied by considering three cases as zero wall velocity, positive and negative wall velocity. Investigation on gap size, wall speed and Reynolds number variation leads to non-linearity and flow separations within the fluid flow.

Valdani and Adamian (2021) presented a parametric study to increase the strength the steel structure under water to mitigate the negative effect of explosive loads. Authors carried out several cases of reinforcing blades attached with the basic steel plate. The resistance of the plate was expressed as contour plots of Von-mises stresses, damage parameter and displacement graphs.

Finite element analysis being most popular among researchers for its capability to handle complex geometry was enhanced its limits with the incorporation of isogeometric analysis (IGA). This reduced the induced error due to data interaction between coding platform and computer drafting interface which uses conventional non-uniform rational basis spline (NURBS). Possible error due to geometric approximation between two separate interfaces can be removed. Hence IGA was getting popularity among the researchers for solving complex problems and literature was available on vibration and buckling response of laminated plates using IGA. Phung-Van et al. (2021) presented an article on this topic in recent years.

An excellent review was presented by Yu and Whittaker (2021) on fluid-structure interaction of cylindrical tanks supported on its base. Lateral movement of the tank, convective and impulsive wave actions under FSI was discussed. Authors reviewed the solutions for FSI stated by Jacobsen, Housner, Veletsos, Chalhoub and Kelly and also pointed out errors if any.

Variation of wall shear stress due to fluid flow for variation of temperature and pressure was reported by Daricik et al. (2022). Change in mechanical and thermal-physical properties of fiber reinforced polymer composites were studied by the authors and wall shear stress and Von-mises stresses were reported.

Response of a curvilinear composite plate within a viscous fluid flow was studied by Liu et al. (2023). Nonlinear FSI was studied for the plate with curvilinear fiber reinforced composite. Authors concluded that nature of flapping changes with change in ply lay-ups and ply angles which confirms that ply orientation and sequence has significant effect on FSI.

Sloshing effect of cylindrical composite tank was analyzed for free vibration response by Tiwari et al. (2023) considering FSI. Direct coupling is used to model the FSI. The analysis was carried out using 3-D finite element method. The effect of ply orientation, dimension ratios was studied thoroughly in this article.

2.5 CRITICAL DISCUSSION

- Composite material is being used as the main structural unit for the formation of plate and shell since long back. It is much popular among the researchers due the flexibility in design the structure by simple modification in ply orientation or sequence. It has also very high stiffness value compared to its weight, which made it popular construction unit in the weight sensitive branches of engineering.
- Various shear deformation theories are proposed at different times for to model the strain displacement relationship matrix. Classical laminated plate theory, first order and higher order shear deformation theory are most popular among them. It is seen from the review that FSDT for thin plates gives almost comparable results with that of higher order theories. Hence to account for the effect of transverse shear FSDT is used in the present formulation.
- Various methods are used by many researchers to model the plates. Finite element, finite difference, boundary value problem are some of them. Finite element method being robust in modelling complex geometry and various loads are adopted in the present study.
- Different aspects of analysis were carried out on plates including static and dynamic response, bending characteristics, failure criteria under various boundary conditions and loads. Dynamic analysis of any structure is very important as it defines the strength and serviceability potential of a structure.
- Dynamic analysis is mainly of two types: free and forced vibration. Free vibration is equally important to observe the pattern of natural frequencies of the structure with that of forced vibration. Free vibration is especially important for composite materials because presence of cracks or cut outs within the plate modifies the frequency values. Hence natural frequency of a composite structure defines the presence of cracks within the structure.
- Forced vibration on the other hand is another important topic of research. Structures throughout its life undergoes various types of loads. The response of the structure under such loads is very important. If any vibration generated with the structure remains

unattained, may lead to uncontrolled vibration or noise within it. Hence a thorough study is required for the presence of external or internal loads for any sort of vibration.

- Structures under strong ground motion is another important topic of research and the above literature survey suggests that it is very important to carry out the structural response under such types of loads. Earthquake load is non periodic and unpredictable in nature. Failure of huge structures due to strong ground motion is catastrophic and must be avoided. A case study on previous earthquake can give us an idea to plan for design of future structures. Earthquake on aged structures is also an important area of research and many researchers have focused on that part as well.
- Liquid retaining structures being huge in mass is of utmost important to study against failure. Response of such structures under dynamic loading needs careful attention. Researchers round the globe have studied the effect of pressure generation under ground motion since long back. Different theories are implemented and further refined to study the response of liquid storage structures. Pressure being the primary variable in such structures, are calculated for various parameters. Most important in such variation is geometric variation and the variation in different ground motions. Corresponding change in pressure is observed and reported by the authors.
- Sloshing in a liquid retaining structure is very important phenomenon and it depends upon many external as well as internal parameters. Effect of sloshing is also very important in designing liquid retaining structures. Many authors have studied mainly the sloshing effect due to external excitations.
- Baffle wall inside a liquid retaining structure is another important topic of research as it modifies the overall response of the structure. Position, number, size of baffle walls and stiffness also modifies overall response of the system.
- Study on variation of pressure under convective wave and impulsive wave is observed in depth. Various software is used to study the response. Presence of free board at the liquid retaining structure is also studied for modification of response. Tank totally filled with liquid and partial fill both were studied.
- Various ground supported concrete tanks were studied for convective an impulsive wave propagation. Tank geometry and support conditions were varied and studied under different ground excitations.

- Finite element method is the common choice for the researchers to model the fluid due to various advantages as mentioned earlier. Study of fluid domain on various aspects were carried out by modelling the fluid using finite element method, but mostly two-dimensional element is used. Analysis of fluid using three-dimensional finite element method is very limited in the research domain. Hence a three-dimensional approach is employed in the present formulation to model the fluid using finite element technique.
- Fluid-structure interaction is another important topic of research since long. Finite element method is used by most of the researchers to study the coupled response of the system.
- Fluid-structure interaction involves in huge mass jointly of the structure as well as the fluid in it. Vibration study thus becomes of immense importance of such system. Free as well as forced vibration response of such combined structure has gained attention of many researchers round the world. Various theories and formulations were proposed to study the dynamics of such structures.
- The modification in sloshing response in fluid retaining structures are conducted to observe the effect of fluid-structure interaction.
- Various cases are there where the structure is stationery and fluid is flowing around it or sometimes fluid is stagnant structure is moving in nature. In both the cases the effect of fluid-structure interaction on various response parameters are studied. Apart from these two cases, both fluid and structure are stationary (retaining structure type) is also studied for dynamic analysis.
- Direct as well indirect coupling is used to deal with fluid-structure interaction problems in the literatures. However, the direct coupling being more versatile is considered by most of the authors.
- External loadings are varied to find the response of the combined structure. Along with transient loading or ground motion, impact load is also played an important component of research criteria. Many practical cases are analysed under impact load (such as impact by ice, impact by birds on fuel tank, blast load etc.) considering fluid-structure interaction.
- The effect of obstruction in fluid flow is studied considering fluid-structure interaction. The modification in flow regime due to the presence of such material is studied.

- Liquid retaining structures analysed for fluid structure interaction mainly focused on materials such as concrete, steel or steel-concrete composite structure. Generation of pressure on the structural part is studied.
- Failure in composite structure under external force is studied considering fluid structure interaction. Matrix cracking and delamination both were considered.
- Composite materials used as the structural unit during fluid-structure interaction problem only in case of helicopter fuel tank or in case of hull of a ship. In both the cases they are absolutely different in nature than the retaining structure. Composites are not used as the construction unit as far the knowledge of the present researchers.

2.6 NOVELTY OF THE PRESENT WORK

A detailed go-through of the critical discussion points out towards the following lacuna of the existing literature:

1. Composites are used as construction unit of liquid retaining structure for fluid-structure interaction problem. In most of the cases the sloshing effect under fluid-structure interaction is studied. No literature on structural response is available.
2. Composite plates are studied for stress and displacement response considering direct coupling effect but mainly for individual structural component, such as hull of a ship.
3. In all cases where fluid-structure interaction is considered for liquid retaining structures, applied loads are mainly impact load, blast load or temperature stress. Effect of structural response considering fluid-structure interaction under transient loading or under ground motion is absent in the literature.

In order to mitigate the above gap, present research is carried out by analyzing a composite tank under transient loading and ground motions. The present research lies in the fact that the more realistic displacement, normal stress, inplane shear stress and transverse shear stress of composite side walls of the liquid tank is obtained and presented under different transient loading as well as under ground motion. For this, a finite element model of composite plate-liquid coupled systems in which the fluid within the tank is simulated as

3-D system. In addition, in the present study, the interaction between composite side walls and the fluid within the tank is incorporated so that the responses of composite side walls will be as realistic as possible. The stresses developed at different ply layers under same loading cases are also presented for different ply angles and geometric variations.

2.7 RESEARCH GOAL

The main objective of present study is to carry out the dynamic analysis of liquid retaining structure considering fluid-structure interaction. Finite element method is used to formulate the side walls and fluid part. Eight node isoparametric element is used for the plate structure and sixteen node brick element is used to formulate the fluid element. Five degrees of freedom per node is considered for plate element as three translation and two rotation and only pressure is the unknown at each node for the fluid element. Direct coupling method is employed to couple the fluid-structure interaction problem and corresponding frequency, displacement and stresses are calculated. Various parametric variations are applied such as change in ply angle, ply layers and orientation, boundary conditions and geometry. Stress contour at different ply layers is obtained and presented.

CHAPTER 3

MATHEMATICAL FORMULATION

3.1 GENERAL

Study of liquid retaining structures having huge mass is very important area of research. Static as well dynamic response of such massive structure is required careful attention. Presence of liquid in the reservoir modifies the overall response of the system due to the coupling between the fluid and structure. Three-dimensional fluid-structure system is modeled and analyzed for different loading and boundary conditions in the present study. The present work starts with modeling of side walls of the tank using composite materials as the construction unit and corresponding responses are noted only for the wall. Finally, the fluid and coupling between the structure and fluid are done and corresponding response is studied. The study is carried out using three-dimensional finite element technique. the side walls are modeled as two dimensional isoparamentric plate elements with eight nodes per element and the fluid part is modeled as three-dimensional sixteen node brick element. Stresses developed at the two side walls under coupling is studied and also stress contour at each layer of the composite plate is presented at the end of the study. Detailed theoretical formulation is presented in the following sections.

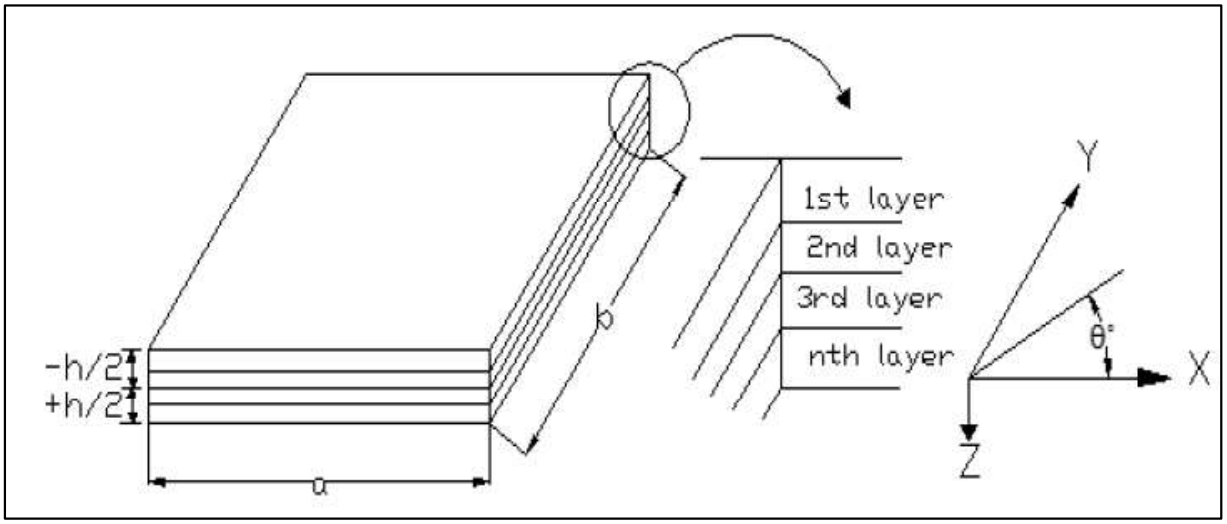

Fig. 3.1 Composite plate with specific layer number and ply angle

3.2 FINITE ELEMENT METHOD (FEM)

In this method, the whole structure is divided into several smaller parts. This is termed as discretization. Individual smaller parts are termed as elements. All the elements are connected at nodes. Number of nodes present in each element depends upon the requirement of the specific problem under consideration. Response of each element (displacement, stress etc.) is obtained at some discrete points within the material. Interpolation functions are used to interpolate and transfer the responses between any point within the material and the nodes. In this method all the responses are calculated at the nodal points and then they are assembled to obtain the overall response of the structure.

3.2.1 Selection of element

Discretization process in FEM and selection of proper element to represent the whole structure is very important. The element is selected in such a way that it can represent the whole structure properly in terms of geometry and displacement field. In the present work a eight nodded quadratic isoparametric element (ref Fig 3.2) with C^0 continuity is chosen to model the plate element. Jacobian matrix is used to transform natural coordinate system to cartesian coordinate system.

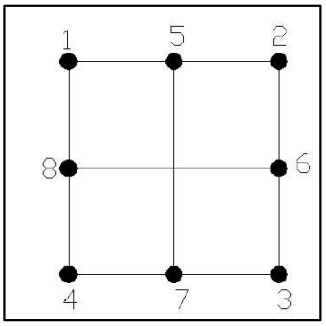

Fig. 3.2 Eight node isoparametric element

3.2.2 Discretisation of element

Plate elements with varying plan dimensions are adopted for present study. The plate is further discretized into smaller elements and the element numbers are optimised for minimum

error. Number of elements along both the axes or the mesh size is obtained by convergence study. After convergence study it was found that a 4×4 meshing of the plate represents the displacement field of the plate most accurately and hence it is followed in the present study. The meshing is presented in Fig. 3.3.

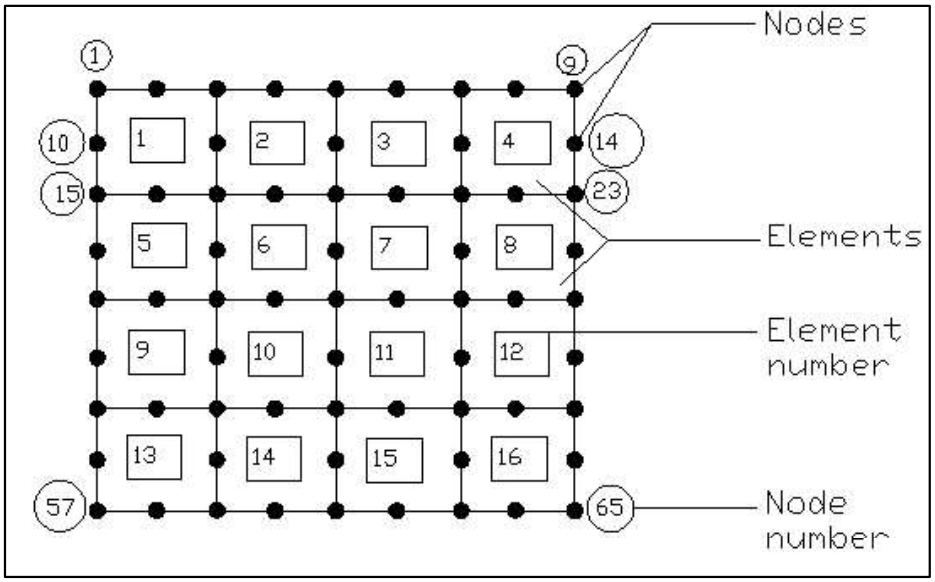

Fig. 3.3 A typical discretization of 4×4 meshing with node and element number

3.2.3 Selection of interpolation function

Interpolation functions relates the displacement values between any point within the element with the nodal points. In order to use the same shape function for displacement as well as coordinates, isoparametric elements are used. A polynomial of displacement in a natural coordinate system is assumed. The same is then solved at the nodal points to achieve the final expressions of shape functions.

Shape functions used for the present eight noded plate elements are

$N_i = \frac{1}{4}(1+\xi\xi_i)(1+\eta\eta_i)(\xi\xi_i+\eta\eta_i-1)$ for i = 1,2,3,4

$N_i = \frac{1}{2}(1-\xi^2)(1+\eta\eta_i)$ for i = 5,7

$$N_i = \frac{1}{2}(1-\eta^2)(1+\xi\xi_i) \qquad \text{for i = 6,8} \qquad (3.1)$$

N_i is the interpolation function of ith node having natural coordinates ξ_i and η_i.

Position of a point inside an element can also be expressed in terms of shape function as $x = \sum N_i x_i$ and $y = \sum N_i y_i$, where x_i and y_i being the geometric coordinates at nodal points with i ranging from 1 to 8.

3.3 FORMULATION OF THE COMPOSITE PLATE USING FEM

3.3.1 Selection of displacement field and degrees of freedom

The plate is discretized with eight nodded isoparametric elements. These elements consist of four corner nodes and four middle side nodes. First order shear deformation theory (FSDT) is applied for thin plates in the present study. The nodes are present in each element along the mid thickness. As thin plate and FSDT is considered hence the plane before bending remains plane after bending not necessarily perpendicular after bending. Hence the thickness dimension is neglected and the plate is modelled as a 2D element. Five degrees of freedom are associated with each nodes as three displacements (u,v and w) along three axes and two rotations (α and β).

Displacement at any point within the element is related to nodal displacement with the following relationship using shape functions.

$$[u] = \sum_{i=1}^{8} N_i u_i \, , [v] = \sum_{i=1}^{8} N_i v_i, [w] = \sum_{i=1}^{8} N_i w_i,$$

$$[\alpha] = \sum_{i=1}^{8} N_i \alpha_i \text{ and } [\beta] = \sum_{i=1}^{8} N_i \beta_i \qquad (3.2)$$

This relationship can be expressed in a generalised form as below.

$$\{u\} = \begin{Bmatrix} u \\ v \\ w \\ \alpha \\ \beta \end{Bmatrix} = \begin{bmatrix} N_i & & & & \\ & N_i & & & \\ & & N_i & & \\ & & & N_i & \\ & & & & N_i \end{bmatrix} \begin{Bmatrix} u_i \\ v_i \\ w_i \\ \alpha_i \\ \beta_i \end{Bmatrix} \qquad (3.3)$$

3.3.2 Strain-displacement relationship

First order shear deformation theory (FSDT) is used for the thin shell to obtain the strain-displacement relationship matrix. Based upon the theory displacement along different layers in a plate element is governed by the following relationships.

$$u = u_0 - z\frac{\partial w}{\partial x},\ \mathrm{v} = v_0 - z\frac{\partial w}{\partial y},\ w = w_0 \tag{3.4}$$

Where u_0, v_0 and w_0 are the displacement at the middle plane and z is the distance of a particular fiber layer from the middle layer.

Now strain can be related with displacement components using shape functions as follows

$$\begin{Bmatrix} \varepsilon_x^0 \\ \varepsilon_y^0 \\ \varepsilon_s^0 \\ \gamma_x \\ \gamma_y \\ \gamma_s \\ \gamma_{xz} \\ \gamma_{yz} \end{Bmatrix} = \sum_{i=1}^{8} \begin{bmatrix} \frac{\delta N_i}{\delta x} & 0 & 0 & 0 & 0 \\ 0 & \frac{\delta N_i}{\delta y} & 0 & 0 & 0 \\ \frac{\partial N_i}{\partial y} & \frac{\partial N_i}{\partial x} & 0 & 0 & 0 \\ 0 & 0 & 0 & -\frac{\partial N_i}{\partial x} & \\ & & & & -\frac{\partial N_i}{\partial y} \\ 0 & 0 & 0 & -\frac{\partial N_i}{\partial y} & -\frac{\partial N_i}{\partial x} \\ 0 & 0 & \frac{\partial N_i}{\partial x} & -N_i & 0 \\ 0 & 0 & \frac{\partial N_i}{\partial y} & 0 & -N_i \end{bmatrix} \begin{Bmatrix} u \\ v \\ w \\ \alpha \\ \beta \end{Bmatrix} \tag{3.5}$$

Where ε_x^0 , ε_y^0 and ε_s^0 are the normal strain, γ_x , γ_y and γ_s are shear strain and γ_{xz} and γ_{yz} are the transverse shear strain. Equation 3.5 can be written in general form as $\{\epsilon\} = [B]\{d_e\}$, $[B]$is the strain displacement-relationship matrix and d_e is the generalized displacement vector. Shape functions are expressed in natural coordinate system and hence requires a conversion parameter between natural coordinate (ξ,η) and Cartesian coordinate system (X,Y) to express the B matrix. This conversion is done by Jacobian matrix [J] and expressed as

$$\begin{Bmatrix} \frac{\delta}{\delta\xi} \\ \frac{\delta}{\delta\eta} \end{Bmatrix} = \begin{bmatrix} \frac{\delta x}{\delta\xi} & \frac{\delta y}{\delta\xi} \\ \frac{\delta x}{\delta\eta} & \frac{\delta y}{\delta\eta} \end{bmatrix} \begin{Bmatrix} \frac{\delta}{\delta x} \\ \frac{\delta}{\delta y} \end{Bmatrix} \tag{3.6}$$

$$\begin{Bmatrix} \frac{\delta}{\delta\xi} \\ \frac{\delta}{\delta\eta} \end{Bmatrix} = [J] \begin{Bmatrix} \frac{\delta}{\delta x} \\ \frac{\delta}{\delta y} \end{Bmatrix} \tag{3.7}$$

Now using shape function in natural coordinate system, Jacobian matrix can be expressed as

$$[J] = \begin{bmatrix} \sum_{i=1}^{8} x_i \frac{\delta N_i}{\delta\xi} \sum_{i=1}^{8} y_i \frac{\delta N_i}{\delta\xi} \\ \sum_{i=1}^{8} x_i \frac{\delta N_i}{\delta\eta} \sum_{i=1}^{8} y_i \frac{\delta N_i}{\delta\eta} \end{bmatrix} \tag{3.8}$$

Now using the conversion parameter Jacobian matrix, *B* matrix can easily be written.

3.3.3 Force-strain relationship of composite plate

Stress strain relationship matrix

$$\begin{Bmatrix} \sigma_1 \\ \sigma_2 \\ \\ \\ \sigma_6 \end{Bmatrix} = \begin{bmatrix} C_{11} & C_{12} & C_{13} & & & \\ C_{21} & C_{22} & C_{23} & & & \\ C_{31} & C_{32} & C_{33} & & & \\ & & & C_{44} & & \\ & & & & C_{55} & \\ & & & & & C_{66} \end{bmatrix} \begin{Bmatrix} \varepsilon_1 \\ \varepsilon_2 \\ \varepsilon_3 \\ \varepsilon_4 \\ \varepsilon_5 \\ \varepsilon_6 \end{Bmatrix} \tag{3.9}$$

Where,

$C_{11} = \frac{1-\nu_{23}\nu_{32}}{E_2 E_3 \Delta}$

$C_{12} = \frac{\nu_{12}+\nu_{13}\nu_{32}}{E_2 E_3 \Delta}$

$C_{22} = \frac{1-\nu_{13}\nu_{31}}{E_1 E_3 \Delta}$

$C_{33} = \frac{1-\nu_{12}\nu_{21}}{E_1 E_2 \Delta}$

$C_{23} = \frac{\nu_{23}+\nu_{21}\nu_{13}}{E_1 E_2 \Delta}$

$$C_{13} = \frac{\nu_{13}+\nu_{21}\nu_{32}}{E_2 E_3 \Delta} \tag{3.10}$$

$$\Delta = \frac{1}{E_1 E_2 E_3}\begin{vmatrix} 1 & -\nu_{21} & -\nu_{31} \\ -\nu_{12} & 1 & -\nu_{32} \\ -\nu_{13} & -\nu_{23} & 1 \end{vmatrix} \tag{3.11}$$

$$\begin{Bmatrix}\sigma_1 \\ \sigma_2 \\ \sigma_6\end{Bmatrix} = \begin{bmatrix} Q_{11} & Q_{12} & 0 \\ Q_{12} & Q_{22} & 0 \\ 0 & 0 & Q_{66}\end{bmatrix}\begin{Bmatrix}\varepsilon_1 \\ \varepsilon_2 \\ \varepsilon_6\end{Bmatrix} \tag{3.12}$$

$$Q_{11} = \frac{E_1}{1-\nu_{12}\nu_{21}} \tag{3.13a}$$

$$Q_{22} = \frac{E_2}{1-\nu_{12}\nu_{21}} \tag{3.13b}$$

$$Q_{12} = \frac{\nu_{12}E_2}{1-\nu_{12}\nu_{21}} \tag{3.13c}$$

$$Q_{66} = G_{12} \tag{3.13d}$$

Conversion between local and global axes

$$\begin{Bmatrix}\sigma_x \\ \sigma_y \\ \sigma_s\end{Bmatrix} = \begin{bmatrix} m^2 & n^2 & -2mn \\ n^2 & m^2 & 2mn \\ mn & -mn & m^2-n^2\end{bmatrix}\begin{Bmatrix}\sigma_1 \\ \sigma_2 \\ \sigma_6\end{Bmatrix}$$

$$= \begin{bmatrix} m^2 & n^2 & -2mn \\ n^2 & m^2 & 2mn \\ mn & -mn & m^2-n^2\end{bmatrix}\begin{bmatrix} Q_{11} & Q_{12} & 0 \\ Q_{12} & Q_{22} & 0 \\ 0 & 0 & Q_{66}\end{bmatrix}\begin{Bmatrix}\varepsilon_1 \\ \varepsilon_2 \\ \varepsilon_6\end{Bmatrix}$$

$$= \begin{bmatrix} m^2 & n^2 & -2mn \\ n^2 & m^2 & 2mn \\ mn & -mn & m^2-n^2\end{bmatrix}\begin{bmatrix} Q_{11} & Q_{12} & 0 \\ Q_{12} & Q_{22} & 0 \\ 0 & 0 & Q_{66}\end{bmatrix}\begin{bmatrix} m^2 & n^2 & 2mn \\ n^2 & m^2 & -2mn \\ -mn & mn & m^2-n^2\end{bmatrix}\begin{Bmatrix}\varepsilon_x \\ \varepsilon_y \\ \frac{\varepsilon_s}{2}\end{Bmatrix} \tag{3.14}$$

$$\begin{Bmatrix}\sigma_x \\ \sigma_y \\ \sigma_s\end{Bmatrix} = \begin{bmatrix} Q_{xx} & Q_{yy} & 2Q_{xs} \\ Q_{ys} & Q_{yy} & 2Q_{ys} \\ Q_{sx} & Q_{sy} & 2Q_{ss}\end{bmatrix}\begin{Bmatrix}\varepsilon_x \\ \varepsilon_y \\ \frac{\varepsilon_s}{2}\end{Bmatrix} \tag{3.15}$$

$$Q_{xx} = m^4Q_{11} + n^4Q_{22}+2m^2n^2Q_{12}+4m^2n^2Q_{66}$$

$$Q_{yy} = n^4Q_{11} + m^4Q_{22}+2m^2n^2Q_{12}+4m^2n^2Q_{66}$$

$$Q_{xy} = m^2n^2Q_{11} + m^2n^2Q_{22}+(m^4 + n^4)Q_{12} - 4m^2n^2Q_{66}$$

$$Q_{xs} = m^3nQ_{11} + mn^3Q_{22}+(\mathrm{mn}^3 - \mathrm{m}^3\mathrm{n})Q_{12} + 2(mn^3 - m^3n)Q_{66}$$

$$Q_{yx} = mn^3Q_{11} - m^3nQ_{22}+(\mathrm{m}^3\mathrm{n} - \mathrm{mn}^3)Q_{12} + 2(m^3n - mn^3)Q_{66}$$

$$Q_{ss} = m^2n^2Q_{11} + m^2n^2Q_{22} - 2m^2n^2Q_{12} + (m^2 - n^2)Q_{66}$$

m=cosθ, n=sinθ

$$\begin{Bmatrix} \varepsilon_x \\ \varepsilon_y \\ \frac{\varepsilon_s}{2} \end{Bmatrix} = \begin{Bmatrix} \varepsilon_x^0 \\ \varepsilon_y^0 \\ \varepsilon_s^0 \end{Bmatrix} + z \begin{Bmatrix} \kappa_x \\ \kappa_y \\ \kappa_s \end{Bmatrix} \tag{3.16}$$

$$\begin{Bmatrix} \sigma_x \\ \sigma_y \\ \sigma_s \end{Bmatrix} = \begin{bmatrix} Q_{xx} & Q_{xy} & 2Q_{xs} \\ Q_{yx} & Q_{yy} & 2Q_{ys} \\ Q_{sx} & Q_{sy} & 2Q_{ss} \end{bmatrix} \begin{Bmatrix} \varepsilon_x^0 \\ \varepsilon_y^0 \\ \varepsilon_s^0 \end{Bmatrix} + z \begin{bmatrix} Q_{xx} & Q_{xy} & 2Q_{xs} \\ Q_{yx} & Q_{yy} & 2Q_{ys} \\ Q_{sx} & Q_{sy} & 2Q_{ss} \end{bmatrix} \begin{Bmatrix} \kappa_x \\ \kappa_y \\ \kappa_s \end{Bmatrix} \tag{3.17}$$

N_X , N_Y = Normal forces acting on unit length

N_S = Inplane shear force acting on unit length

M_X, M_Y = Bending moment acting on unit length

M_S = Twisting moment acting on unit length

Force and Moment for individual layer:

$$N_x = \int_{dk} \sigma_x dz$$

$$M_x = \int_{dk} \sigma_x z dz$$

$$N_y = \int_{dk} \sigma_y dz$$

$$M_y = \int_{dk} \sigma_y z dz$$

$$N_s = \int_{dk} \sigma_s dz$$

$$M_s = \int_{dk} \sigma_s z dz \tag{3.18}$$

Force and Moment for all the layers:

$$\begin{Bmatrix} N_x \\ N_y \\ N_s \end{Bmatrix} = \sum_{K=1}^{n} \int_{z_{k-1}}^{z_k} \begin{Bmatrix} \sigma_x \\ \sigma_y \\ \sigma_s \end{Bmatrix}_k dz \tag{3.19}$$

$$\begin{Bmatrix} M_x \\ M_y \\ M_s \end{Bmatrix} = \sum_{K=1}^{n} \int_{z_{k-1}}^{z_k} \begin{Bmatrix} \sigma_x \\ \sigma_y \\ \sigma_s \end{Bmatrix}_k z dz \tag{3.20}$$

$$\begin{Bmatrix} N_x \\ N_y \\ N_s \end{Bmatrix} = \sum_{K=1}^{n} \begin{bmatrix} Q_{xx} & Q_{xy} & Q_{xs} \\ Q_{yx} & Q_{yy} & Q_{ys} \\ Q_{sx} & Q_{sy} & Q_{ss} \end{bmatrix}_k \begin{Bmatrix} \varepsilon_x^0 \\ \varepsilon_y^0 \\ \varepsilon_s^0 \end{Bmatrix} \int_{Z_{K-1}}^{Z_K} dz + \begin{bmatrix} Q_{xx} & Q_{xy} & Q_{xs} \\ Q_{yx} & Q_{yy} & Q_{ys} \\ Q_{sx} & Q_{sy} & Q_{ss} \end{bmatrix}_k \begin{Bmatrix} \kappa_x \\ \kappa_y \\ \kappa_s \end{Bmatrix} \int_{Z_{K-1}}^{Z_K} z dz \tag{3.21}$$

$$\begin{Bmatrix} M_x \\ M_y \\ M_s \end{Bmatrix} = \sum_{K=1}^{n} \begin{bmatrix} Q_{xx} & Q_{xy} & Q_{xs} \\ Q_{yx} & Q_{yy} & Q_{ys} \\ Q_{sx} & Q_{sy} & Q_{ss} \end{bmatrix}_k \begin{Bmatrix} \varepsilon_x^0 \\ \varepsilon_y^0 \\ \varepsilon_s^0 \end{Bmatrix} \int_{Z_{K-1}}^{Z_K} z dz + \begin{bmatrix} Q_{xx} & Q_{xy} & Q_{xs} \\ Q_{yx} & Q_{yy} & Q_{ys} \\ Q_{sx} & Q_{sy} & Q_{ss} \end{bmatrix}_k \begin{Bmatrix} \kappa_x \\ \kappa_y \\ \kappa_s \end{Bmatrix} \int_{Z_{K-1}}^{Z_K} z^2 dz \tag{3.22}$$

$$\{N\} = \sum_{K=1}^{n} \left[[Q][z_K - z_{K-1}]\right]\{\varepsilon^0\} + \sum_{K=1}^{n} \frac{1}{2}\left[[Q][z_k^2 - z_{k-1}^2]\right]\{\kappa\} \tag{3.23}$$

$$\{M\} = \sum_{K=1}^{n} \frac{1}{2}\left[[Q][z_k^2 - z_{k-1}^2]\right]\{\varepsilon^0\} + \sum_{K=1}^{n} \frac{1}{3}\left[[Q][z_k^3 - z_{k-1}^3]\right]\{\kappa\} \tag{3.24}$$

$$\{N\} = [A]\{\varepsilon^0\} + [B]\{\kappa\} \tag{3.25}$$

$$\{M\} = [B]\{\varepsilon^0\} + [D]\{\kappa\} \tag{3.26}$$

Where,

$A_{ij} = \sum_{K=1}^{n} Q_{ij}^{K}(z_K - z_{K-1})$

$B_{ij} = \sum_{K=1}^{n} \frac{1}{2} Q_{ij}^{K}(z_k^2 - z_{k-1}^2)$

$D_{ij} = \sum_{K=1}^{n} \frac{1}{3} Q_{ij}^{K}(z_k^3 - z_{k-1}^3)$

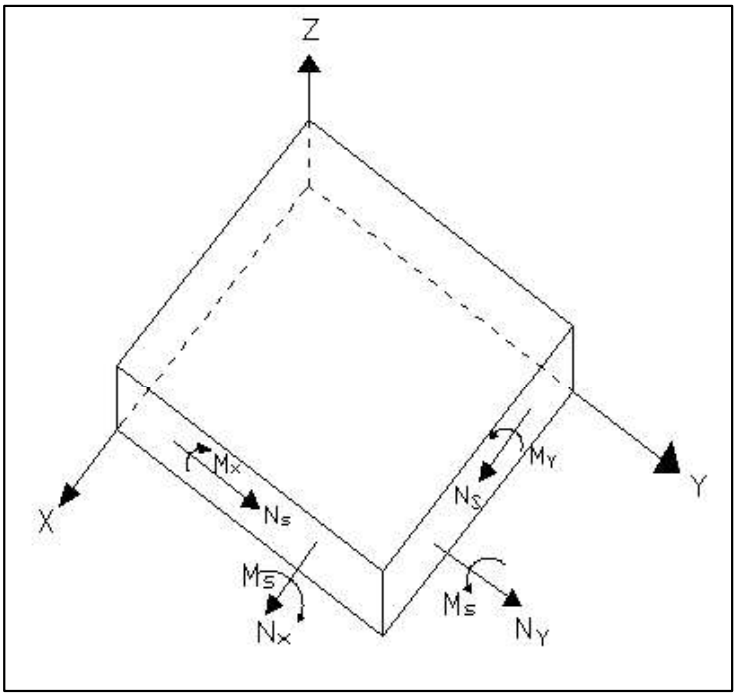

Fig. 3.4 Direction of various forces and moments in a lamina

$$\begin{Bmatrix} N \\ M \end{Bmatrix} \begin{bmatrix} A_{ij} & B_{ij} \\ B_{ij} & D_{ij} \end{bmatrix} \begin{Bmatrix} \varepsilon^0 \\ \kappa \end{Bmatrix} \tag{3.27}$$

$$A_{ij} = \begin{bmatrix} A_{xx} & A_{xy} & A_{xs} \\ A_{yx} & A_{yy} & A_{ys} \\ A_{sx} & A_{sy} & A_{ss} \end{bmatrix}$$

$$B_{ij} = \begin{bmatrix} B_{xx} & B_{xy} & B_{xs} \\ B_{yx} & B_{yy} & B_{ys} \\ B_{sx} & B_{sy} & B_{ss} \end{bmatrix}$$

$$D_{ij} = \begin{bmatrix} D_{xx} & D_{xy} & A_{xs} \\ A_{yx} & A_{yy} & A_{ys} \\ A_{sx} & A_{sy} & A_{ss} \end{bmatrix}$$

$$\begin{Bmatrix} N_x \\ N_y \\ N_s \\ M_x \\ M_y \\ M_s \end{Bmatrix} = \begin{bmatrix} A_{xx} & A_{xy} & A_{xs} & B_{xx} & B_{xy} & B_{xs} \\ A_{yx} & A_{yy} & A_{ys} & B_{yx} & B_{yy} & B_{ys} \\ A_{sx} & A_{sy} & A_{ss} & B_{sx} & B_{sy} & B_{ss} \\ B_{xx} & B_{xy} & B_{xs} & D_{xx} & D_{xy} & D_{xs} \\ B_{yx} & B_{yy} & B_{ys} & D_{yx} & D_{yy} & D_{ys} \\ B_{sx} & B_{sy} & B_{ss} & D_{sx} & D_{sy} & D_{ss} \end{bmatrix} \begin{Bmatrix} \varepsilon_x^0 \\ \varepsilon_y^0 \\ \varepsilon_s^0 \\ \kappa_x^0 \\ \kappa_y^0 \\ \kappa_s^0 \end{Bmatrix} \tag{3.28}$$

$$\begin{Bmatrix} N_x \\ N_y \\ N_s \\ M_x \\ M_y \\ M_s \\ Q_x \\ Q_y \end{Bmatrix} = \begin{bmatrix} A_{xx} & A_{xy} & A_{xs} & B_{xx} & B_{xy} & B_{xs} & 0 & 0 \\ A_{yx} & A_{yy} & A_{ys} & B_{yx} & B_{yy} & B_{ys} & 0 & 0 \\ A_{sx} & A_{sy} & A_{ss} & B_{sx} & B_{sy} & B_{ss} & 0 & 0 \\ B_{xx} & B_{xy} & B_{xs} & D_{xx} & D_{xy} & D_{xs} & 0 & 0 \\ B_{yx} & B_{yy} & B_{ys} & D_{yx} & D_{yy} & D_{ys} & 0 & 0 \\ B_{sx} & B_{sy} & B_{ss} & D_{sx} & D_{sy} & D_{ss} & 0 & 0 \\ 0 & 0 & 0 & 0 & 0 & 0 & A_{xx}^z & A_{xy}^z \\ 0 & 0 & 0 & 0 & 0 & 0 & A_{yx}^z & A_{yy}^z \end{bmatrix} \begin{Bmatrix} \varepsilon_x^0 \\ \varepsilon_y^0 \\ \varepsilon_s^0 \\ \kappa_x \\ \kappa_y \\ \kappa_s \\ \varepsilon_{xz}^0 \\ \varepsilon_{yz}^0 \end{Bmatrix} \tag{3.29}$$

$$\{F\} = [D]\{\varepsilon\} \tag{3.30}$$

Formation of Mass Matrix

$$[M_e] = \iint_A [N]^T [m][N] dx dy \{\ddot{d}_e\} \tag{3.31}$$

3.3.4 Formation of Inertia matrix

The inertia matrix consists of linear and rotary inertia terms.

Mass per unit area is denoted by

$$m = \rho h \tag{3.32}$$

Here ρ is considered as the mass density of plate and h is the thickness of the plate.

Moment of inertia per unit area is denoted by I and represented by

$$I = \frac{\rho h^3}{12} \tag{3.33}$$

Generalized inertia matrix is represented as follows:

$$[m] = \begin{bmatrix} m & 0 & 0 & 0 & 0 \\ 0 & m & 0 & 0 & 0 \\ 0 & 0 & m & 0 & 0 \\ 0 & 0 & 0 & I & 0 \\ 0 & 0 & 0 & 0 & I \end{bmatrix} \tag{3.34}$$

3.3.5 Formulation of equation of motion for vibration problem

General variational method:

We assume that y is a function of x. So it can be written as (y,y',y") is a functional. It is required to find $y=y(x)$, such that the first variance of $I = \int_{x_1}^{x_2} F(y, y', y")dx$. It is obvious that I must be made stationary by satisfying the boundary conditions. In elasticity problems potential energy term is such functional.

In the present study it is required to find the solution of first variance with $\delta I = 0$

$$\int_{x_1}^{x_2} F(y, y', y")dx = 0$$

$$\Rightarrow \int_{x_1}^{x_2} \left(\frac{\delta F}{\delta y}\delta y + \frac{\delta F}{\delta y'}\delta y' + \frac{\delta F}{\delta y"}\delta y"\right)dx = 0 \tag{3.35}$$

Applying integration by parts on second and third term, we have,

$$\int_{x_1}^{x_2} \frac{\delta F}{\delta y'}\delta y' dx = \left[\frac{\delta F}{\delta y'}\delta y'\right]_{x_1}^{x_2} - \int_{x_1}^{x_2} \frac{d}{dx}\left(\frac{\delta F}{\delta y'}\right)\delta y dx$$

$$\int_{x_1}^{x_2} \frac{\delta F}{\delta y''}\delta y'' dx = \left[\frac{\delta F}{\delta y''}\delta y'\right]_{x_1}^{x_2} - \left[\frac{d}{dx}\left(\frac{\delta F}{\delta y''}\right)\delta y\right]_{x_1}^{x_2} + \int_{x_1}^{x_2} \frac{d^2}{dx^2}\left(\frac{\delta F}{\delta y''}\right)\delta y dx \tag{3.36}$$

Putting these terms in the original equation

$$\int_{x_1}^{x_2}\left(\frac{\delta F}{\delta y}-\frac{d}{dx}\left(\frac{\delta F}{\delta y\prime}\right)+\frac{d^2}{dx^2}\left(\frac{\delta F}{\delta y\prime\prime}\right)\right)\delta y dx+\left[\left\{\frac{\delta F}{\delta y\prime}-\frac{d}{dx}\left(\frac{\delta F}{\delta y\prime\prime}\right)\right\}\delta y\right]_{x_1}^{x_2}+\left[\frac{\delta F}{\delta y\prime\prime}\delta y'\right]_{x_1}^{x_2}=0 \tag{3.37}$$

Since δy is arbitrary, hence all the three terms of the above equation are zero.

Hence,

$$\frac{\delta F}{\delta y}-\frac{d}{dx}\left(\frac{\delta F}{\delta y\prime}\right)+\frac{d^2}{dx^2}\left(\frac{\delta F}{\delta y\prime\prime}\right)=0 \tag{3.38}$$

$$\frac{\delta F}{\delta y\prime}-\frac{d}{dx}\left(\frac{\delta F}{\delta y\prime\prime}\right)=0 \tag{3.39}$$

$$\frac{\delta F}{\delta y\prime\prime}\delta y'=0 \tag{3.40}$$

The first of these three equations are known as Eular-Lagrange equation which is

$$\frac{\delta F}{\delta y}-\frac{d}{dx}\left(\frac{\delta F}{\delta y\prime}\right)+\frac{d^2}{dx^2}\left(\frac{\delta F}{\delta y\prime\prime}\right)=0$$

For the present formulation if the functional F is taken as the total energy stored within an element due to applied load q, we have

Potential energy stored = $U = \int_V \frac{1}{2}\sigma\varepsilon dv$ (3.41)

Kinetic energy stored = $V = \int_V \frac{1}{2}MV^2 dv$ (3.42)

Applied load = Q

Total energy in the element = $(U\text{-}V\text{-}Q) = F$ (3.43)

Potential energy stored will be = $U = \int_V \frac{1}{2}\sigma\varepsilon dv = \int \frac{1}{2}[B]^T\{d_e\}^T[D][B]\{d_e\}dv$

(3.44)

Kinetic energy will be = $\int_V \frac{1}{2} MV^2 dv = \int_V \frac{1}{2} \{\dot{d_e}\}^T [N]^T [m][N]\{\dot{d_e}\} dv$

(3.45)

Work done by the applied load = $\int_V Q\{d_e\} dv = \int_V [N]^T \{q\}\{d_e\} dv$ (3.46)

$$F = \left[\int_V \frac{1}{2}[B]^T \{d_e\}^T [D][B]\{d_e\} dv - \int_V \frac{1}{2}\{\dot{d_e}\}^T [N]^T [m][N]\{d_e\} dv - \int_V \dot{[N]}^T \{d_e\}\{q\} dv\right]$$

(3.47)

Applying Eular-Lagrange equation on this functional, we have

$$\frac{\delta F}{\delta u} - \frac{d}{dt}\left(\frac{\delta F}{\delta \dot{u}}\right) + \frac{d^2}{dt^2}\left(\frac{\delta F}{\delta \ddot{u}}\right) = 0$$

$$\int_V [[B]^T [D][B]\{d_e\} - [N]^T \{q\}] dv - \frac{d}{dt}[-\int_V [N]^T [m][N]\{\dot{d_e}\} dv]$$

$$\int_A [K]\{d_e\} t dx dy + \int_A [M]\{\ddot{d_e}\} t dx dy = \int_A [N]^T \{q\} t dx dy \quad (3.48)$$

For free vibration, $\{q\} = 0$

$$[M]\{\ddot{d_e}\} + [K]\{d_e\} = 0 \quad (3.49)$$

Element stiffness matrix is given as $[K] = \int_A [B]^T [D][B] dx dy$ (3.50)

Element mass matrix is given as $[M] = \int_A [N]^T [m][N] dx dy$ (3.51)

Element load vector is given as $[Q] = \int_A [N]^T \{q\} dx dy$ (3.52)

The above integrals are converted to natural coordinates using Jacobian matrix as follows

$$[K] = \int_{-1}^{+1}\int_{-1}^{+1}[B]^T[D][B]|J|d\xi d\eta \quad (3.53)$$

$$[M] = \int_{-1}^{+1}\int_{-1}^{+1}[N]^T[m][N]|J|d\xi d\eta \quad (3.54)$$

$$[Q] = \int_{-1}^{+1}\int_{-1}^{+1}[N]^T\{q\}|J|d\xi d\eta \quad (3.55)$$

Numerical integration on the above equations is performed using Gauss quadrature rule. 3×3 Gauss quadrature rule is applied to solve bending stress and 2×2 Gauss quadrature rule i.e., reduced integration technique is applied on shear stress calculation to avoid shear locking.

Elemental stiffness and mass matrix is transformed from local axis system to to global matrix using transformation matrix. Global stiffness and mass matrix is assembled properly.

Thus, the global stiffness matrix, mass matrix and load vector is given as

$$[K] = \sum_{i=1}^{n}[K_e]\ ,\ [M] = \sum_{i=1}^{n}[M_e] \text{ and } [Q] = \sum_{i=1}^{n}[Q_e] \quad (3.56)$$

Applying numerical integration and neglecting thickness,

$$[K]\{d\} + [M]\{\ddot{d}\} = Q \quad (3.57)$$

3.3.6 Application of boundary condition and solution procedure

Imposition of boundary condition means whether a specified degree of freedom has null value or not. In the present formulation five numbers of degrees of freedom is selected at each node. Three displacements oriented along *X, Y* and *Z* axis (*u, v* and *w* respectively) and two rotations (α and β). Zero displacement or rotation boundary condition is imposed by deleting corresponding row and column from the global matrix and load vector. General dynamic problem is formulated first then static and dynamic problem is deduced from it as two special cases.

3.3.7 Formulation of static analysis problem

Static problem can be easily obtained from Equation 3.57 by neglecting the inertia term in the equation. The displacement and load vectors in the present formulation are assumed to be time independent. Hence the static analysis equation is reduced to

$$[\mathrm{K}]\{d\} = Q \tag{3.58}$$

Gauss elimination technique is employed to obtain global displacement vector from which ultimately local displacement vector is obtained.

3.3.8 Formulation of free vibration problem

If the load vector is dropped from equation 3.57 then the free vibration equation can be obtained and can be written as follows

$$[\mathrm{K}]\{d\} + [M]\{\ddot{d}\} = 0 \tag{3.59}$$

In the above equation, displacement $\{d\}$ is a function dependent upon space and time.

Hence $\{d\}$ can be expressed as $\{\mathrm{d}\} = \mathrm{a}e^{\mathrm{i}\omega\mathrm{t}}\varphi$ (3.60)

$\mathrm{a}e^{\mathrm{i}\omega\mathrm{t}}$ is the time dependent part and φ is the time-independent term.

Hence $\{\dot{d}\} = -\omega \mathrm{a}e^{\mathrm{i}\omega\mathrm{t}}\varphi$ and $\{\ddot{d}\} = -\omega^2 \mathrm{a}e^{\mathrm{i}\omega\mathrm{t}}\varphi$

Now if the inertia term is replaced with the above expressions, then equation 3.59 can be written as

$$-\omega^2 \mathrm{a}e^{\mathrm{i}\omega\mathrm{t}}\varphi[M] + \mathrm{a}e^{\mathrm{i}\omega\mathrm{t}}\varphi[K] = 0 \tag{3.61}$$

$$\mathrm{a}e^{\mathrm{i}\omega\mathrm{t}}([K]\{\varphi\} - \omega^2\{\varphi\}[M]) = 0 \tag{3.62}$$

$$([K] - \omega^2[M])\{\varphi\} = 0 \qquad \text{As } ae^{i\omega t} \neq 0 \text{ is assumed} \tag{3.63}$$

Eigen solution is applied on the above equation to obtain the fundamental frequency ω and mode shape $\{\varphi\}$ of the structure. Damping of the structure is not considered in the present study. A computer code is written in the MATLAB environment to perform the Eigen solution.

3.3.9 Formulation of forced vibration problem

If the load vector in Equation 3.57 is transient in nature, then it represents the basic forced vibration type equation. The forced vibration equation is solved using Newmark average integration method and is given as

$$\dot{u}_{j+1} = \dot{u}_j + (1-\gamma)\Delta t\ddot{u}_j + \gamma\Delta t\ddot{u}_j \tag{3.64}$$

$$u_{j+1} = u_j + \Delta t\dot{u}_j + \left(\frac{1}{2} - \beta\right)\Delta t^2\ddot{u}_j + \beta\Delta t^2\ddot{u}_j \tag{3.65}$$

The time history solution is obtained using Newmark's average integration scheme by iterative method. In this method initial conditions are assumed as zero values. Stiffness of the structure is computed with zero damping. Using the initial conditions the effective load at next iteration is found out considering $\beta = \frac{1}{4}$ and $\gamma = \frac{1}{2}$. From effective load and stiffness, the displacement is calculated, which is then utilized to obtain the velocity and acceleration at the next time step. These displacement, velocity and acceleration are again fed to the effective load equation as the initial condition to obtain displacement parameters for the higher time steps.

3.3.10 Ground motion data

Ground motion data used in the present are Koyna and El-centro ground motion. Details of which are provided below.

Koyna earthquake occurred in 1967 is extensively available in literature such as Chopra and Chakrabarty (1972). In the present study the authors have used the horizontal component of the ground motion as shown in Fig. 3.5 with PGA of 0.49g [Chopra and Chakrabarty (1972)].

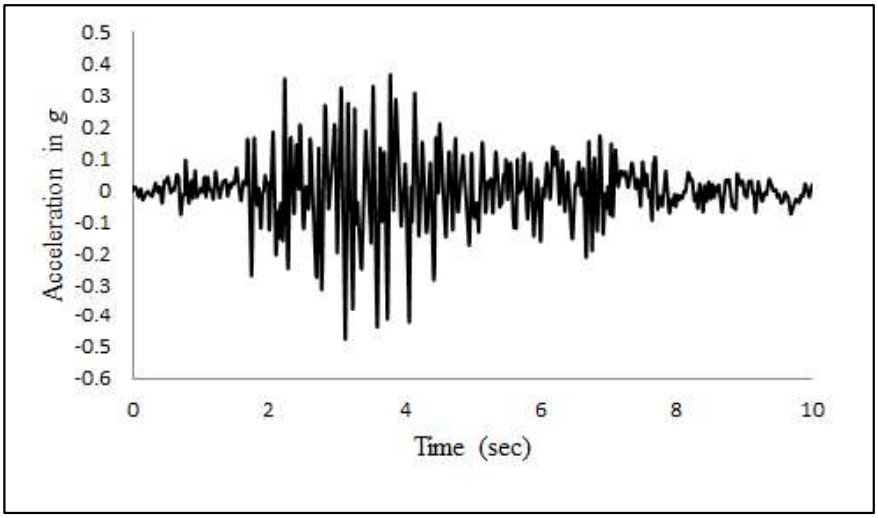

Fig. 3.5 Horizontal component of Koyna earthquake acceleration recorded on 11th December 1967

El Centro ground motion (recorded on 19th May 1940) is considered for present study and the acceleration magnitude is shown in Fig. 3.6.

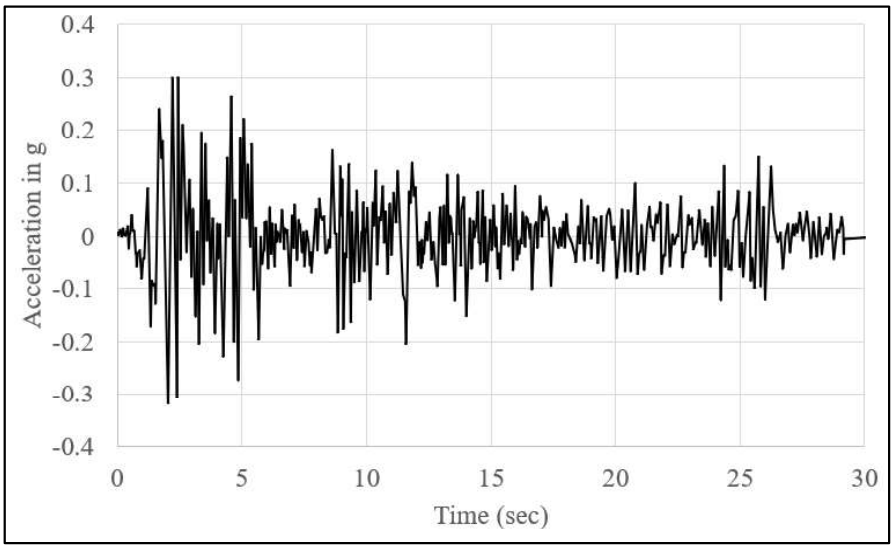

Fig. 3.6 Horizontal component of El Centro earthquake acceleration recorded on 19th May 1940

Forcing frequency other than ground motion accelerations used in the present study are Fundamental frequency and 0.1 times and 3 times of fundamental frequency. Corresponding frequency values are mentioned at the respective sections.

3.3.11 Computation of stresses in side walls

Stresses in finite element analysis is obtained from nodal displacement vector. In the present case the stress developed at two side plates are obtained from the developed nodal displacement vector. Using constitutive relationship matrix [D] and strain-displacement relationship [B] elemental stress vector $\sigma_e$can be calculated as

$$\sigma_e = [D][B]\{u_e\} \tag{3.66}$$

where $\{u_e\}$ is the elemental displacement vector. Once the stresses are obtained at nodal points from the displacement vector, it is observed that the stress values are discontinuous at the nodal points. Moreover, it was demonstrated by Zienkiewich and Taylor (2000) that it gives very poor results for stress if node points are considered as the sampling points. It was further reported by many researchers that Gauss points within the element can be treated as good sampling points for stress calculation. Hence in present formulation, stresses are obtained at 2×2 Gauss point within the plate and bilinear extrapolation is performed to obtain the stresses at the nodal points using the 'local stress smoothing' technique as suggested by Hinton and Cambell (1974).

Bilinear extrapolation for a 2 × 2 Gauss point is performed as followed:

$\bar{\sigma}_1, \bar{\sigma}_2, \bar{\sigma}_3, \bar{\sigma}_4, \bar{\sigma}_5, \bar{\sigma}_6, \bar{\sigma}_7, \bar{\sigma}_8$ be the stresses at the node points (normal stress or inplane shear stress or transverse shear stress) which can be obtained by extrapolation from the stresses at the Gauss points say $\bar{\sigma}_{1g}$, $\bar{\sigma}_{2g}$, $\bar{\sigma}_{3g}$, $\bar{\sigma}_{4g}$. In a two-point Gauss point integration, the Gauss points are (0.57735,0.57735) or $\left(\frac{1}{\sqrt{3}}, \frac{1}{\sqrt{3}}\right)$ from the center point. To find $\bar{\sigma}_1$, $\bar{\sigma}_2$, $\bar{\sigma}_3$, $\bar{\sigma}_4$ it is required to calculate $\acute{\sigma}_1$, $\acute{\sigma}_2$, $\acute{\sigma}_3$, $\acute{\sigma}_4$, $\acute{\sigma}_5$, $\acute{\sigma}_6$, $\acute{\sigma}_7$, $\acute{\sigma}_8$ which are the stresses as shown in Figure 3.5. $\acute{\sigma}_1$,.. $\acute{\sigma}_8$ are the stress values which can be obtained by extrapolation from the Gauss point stresses i.e $\bar{\sigma}_{1g}$,.. $\bar{\sigma}_{4g}$.

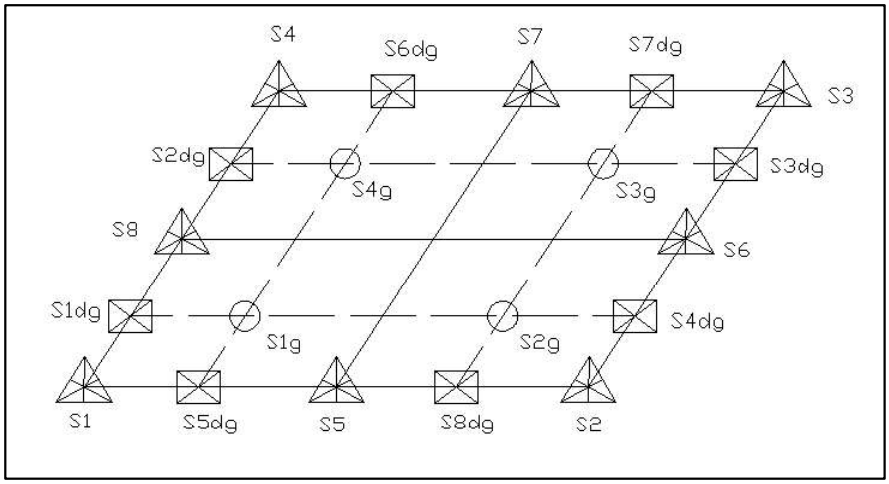

Fig. 3.7 Various stress points in the plate element. S1g to S4g represents $\bar{\sigma}_{1g}$, $\bar{\sigma}_{2g}$, $\bar{\sigma}_{3g}$, $\bar{\sigma}_{4g}$ (stresses at Gauss points), S1dg to S8dg represents $\acute{\sigma}_1$, $\acute{\sigma}_2$, $\acute{\sigma}_3$, $\acute{\sigma}_4$, $\acute{\sigma}_5$, $\acute{\sigma}_6$, $\acute{\sigma}_7$, $\acute{\sigma}_8$ (stresses at point on the edge of the plate, extrapolated from Gauss points) and S1 to S8 represents $\bar{\sigma}_1$, $\bar{\sigma}_2$, $\bar{\sigma}_3$, $\bar{\sigma}_4$, $\bar{\sigma}_5$, $\bar{\sigma}_6$, $\bar{\sigma}_7$, $\bar{\sigma}_8$ (stresses at the nodal points).

$$\acute{\sigma}_1 = \sigma_{1g} + \left(\sigma_{1g} - \sigma_{2g}\right)\left(\frac{\sqrt{3}}{2} - \frac{1}{2}\right) \tag{3.67}$$

$$\acute{\sigma}_2 = \sigma_{4g} + \left(\sigma_{4g} - \sigma_{3g}\right)\left(\frac{\sqrt{3}}{2} - \frac{1}{2}\right) \tag{3.68}$$

In order to get the nodal stress value at node 1 $\bar{\sigma}_1$, linearly extrapolating between edge stresses of $\acute{\sigma}_1$ and $\acute{\sigma}_2$ we can get the following:

$$\bar{\sigma}_1 = \acute{\sigma}_1 + (\acute{\sigma}_1 - \acute{\sigma}_2)\left(\frac{\sqrt{3}}{2} - \frac{1}{2}\right) \tag{3.69}$$

$$=\sigma_{1g} + \left(\sigma_{1g} - \sigma_{2g}\right)\left(\frac{\sqrt{3}}{2} - \frac{1}{2}\right) + \left[\sigma_{1g} + \left(\sigma_{1g} - \sigma_{2g}\right)\left(\frac{\sqrt{3}}{2} - \frac{1}{2}\right) - \sigma_{4g} - \left(\sigma_{4g} - \sigma_{3g}\right)\left(\frac{\sqrt{3}}{2} - \frac{1}{2}\right)\right] \times \left(\frac{\sqrt{3}}{2} - \frac{1}{2}\right)$$

$$= \quad \sigma_{1g}\left(1 + \frac{\sqrt{3}}{2}\right) - \frac{1}{2}\sigma_{2g} + \sigma_{3g}\left(1 - \frac{\sqrt{3}}{2}\right) - \frac{1}{2}\sigma_{4g}$$

Hence,

$$\bar{\sigma}_1 = \sigma_{1g}\left(1 + \frac{\sqrt{3}}{2}\right) - \frac{1}{2}\sigma_{2g} + \sigma_{3g}\left(1 - \frac{\sqrt{3}}{2}\right) - \frac{1}{2}\sigma_{4g} \tag{3.70}$$

Similarly, the stresses at other node points are obtained in the same manner and relation between nodal stress and stress at Gauss points are related in the following matrix.

$$\begin{bmatrix}\sigma_1\\ \sigma_2\\ \sigma_3\\ \sigma_4\\ \sigma_5\\ \sigma_6\\ \sigma_7\\ \sigma_8\end{bmatrix} = \begin{bmatrix}(1+\sqrt{3}/2) & -0.5 & (1-\sqrt{3}/2) & -0.5\\ -0.5 & (1+\sqrt{3}/2) & -0.5 & (1-\sqrt{3}/2)\\ (1-\sqrt{3}/2) & -0.5 & (1+\sqrt{3}/2) & -0.5\\ -0.5 & (1-\sqrt{3}/2) & -0.5 & (1+\sqrt{3}/2)\\ (1+\sqrt{3}/4)(1+\sqrt{3}/4) & (1-\sqrt{3}/4)(1-\sqrt{3}/4) & & \\ (1-\sqrt{3}/4)(1+\sqrt{3}/4) & (1+\sqrt{3}/4)(1-\sqrt{3}/4) & & \\ (1-\sqrt{3}/4)(1-\sqrt{3}/4) & (1+\sqrt{3}/4)(1+\sqrt{3}/4) & & \\ (1+\sqrt{3}/4)(1-\sqrt{3}/4) & (1-\sqrt{3}/4)(1+\sqrt{3}/4) & & \end{bmatrix} \begin{Bmatrix}\sigma_{1g}\\ \sigma_{2g}\\ \sigma_{3g}\\ \sigma_{4g}\end{Bmatrix} \quad (3.71)$$

Here, $\bar{\sigma}_1$, $\bar{\sigma}_2$, $\bar{\sigma}_3$, $\bar{\sigma}_4$, $\bar{\sigma}_5$, $\bar{\sigma}_6$, $\bar{\sigma}_7$, $\bar{\sigma}_8$ are the nodal stresses after application of local smoothing technique. These smoothened stresses are modified or averaged for a particular node, where more than one element is connected to obtain the final stress value.

3.4 Formulation for fluid

3.4.1 Theoretical formulation

Total stress of Newtonian fluid can be expressed as:

$$T_{ij} = -p\delta_{ij} + \mu\left(\frac{\delta u_i}{\delta x_k} + \frac{\delta u_k}{\delta x_i}\right) + \lambda\frac{\delta u_j}{\delta x_i}\delta_{ij} \quad (3.72)$$

T_{ij} represents the total stress, u_i is velocity of fluid, x_i is coordinate and p is hydrostatic pressure. δ_{ij} is the Kronecker delta.

Coefficient of bulk viscosity is given as $\mu_b = \left(\frac{2}{3}\mu + \lambda\right)$ (3.73)

Hence by separating isotropic and deviatoric parts of equation 3.72 can be written as

$$T_{ij} = -p\delta_{ij} + \mu\left(\frac{\delta u_i}{\delta x_k} + \frac{\delta u_k}{\delta x_i} - \frac{2}{3}\frac{\delta u_j}{\delta x_j}\delta_{ij}\right) + \mu_b\frac{\delta u_j}{\delta x_i}\delta_{ij} \quad (3.74)$$

Now neglecting non-linear deviatoric stress parts equation 3.74 can be written as

$$T_{ij} = -p\delta_{ij} + \mu\left(-\frac{2}{3}\frac{\delta u_j}{\delta x_j}\delta_{ij}\right) + \mu_b \frac{\delta u_j}{\delta x_i}\delta_{ij} \quad (3.75)$$

Bulk viscosity for compressible fluid is considered as zero. Hence equation 3.75 is reduced to

$$T_{ij} = -p\delta_{ij} - \mu\left(\frac{2}{3}\frac{\delta u_j}{\delta x_j}\delta_{ij}\right) \quad (3.76)$$

Now, neglecting the viscosity of the fluid for simplicity, the total stress tensor reduces as:

$$T_{ij} = -p\delta_{ij} \quad (3.77)$$

Navier-Stokes equation of motion can be written as :

$$\rho\left(\frac{\partial v_i}{\partial t} + V_j\frac{\partial v_i}{\partial x_j}\right) = \frac{\partial T_{ij}}{\partial x_j} + \rho B_i \quad (3.78)$$

Here ρ is the density of fluid and B_i is the body force. If equation 3.77 is substituted in equation 3.78, we can obtain

$$\rho\left(\frac{\partial v_i}{\partial t} + V_j\frac{\partial v_i}{\partial x_j}\right) = -\frac{\partial p}{\partial x_i} + \rho B_i \quad (3.79)$$

Disregarding the body forces and convective terms in equation 3.79, following equation can be obtained.

$$\frac{1}{\rho}\frac{\partial p}{\partial x} + \frac{\partial u}{\partial t} = 0 \quad (3.80)$$

$$\frac{1}{\rho}\frac{\partial p}{\partial y} + \frac{\partial v}{\partial t} = 0 \quad (3.81)$$

$$\frac{1}{\rho}\frac{\partial p}{\partial z} + \frac{\partial w}{\partial t} = 0 \quad (3.82)$$

Here *u, v* and *w* are the components of velocity of the fluid along the three orthogonal directions. The continuity equation in the three dimensions can be written as

$$\frac{\partial p}{\partial t} + \rho\alpha^2\left(\frac{\partial u}{\partial x} + \frac{\partial v}{\partial y} + \frac{\partial w}{\partial z}\right) = 0 \tag{3.83}$$

$\boldsymbol{\alpha}$ is the acoustic velocity of the wave in the fluid domain.

Differentiating equations 3.80 to 3.82, with respect to *x, y* and *z* respectively, the following equations can be obtained.

$$\frac{1}{\rho}\frac{\partial^2 p}{\partial x^2} + \frac{\partial}{\partial x}\left(\frac{\partial u}{\partial t}\right) = 0 \tag{3.84}$$

$$\frac{1}{\rho}\frac{\partial^2 p}{\partial y^2} + \frac{\partial}{\partial x}\left(\frac{\partial v}{\partial t}\right) = 0 \tag{3.85}$$

$$\frac{1}{\rho}\frac{\partial^2 p}{\partial z^2} + \frac{\partial}{\partial x}\left(\frac{\partial w}{\partial t}\right) = 0 \tag{3.86}$$

Adding equations 3.84 to 3.86, we obtain

$$\frac{1}{\rho}\frac{\partial^2 p}{\partial x^2} + \frac{1}{\rho}\frac{\partial^2 p}{\partial y^2} + \frac{1}{\rho}\frac{\partial^2 p}{\partial z^2} + \frac{\partial}{\partial x}\left(\frac{\partial u}{\partial t}\right) + \frac{\partial}{\partial x}\left(\frac{\partial v}{\partial t}\right) + \frac{\partial}{\partial x}\left(\frac{\partial w}{\partial t}\right) = 0 \tag{3.87}$$

Now differentiating the terms in equation 3.83, with respect to time, *t*, the following equation can be obtained.

$$\frac{\partial^2 p}{\partial t^2} + \rho\alpha^2\left\{\frac{\partial}{\partial x}\left(\frac{\partial u}{\partial t}\right) + \frac{\partial}{\partial y}\left(\frac{\partial v}{\partial t}\right) + \frac{\partial}{\partial z}\left(\frac{\partial w}{\partial t}\right)\right\} = 0 \tag{3.88}$$

which can further be written as

$$\left\{\frac{\partial}{\partial x}\left(\frac{\partial u}{\partial t}\right) + \frac{\partial}{\partial y}\left(\frac{\partial v}{\partial t}\right) + \frac{\partial}{\partial z}\left(\frac{\partial w}{\partial t}\right)\right\} = -\frac{1}{\rho\alpha^2}\left(\frac{\partial^2 p}{\partial t^2}\right) \tag{3.89}$$

Now using the expression of equation 3.89 in equation 3.87, we can obtain the following

$$\frac{1}{\rho}\frac{\partial^2 p}{\partial x^2} + \frac{1}{\rho}\frac{\partial^2 p}{\partial y^2} + \frac{1}{\rho}\frac{\partial^2 p}{\partial z^2} - \frac{1}{\rho\alpha^2}\left(\frac{\partial^2 p}{\partial t^2}\right) = 0 \tag{3.90}$$

Simplifying equation 3.90 the equation for compressible fluid in three dimensions can be obtained as

$$\nabla^2 p(x,y,z,t) = \frac{1}{\alpha^2}\ddot{p}(x,y,z,t) \qquad (3.91)$$

This equation is known as Helmholtz's equation for compressible liquid. Here ∇^2 is a three-dimensional Laplacian operator since we have considered a three-dimensional fluid-structure coupled system for our analysis as shown in figure 3.8. Fluid is assumed as compressible and non-viscous. The fluid domain has been discretized by three-dimensional twenty node brick elements.

Hydrodynamic pressure at any point within the liquid can be obtained by applying boundary conditions to equation 3.91.

The six surfaces of the liquid are marked surface I to VI as shown in Fig. 3.9.

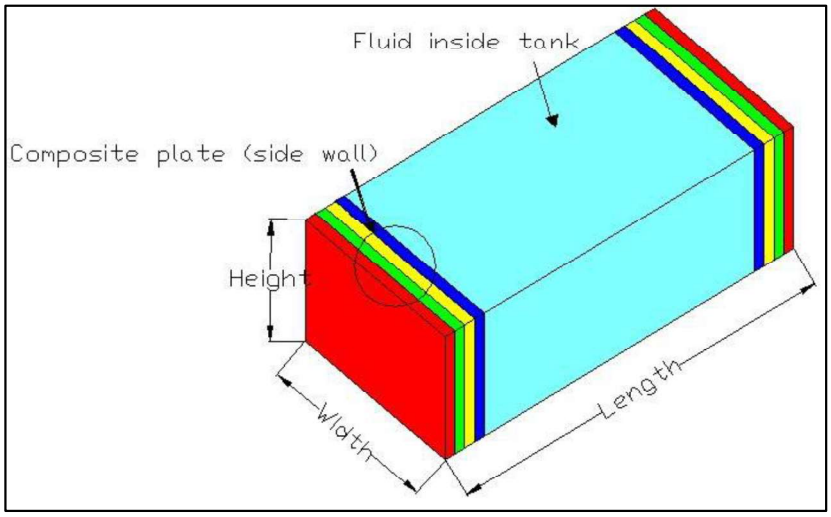

Fig. 3.8 Geometry of fluid-structure coupled system

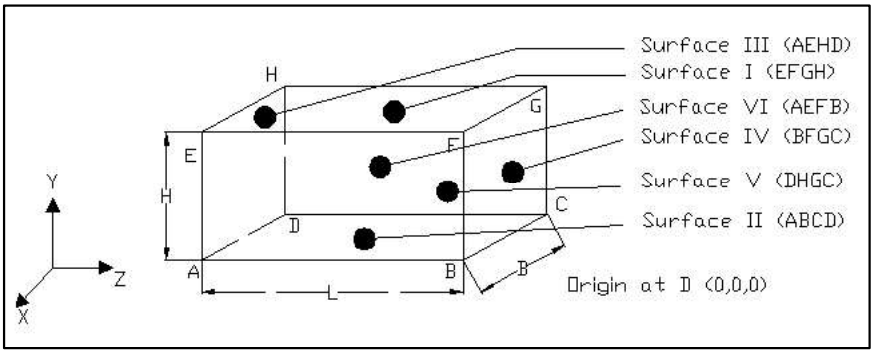

Fig. 3.9 Nomenclature of various surface conditions of the 3D fluid element

Various boundary conditions considered for different surface conditions are as mentioned below:

1) At surface I (EFGH)

Boundary condition at the top surface of the liquid considered as

$$\frac{1}{g}\ddot{P}(x,H,z,t)+\frac{\partial P(x,H,z,t)}{\partial y}=0 \quad (3.92)$$

2) At surface II (ABCD)

Pressure gradient along this surface should be considered as zero. Hence applied boundary condition will be

$$\frac{\partial P}{\partial y}(x,0,z,t)=0.0 \quad (3.93)$$

3) At surface III (AEHD)

At liquid-wall interface at the left face, the pressure gradient should satisfy

$$\frac{\partial P(x,y,0,t)}{\partial z}=\rho_f a' \quad (3.94)$$

Where, ρ_f and a' are fluid density and horizontal ground acceleration respectively.

Various boundary conditions considered for different surface conditions are as mentioned below:

4) At surface IV (BFGC)

At liquid-wall interface at the right face, the pressure gradient should satisfy

$$\frac{\partial P(x,y,L,t)}{\partial z}=\rho_f a' \quad (3.95)$$

5) At surface V (DHGC)

Pressure gradient along this surface should be considered as zero.

$$\frac{\partial P}{\partial x}(0, y, z, t) = 0.0 \tag{3.96}$$

6) At surface VI (AEFB)

Pressure gradient along this surface should also be considered as zero.

$$\frac{\partial P}{\partial x}(B, y, z, t) = 0.0 \tag{3.97}$$

3.4.2 Finite element formulation

Eq. (3.91) may be expressed in discretized form as eq. (3.98) using Galerkin approach. The only nodal variable considered in the expression is pressure

$$\int_{\Omega} N_r[\nabla^2 \sum P_i - \frac{1}{\alpha^2}\sum \ddot{P}_i]d\Omega = 0 \tag{3.98}$$

Where, N_r is the shape function for the reservoir domain, Ω.

Appling Green's theorem eq. (3.98) may be reduced to

$$-\int_{\Omega} \left(\frac{\delta N_r}{\delta x}\frac{\delta P}{\delta x} + \frac{\delta N_r}{\delta y}\frac{\delta P}{\delta y} + \frac{\delta N_r}{\delta z}\frac{\delta P}{\delta z}\right) d\Omega + \int_{\Gamma} N_r \left(\frac{\delta P}{\delta x} + \frac{\delta P}{\delta y} + \frac{\delta P}{\delta z}\right) d\Gamma - \frac{1}{\alpha^2}\int_{\Omega} \left(N_r \frac{\delta^2 P}{\delta t^2}\right) d\Omega = 0 \tag{3.99}$$

First part of the equation 3.99 can be expressed as

$$\int_{\Omega} \left(\frac{\delta N_r}{\delta x}\frac{\delta P}{\delta x} + \frac{\delta N_r}{\delta y}\frac{\delta P}{\delta y} + \frac{\delta N_r}{\delta z}\frac{\delta P}{\delta z}\right) d\Omega = \int_{\Omega} \begin{bmatrix} \frac{\delta N_r}{\delta x} & \frac{\delta N_r}{\delta y} & \frac{\delta N_r}{\delta z} \end{bmatrix} \begin{bmatrix} \frac{\delta N_r}{\delta x} \\ \frac{\delta N_r}{\delta y} \\ \frac{\delta N_r}{\delta z} \end{bmatrix} p d\Omega = \int_{\Omega} B^T B p d\Omega$$

Surface and boundary of the fluid domain is represented by Ω and Γ respectively and n is normal to the boundary surface. The second term of eq. (3.99) may be expressed as

$$\bar{F} = \int_{\Gamma} N_r \frac{\partial P}{\partial n} d\Gamma = \int_{\Gamma} N_r^T N_r \frac{\partial p}{\partial n} d\Gamma \tag{3.100}$$

In matrix form the eq. (3.99) may be written as

$$\left(\overline{E}\right)\ddot{P} + (\bar{G})P = \overline{F} \tag{3.101}$$

In which,

$$\overline{E} = \frac{1}{\alpha^2}\sum \int_{\Omega} N_r^T N_r d\Omega \tag{3.102}$$

$$\bar{G} = \int_{\Omega} B^T B d\Omega \tag{3.103}$$

$$\bar{F} = \sum \int_{\Gamma} N_r^T \frac{\partial P}{\partial n} d\Gamma = \bar{F}_I + \bar{F}_{II} + \bar{F}_{III} + \bar{F}_{IV} + \bar{F}_V + \bar{F}_{VI} \tag{3.104}$$

Here, *I*, *II*, *III, IV, V and VI* represent different surface boundary as shown in Fig. 3.7.

To account for sloshing effect of the free surface, equation 3.92 can be expressed as

$$\bar{F}_I = -\frac{1}{g} S_I \ddot{\bar{P}} \tag{3.105}$$

Where,

$$S_I = \sum \int_{\Gamma} N_r^T N_r d\Gamma \tag{3.106}$$

At tank bottom surface, *II*

$$\bar{F}_{II} = 0$$

At tank-fluid interfaces i.e. at surface III and surface IV, $\{ a' \}$ is the nodal acceleration vector in generalized coordinates, and expressed as

$$\bar{F}_{III} = -\rho_f S_{III} a \tag{3.107}$$

$$\bar{F}_{IV} = -\rho_f S_{IV} a \tag{3.108}$$

In which,

$$S_{III} = \sum \int_{\Gamma} N_r^T N_r d\Gamma \quad (3.109)$$

$$S_{IV} = \sum \int_{\Gamma} N_r^T N_r d\Gamma \quad (3.110)$$

At back and front surface of the tank, surface V and VI

$$\bar{F}_V = 0 \text{ and } \bar{F}_{VI} = 0 \quad (3.111)$$

After imposing all boundary condition, equation (3.101) becomes

$$(E)\ddot{P} + (G)P = F \quad (3.112)$$

$$E = \bar{E} + \frac{1}{g} S_I \quad (3.113)$$

$$F = -\rho_f S_{III} a - \rho_f S_{IV} a \quad (3.114)$$

$$G = \bar{G}$$

Hydrodynamic pressure is obtained after solving eq. (3.112) for given acceleration at the tank-fluid interface.

3.5 Formulation of direct coupling between fluid and structure

Structure and fluid in fluid-structure interaction problem does not vibrate as individual entity, rather they act together in a coupled way. Hence such problem must be solved in a coupled way. Direct coupling method is most effective, hence the same is employed to formulate the interaction problem under external excitation. The finite element equation for the structural part, left wall (l) and right wall (r) are written as

$$[M_l]\{\ddot{u}_l\} + [K_l]\{u_l\} - [Q_l]\{p\} - \{F_{dl}\} = 0 \quad (3.115)$$

$$[M_r]\{\ddot{u}_r\} + [K_r]\{u_r\} - [Q_r]\{p\} - \{F_{dr}\} = 0 \quad (3.116)$$

The term $[Q]$ arises to satisfy the compatibility condition at the tank-wall interface as mentioned by Zienkiewicz and Newton (1969). Extra amount of force developed due to hydrodynamic

pressure is taken care by the term $[Q]\{p\}$ within the water near the tank wall. Similarly $[Q]\{\ddot{u}\}$ is the other term that takes care the additional pressure due to acceleration of the flexible walls in the present study.

$$\int_{\Gamma_s} N_S^T n p d\Gamma = \left(\int_{\Gamma_s} N_S^T n N_f d\Gamma\right) p = [Q]\{p\} \tag{3.117}$$

N_s is the interpolation function of the structure and N_f is the interpolation function of the fluid respectively and n is direction vector normal with the surface of the tank.

The coupled equation for fluid and elastic structure in finite element can be written as

$$[E]\{\ddot{P}\} + [G]\{P\} + [Q_l^T]\{\ddot{u}_l\} + [Q_r^T]\{\ddot{u}_r\} = \{F_l\} \tag{3.118}$$

Now equations 3.115, 3.116 and 3.118 are coupled in a second order differential equation to express the complete coupled fluid-structure problem. Damping of the system is neglected. The equations can be written in matrix form as

$$\begin{bmatrix} M_l & 0 & 0 \\ Q_l^T & E & Q_r^T \\ 0 & 0 & M_r \end{bmatrix} \begin{Bmatrix} \ddot{u}_l \\ \ddot{p} \\ \ddot{u}_r \end{Bmatrix} + \begin{bmatrix} K_l & -Q_l & 0 \\ 0 & G & 0 \\ 0 & -Q_r & K_r \end{bmatrix} \begin{Bmatrix} u_l \\ p \\ u_r \end{Bmatrix} = \begin{Bmatrix} F_{dl} \\ F_l \\ F_{dr} \end{Bmatrix} \tag{3.119}$$

Equation 3.119 is solved to obtain the coupled response of the tank.

CHAPTER 4

RESULTS AND DISCUSSIONS

4.1 GENERAL

A computer code is prepared in the MATLAB environment to model a composite plate in 2D and fluid in 3D in the present formulation. The solid and fluid parts are modeled separately and then their interaction effects are simulated numerically. Present algorithm can be used to evaluate the dynamic response of the coupled fluid-structure system under various boundary conditions against different excitations. Nodal displacement and various stress parameters within the composite plate can be estimated using the code. The stress contour at various ply levels in the composite plate can also be obtained using Origin-Pro software. The study is divided into mainly three parts. Initially the plate is modelled using isoparametric element and validated with the existing literature. The fluid is then modelled as 3-D brick element and again it is validated with the literature. Finally, the plate and fluid is coupled in a direct way and in depth study is carried out on composite plate considering composite-fluid interaction.

4.2 ANALYSIS OF COMPOSITE PLATES WITHOUT INTERACTING WITH FLUID

Composite plate is modelled in 2D framework using MATLAB coding. Graphite-epoxy is used as the composite material with material properties E_1/E_2=25, G_{12}/E_2=0.5, G_{13}/E_2= 0.5, G_{23}/E_2=0.2, and Poisson's ration v_{12}=0.25, ρ=1. In this section, the convergence study for suitable mesh size is carried out. Convergence study for the time step in dynamic analysis is also carried out. The plate response under static as well as dynamic loading is determined and compare with the result published in existing literatures to validate the present algorithm. The composite plate is then studied for fundamental frequency under various parametric variations. Finally, the dynamic analysis of coupled composite-fluid coupled system is carried out to study the effect of coupling between composite plate and fluid under sinusoidal excitation with different frequencies and earthquake excitations.

4.2.1 Convergence study of mesh size

Dimensionless fundamental frequency, $\lambda = \omega a^2\left(\frac{\rho}{E_2 h^2}\right)^{\frac{1}{2}}$ of a square simply supported angle-ply (*30°/-30°/30°/-30°*) laminated plate with *a/h* =10 is considered. To optimize the mesh size, it is varied from 2×2 to 10×10 and corresponding fundamental frequency values are plotted. Effect of mesh size presented along with the already published results in Fig. 4.1 .From this figure, it can be concluded that magnitude of the fundamental frequency jumps from meshing 2×2 to 4×4. However, the same increment almost ceases for mesh size increment from 4×4 to higher meshes. As the mesh size increases beyond 4×4, results converge more accurately, but at the same time the computation time also increases significantly and the percentage of errors induced in the final results due to mesh optimisation is almost 0.23. Hence to optimize the results between accuracy and consumption of time, 4×4 mesh size found to be most effective and used in the further study, unless otherwise mentioned.

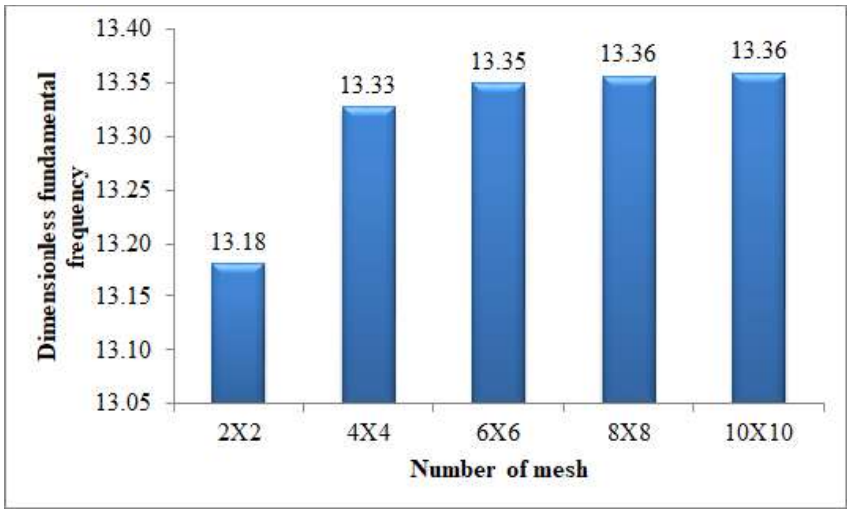

Fig. 4.1 Variation of fundamental frequencies with increment of meshes for anti-symmetric *30°* lamination

4.2.2 Convergence study of time step

Newmark's average integration technique is unconditional stable; still the responses of composite plate are quite sensitive to the time step. In order to obtain a suitable time step, a 2-

layer composite plate with ply angle *45˚/-45˚* is considered. The geometry of the plate is considered as *a/b*=1.5, *a/h*=10. The elastic properties of the plate are same as section 4.1. The time histories of the central transverse deflection due to a sinusoidal acceleration of frequency 20% of fundamental frequency of this plate for various time steps are presented in Fig. 4.2 (a). It can be seen from the figure that the central displacement is converged at a time step of 200. If the percentage of errors induced in the final results due to time step convergence is obtained in terms of percentage, then the value comes as 0.03% as shown in Fig. 4.2 (b) which can be neglected. Thus, the step size (Δt) for the time history analysis is adopted as *T/200;* where *T* is the fundamental time period for all the cases unless it is mentioned.

Cumulatively if maximum error inclusion percentage is calculated from mesh size and time step optimization, then the value results to be 0.53% which is very nominal if compared to computation time and hence such error is neglected.

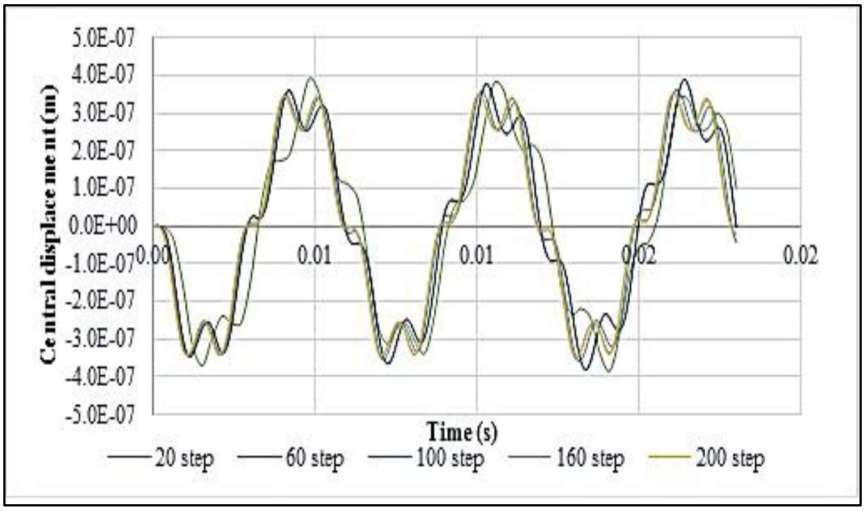

(a)

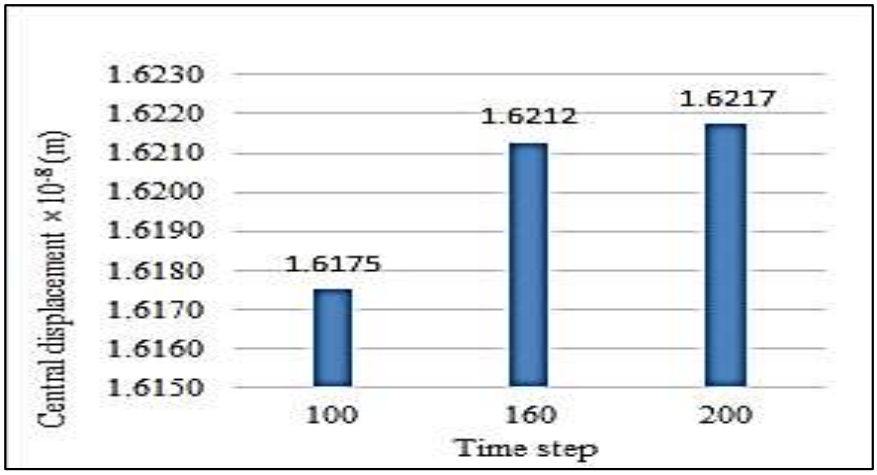

(b)

Fig. 4.2 a) Variation of central deflection b) Percentage of error for different time step against sinusoidal excitation

4.2.3 Validation of the proposed algorithm

The MATLAB code proposed in the present study is validated by comparing the fundamental frequency of a square composite plate obtained from the present study and the results presented by Chattopadhyay et al. (1992) in this section. The material properties which were used in the reference study are also used in the present case. The comparison is presented in Table 4.1 and found to have more than 90% accuracy ('+' means results are on the higher side) value for all the results.

Table 4.1 Dimensionless fundamental frequency $\lambda=\omega a^2(\rho/E_2h^2)^{1/2}$ for square simply supported laminated plates. Anti-symmetric angle-ply ($30°$) laminations with a/h =10.

Number of layers	Reddy (1979)	Chattopadhyay et al. (1992)	Present	Accuracy in result compared with Reddy (1979)
2	15.00	14.59	15.84	94.40 (+)
4	17.69	17.61	19.10	92.03 (+)
6	18.00	17.94	19.67	90.72 (+)
8	18.10	18.04	19.56	91.93 (+)

Same code is further developed for transient response. Here, *0°/90°* laminated plate is studied under uniformly distributed load and the time history plot is compared with that of Reddy (2004) and presented in Fig. 4.3.

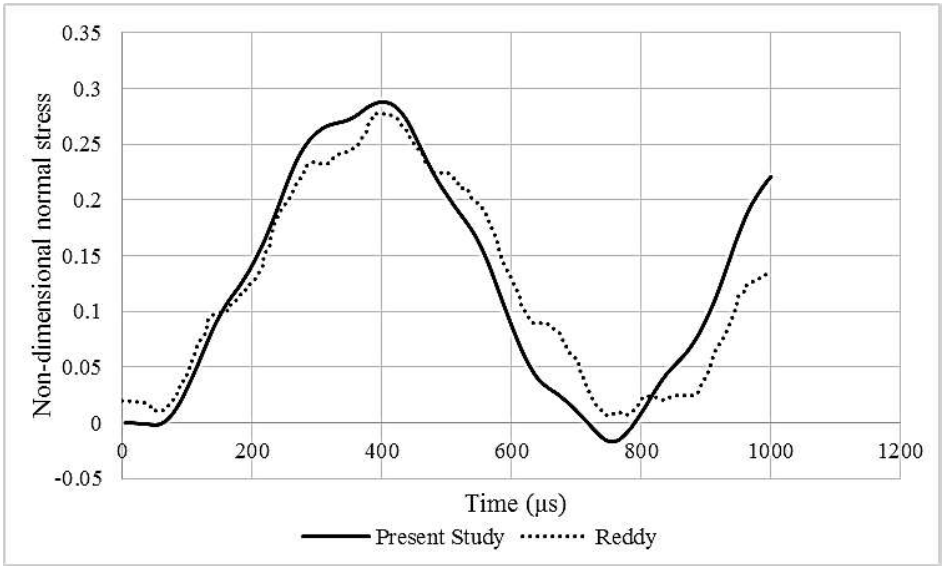

Fig. 4.3 Comparison of normal stress at different time

4.2.4 Effect of Various Parameters on Fundamental Frequency

A composite plate square in dimension is analyzed using finite element method in this section. A 4×4 meshing is considered in all the cases. Plan to thickness ratio is considered as *a/h=10*. Material property used in the present case is maintained unchanged as mentioned in section 4.1. Ply layers are increased in subsequent Tables 4.2-4.5 and corresponding frequencies are reported.

Table 4.2 Dimensionless fundamental frequency, $\lambda = \omega a^2(\rho/E_2h^2)^{1/2}$ for imply supported laminated plates square in plan.

Lamination type	Lamination angle	Fundamental frequency
Cross-ply	0°/90°	15.36
Angle-ply	15°/-15°	14.85
	30°/-30°	15.84
	45°/-45°	16.59

	60°/-60°	15.84
	75°/-75°	14.85

Table 4.3 Dimensionless fundamental frequency, $\lambda = \omega a^2(\rho/E_2h^2)^{1/2}$ for square simply supported laminated plates.

Lamination type	Lamination angle	Fundamental frequency
Cross-ply	0°/90°/0°/90°	15.36
Angle-ply	15°/-15°/15°/-15°	16.72
	30°/-30°/30°/-30°	19.10
	45°/-45°/45°/-45°	20.09
	60°/-60°/60°/-60°	19.10
	75°/-75°/75°/-75°	16.72

Table 4.4 Dimensionless fundamental frequency, $\lambda = \omega a^2(\rho/E_2h^2)^{1/2}$ for square simply supported laminated plates.

Lamination type	Lamination angle	Fundamental frequency
Cross-ply	0°/90°/0°/90°/0°/90°	15.53
Angle-ply	15°/-15°/15°/-15°/15°/-15°	17.15
	30°/-30°/30°/-30°/30°/-30°	19.67
	45°/-45°/45°/-45°/45°/-45°	20.66
	60°/-60°/60°/-60°/60°/-60°	19.67
	75°/-75°/75°/-75°/75°/-75°	17.15

Table 4.5 Dimensionless fundamental frequency, $\lambda = \omega a^2(\rho/E_2h^2)^{1/2}$ for square simply supported laminated plates.

Lamination type	Lamination angle	Fundamental frequency
Cross-ply	0˚/90˚/0˚/90˚/0˚/90˚/0˚/90˚	15.36
Angle-ply	15˚/-15˚/15˚/-15˚/15˚/-15˚/15˚/-15˚	17.03
	30˚/-30˚/30˚/-30˚/30˚/-30˚/30˚/-30˚	19.56
	45˚/-45˚/45˚/-45˚/45˚/-45˚/45˚/-45˚	20.55
	60˚/-60˚/60˚/-60˚/60˚/-60˚/60˚/-60˚	19.56
	75˚/-75˚/75˚/-75˚/75˚/-75˚/75˚/-75˚	17.03

An important observation is that about the 45˚ angle the frequency values are symmetric. 45˚ lamina sequence show highest frequency among all the lamination angles, which is more than cross-ply laminations. It is mentioned in Table 4.3-4.5 that, number of ply layers are increased as 4,6 and 8 respectively. Same trend is maintained for increment of layers with 45˚ angle having highest value. 45˚ lamination can handle shear and bending effectively than any other lamination, which is the reason for obtaining the highest frequency for 45˚ lamination. As the number of ply layer is increased, the frequency values also increase and the increment is about 24% for the eight-layer if compared with the two-layer.

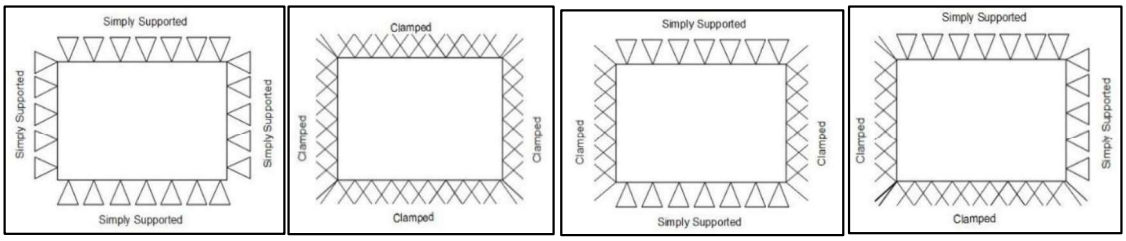

(a) (b) (c) (d)

Fig. 4.4 Different boundary conditions (a) all four edges simply supported (SSSS) (b) all four edges clamped (CCCC) (c) Two opposite edges clamped and simply supported (CSCS) and (d) two adjacent edges simply supported and other adjacent edges clamped (CCSS).

4.2.5 Transient Response of Laminated composite plate

In this section, the central deflection and normal and shear stresses of composite plates are obtained. The geometric and elastic properties of the plate are as follows: a=1.5m, b=1.0m and h = 0.15m (unless otherwise specified), E_1=5.25×10^{11} N/m^2, E_2=2.1×10^{10} N/m^2, G_{12}=1.05×10^{10} N/m^2, G_{23}=4.2×10^9 N/m^2, v_{12}=0.25, ρ=800 kg/m^3. The plates are subjected to sinusoidal acceleration of three different frequencies such as 0.1, 1.0 and 3.0 times fundamental frequency of the composite plate with the amplitude of *1.0g*. In all, the time history response figures presented here have displacement/stress along Y axis and number of cycles of loading along X axis unless specifically mentioned.

4.2.5.1: Problem 1: In this section, the central transverse deflection of the laminated composite plate is studied. The plate is simply supported in all four edges and *a/b* and *a/h* are assumed to be 1.5 and 10 respectively.

The central transverse deflection of the plate is plotted against ratio of time step with forcing frequency 10% of natural frequency of the plate. The variation of displacement for a two layered plate is shown in Fig. 4.5. Fig. 4.5 shows that *45°* symmetric lamination shows highest displacement and anti-symmetric cross or angle ply lamination show least displacement. Further the number of layers for the anti-symmetric *45°* lamination is increased from 2, 4 and 6 keeping the total thickness same, to study its effect. It is found from Fig. 4.6 that with increment of layers from 2 to 4, displacement is greatly reduced however, with increment of layers from 4 to 6, increment of displacement is almost negligible.

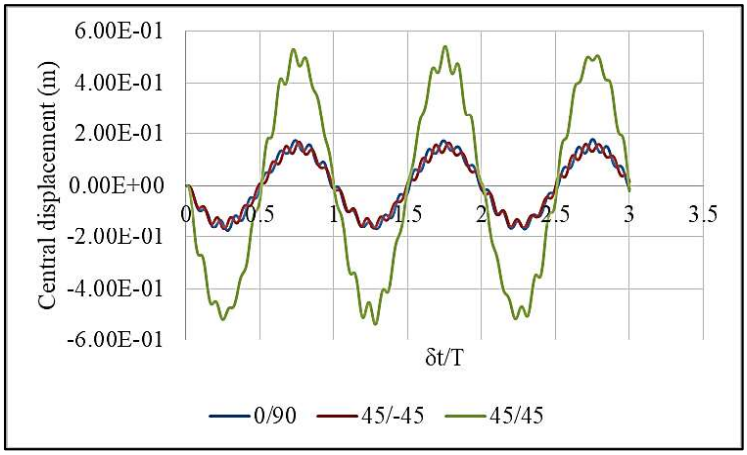

Fig. 4.5 Central displacement of the plate due to sinusoidal acceleration for cross ply and angle ply lamination

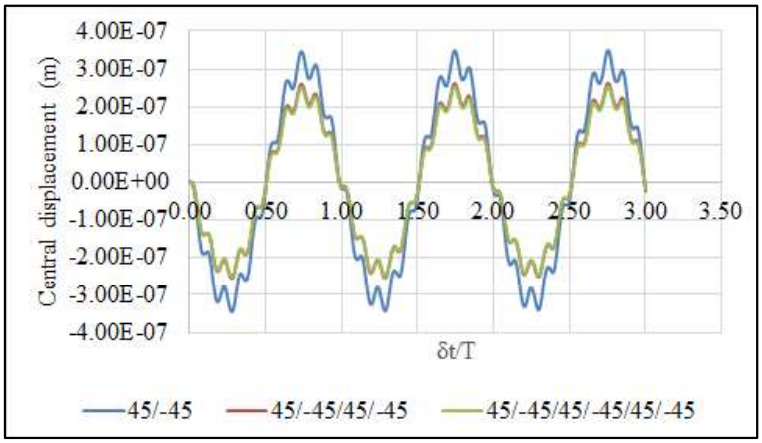

Fig. 4.6 Central transverse deflection of anti-symmetric 45° lamination with increasing ply layers

As the next step, the loading on the plate is varied and corresponding response is presented. The plate is loaded with sinusoidal acceleration with forcing frequency as fundamental frequency and 3 times of fundamental frequency and the corresponding responses are presented in Fig. 4.7.a and 4.7.b respectively. Resonance response can be observed in case of natural frequency in Fig. 4.7.a. and 0° lamination for both the excitation frequencies shows maximum displacement response.

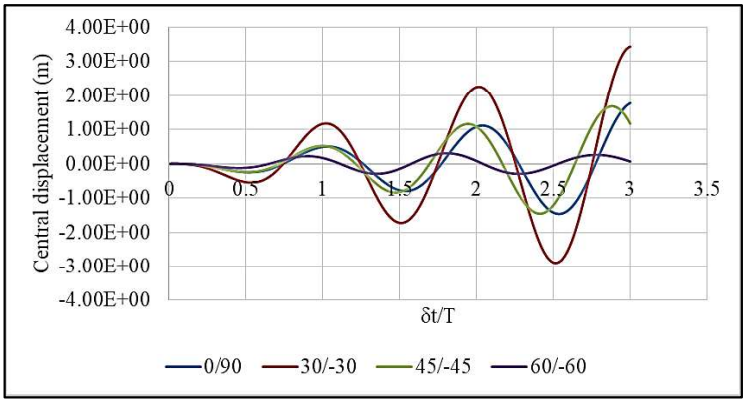

(a)

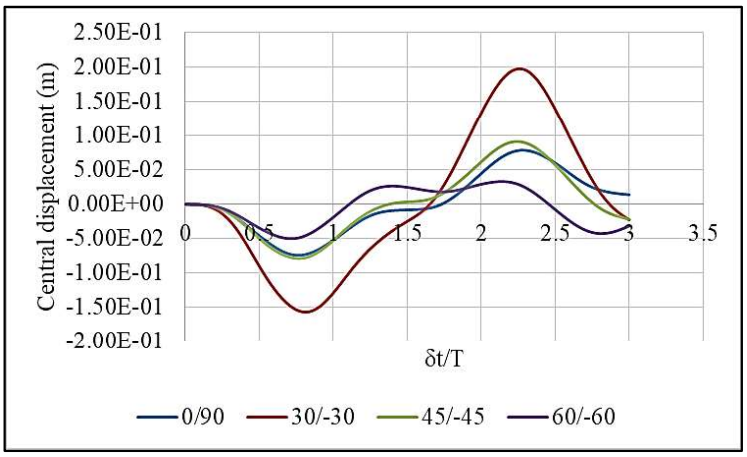

(b)

Fig. 4.7 Central displacement of the plate due to sinusoidal acceleration having forcing frequency (a) Same as natural frequency of plate (b) 3 times natural frequency of the plate

4.2.5.2: Problem 2: Transient response of the central transverse deflection of composite plate with varying geometry and boundary conditions are presented in this section. To study the effect of geometry on central deflection, the value of '*a*' is always kept fixed as 1.5m and *a/b* or *a/h* ratio is modified accordingly. Elastic properties remained same.

The variation of *a/b* ratio (0.75, 1.0 and 1.5) is presented for CSCS boundary condition in Fig. 4.8. For CSCS type boundary condition and *0°/90°* lamination, for a/b = 0.75, simply supported direction is longer in length showing higher deflection. As 0° and 90° both plies are oriented along both direction in equal quantity so fibre has no influence on deflection here. On the other hand for a/b 1.5 simply supported direction has shorter length hence it shows lesser deflection. Finally a/b

=1 being in between showing deflection value in between the rest. The deflection can be controlled by providing more fibres along clamped direction for a/b = 0.75.

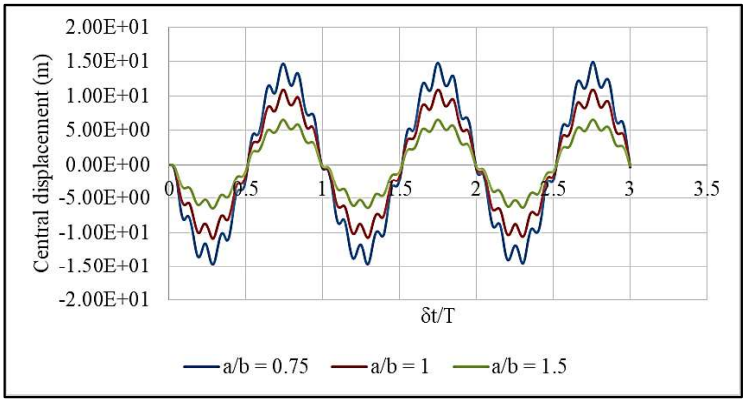

Fig. 4.8 Central displacement of plate (CSCS) due to sinusoidal acceleration with varying *a/b* ratio for *0°/90°* lamination

As the next step, the thickness of the plate is varied and the response under same loading is reported in Table 4.6. As the *a/h* ratio increases from 50 to 100, for a 2 layered (*45°/45°*) composite, the displacement increases drastically.

Table 4.6. Variation of central displacement with varying total thickness of the plate

Displacement in m (×10^-4)		
δt/T	**a/h=50**	**a/h=100**
0.25	-0.3294	-1.2101
0.50	-0.0301	-0.1091
0.75	0.3720	1.3655
1.00	-0.0154	-0.0581
1.25	-0.3150	-1.1595
1.50	-0.0433	-0.1633
1.75	0.3823	1.3988
2.00	-0.0258	-0.0995
2.25	-0.3096	-1.1396
2.50	-0.0493	-0.1831

2.75	0.3828	1.4084
3.00	-0.0268	-0.0945

The effect of boundary conditions on transverse displacement with forcing frequency same as 10% of natural frequency of a composite plate is studied keeping the geometry constant and presented in Fig. 4.9. The simply supported (SSSS) boundary shows maximum displacement among all as expected, whereas clamped edged plate experiences least transverse deflection.

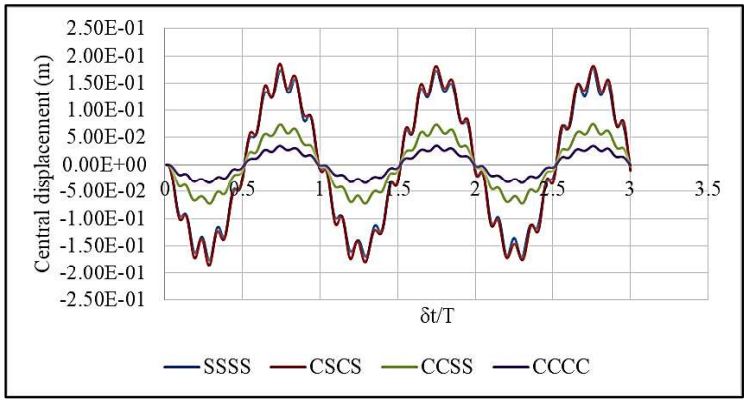

Fig. 4.9 Central displacement of *0˚/90˚* laminated plate with different support conditions

4.2.5.3: Problem 3: The normal stress developed at the central node and top most layer of a simply supported plate is studied in this problem. Two layered cross/angle-ply lamination with symmetric/anti-symmetric ply orientation is considered. Material, geometric property as well as loadings are kept same.

Normal stress along X axis (in N/m^2) is plotted in Fig. 4.10 of a composite plate having *a/b*=1.5 and *a/h*=10. In case of 0/90 lamination cross ply layers are present at both the orthogonal directions, which can manage the normal stress efficiently. Hence the developed stress is minimum. On the other hand, 45 angle ply lamination only has component along the X direction. Hence they develop higher stress values. Again symmetric lamination does not have any bending-stretching coupling between layers, so they contribute lesser stress value. But anti-symmetric lamination having bending-stretching coupling effect shown highest stress values.

To study the effect of increase in ply-layers on stress value, anti-symmetric 45° lamination is considered and the number of layers is increased in pairs from 2 to 4 to 6. It is noted that the stress value decreases drastically with increase in layers from 2 to 4, but the decrement is almost negligible when the ply layers are further increased.

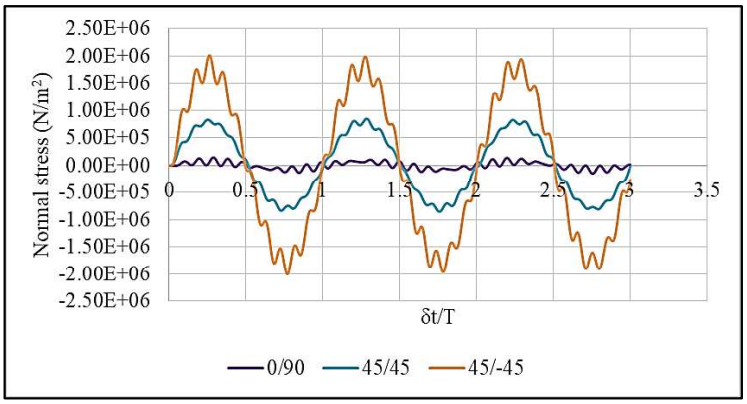

(a)

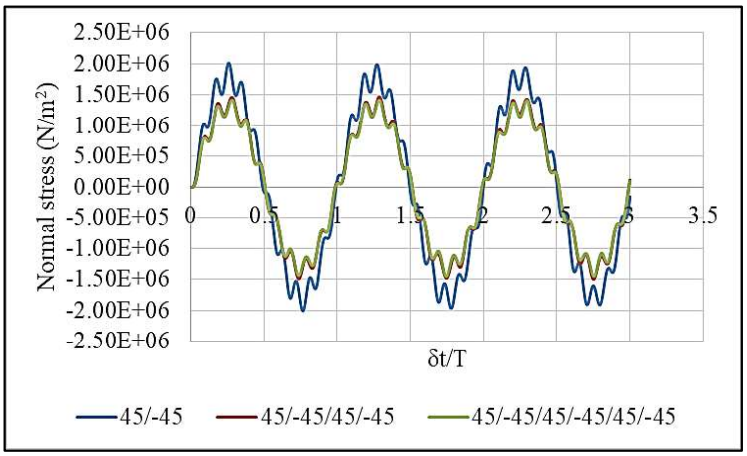

(b)

Fig. 4.10 Normal stress developed at the central node and at top-most layer
(a) Cross and angle ply laminations (b) Anti-symmetric lamination with increased layers

4.2.6 Contour plot for normal stress, inplane shear stress and transverse shear stress

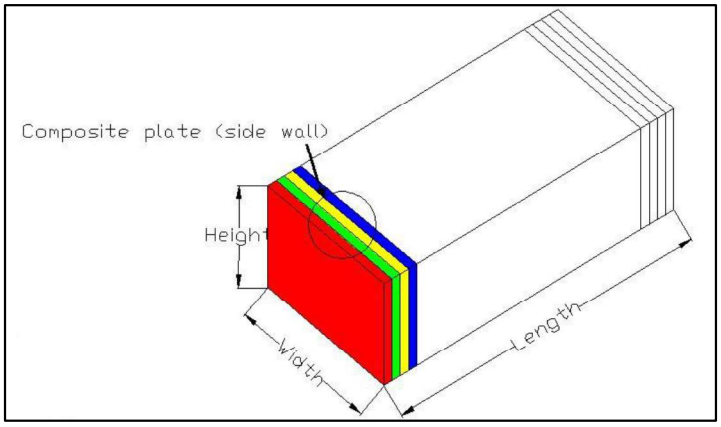

Fig. 4.11.a Side wall of water tank layer sequence of composite plate

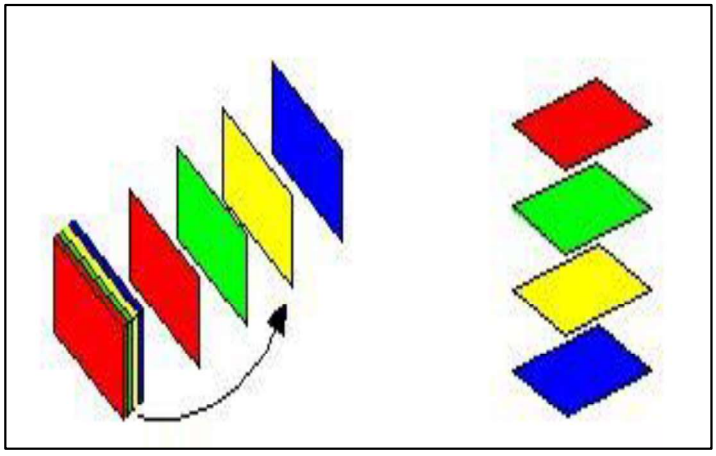

Fig. 4.11.b Side wall of water tank layer sequence with comparison to the stress contour

4.2.6.1: Problem 1: Variation of stresses across different layers in a plate with constant thickness is studied in this problem for a simply supported plate. Three stresses such as normal stress along X axis, inplane shear stress and transverse shear stress are considered for present study. Corresponding stresses are obtained at 0.75μs, 0.25μs and 0.75μs respectively.

Fig. 4.12 shows the variation of normal stresses along X axis at different layers in a laminate of varying ply angles. Among different lamination schemes the cross-ply laminations, always show

higher stress values compared to angle-ply laminations. In case of cross-ply laminations, plies oriented along 0°(along the X axis) always carry highest stress value, whereas the 90° ply angle show very negligible amount of normal stress. It can also be observed that the position of the ply layer in the pack is also important. The stress in central lamina for a 0° lamination is always lower compared to outer layers. For the four layered 0° lamination all the plies are oriented along the X axis and hence it is capable of carrying the stress along that direction most efficiently. If the symmetric and anti-symmetric laminations are compared (Fig. 4.12.b and Fig. 4.12.c), maximum and minimum stress developed for the $0^{\circ}/90^{\circ}/0^{\circ}/90^{\circ}$ orientation is around 26,000 N/m^2 and 5800 N/m^2 respectively, but this range is narrower in case of symmetric lamination ($0^{\circ}/90^{\circ}/90^{\circ}/0^{\circ}$). Moreover, the stress along different layers are evenly distributed for symmetric lamination but for anti-symmetric lamination stresses are concentrated at certain layers.

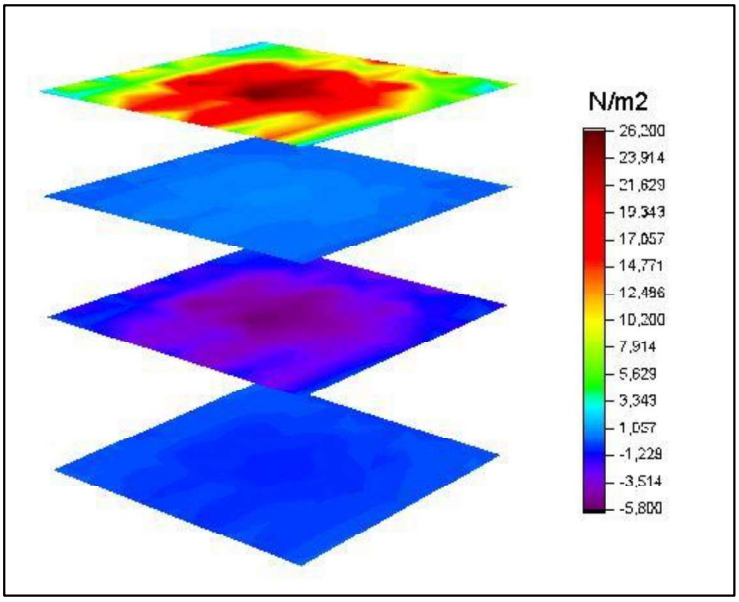

(a)

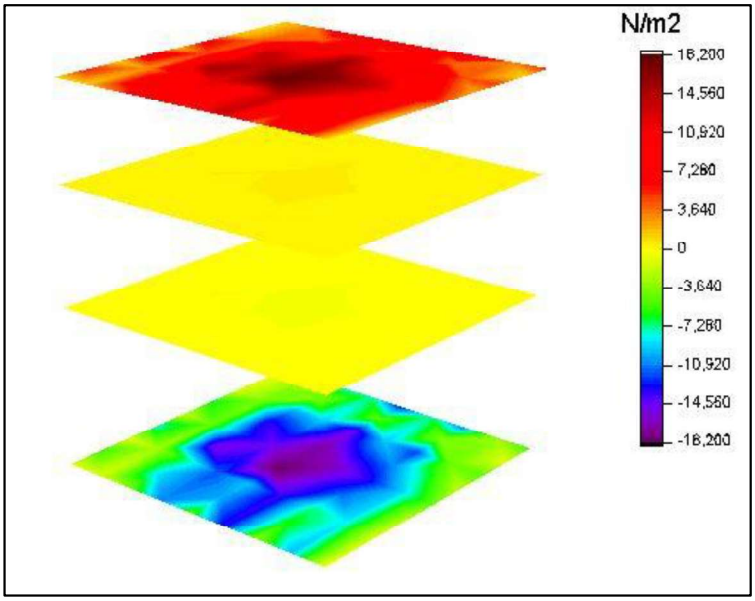
N/m2
18,200
14,560
10,920
7,280
3,640
0
-3,640
-7,280
-10,920
-14,560
-18,200

(b)

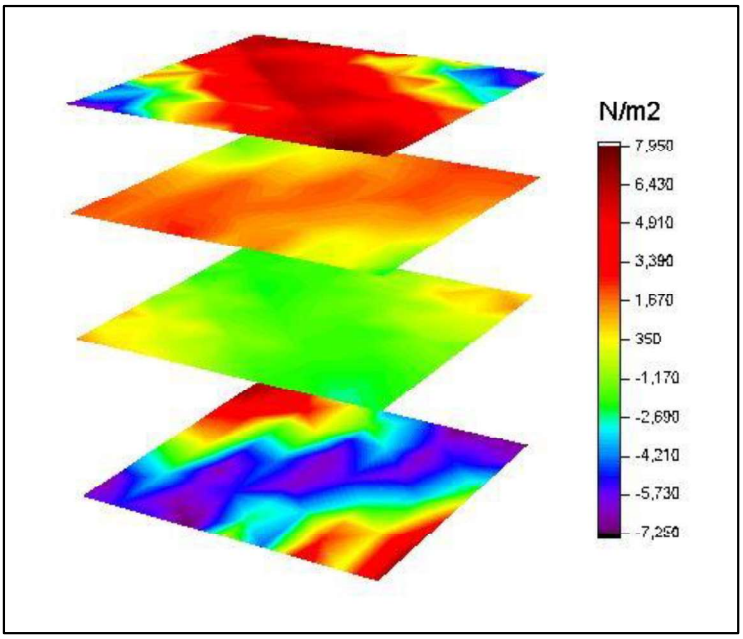
N/m2
7,950
6,430
4,910
3,390
1,870
350
-1,170
-2,690
-4,210
-5,730
-7,250

(c)

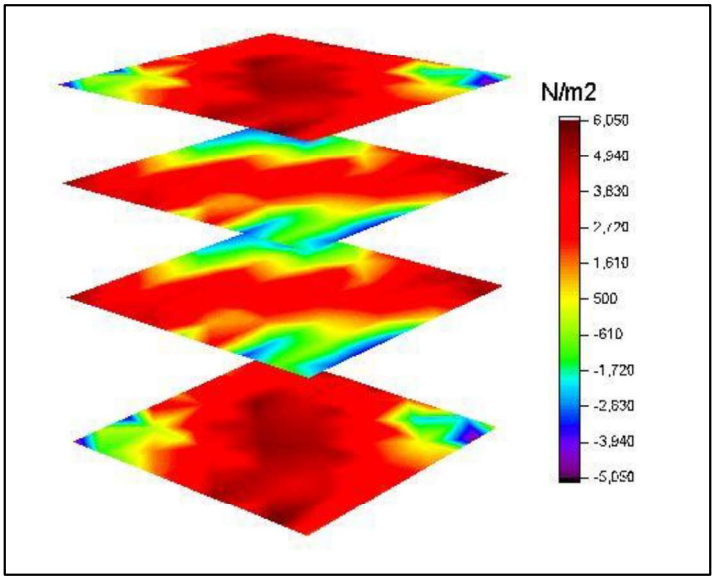

(d)

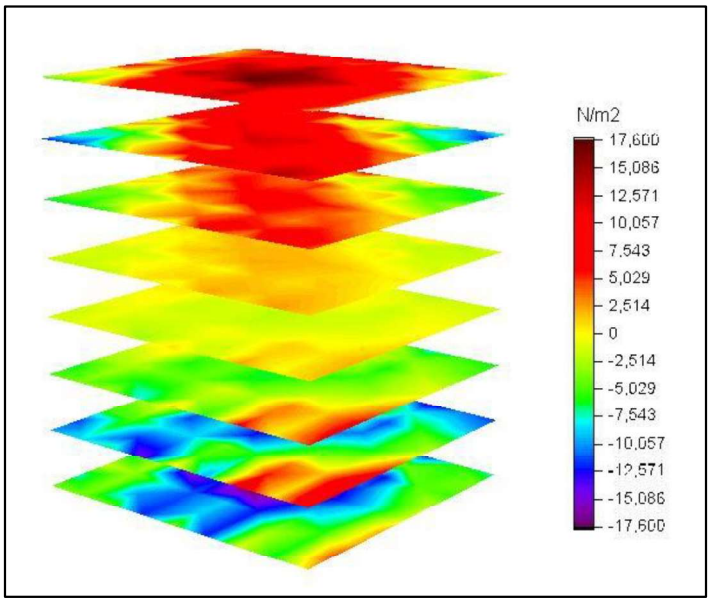

(e)

Fig. 4.12 Contour plot of normal stresses across layers for SSSS boundary condition (a) *0˚/90˚/0˚/90˚* (b) *0˚/90˚/90˚/0˚* (c) *45˚/-45˚/45˚/-45˚* (d) *45˚/-45˚/-45˚/45˚* (e) *0˚/30˚/45˚/60˚/-60˚/-45˚/-30˚/0˚*

On the other hand, if the stresses in angle ply laminations are compared, normal stress distribution along the layers is more even. The distribution of stress across the layers of angle-ply laminates, it decreases as the layers approached towards center then again increases for both symmetric and anti-symmetric laminations. If the angles are oriented in $\theta^{\circ}/\theta^{\circ}$ fashion, the normal stress distribution over the plate at any layer is varying significantly. The variation of stress is parallel to the orientation of the ply angle for that particular layer. The normal stress component is divided into two components, one along the ply layers and the other perpendicular to the ply layer. As a result, the normal stress is concentrated along the diagonal of the plate, for a particular laminate. Fig. 4.12.g shows the variation of stress for an eight-layer plate having total thickness same with different ply angles usually found in literature.

As of now, the variation of different stress parameters across layers is studied for different ply angles but for same boundary conditions. The change in stress values with changing boundary conditions is a very important aspect of study for a particular ply orientation. This specific study is carried out in the next problem.

4.2.6.2: Problem 2: Comparative study of normal stress, inplane shear stress and transverse shear stress for anti-symmetric angle-ply and symmetric cross-ply lamination under different boundary conditions are presented in this problem.

Normal stress developed along X axis for anti-symmetric angle ply laminated plate for four different boundary conditions are shown in Fig. 4.13. It can be observed that the bottommost layer of the plate with all the edges simply supported, carries maximum amount of stress.

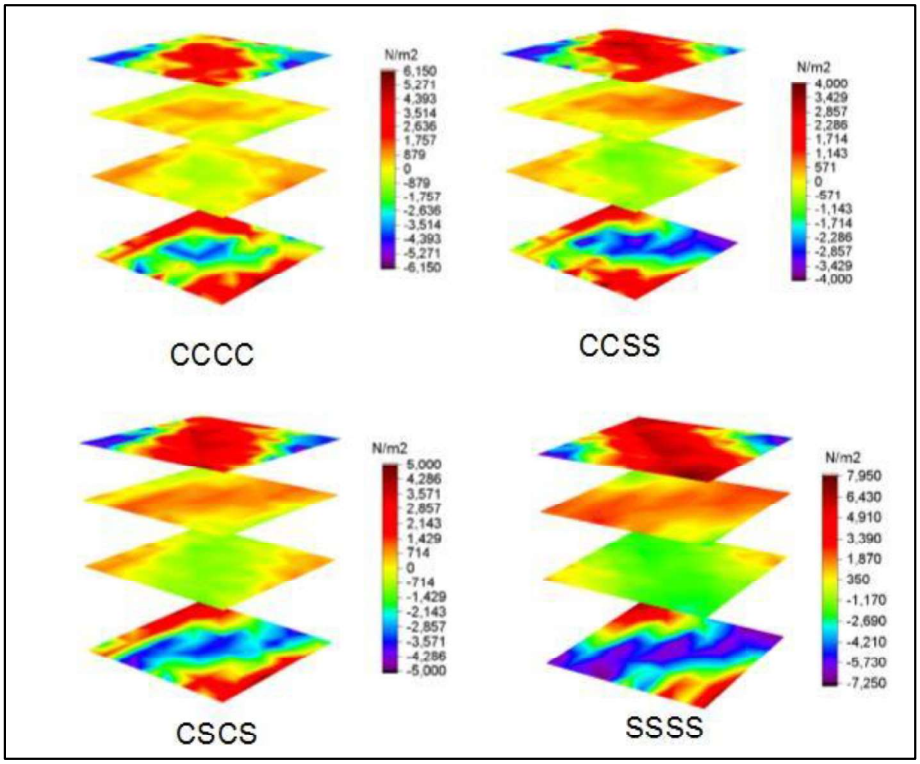

Fig. 4.13 Comparison of normal stress for *45°/-45°/45°/-45°* lamination for varying support conditions

Inplane shear stress distribution for a four layered *45°* anti-symmetric laminated plate is presented in Fig. 4.14. It can be observed from the figure that the inplane shear stress is also shifted towards the simply supported edges and for clamped edged plate the maximum stress is mostly concentrated at the central positions. In all the other cases, a highest stress band can be observed along the diagonal of the plate for all the layers.

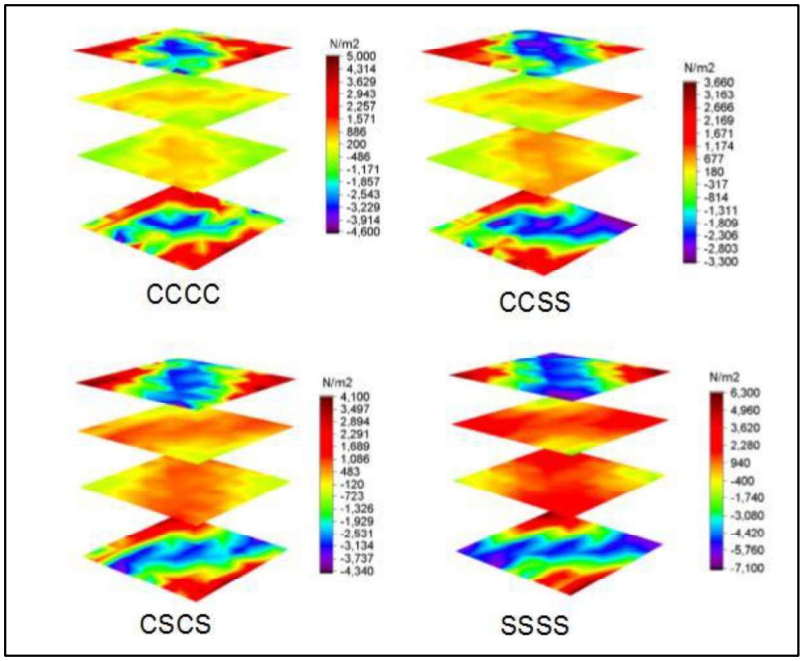

Fig. 4.14 Comparison of inplane shear stress for *45°/-45°/45°/-45°* lamination for varying support conditions

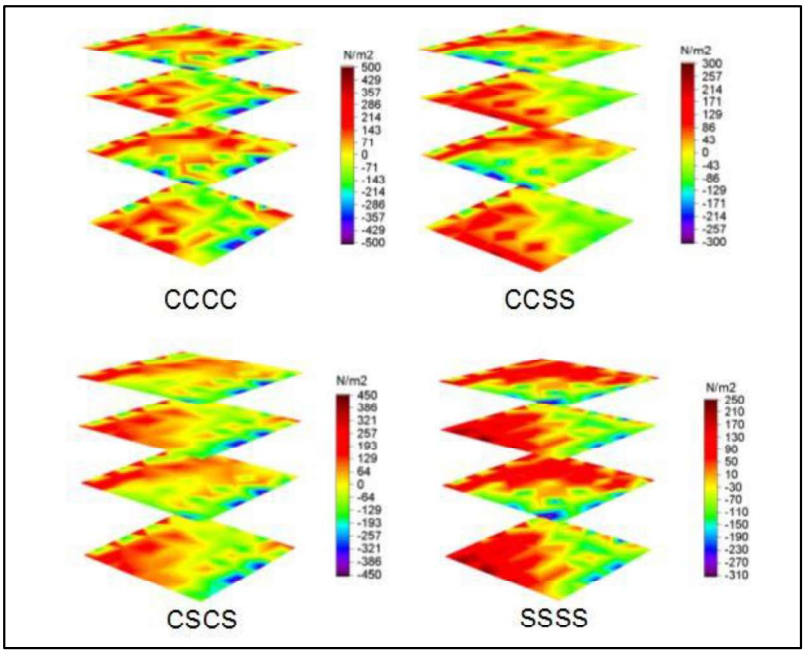

Fig. 4.15 Comparison of transverse shear stress for *45°/-45°/45°/-45°* lamination for varying support conditions

It can be observed from Fig. 4.15 that the magnitude of the transverse shear stress developed for all the support conditions is very less compared to other stress values (i.e. normal stress and

inplane shear stress). From the figure it can also be observed that the positive and negative stress distribution in all the individual layers are almost half of the layers, i.e. diagonal half of the plate is carrying positive shear and the other half carries negative shear.

Stresses in different layers for a composite plate are presented in problems 5 and 6. In problem 5 the boundary conditions are kept constant and the ply angles were varied, whereas in problem 6 the ply angles kept constant and the boundary conditions were varied. It is very important to study the variation of all the stresses with same ply angle and boundary conditions. This will help to find which stress will reach its peak value for same parameters, during the design of plate. It will also help to conclude, which stress will reach the failure stress first.

4.2.7 Numerical study of time history response with parametric variation

Square composite plates (unless mentioned otherwise) with varying boundary conditions and ply angles are studied in this section under Koyna ground motion [Chopra and Chakrabarty (1972)]. Time history response of central displacement and stresses are obtained and presented in subsequent sections. In all the graphs of time history responses, time-steps in seconds are marked along X axis and central displacement or stress are marked along Y axis unless otherwise mentioned.

In the present study, seismic analysis of composite plate is performed considering the Koyna earthquake frequency. Frequency of the composite plate under consideration has similar frequency range with that of Koyna ground motion. Hence the Koyna ground acceleration record is selected for observation.

Koyna earthquake occurred in 1967 is extensively available in literature such as Chopra and Chakrabarty (1972). In the present study the authors have used the horizontal component of the ground motion as shown in Fig. 4.16 with PGA of 0.49g [Chopra and Chakrabarty (1972)].

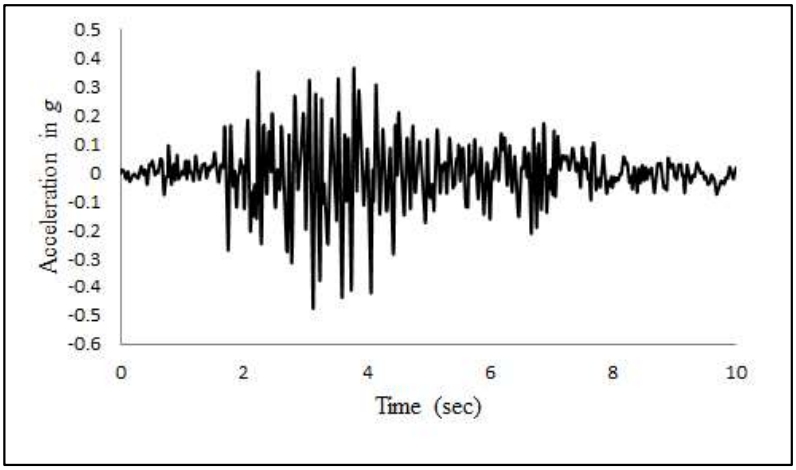

Fig. 4.16 Horizontal component of Koyna earthquake acceleration recorded on 11th December 1967

4.2.7.1: Problem 1: Central displacement of a square composite plate with all the edges fixed is studied in this problem. Ply angles and number of ply layers are varied and displacement of the central node is presented here under Koyna earthquake frequency. The side to thickness ratio is considered as 10. The material properties considered here are E_1=5.25×10^{11} N/m^2, E_2=2.1×10^{10} N/m^2, G_{12}=1.05×10^{10} N/m^2, G_{23}=4.2×10^9 N/m^2, v_{12}=0.25, ρ=800 kg/m^3.

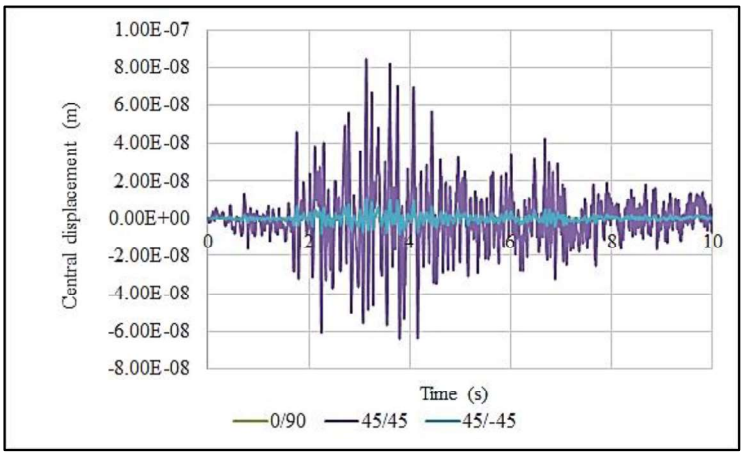

Fig. 4.17 Comparative time history study of two layer plate for Cross-ply and Angle ply lamination

Transverse displacement of the central node of a clamped plate is presented in Fig. 4.17. The ply angles of the plate are varied between two layers of $0^\circ/90^\circ$ and corresponding displacements are reported in Fig. 4.17. It can be observed from the figure that two layered $0^\circ/90^\circ$ laminated plate shows very small deflection value which is not even visible in the figure. On the other hand, if cross and angle-ply laminations are compared, then $45^\circ/45^\circ$ lamination show much higher deflection values compared to the cross-ply laminated plates as mentioned in Fig. 4.17. Anti-symmetric lamination with its bending –stretching coupling effect manages the deflection in better way compared to its symmetric counterpart as shown in the figure.

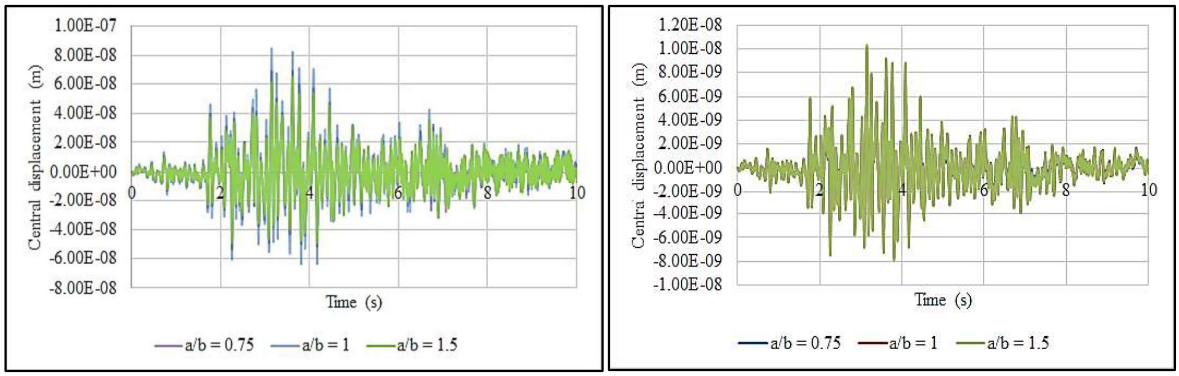

(a) (b)

Fig. 4.18 Effect of geometry of the plate on central displacement on the clamped plate (a) $0^\circ/90^\circ$ (b) $45^\circ/45^\circ$

As a next step, the plan dimension of the plate is varied and corresponding displacements are reported in Fig. 4.18. In all the cases, b value in the plan of the plate is kept constant and the other dimension is varied. As it is seen in Fig. 4.18(a) that as the plies are oriented equally in both the directions, so the square plate shows minimum deflection compared to other values. The same variation when checked with 45° symmetric angle-ply lamination, it can be found that only in case of the square plate (a/b=1), the displacement is minimum; whenever the plate becomes rectangular, it shows higher values.

4.2.7.2: Problem 2: The variation of stresses with time of a square composite plate with all the edges fixed is studied in this problem. Normal stress and inplane shear stress are studied in this problem. Ply angles and ply layers are varied keeping the total thickness of

the plate constant. The geometric and material properties of the plate are kept same as that of previous problems.

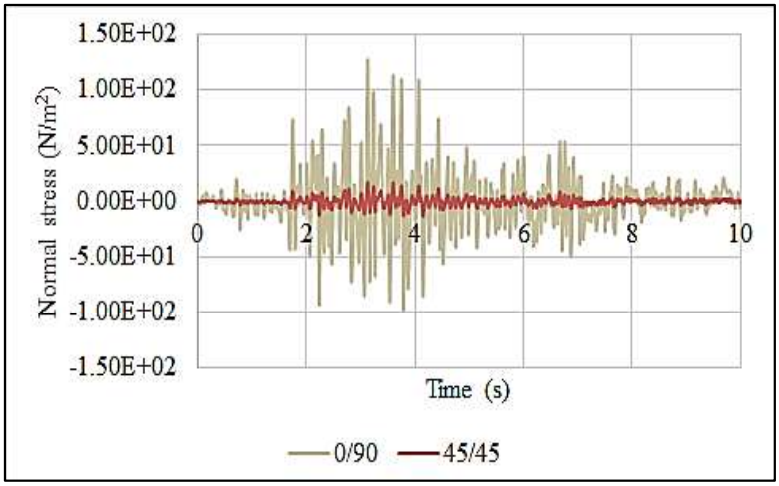

Fig. 4.19 Normal stress variation for two layered plate for cross-ply and angle-ply lamination

The normal stress variation in a clamped edged plate is studied in Fig. 4.19. The stress variation for cross-ply lamination in Fig. 4.19 shows that $0^{\circ}/90^{\circ}$ lamination give maximum stress value as fibres are present along both the orthogonal directions. 45 lamination has always a component in resisting the normal stress hence it shows lesser values compared to cross-ply lamination.

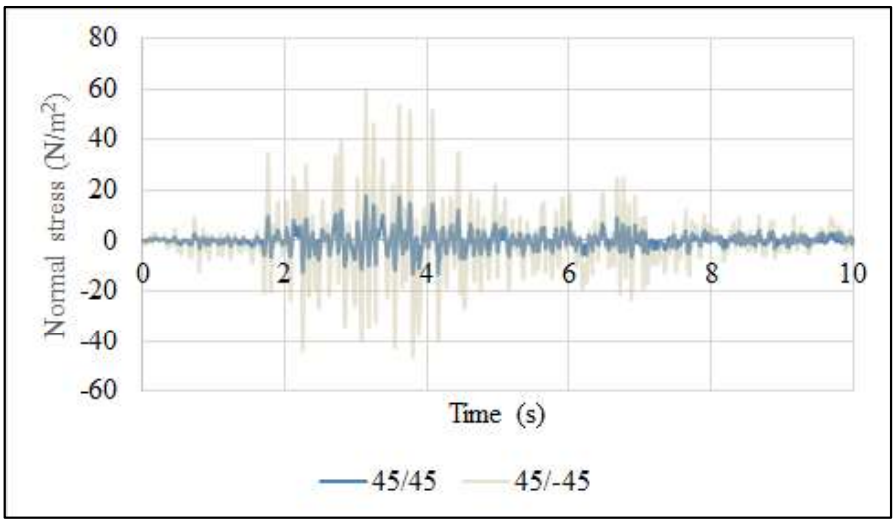

Fig. 4.20 Normal stress variation for two layered symmetric and anti-symmetric plate

The variation of normal stress across layers for angle-ply symmetric and anti-symmetric ply layers are presented in Fig. 4.20. Anti-symmetric angle-ply laminated plate carries much higher stress values compared to symmetric lamination due to its bending-stretching coupling effect of plies.

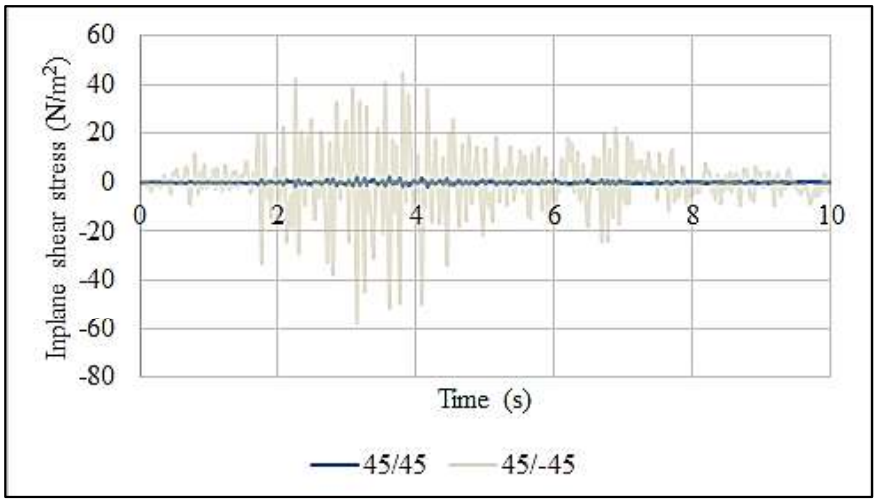

Fig. 4.21 Inplane shear stress variation for two layered symmetric and anti-symmetric plate

Fig. 4.21 shows the variation of inplane shear stress for two layered 45° angle-ply laminated clamped edged plate. The difference in magnitude between symmetric and anti-symmetric lamination is quite large. The maximum stress response of the anti-symmetric lamination is almost 20 times that of the maximum response of the symmetric one. This is due to the fact that as the [B] matrix is non-zero for anti-symmetric lamination, hence extra amount of inplane and transverse shear stress generates in case of anti-symmetric lamination, which is represented in the figure also.

Fig. 4.22 shows the comparative study of increase of layers on inplane shear stress for anti-symmetric lamination, keeping total thickness constant. The result is in line with that of the normal stress results. It shows variation in response. Increase in number of layers decreases the shear stress values.

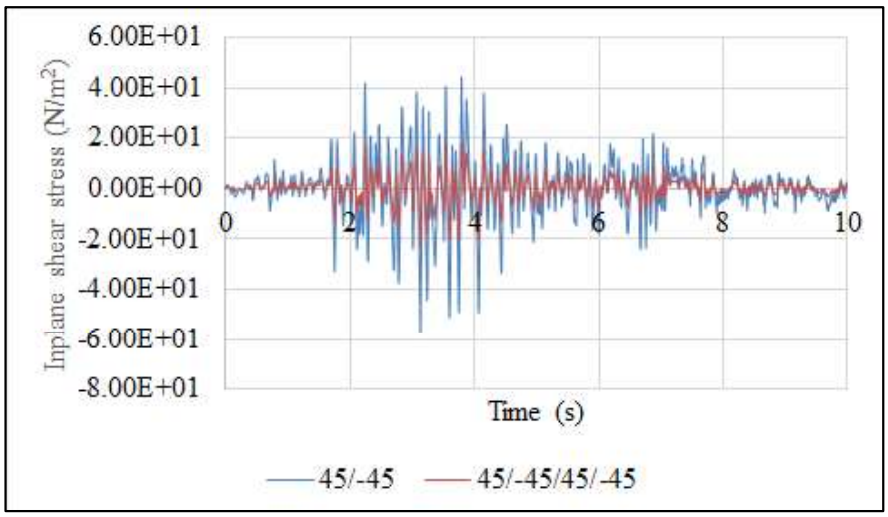

Fig. 4.22 Effect of increase in number of layers on inplane shear stress in angle-ply laminated plate

4.2.8 Numerical study of stresses developed at various ply layers in a plate and corresponding contour plots

Square composite plates (unless mentioned otherwise) with varying boundary conditions and ply angles are studied in this section under Koyna ground motion for normal stress, inplane shear stress and transverse shear stress. Parametric variations are made and change in the nature of stress at each ply layer is presented as contour plots in the subsequent sections.

4.2.8.1: Problem 1: The variation of normal stress across layers in a composite clamped square plate is studied with a/h =10. The forcing frequency remained same that of Koyna earthquake frequency and the stresses are recorded at time step of 3.14s, where the maximum displacement takes place. Ply orientations and number of ply layers are varied and corresponding contours are plotted and presented here.

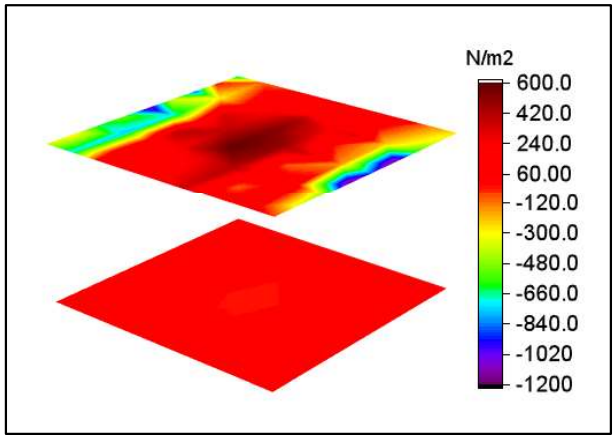

Fig. 4.23 Variation of normal stress across layers of a clamped two layered plate $0^{\circ}/90^{\circ}$

Normal stress in a clamped plate does not remain uniform throughout the surface of the plate. The value of normal stress varies at different locations of the plate. Moreover, the variation is also not uniform across the layers of the plate. Hence the stress contour plot of the plates is very important. Fig. 4.23 shows the variation of normal stress for different layers of a $0^{\circ}/90^{\circ}$ plates. In this case, the 0° layer carries much higher stresses compared to the 90° layer. 90° layer almost carries null stress, whereas the 0° layer carries nearly 1200 N/m^2 stress at certain points on the plate.

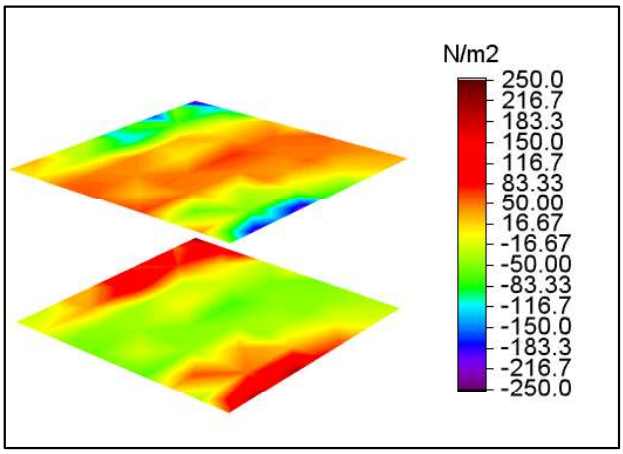

(a)

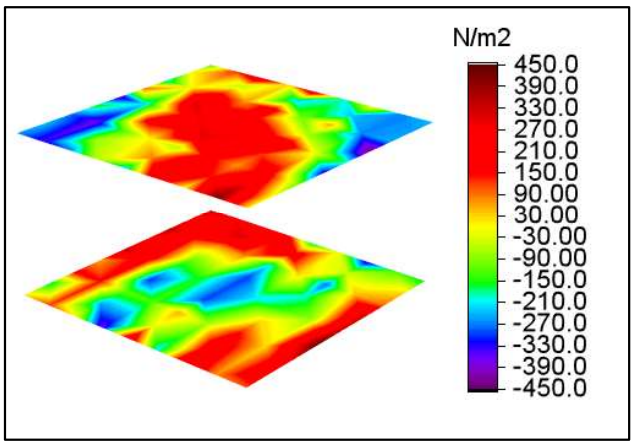

(b)

Fig. 4.24 Variation of normal stress across layers (a) *45°/45°* (b) *45°/-45°*

The stress contour for a two layered plate with *45°* lamination is presented in Fig. 4.24. Symmetric ply variation is presented in Fig. 4.24(a) which shows that the middle portion of the plate carries lower stress values and maximum stress is concentrated along the corners. For anti-symmetric angle-ply lamination, the stress contour is plotted in Fig. 4.24(b), where the maximum stress is at the center as well as at the corners and oriented along the ply directions. Stress in the anti-symmetric lamination is almost twice in magnitude compared to the symmetric one.

4.3 ANALYSIS OF COMPOSITE PLATE INTERACTING WITH ADJACENT FLUID

A 3D tank filled with water is studied for the fluid structure interaction. The opposite side walls are made of composite plates of 0.01 m thickness. Rest of the sides are assumed to be rigid. The height and width of the wall is kept constant as 6 m and 40 m respectively unless mentioned otherwise. Length of the tank is also kept constant as 40 m.

The study of the tank started with the effect of various parameters (ply angle, number of layers, boundary conditions etc.) on the coupled natural frequency of the tank. The central displacement of left and right wall of the tank is studied under transient loading and ground motions in steps. Finally, the stresses (normal stress, inplane shear stress and transverse shear stress) developed at the side walls along with the stress contour at different ply layers under various loading conditions are presented.

4.3.1 Convergence study for mesh size for 3D tank

Convergence study of mesh size is performed to obtain as accurate result as possible. The tank with side plate of dimension 0.5 m height and 2.5 m width and 0.5 mm thickness with a tank length of 1.5 m is used for convergence study. The composite plate (tank side wall) has even number of ply layers with 0°/90° lamination scheme and all the edges are clamped. The mesh size is varied from 2 × 2 to 8 × 8 and corresponding coupled fundamental frequency of the tank is plotted in Fig. 4.25 and 4.26. It can be observed from the two figures that with increase in mesh size, frequency value decreases but beyond 4×4 meshing, the frequency values hardly change. The trend is common for both 2 and 4 number of ply layers. Hence in the present study a 4 × 4 meshing is selected throughout to analyze the tank to obtain coupled frequency values.

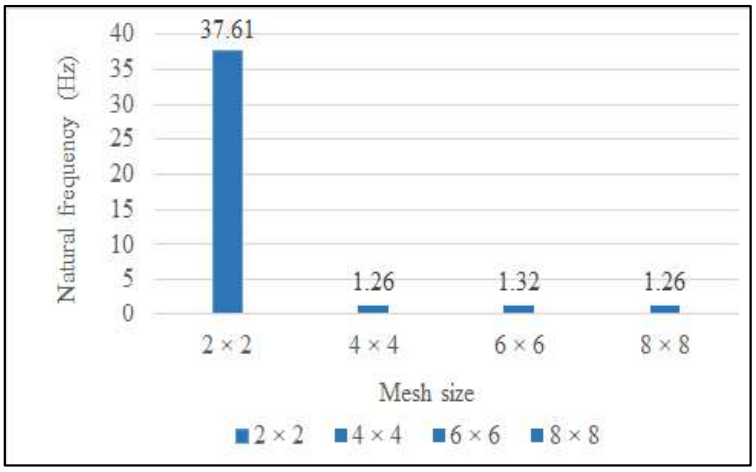

Fig. 4.25 Coupled natural frequency with increase in mesh size (2 layer)

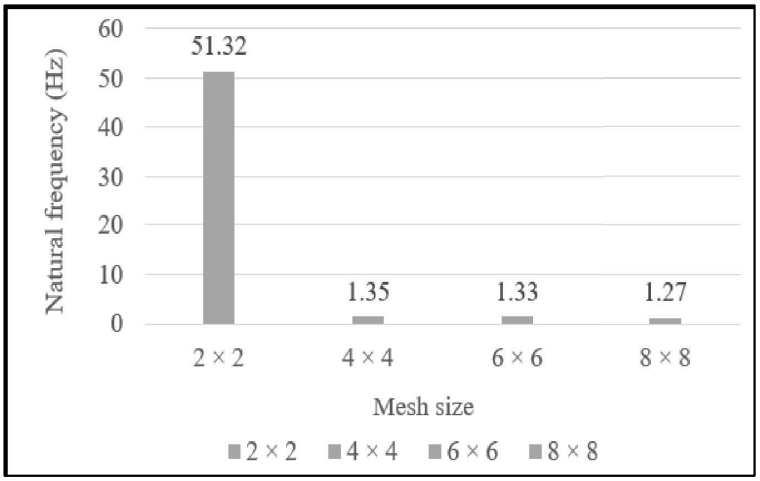

Fig. 4.26 Coupled natural frequency with increase in mesh size (4 layer)

4.3.2 Validation of the proposed algorithm for uncoupled fluid

The fluid part in the present formulation is separately studied its accuracy with published literature. As suggested by Jain and Jaiswal (2005) the time period for a rectangular tank is studied and the results are presented in a graphical form in Fig. 4.27. According to the literature, the time period is constant beyond height to length ratio (*h/L*) of 0.8. Hence the present study is limited within the range of 0.1 to 0.9 of *h/L* of the tank. The figure shows time period values obtained from present formulation is in good agreement with that of the published literature.

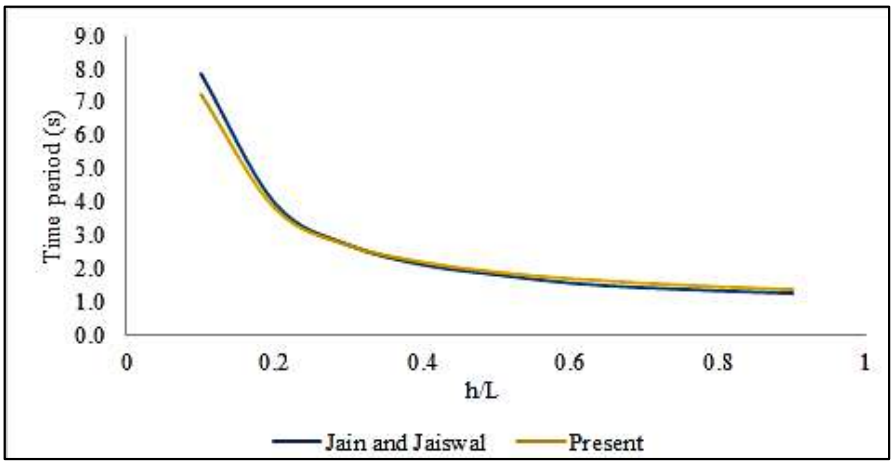

Fig. 4.27 Comparison of time period for height to length ratio between 0.1 to 0.9

4.3.3 Analysis of central displacement of the side walls for the coupled system under different forcing frequencies

Central displacement of the left tank wall is presented in Fig. 4.28 with different ply angles. Response of the plate under forcing frequency of 10% of that of fundamental frequency (FF) is used. Cross-ply as well as angle-ply laminations are used to check the variation in response. It was observed that except anti-symmetric 45° lamination, rest of the ply angles give similar results. Only in case of 45°/-45° lamination, it shows higher deflection compared to the rest of the results.

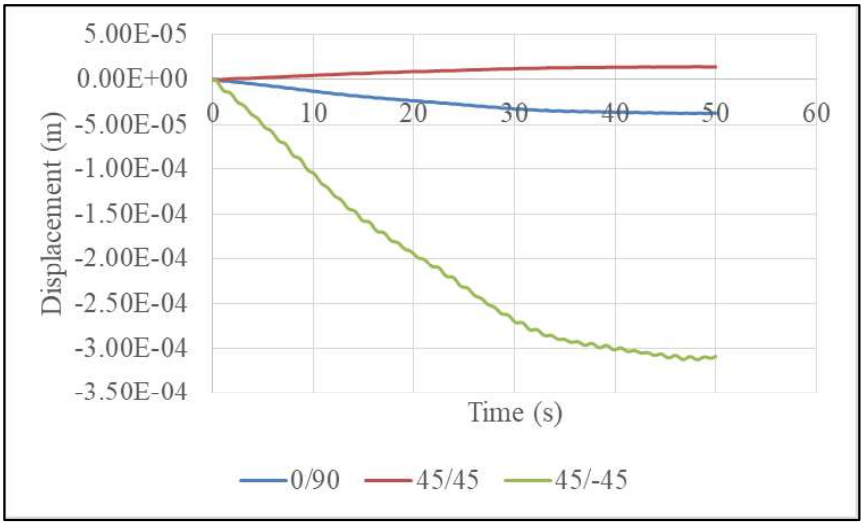

Fig. 4.28 Variation of central displacement of the left tank wall (CCCC) under forcing frequency as 10% of fundamental frequency for different ply angles

Variation of central displacement for an all edges clamped tank wall with varying thickness is presented in Fig. 4.29. The thickness of the plate is varied in steps from 0.1 m to 0.001 m. The plate displacement increases as thickness decreases. In case of 0.001m thick plate, displacement is quite large, as it may experience instability due to very thin plate. The variation in displacement is shown for two layered 0°/90° (Fig. 4.29) and anti-symmetric 45° (Fig. 4.30) lamination ply layers.

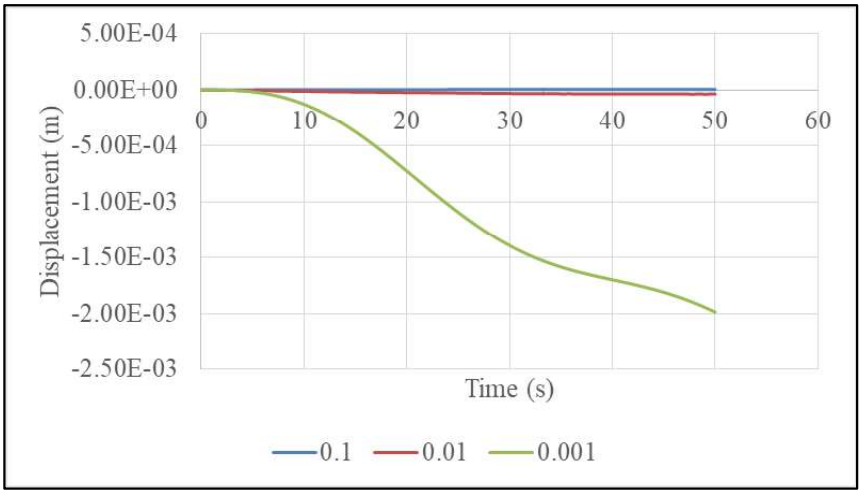

Fig. 4.29 Variation of central displacement of the left tank wall (CCCC) under forcing frequency as 10% of fundamental frequency for various plate thickness (0°/90° lamination)

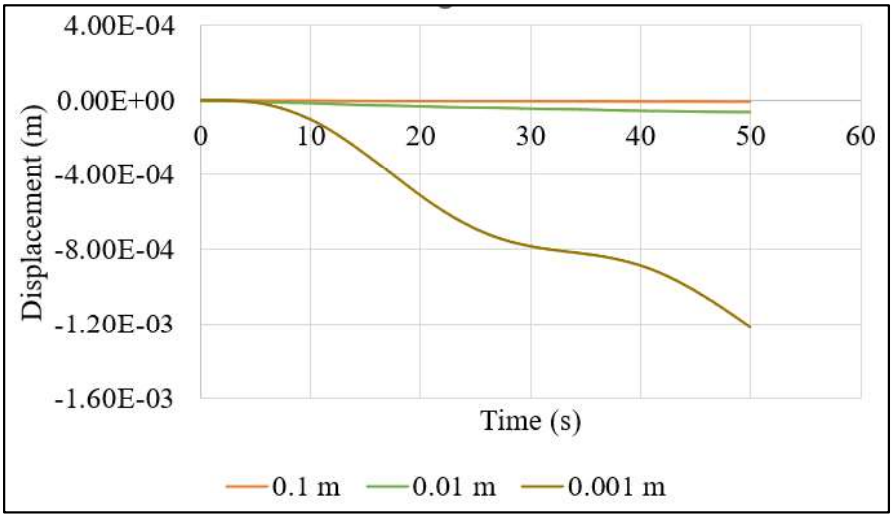

Fig. 4.30 Variation of central displacement of the left tank wall (CCCC) under forcing frequency as 10% of fundamental frequency for various plate thickness (45°/-45° lamination)

As the next step the forcing frequency is changed to 3 times fundamental frequency to check the variation in response in terms of central displacement of the left tank wall. Initially the effect of various ply angles is presented in Fig. 4.31 and similar trend for ply angle variation as that of fundamental frequency is obtained. The plate thickness is then varied and the result is presented (Fig. 4.32 and Fig. 4.33) for 90° and 45° laminations. Huge displacement is found for thin plate for both the ply angles.

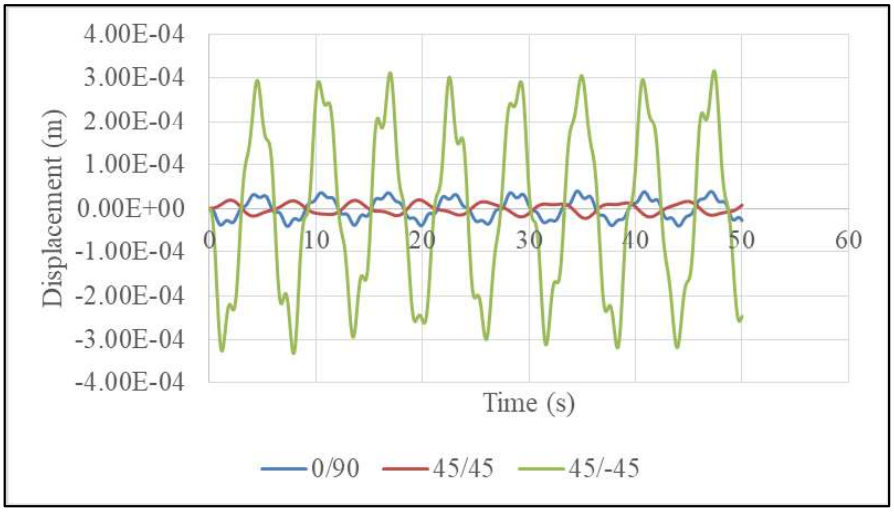

Fig. 4.31 Variation of central displacement of the left tank wall (CCCC) under forcing frequency as 3 times fundamental frequency for different ply angles

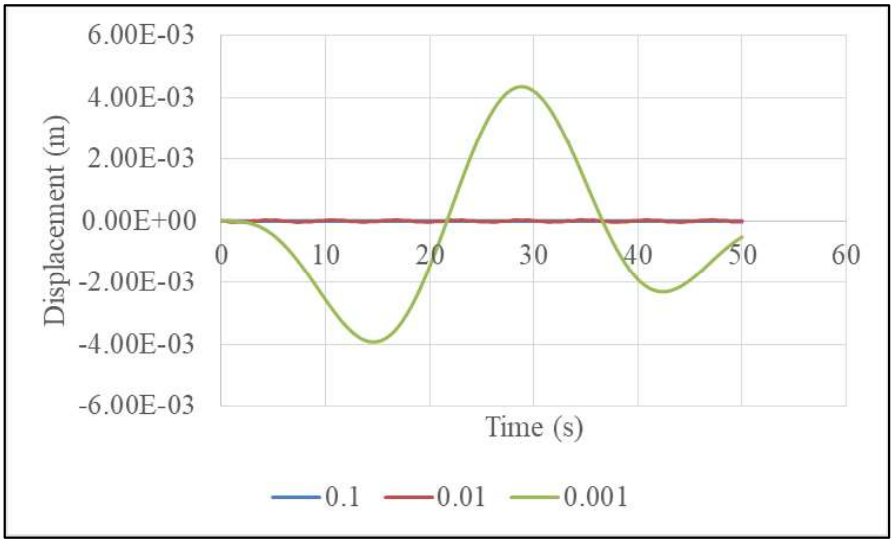

Fig. 4.32 Variation of central displacement of the left tank wall (CCCC) under forcing frequency as 3 times fundamental frequency for different plate thickness (0°/90° lamination)

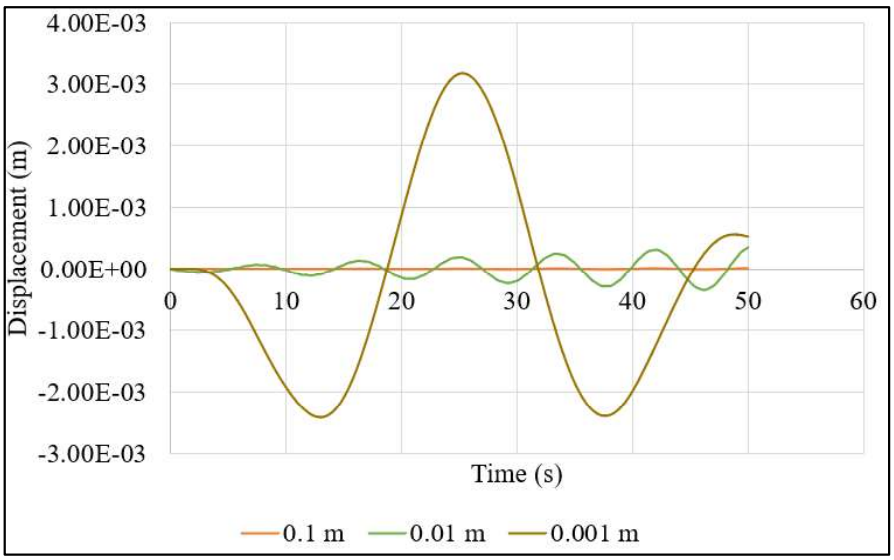

Fig. 4.33 Variation of central displacement of the left tank wall (CCCC) under forcing frequency as 3 times fundamental frequency for various plate thickness (45°/-45° lamination)

The same result is again studied for fundamental frequency values as shown in Fig. 4.34. Similar trend is maintained for variation of ply angle. In all the cases 45°/-45° lamination shows maximum amount of deflection in all the cases.

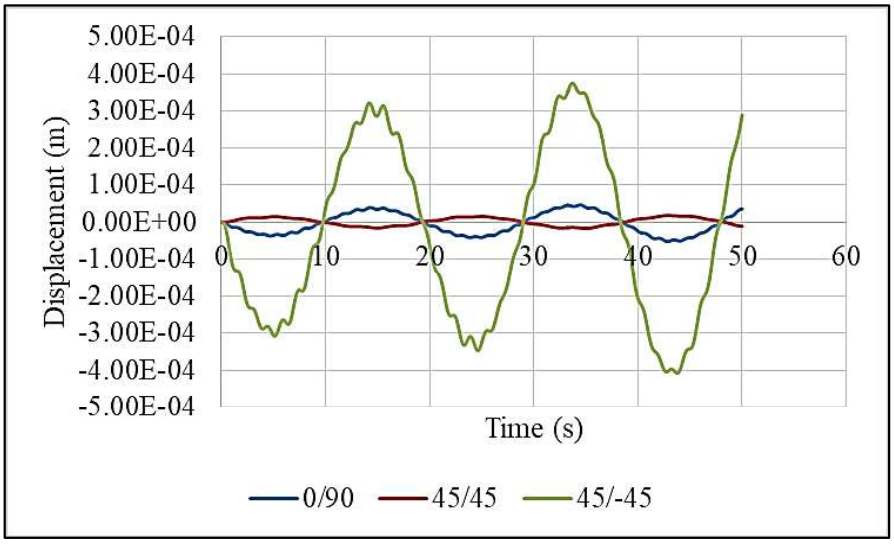

Fig. 4.34 Variation of central displacement of the left tank wall (CCCC) under forcing frequency as fundamental frequency for different ply angles

Variation of central displacement of the left tank wall for cross-ply and angle-ply lamination is presented in the Figs. 4.35 and 4.36. Four different boundary conditions are studied as CCCC (all edges clamped), SSSS (all edges simply supported), CCCF (all edges clamped except top layer which is free) and SCSF (two sides are simply supported, bottom edge is clamped and top edge is free). 3 times FF is used as the forcing frequency. In both the ply angles, SCSF boundary condition shows maximum deflection. In case of angle ply lamination, SSSS in some cases is showing higher displacement values.

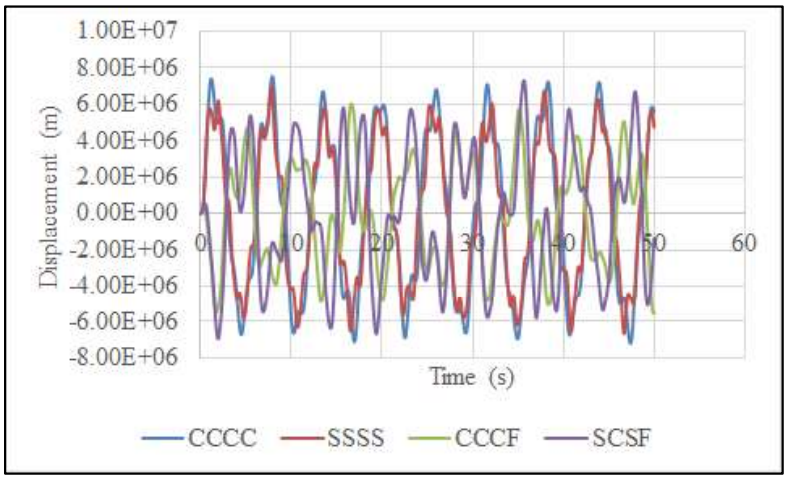

Fig. 4.35 Variation of central displacement of the left tank wall under forcing frequency as 3 times fundamental frequency for different boundary conditions (45°/-45° lamination)

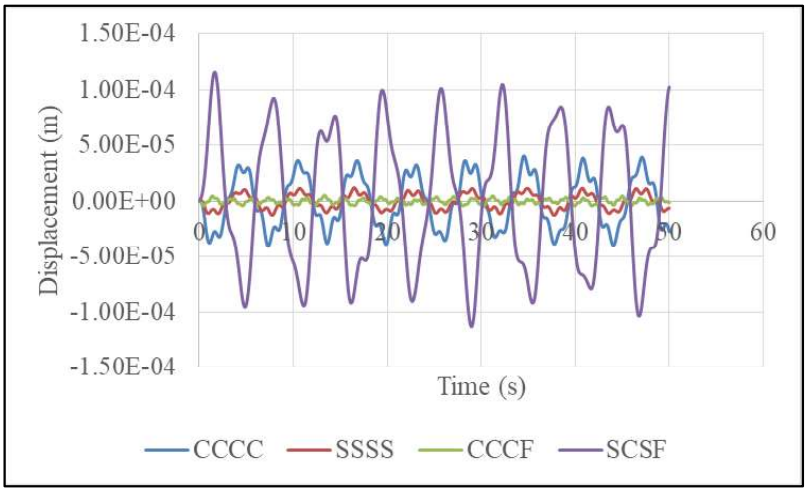

Fig. 4.36 Variation of central displacement of the left tank wall under forcing frequency as 3 times fundamental frequency for different boundary conditions (0°/90° lamination)

Effect of boundary conditions is checked for another frequency value. The forcing frequency is changed to fundamental frequency and effect of boundary condition on central displacement for cross as well as angle ply lamination is studied as presented in Figs. 4.37 and 4.38. Same trend which was seen before is also obtained here. SCSF boundary condition gives maximum displacement among the set of boundary conditions.

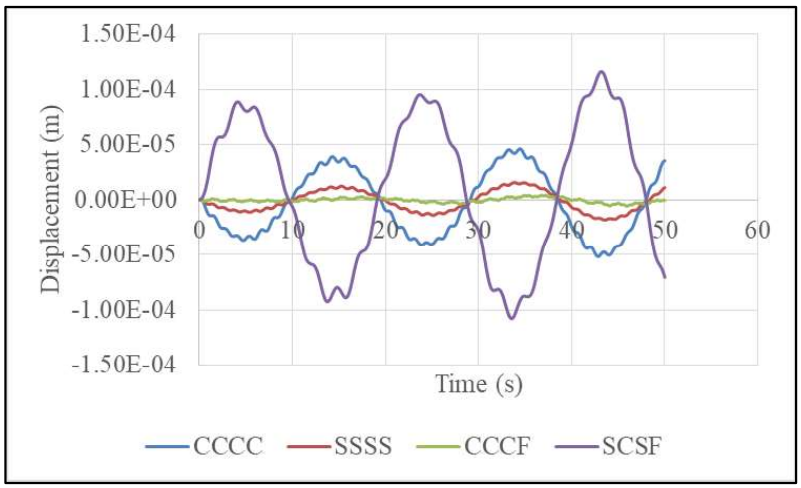

Fig. 4.37 Variation of central displacement of the left tank wall under forcing frequency as fundamental frequency for different boundary conditions (0°/90° lamination)

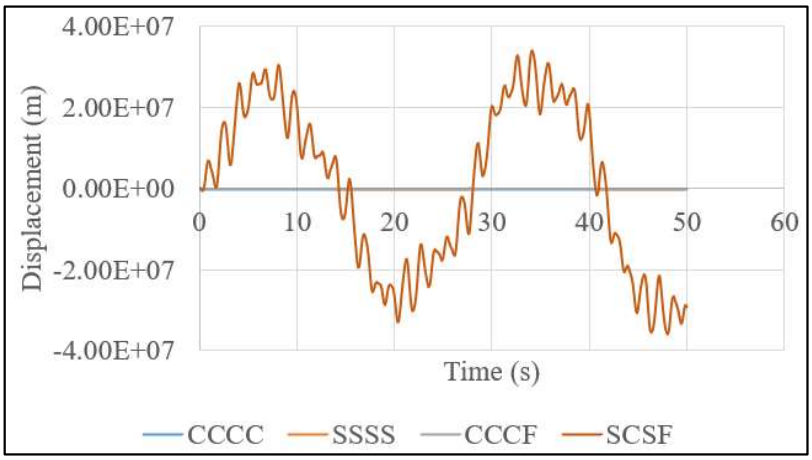

Fig. 4.38 Variation of central displacement of the left tank wall under forcing frequency as fundamental frequency for different boundary conditions (45°/-45° lamination)

The effect of number of ply layers on displacement of side wall under dynamic loading is studied keeping the total thickness constant as 0.01 m. The study includes both the effect of cross and angle ply laminations. It is observed that the displacement values are increased upto four layer cross ply lamination, then the values decreased. The level of decrement is drastic in case of angle ply lamination, whereas it is gradual in case of cross-ply laminations. cross ply lamination does not have any influence due to increase in number of ply layers as shown in Fig. 4.40, whereas in case of angle ply laminations, displacement values drastically decrease with increase in number of layers shown in Fig. 4.39.

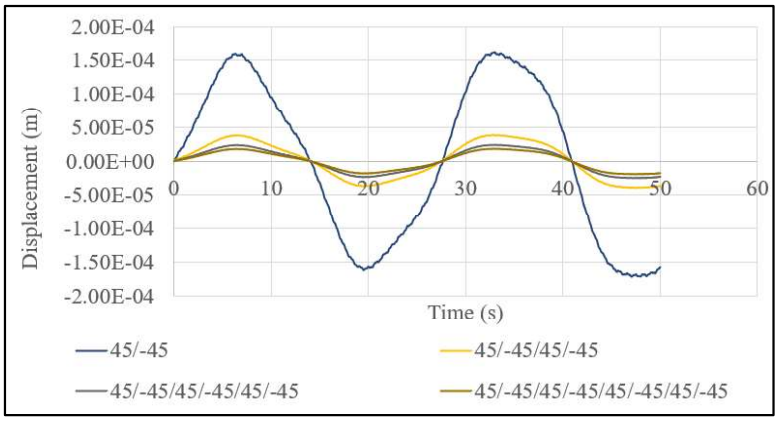

Fig. 4.39 Variation of central displacement of the left tank wall (SSSS) under forcing frequency as fundamental frequency for increasing number of layers (angle ply laminations)

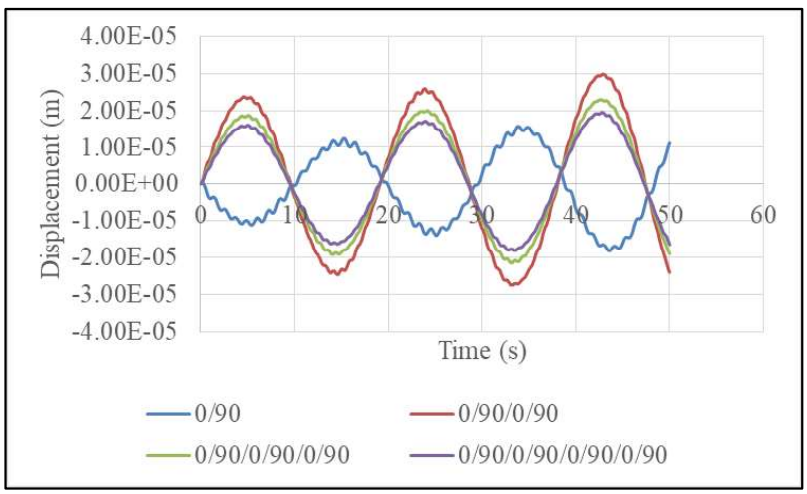

Fig. 4.40 Variation of central displacement of the left tank wall (SSSS) under forcing frequency as fundamental frequency for increasing number of layers (cross-ply laminations)

The next step of study includes the variation in geometry of the plate. The width and length of the tank is kept constant as 40 m and the height of the side walls are increased from 1.1 m to 6.1 m in steps as presented in Fig. 4.41 and Fig. 4.42. In all the cases the tank is assumed to totally filled with water, which means wall height and water height is same in all cases. Central displacement of the plate increases with increase in tank height. Only in case of cross ply lamination displacement values decrease beyond the tank height of 5.1m. Boundary condition considered here is SCSF and cross as well as angle ply laminations are studied and presented here.

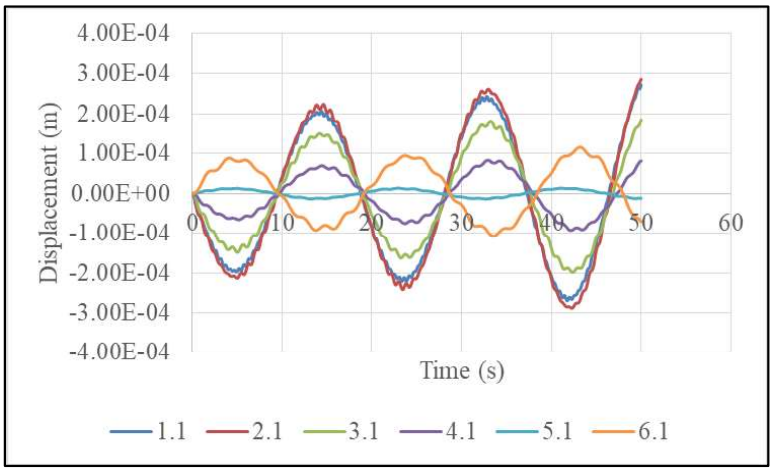

Fig. 4.41 Variation of central displacement of the left tank wall (SCSF) with fundamental frequency as the forcing frequency for increase in tank height (0°/90° laminations)

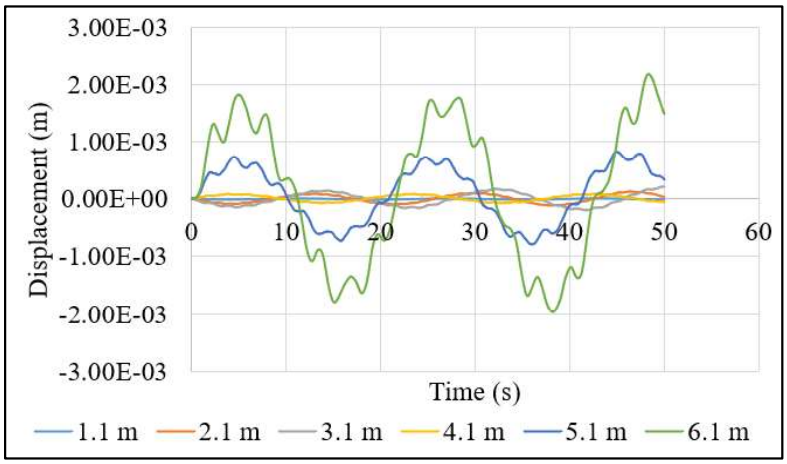

Fig. 4.42 Variation of central displacement of the left tank wall (SCSF) with fundamental frequency as the forcing frequency for increase in tank height (45°/-45° laminations)

The length of the tank is varied in steps to check the effect on central displacement of the left plate keeping the height as 6.1m and width of the plate 40m and presented in Fig. 4.43 and 4.44. The response is studied for a tank with edges SCSF condition and found to increase the displacement values with length of the plate. The study is carried out for cross and angle ply laminations and found to have similar results with increase in displacement with increase in length.

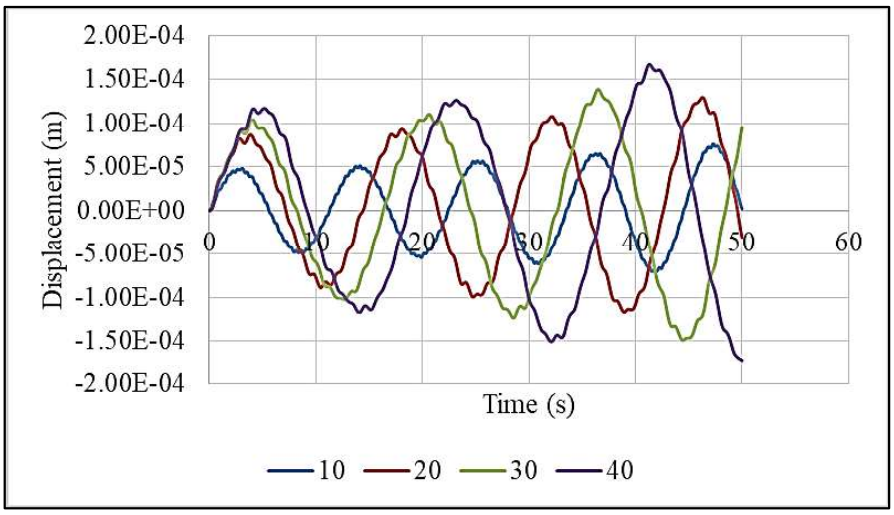

Fig. 4.43 Variation of central displacement of the left tank wall (SCSF) with fundamental frequency as the forcing frequency for increase in tank length (0°/90° laminations)

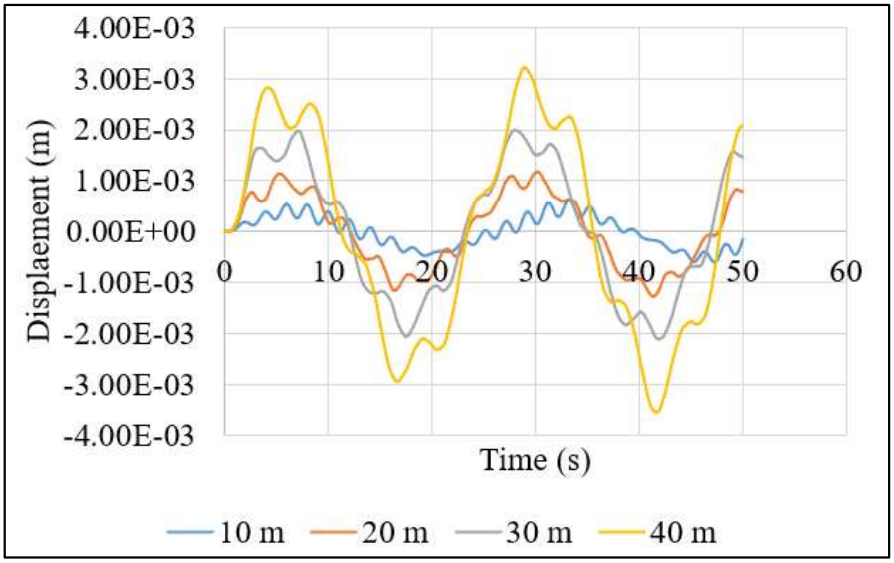

Fig. 4.44 Variation of central displacement of the left tank wall (SCSF) with fundamental frequency as the forcing frequency for increase in tank length (45°/-45° laminations)

Finally, the variation in geometry is studied for different width of the tank keeping the height and length of the tank constant as 6.1 m and 40 m. The study includes the effect of cross ply laminations (Fig. 4.45) and 45° anti-symmetric laminations (Fig. 4.46) for SCSF boundary conditions. The forcing frequency to study the effect of geometry is always maintained as the fundamental frequency. Unlike to the previous results for geometric variations, central displacement values decrease with increase in tank width.

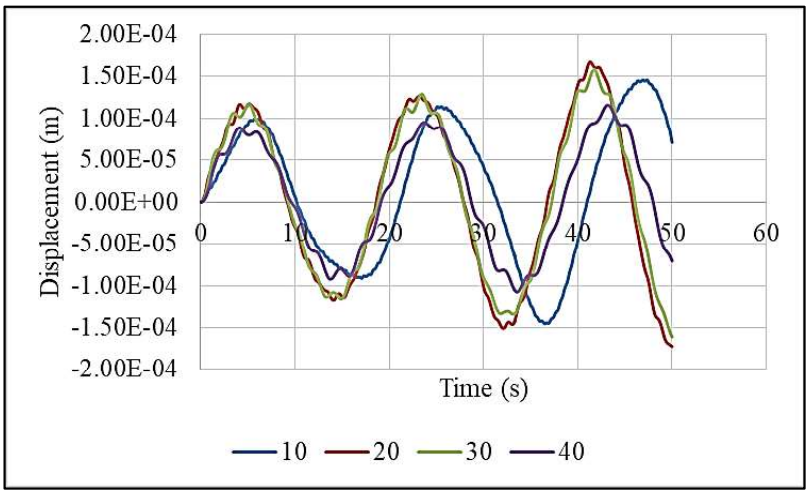

Fig. 4.45 Variation of central displacement of the left tank wall (SCSF) with fundamental frequency as the forcing frequency for increase in tank width (0°/90° laminations)

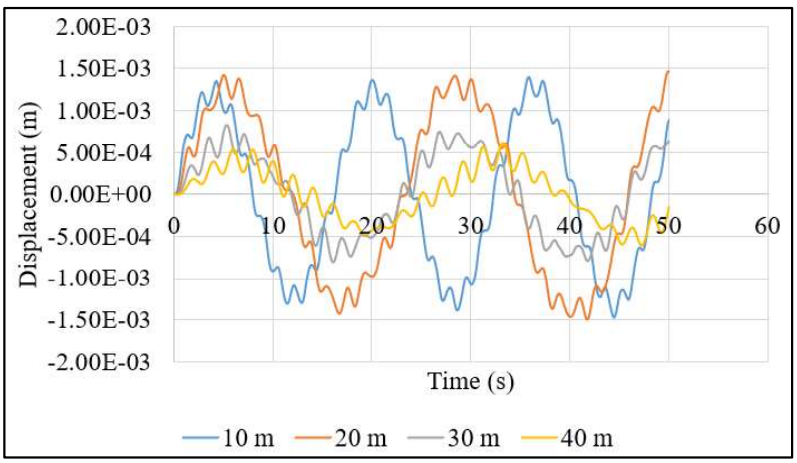

Fig. 4.46 Variation of central displacement of the left tank wall (SCSF) with fundamental frequency as the forcing frequency for increase in tank width (45°/-45° laminations)

The comparison of central displacement of the two walls of the tank is studied under dynamic loading as shown in Fig. 4.47 (cross-ply laminations) and Fig. 4.48 (angle-ply laminations). Initially the displacement of both the walls are same, but as time progresses, there is a variation in values between the two. This happened due to the effect of coupling between plate and fluid, which tend to resist the two plate to behave synchronously. The variation is more prominent in case of simply supported edges, hence the result for SSSS plate is presented here. Angle-ply laminations always show higher displacement values compared to its cross-ply counterpart as it is seen earlier. Similar trend is also seen here. Angle-ply lamination shows higher difference in magnitude between left and right plate. There is basically becomes a phase difference as time progresses. The phase difference is more prominent in case of cross-ply lamination compared to angle ply one.

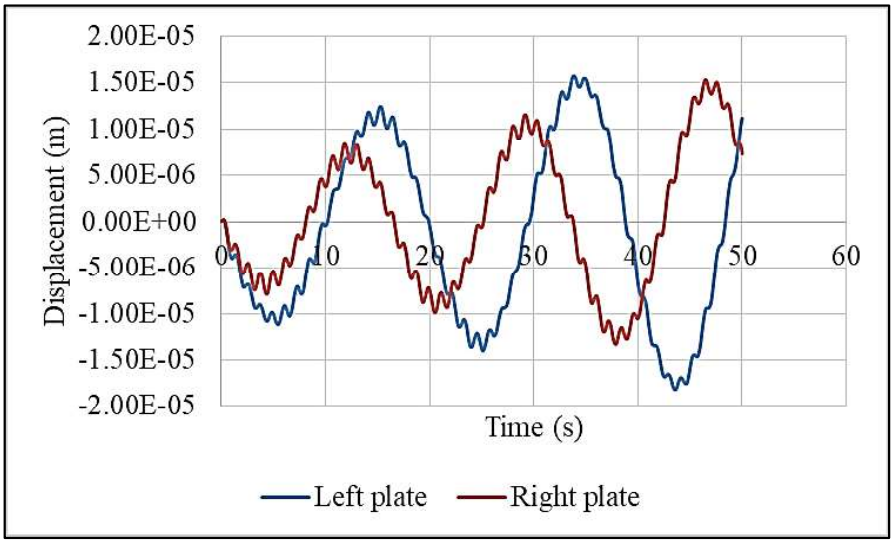

Fig. 4.47 Variation of central displacement of the tank wall (SSSS) under fundamental frequency as forcing frequency for left wall and right wall of the tank (0°/90° lamination)

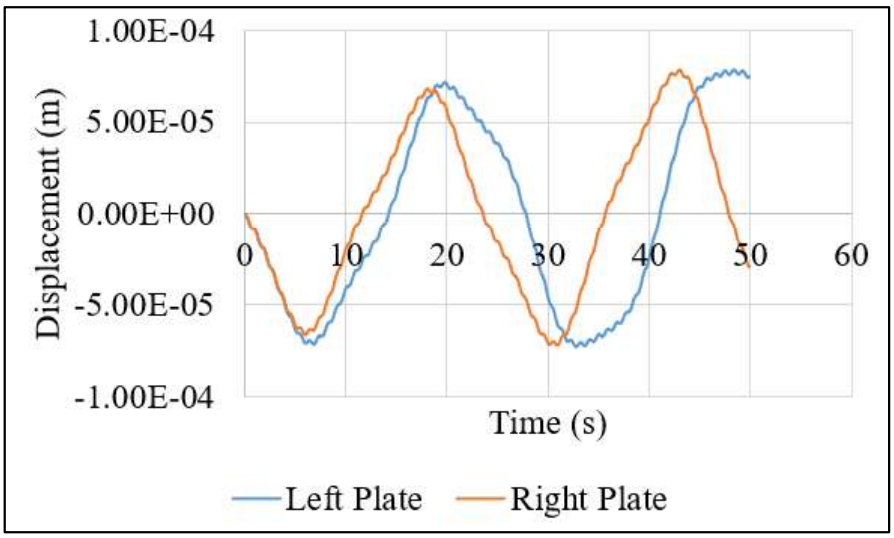

Fig. 4.48 Variation of central displacement of the tank wall (SSSS) under forcing frequency as fundamental frequency for left wall and right wall of the tank (45°/-45° lamination)

4.3.4 Analysis of various stresses developed at the tank wall for the tank-fluid coupled system

Normal stress, inplane shear stress and transverse shear stress developed in the left plate under fundamental frequency as forcing frequency is presented in the following section. Normal stress is calculated at the central position and at the top-most layer of the wall. Inplane shear stress is calculated at the top corner of the wall and at the top most layer. Transverse shear stress is calculated at the middle of the left edge and at the middle of the layers.

The wall is considered to be clamped in all the four edges. Cross ply lamination is studied for normal stress variation as shown in Fig. 4.49 and 0°/90° lamination gives higher stress value compared to 45° ply angle lamination. Symmetric and anti-symmetric angle ply lamination is studied and it was found to have higher stress values for anti-symmetric laminations due to the bending-stretching coupling effect of composites. . Same ply angles were used to check the inplane (Fig. 4.50) and transverse shear stress (Fig. 4.51) values. Inplane shear stress for cross ply laminations give highest results with anti-symmetric lamination as ply coupling effect give rise to inplane shear stresses. At the same time symmetric 45° angle ply laminations give higher values than the anti-symmetric one. Comparison of transverse shear stress for various ply angle shows a different trend than the previous two cases. In this case, symmetric 45° angle ply laminations shows highest stress values among the set. So, in a nutshell it can be concluded that, angle-ply

laminations always shows higher stress values than cross ply ones. Anti-symmetric lamination shows higher values in normal stress inplane shear stress and symmetric laminations shows higher stress values in transverse shear stresses (transverse).

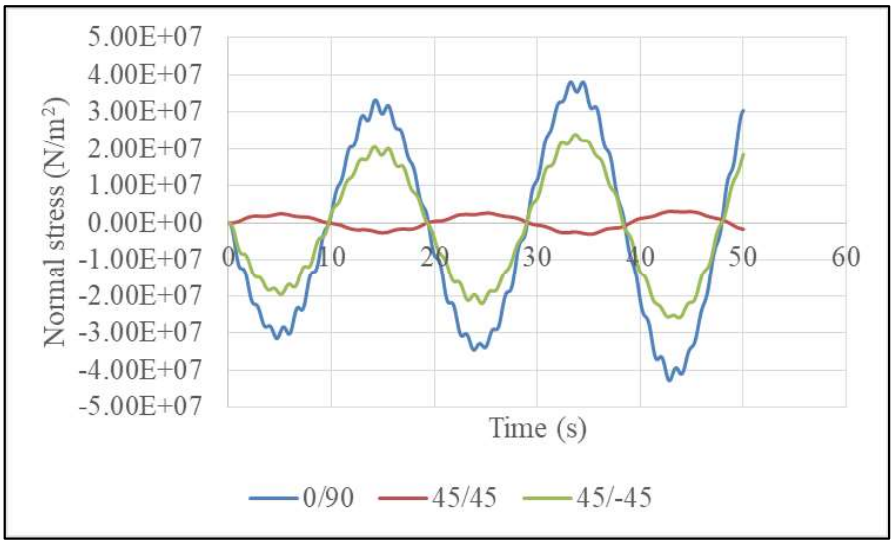

Fig. 4.49 Variation of normal stress of the left tank wall (CCCC) under forcing frequency as fundamental frequency for different ply angle

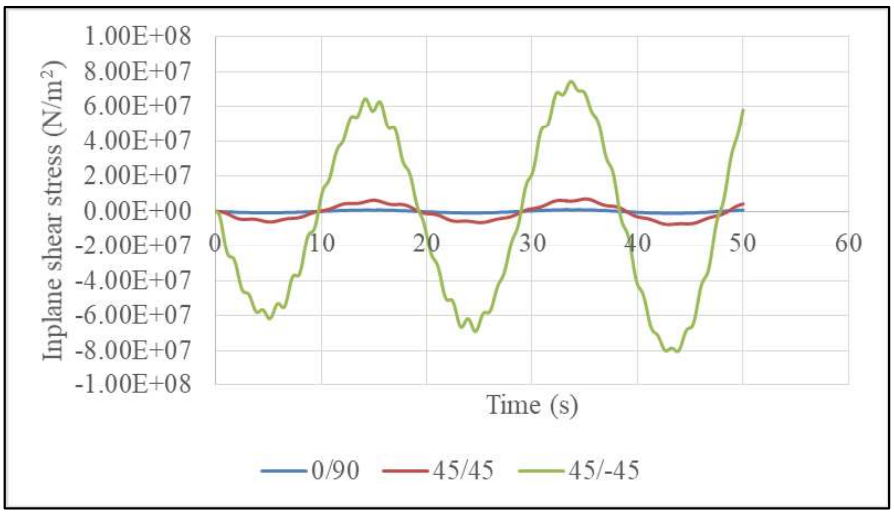

Fig. 4.50 Variation of inplane shear stress of the left tank wall (CCCC) under forcing frequency as fundamental frequency for different ply angles

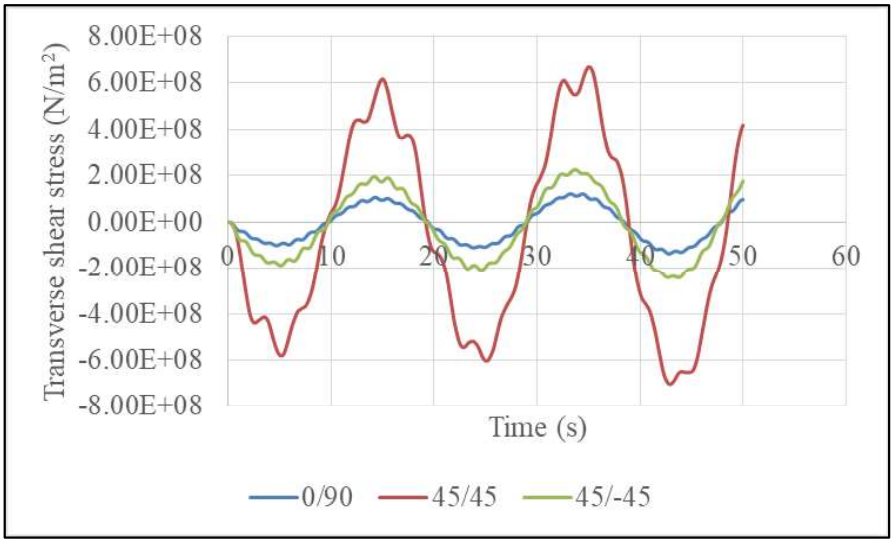

Fig. 4.51 Variation of transverse shear stress of the left tank wall (CCCC) under forcing frequency as fundamental frequency for different ply angles

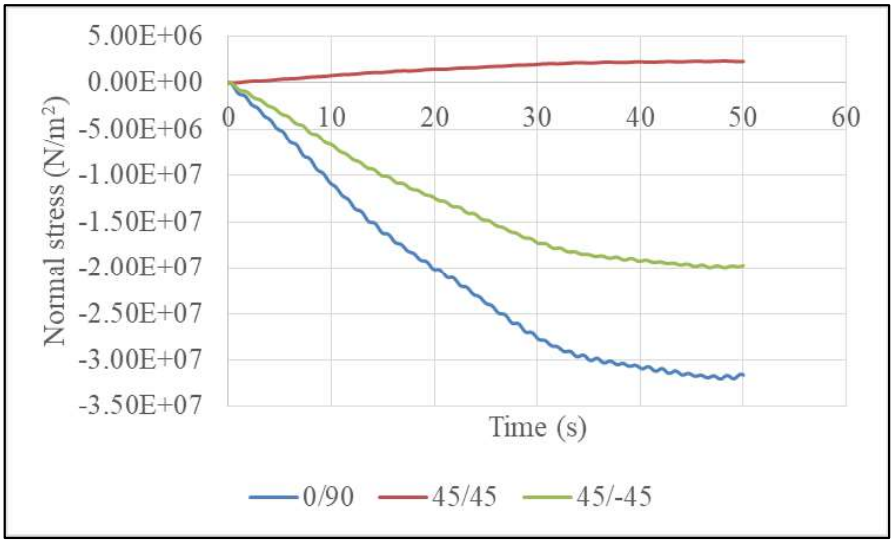

Fig. 4.52 Variation of normal stress of the left tank wall (CCCC) under forcing frequency as 10% of fundamental frequency for different ply angle

The forcing frequency is changed to 10% and 3 times that of fundamental frequency and the stress results are presented in sequence. Figs. 4.52 – 4.54 shows variation of stress for forcing frequency 10% of natural frequency and Figs. 4.55 – 4.57 shows variation of stress for forcing frequency 3 times of natural frequency. Same trend of stress variations for cross and angle ply

laminations are obtained. Variation of forcing frequency does not have any impact on stress values. In all the cases 0/90 lamination gives highest normal stress values and 45° anti-symmetric laminations gives highest inplane shear stress value and symmetric lamination gives maximum transverse shear stress values.

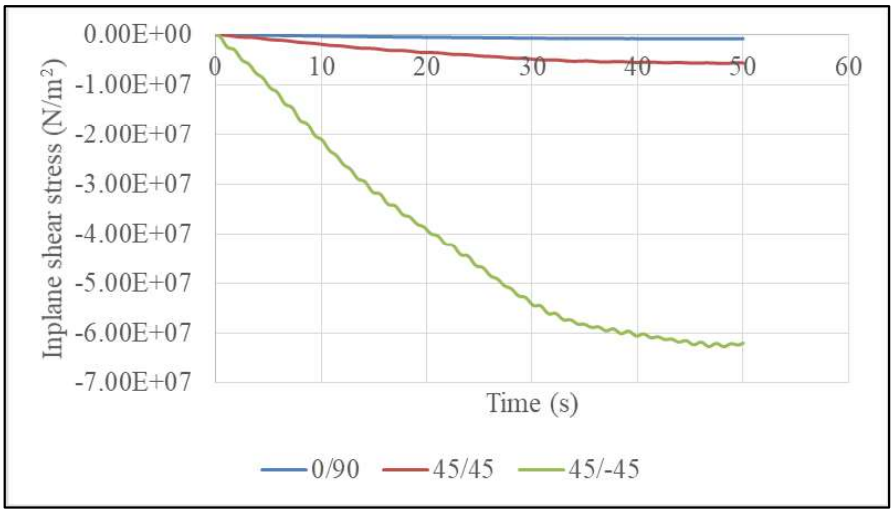

Fig. 4.53 Variation of inplane shear stress of the left tank wall (CCCC) under forcing frequency as 10% of fundamental frequency for different ply angle

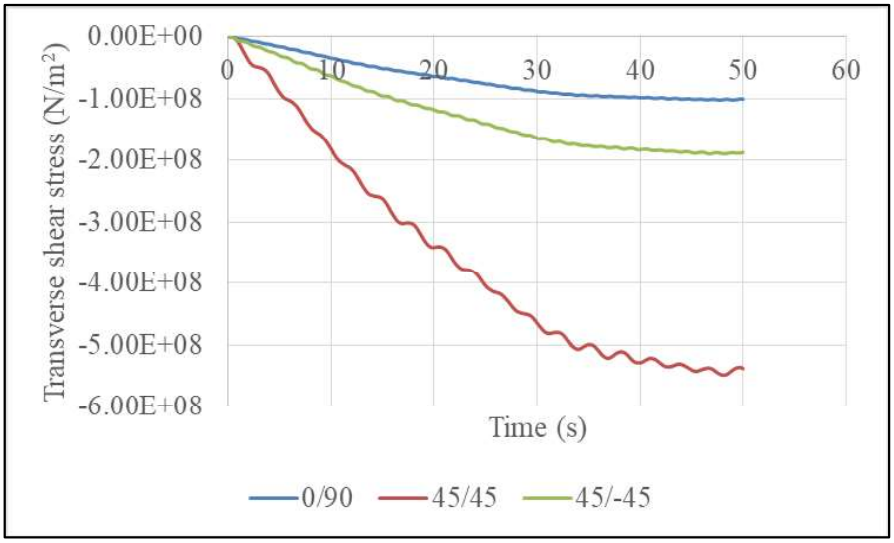

Fig. 4.54 Variation of transverse shear stress of the left tank wall (CCCC) under forcing frequency as 10% of fundamental frequency for different ply angle

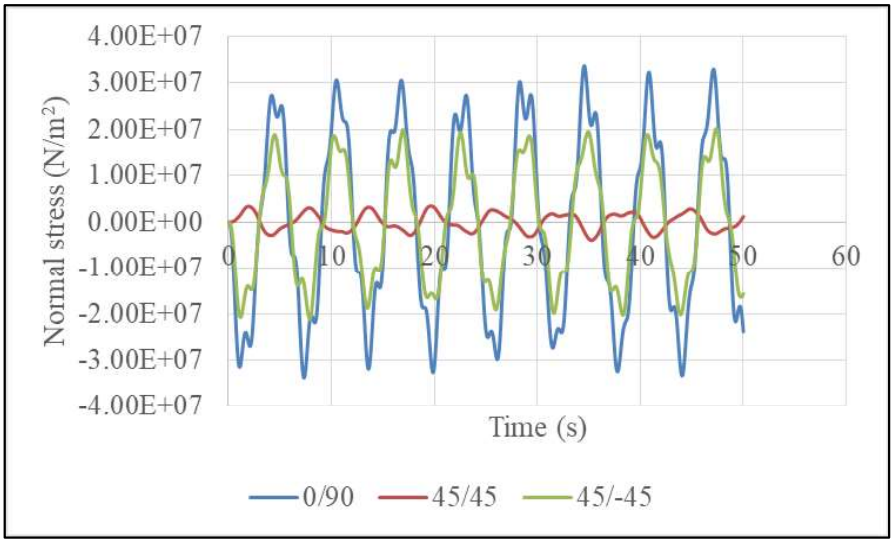

Fig. 4.55 Variation of normal stress of the left tank wall (CCCC) under forcing frequency as 3 times of fundamental frequency for different ply angle

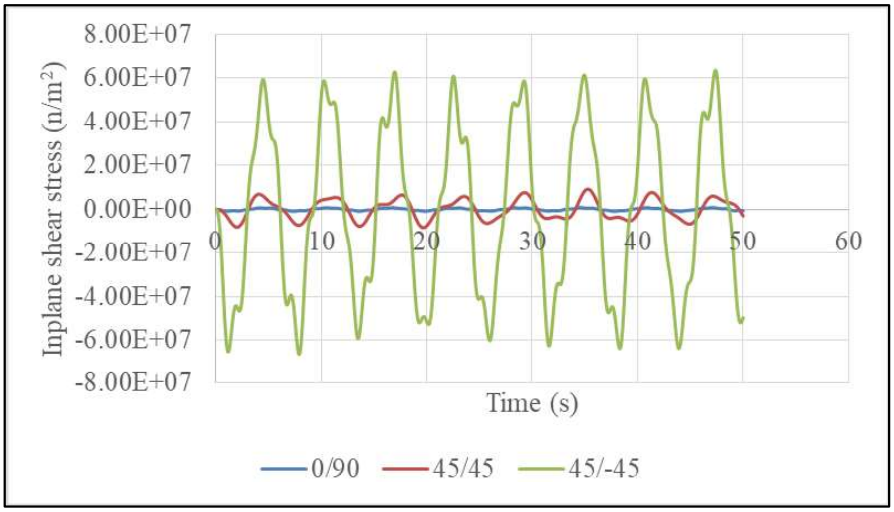

Fig. 4.56 Variation of inplane shear stress of the left tank wall (CCCC) under forcing frequency as 3 times of fundamental frequency for different ply angle

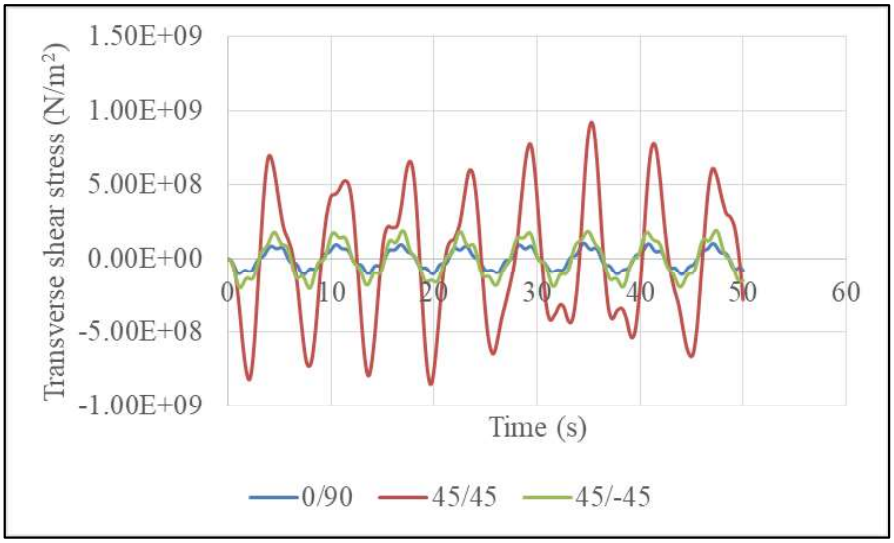

Fig. 4.57 Variation of transverse shear stress of the left tank wall (CCCC) under forcing frequency as 3 times of fundamental frequency for different ply angle

Boundary conditions of the side walls are varied as CCCC, SSSS, CCCF and SCSF and corresponding stress variations are reported for cross as well angle ply laminations. In case of normal stress values, maximum stress for cross ply lamination is obtained for SSSS boundary condition and that for angle ply (45°/-45°) lamination can be obtained for SCSF boundary condition as shown in Figs. 4.58 – 4.59. Minimum normal stress is generated for SCSF boundary condition in case of cross ply lamination but SSSS boundary condition gives minimum value for angle ply laminations.

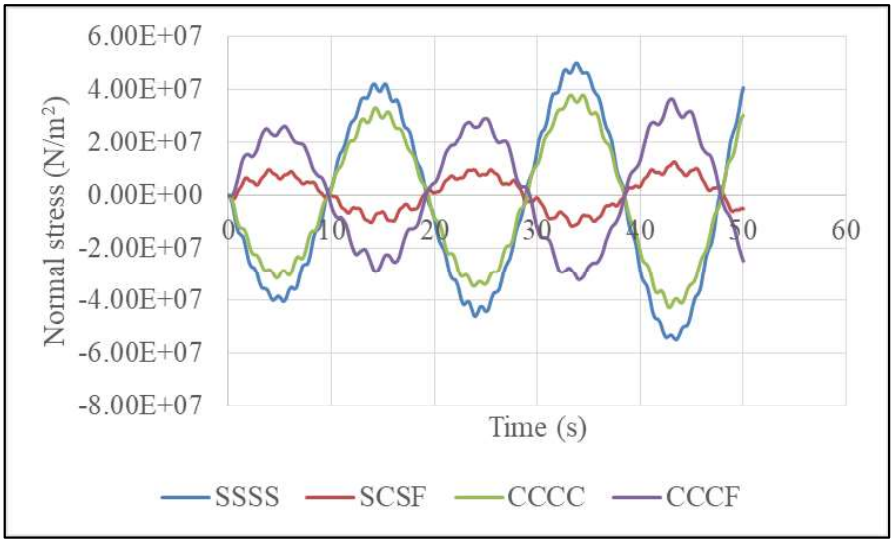

Fig. 4.58 Variation of normal stress of the left tank wall under forcing frequency as fundamental frequency for different boundary conditions (0°/90°)

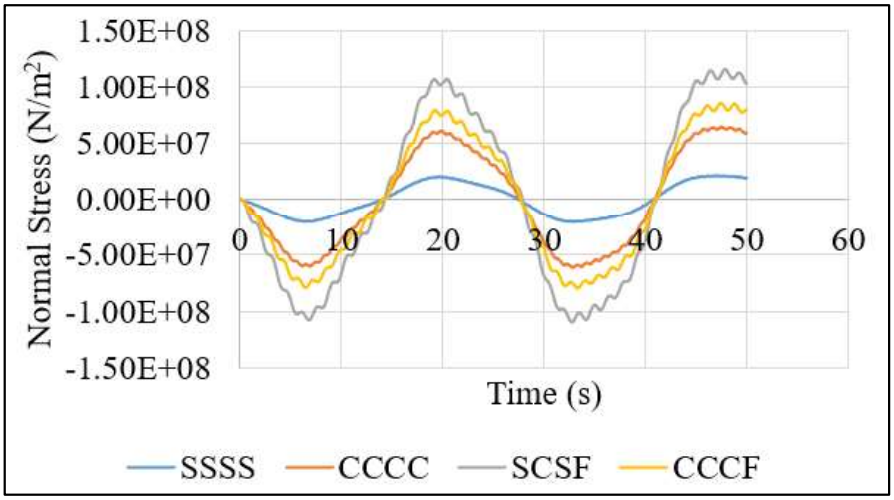

Fig. 4.59 Variation of normal stress of the left tank wall under forcing frequency as fundamental frequency for different boundary conditions (45°/-45°)

Inplane shear stress on the other hand shows different nature for varying boundary conditions as given in Figs. 4.60 – 4.61. In case of 0°/90° lamination maximum stress is generated when all the sides of the wall is clamped and SSSS being the least among the set. Inplane shear stress for angle ply anti symmetric laminations, SCSF boundary condition shows maximum stress values. SSSS shows minimum stress value, same that of cross ply lamination.

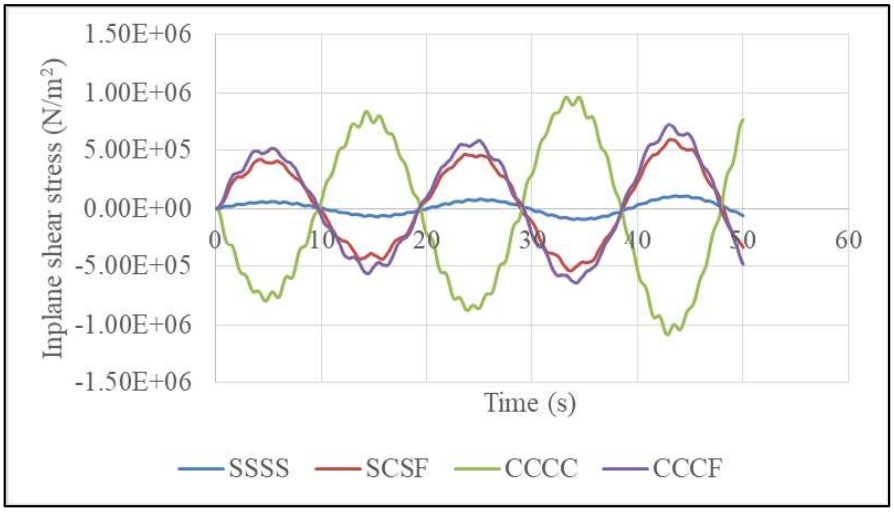

Fig. 4.60 Variation of inplane shear stress of the left tank wall under forcing frequency as fundamental frequency for different boundary conditions (0°/90°)

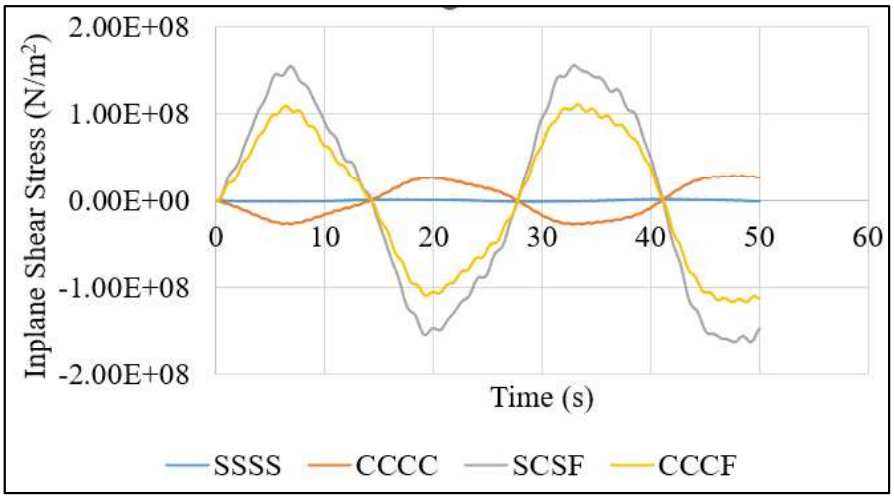

Fig. 4.61 Variation of inplane shear stress of the left tank wall under forcing frequency as fundamental frequency for different boundary conditions (45°/-45°)

Effect of boundary condition on transverse shear stress is presented at the next part in Figs. 4.62 – 4.63. The variation of stress for different boundary conditions is very much different for cross and angle ply laminations. In case of cross ply laminations, tank wall with all edges clamped shows highest stress values and plate with SSSS boundary condition gives minimum stress values. Same thing if studied for angle ply (45°/-45°) laminations, then plate with top edge free and other edges

clamped is showing highest transverse shear stress values. Simply supported and clamped plates are showing almost comparing results. Plates with edges SCSF and CCCF are more responsive in terms of transverse shear stress

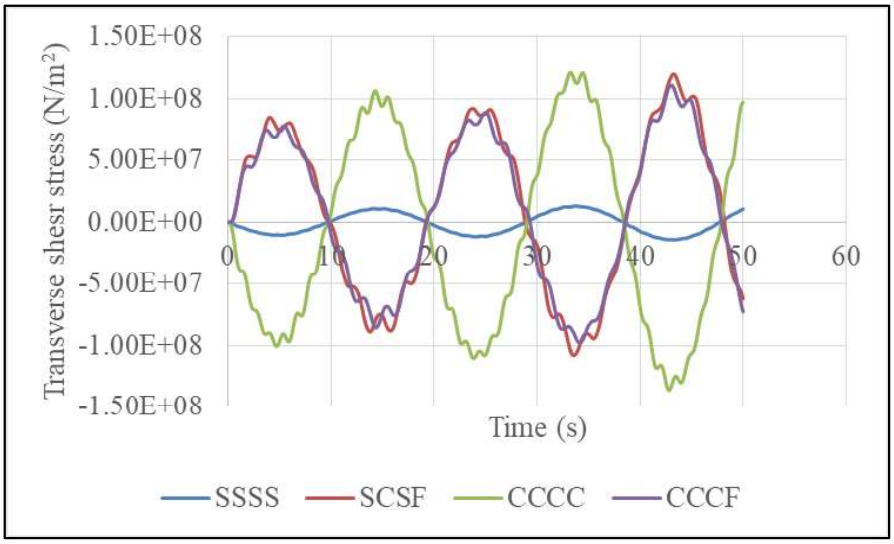

Fig. 4.62 Variation of transverse shear stress of the left tank wall under forcing frequency as fundamental frequency for different boundary conditions (0°/90°)

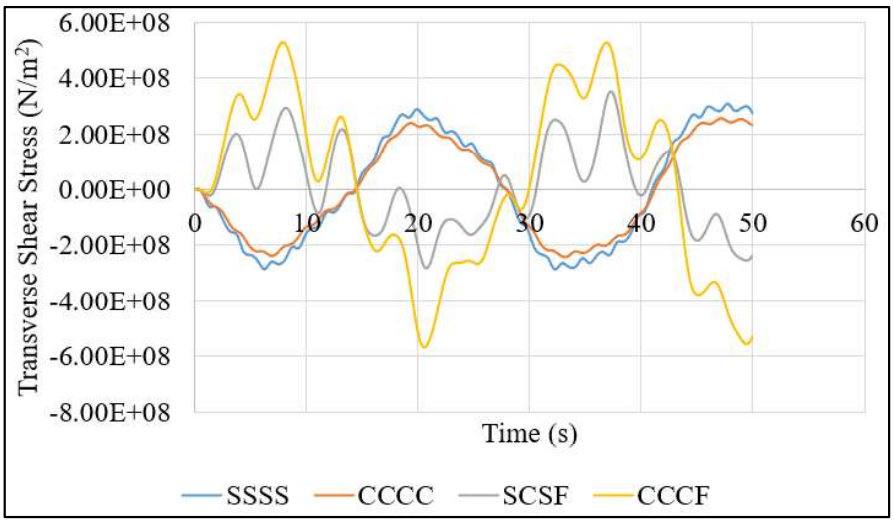

Fig. 4.63 Variation of transverse shear stress of the left tank wall under forcing frequency as fundamental frequency for different boundary conditions (45°/-45°)

Variation of stresses with increased number of ply layers is presented in the next section in Figs. 4.64 – 4.66 with 45° anti-symmetric angle ply laminations. It is observed that 2 layered plate gives

maximum normal stress and transverse shear stress values and with increment of number of ply layers, stress value decreases and becomes almost constant. Same layer variation for inplane shear stress shows increment of stress value with higher ply layer numbers. Inplane shear stress is minimum for two layered plates.

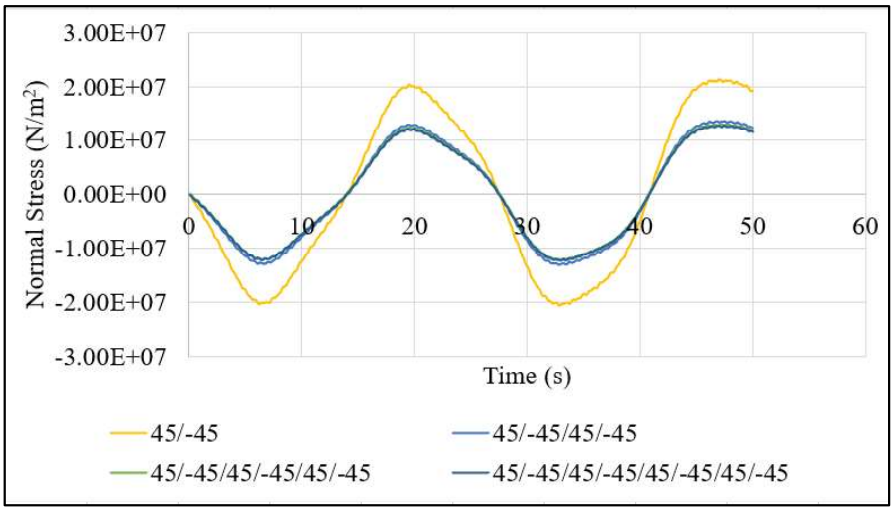

Fig. 4.64 Variation of normal stress of the left tank wall (SSSS) under forcing frequency as fundamental frequency for increasing number of layers (angle-ply laminations)

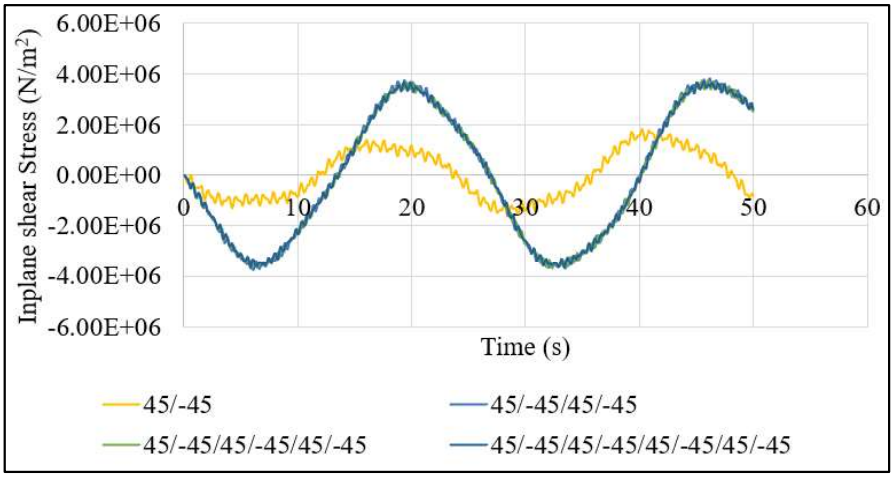

Fig. 4.65 Variation of inplane shear stress of the left tank wall (SSSS) under forcing frequency as fundamental frequency for increasing number of layers (angle-ply laminations)

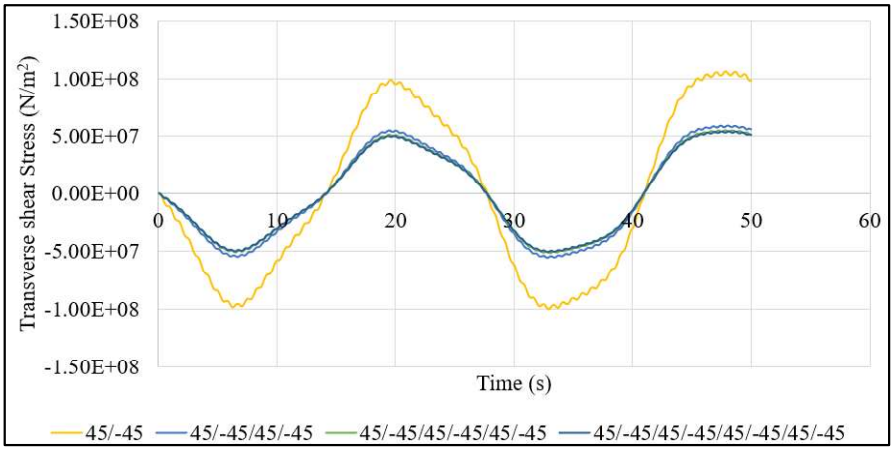

Fig. 4.66 Variation of transverse shear stress of the left tank wall (SSSS) under forcing frequency as fundamental frequency for increasing number of layers (angle-ply laminations)

Effect of geometry of the tank on stress parameters is presented in the next step. Height of the tank wall is studied and the tank is always considered full with water. The variation of normal stress for cross and angle ply laminations is shown. In case of cross ply laminations, the stress values show peak value at height 4.1m shown in Fig. 4.67 then it marginally decreases, but in case of anti-symmetric angle ply laminations (Figs. 4.68), with increment of ply angle, stress values increase. This variation is consistent in case of angle ply laminations.

Variation of inplane shear stress for cross and angle ply variations are almost same (Figs. 4.69 and 4.70) in trend only the magnitude varies. In all the cases height increment leads to increment in stress values. Transverse shear stress variation for cross ply lamination is more prominent compared to the angle ply laminations. Stress value increases with increment in tank height as shown in Figs. 4.71 and 4.72.

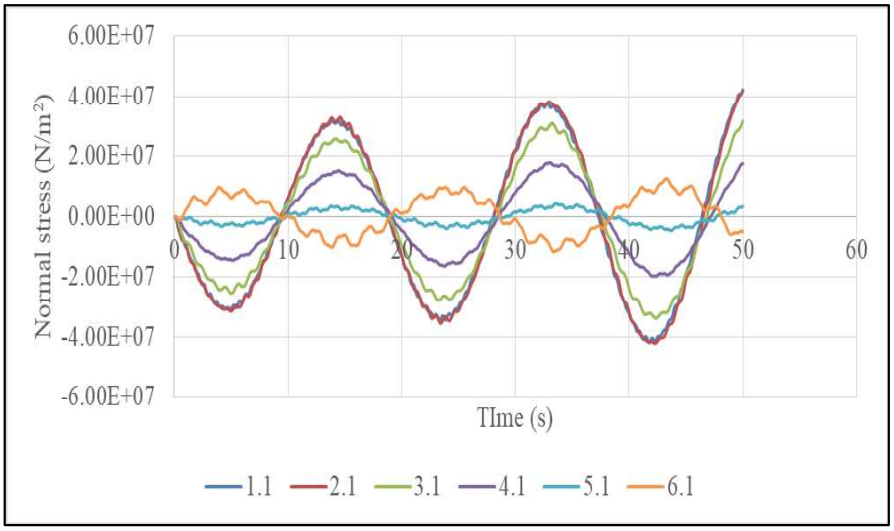

Fig. 4.67 Variation of normal stress of the left tank wall (SCSF) with fundamental frequency as the forcing frequency for increase in tank height (0°/90° laminations)

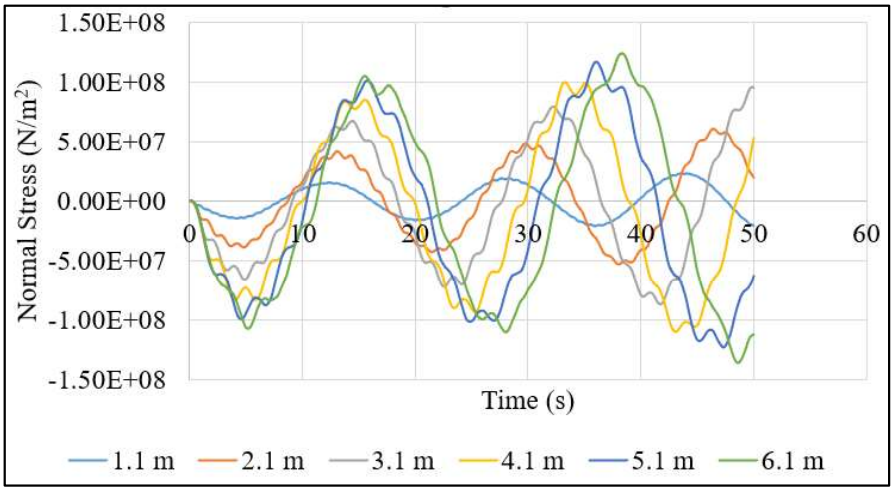

Fig. 4.68 Variation of normal stress of the left tank wall (SCSF) with fundamental frequency as the forcing frequency for increase in tank height (45°/-45° laminations)

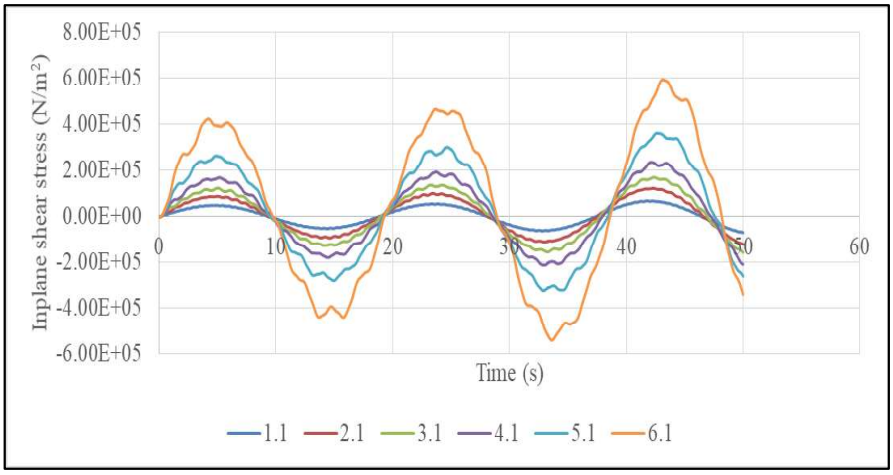

Fig. 4.69 Variation of inplane shear stress of the left tank wall (SCSF) with fundamental frequency as the forcing frequency for increase in tank height (0°/90° laminations)

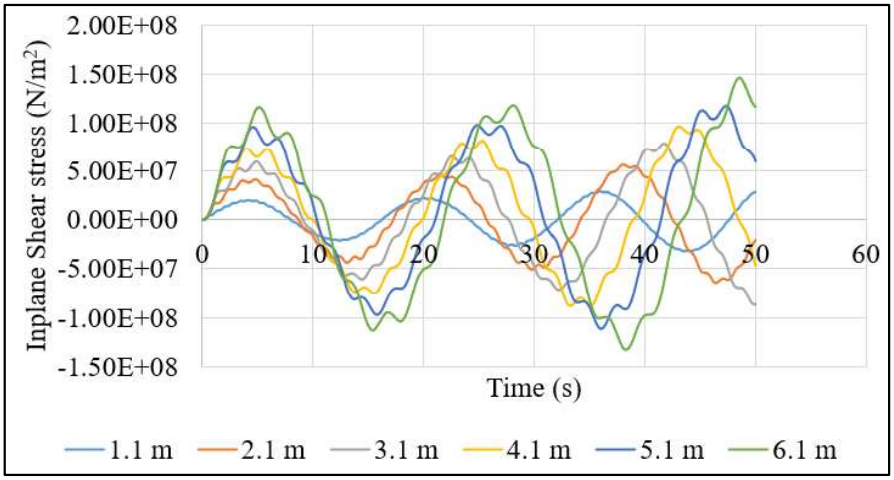

Fig. 4.70 Variation of inplane shear stress of the left tank wall (SCSF) with fundamental frequency as the forcing frequency for increase in tank height (45°/-45° laminations)

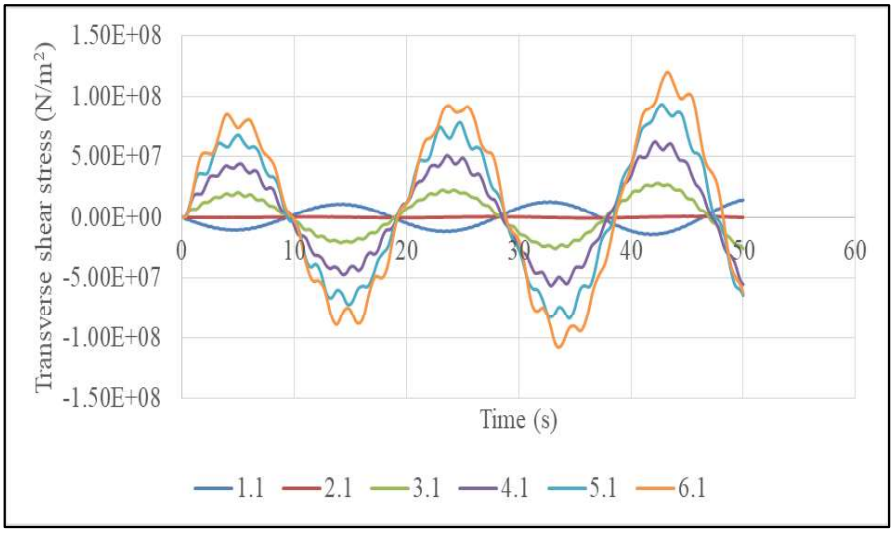

Fig. 4.71 Variation of transverse shear stress of the left tank wall (SCSF) with fundamental frequency as the forcing frequency for increase in tank height (0°/0° laminations)

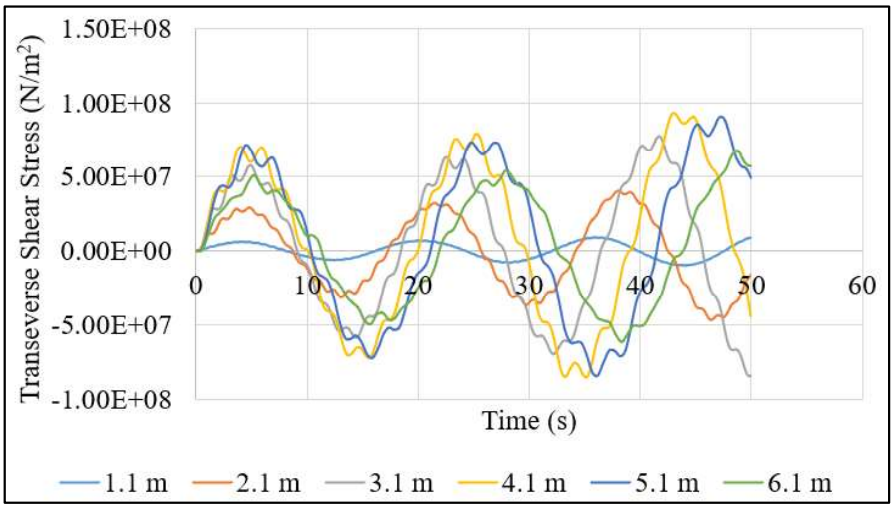

Fig. 4.72 Variation of transverse shear stress of the left tank wall (SCSF) with fundamental frequency as the forcing frequency for increase in tank height (45°/-45° laminations)

The tank length is then varied in steps from 10 m to 40 m and corresponding response of left tank wall is studied in Figs. 4.73 – 4.78. In all the cases, length increment leads to decrease in normal stress for cross ply lamination and remains almost same for angle ply laminations. Inplane shear stress increases with tank length for cross ply lamination but remains almost unchanged for

angle ply laminations. Transverse shear stress increases both in case of cross as well angle ply laminations.

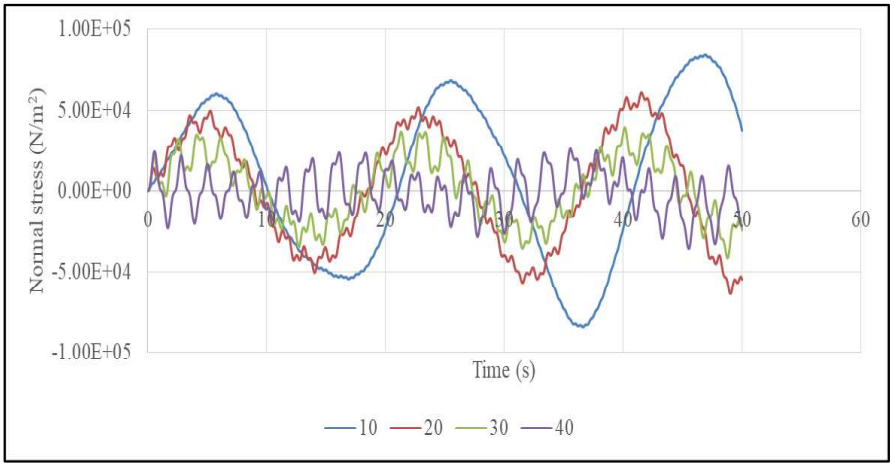

Fig. 4.73 Variation of normal stress of the left tank wall (SCSF) with fundamental frequency as the forcing frequency for increase in tank length (0°/90° laminations)

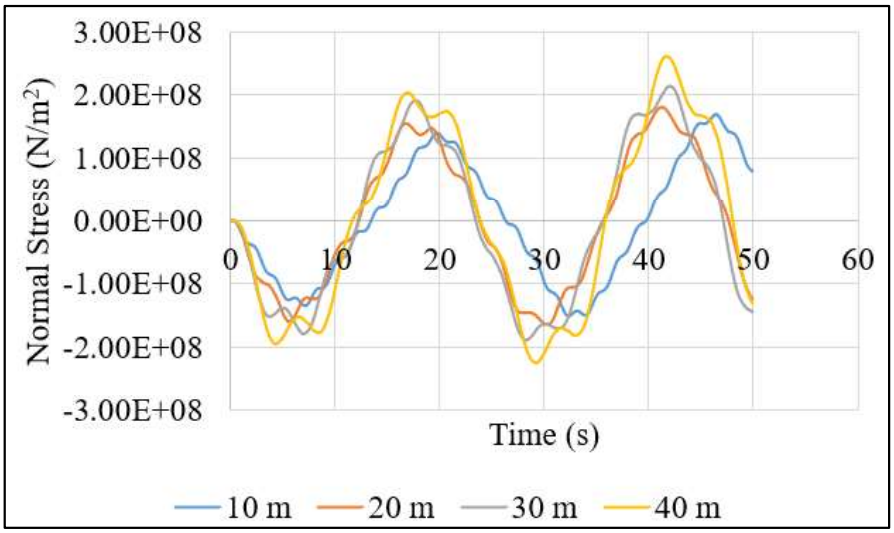

Fig. 4.74 Variation of normal stress of the left tank wall (SCSF) with fundamental frequency as the forcing frequency for increase in tank length (45°/-45° laminations)

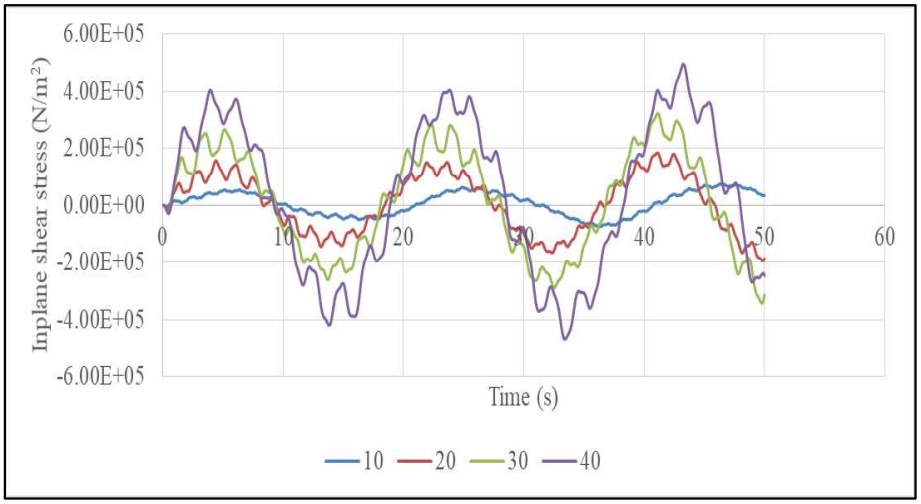

Fig. 4.75 Variation of inplane shear stress of the left tank wall (SCSF) with fundamental frequency as the forcing frequency for increase in tank length (0°/90° laminations)

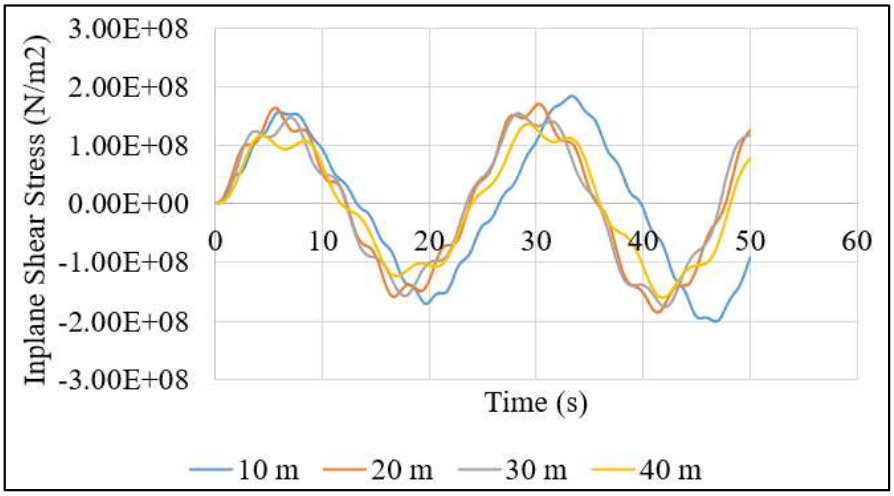

Fig. 4.76 Variation of inplane shear stress of the left tank wall (SCSF) with fundamental frequency as the forcing frequency for increase in tank length (45°/-45° laminations)

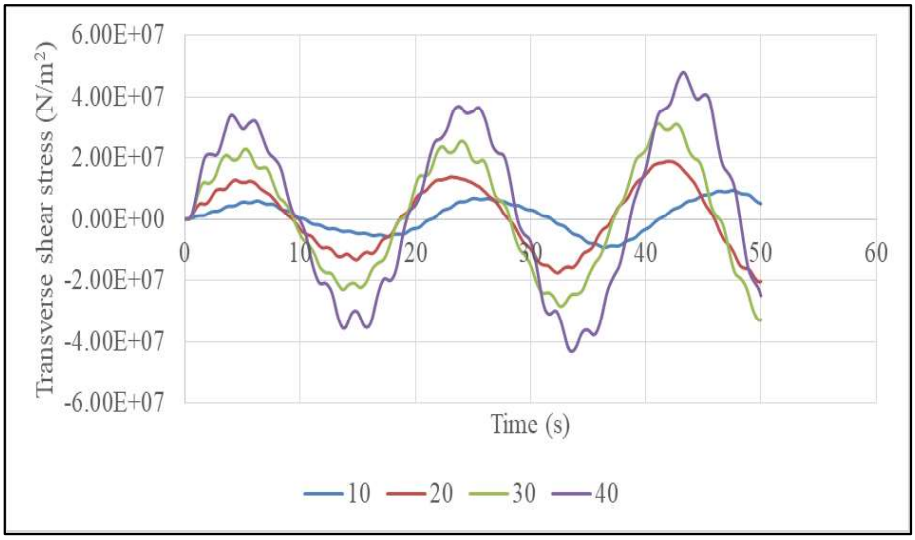

Fig. 4.77 Variation of transverse shear stress of the left tank wall (SCSF) with fundamental frequency as the forcing frequency for increase in tank length (0°/90° laminations)

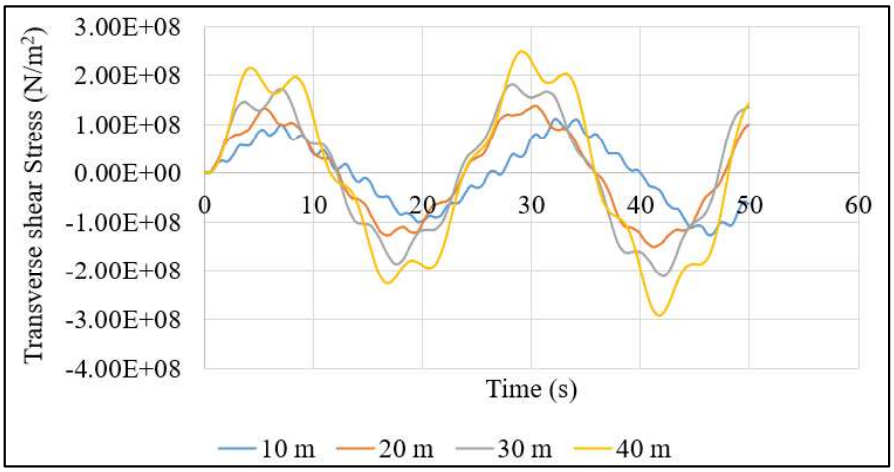

Fig. 4.78 Variation of transverse shear stress of the left tank wall (SCSF) with fundamental frequency as the forcing frequency for increase in tank length (45°/-45° laminations)

The width of the tank is carried in steps from 10 m to 40 m and the results are shown in Figs. 4.79 – 4.84. It is observed that for normal stress, inplane shear stress and transverse shear stress magnitude increases with increase in width of the tank for both cross and angle ply laminations.

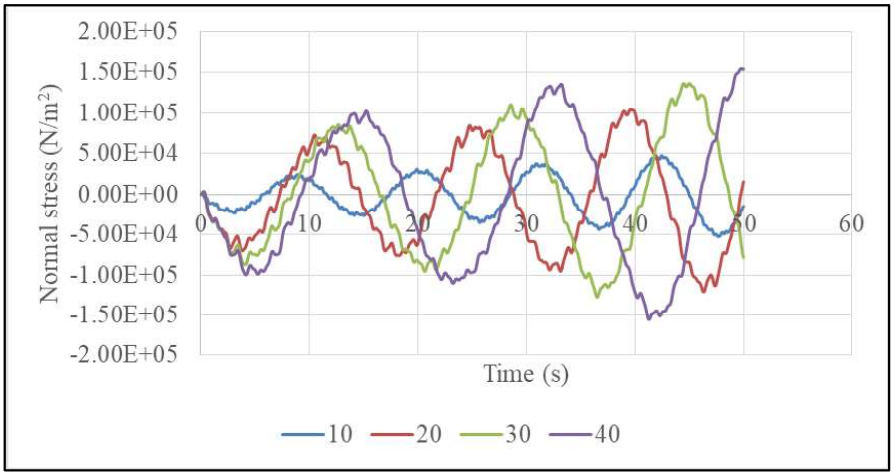

Fig. 4.79 Variation of normal stress of the left tank wall (SCSF) with fundamental frequency as the forcing frequency for increase in tank width (0°/90° laminations)

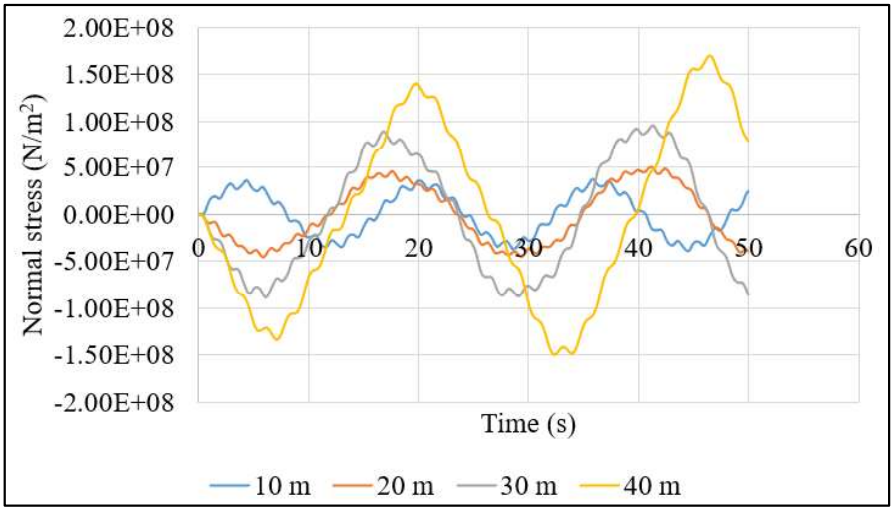

Fig. 4.80 Variation of normal stress of the left tank wall (SCSF) with fundamental frequency as the forcing frequency for increase in tank width (45°/-45° laminations)

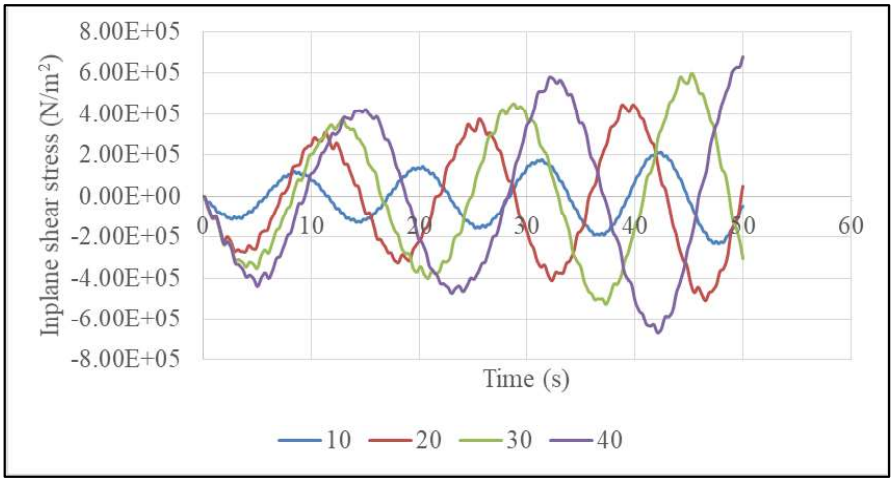

Fig. 4.81 Variation of inplane shear stress of the left tank wall (SCSF) with fundamental frequency as the forcing frequency for increase in tank width (0°/90° laminations)

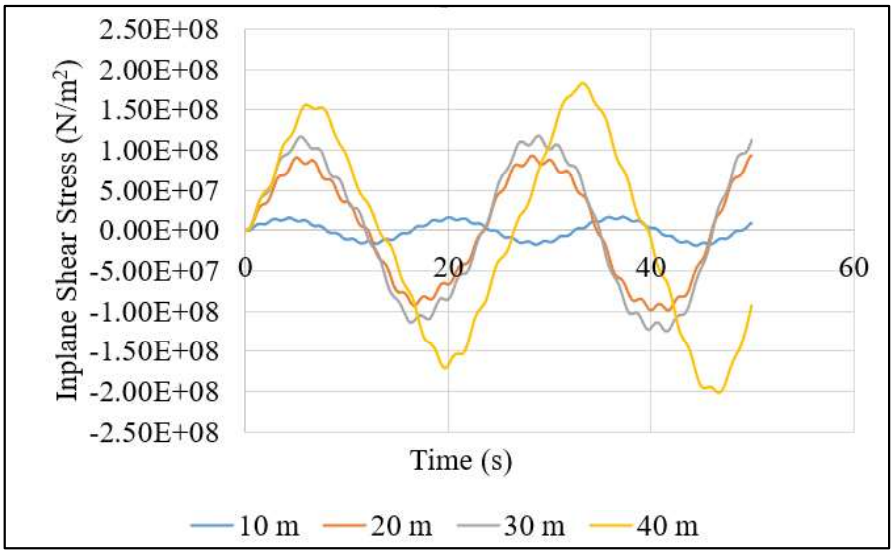

Fig. 4.82 Variation of inplane shear stress of the left tank wall (SCSF) with fundamental frequency as the forcing frequency for increase in tank width (45°/-45° laminations)

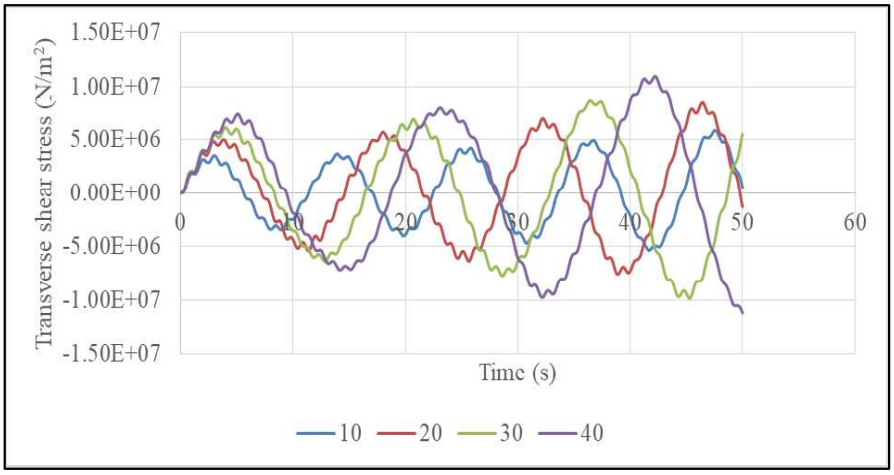

Fig. 4.83 Variation of transverse shear stress of the left tank wall (SCSF) with fundamental frequency as the forcing frequency for increase in tank width (0°/90° laminations)

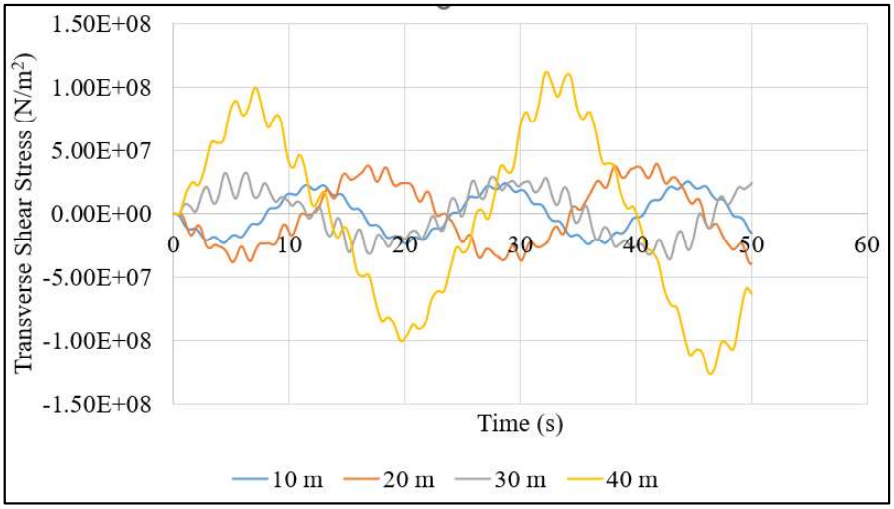

Fig. 4.84 Variation of transverse shear stress of the left tank wall (SCSF) with fundamental frequency as the forcing frequency for increase in tank width (45°/-45° laminations)

4.3.5 Analysis of contour plot of various stresses developed across different layers in the tank wall for the coupled system

The stress developed at different layers in the plate under dynamic loading is presented in the following part. Layer numbers considered in the present study are 2 layer (45°/-45°, 45°/45°, 0°/90°), 4 layer (0°/90°/90°/0°, 0°/90°/0°/90°, 45°/-45°/-45°/45°, 45°/-45°/45°/-45°) and 6 layer

(45°/-45°/45°/45°/-45°/45°). Normal stress, inplane shear stress and transvese shear stress developed at each layer for left tank wall with all sides clamped are presented. The stress is calculated at 8.25s as it is mostly peak for the first cycle. Finally comparative study of various stresses are reported.

The study starts with normal stress contour for 6 layer, 4 layer and 2 layered plate for cross and angle ply laminations under fundamental frequency as forcing frequency. Respective contour plots are shown in Fig. 4.85 to 4.92. Angle ply 45° laminations shows diagonal stress variation as expected. Corners carry higher normal stress and middle portions has lower stress value. Cross ply lamination shows on the other hand higher stress band variation paraller to base at upper portion of the plate. Higher stresses are present at the opposite corners. Rest of the contour plots are similar to higher ply layer variations.

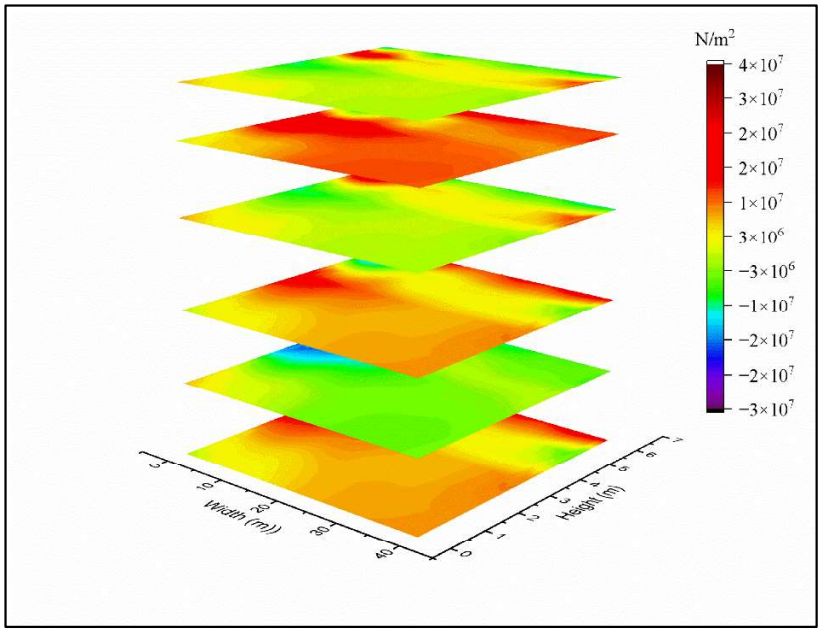

Fig. 4.85 Variation of normal stress of the left tank wall (CCCC) with fundamental frequency as the forcing frequency for various layers (45/-45/45/45/-45/45 laminations)

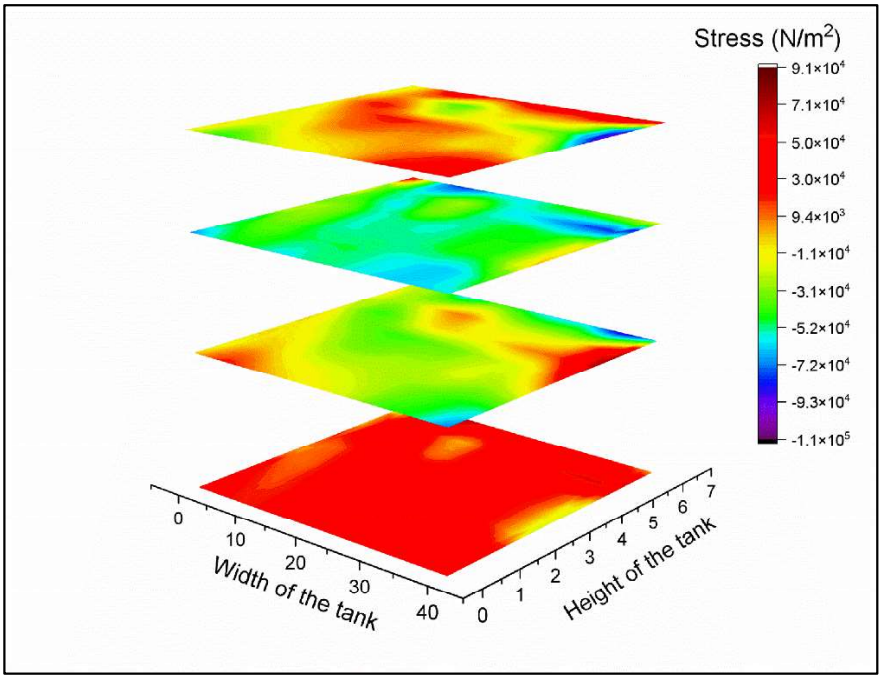

Fig. 4.86 Variation of normal stress of the left tank wall (CCCC) with fundamental frequency as the forcing frequency for various layers (45/-45/45/-45 laminations)

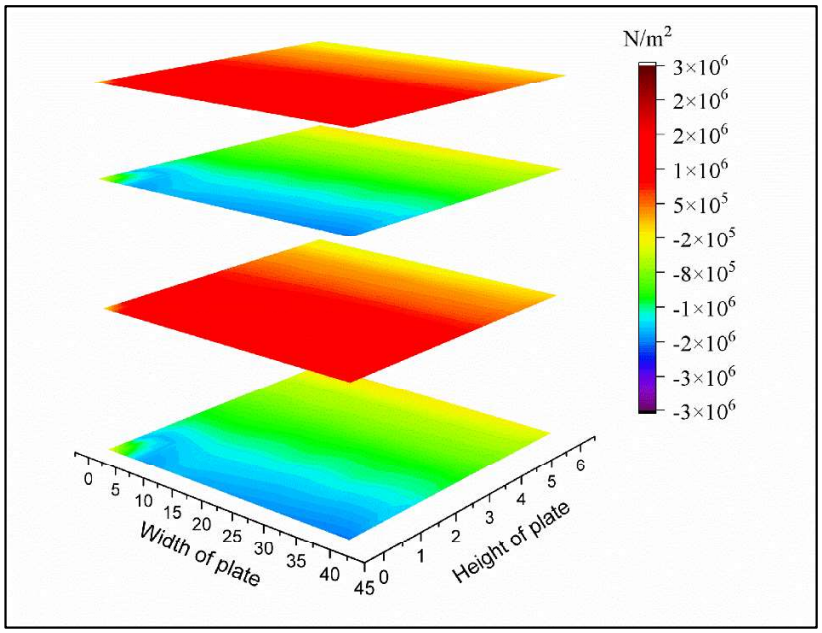

Fig. 4.87 Variation of normal stress of the left tank wall (CCCC) with fundamental frequency as the forcing frequency for various layers (45/-45/-45/45 laminations)

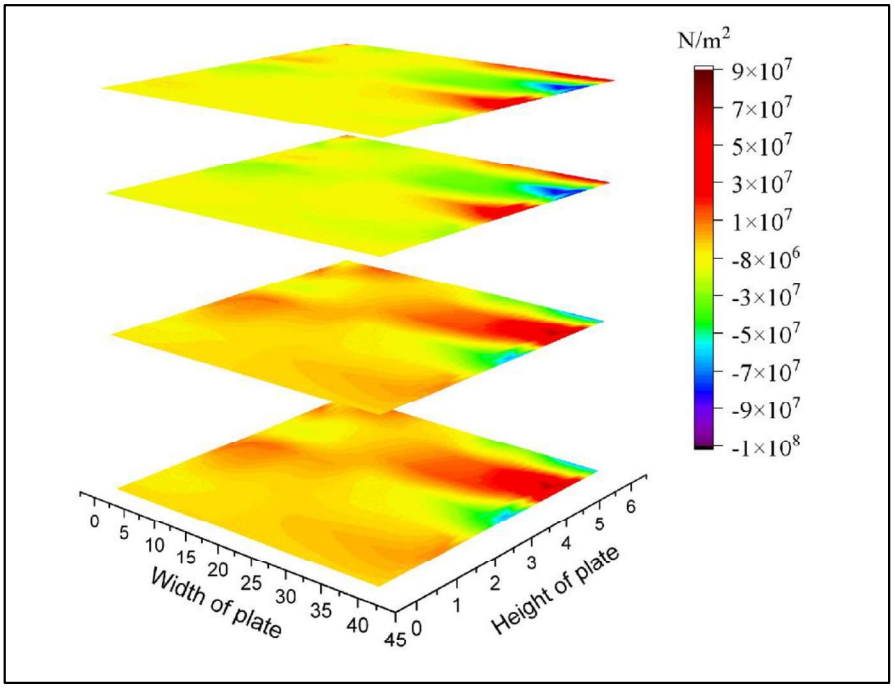

Fig. 4.88 Variation of normal stress of the left tank wall (CCCC) with fundamental frequency as the forcing frequency for various layers (0/90/0/90 laminations)

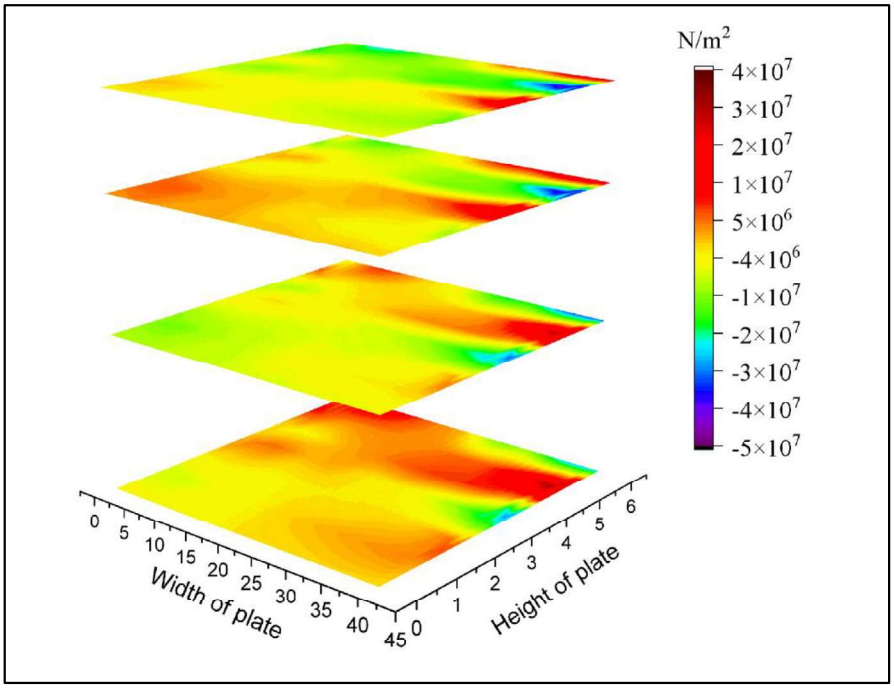

Fig. 4.89 Variation of normal stress of the left tank wall (CCCC) with fundamental frequency as the forcing frequency for various layers (0/90/90/0 laminations)

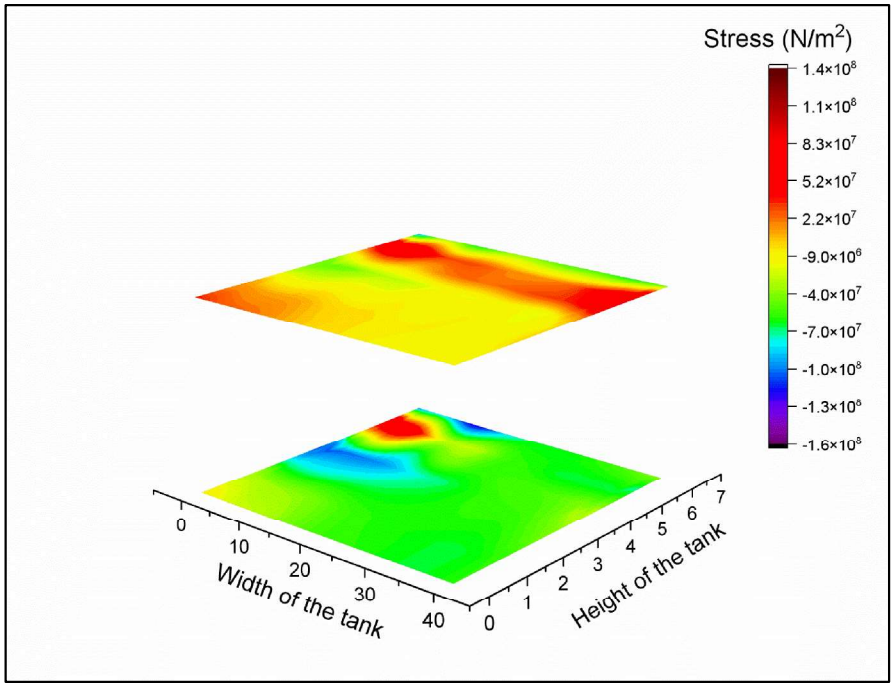

Fig. 4.90 Variation of normal stress of the left tank wall (CCCC) with fundamental frequency as the forcing frequency for various layers (45/-45 laminations)

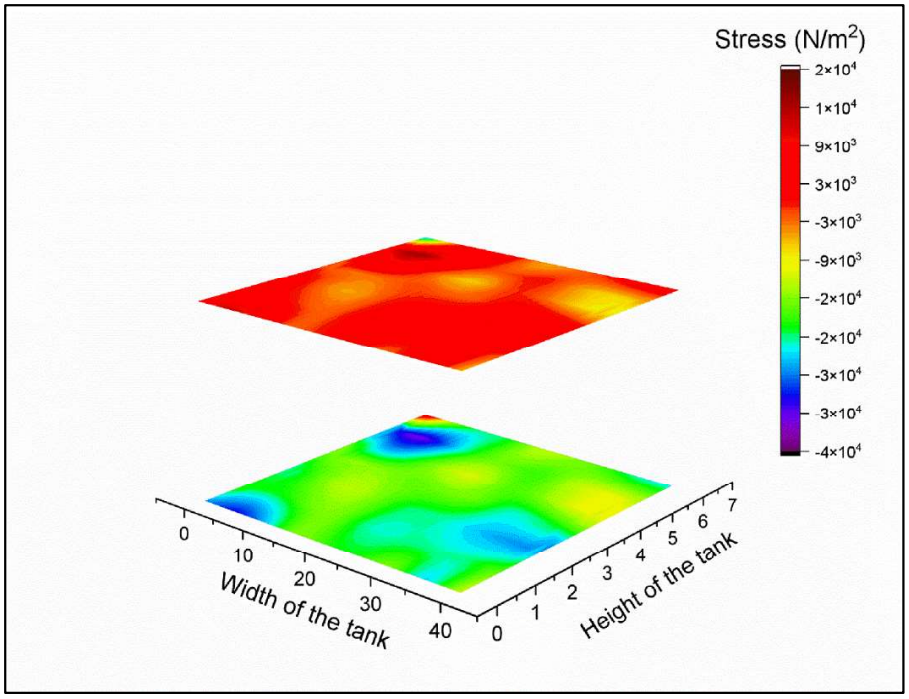

Fig. 4.91 Variation of normal stress of the left tank wall (CCCC) with fundamental frequency as the forcing frequency for various layers (45/45 laminations)

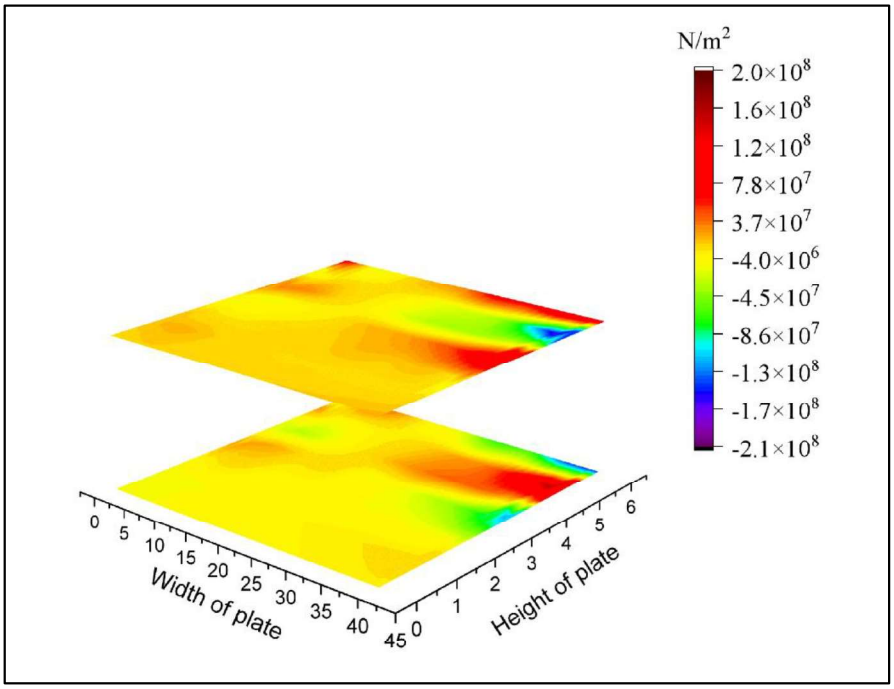

Fig. 4.92 Variation of normal stress of the left tank wall (CCCC) with fundamental frequency as the forcing frequency for various layers (0/90 laminations)

Variation of inplane shear stress variation across various layers is presented in the next part from Fig. 4.93 to 4.100. In case of 45° 4-layer anti symmetric lamination, higher stress values can be obtained in the outer layers and inner layers have lower stress values, also higher stress values are concentrated within the central portion of the plate. 45° four-layer symmetric lamination shows lower stress band along the diagonal and maximum stress is concentrated at the bottom right corners. Cross ply lamination shows lower stress band parallel to the base at the upper portion of the plate and higher stress is concentrated at the base portions. Otherwise, as a whole the plate carries lower inplane shear stress. 2 layer cross and angle play lamination shows similar stress contour variation that of four layered plate and also 8 layered 45° laminated plate gives similar result that of lower number of layers.

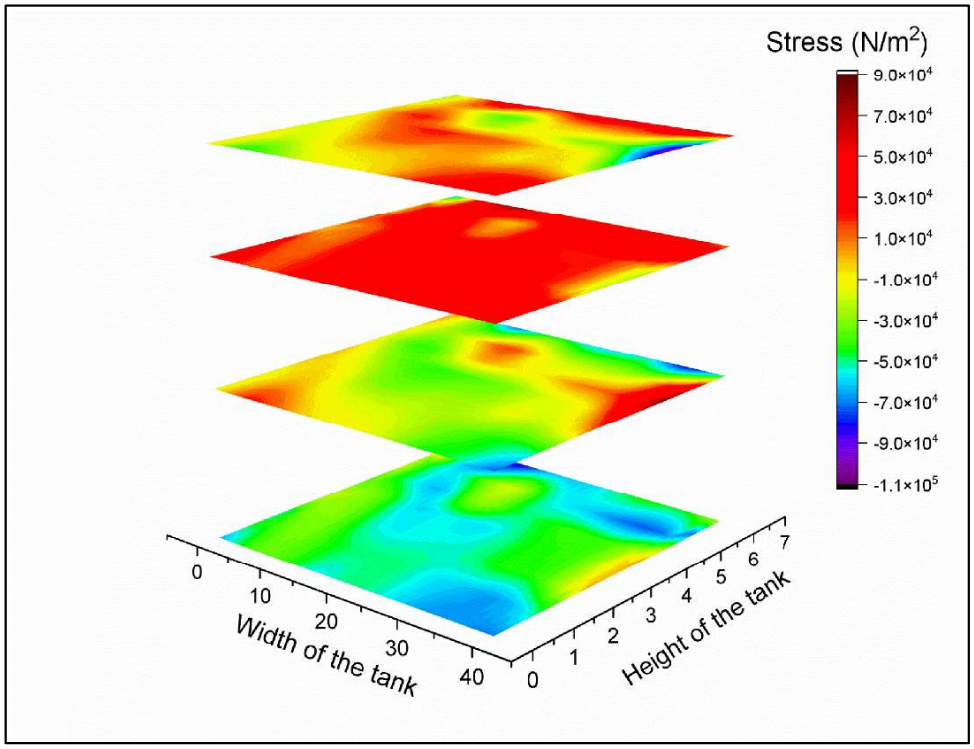

Fig. 4.93 Variation of inplane shear stress of the left tank wall (CCCC) with fundamental frequency as the forcing frequency for various layers (45/-45/45/-45 laminations)

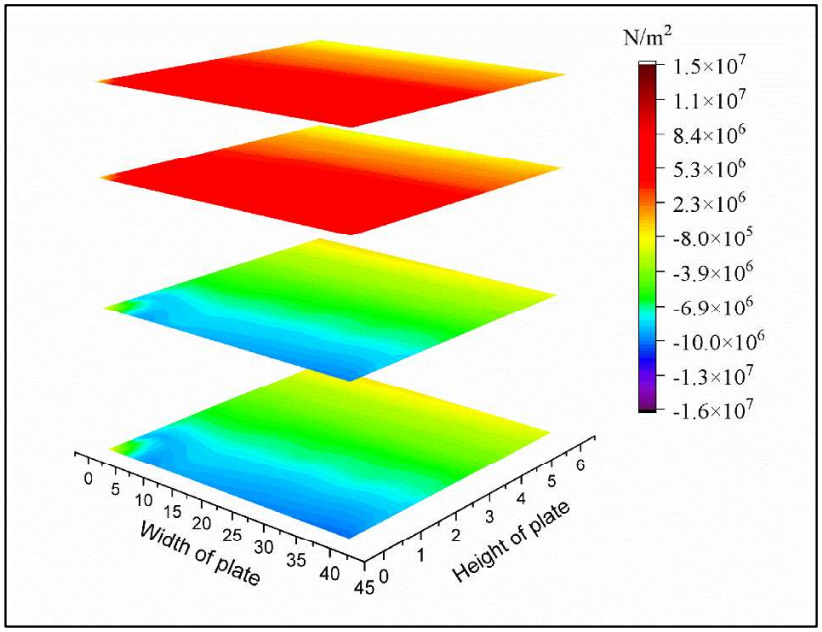

Fig. 4.94 Variation of inplane shear stress of the left tank wall (CCCC) with fundamental frequency as the forcing frequency for various layers (45/-45/-45/45 laminations)

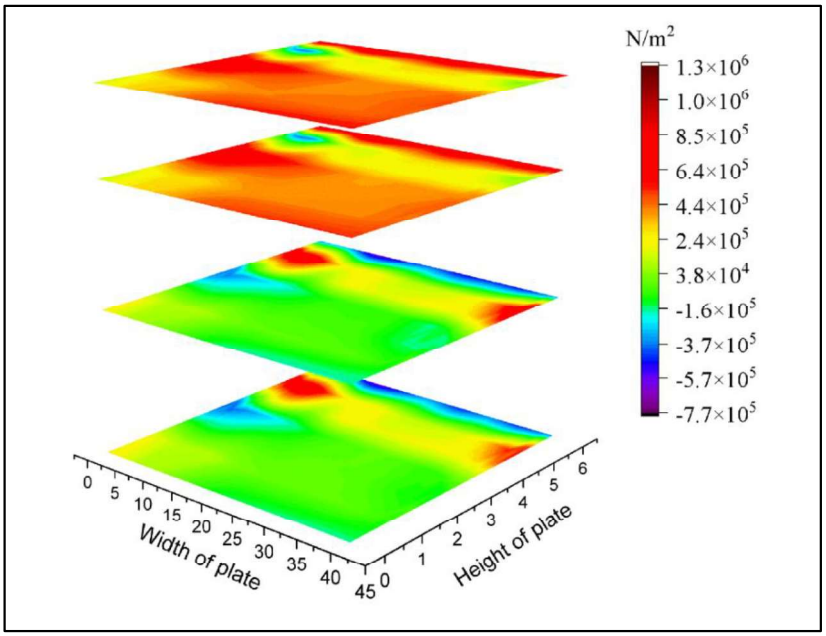

Fig. 4.95 Variation of inplane shear stress of the left tank wall (CCCC) with fundamental frequency as the forcing frequency for various layers (0/90/0/90 laminations)

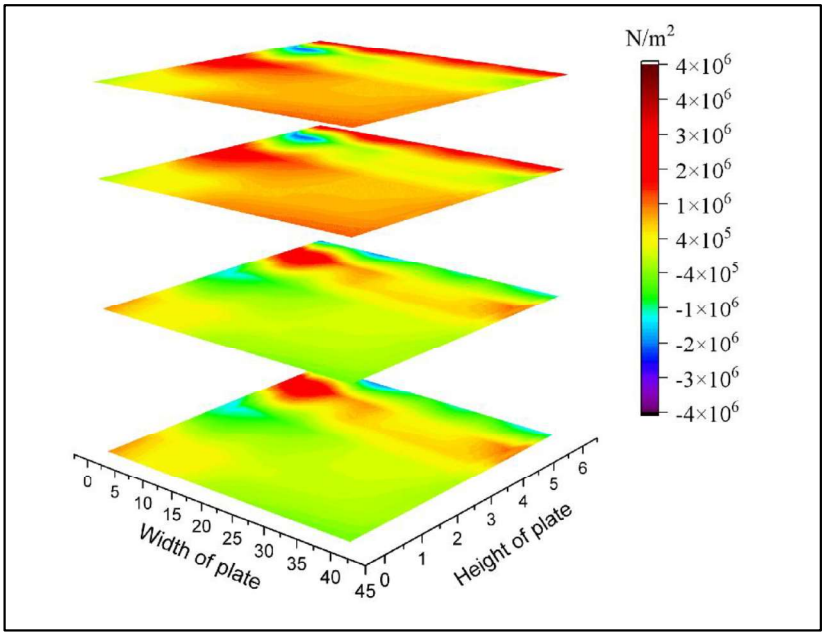

Fig. 4.96 Variation of inplane shear stress of the left tank wall (CCCC) with fundamental frequency as the forcing frequency for various layers (0/90/90/0 laminations)

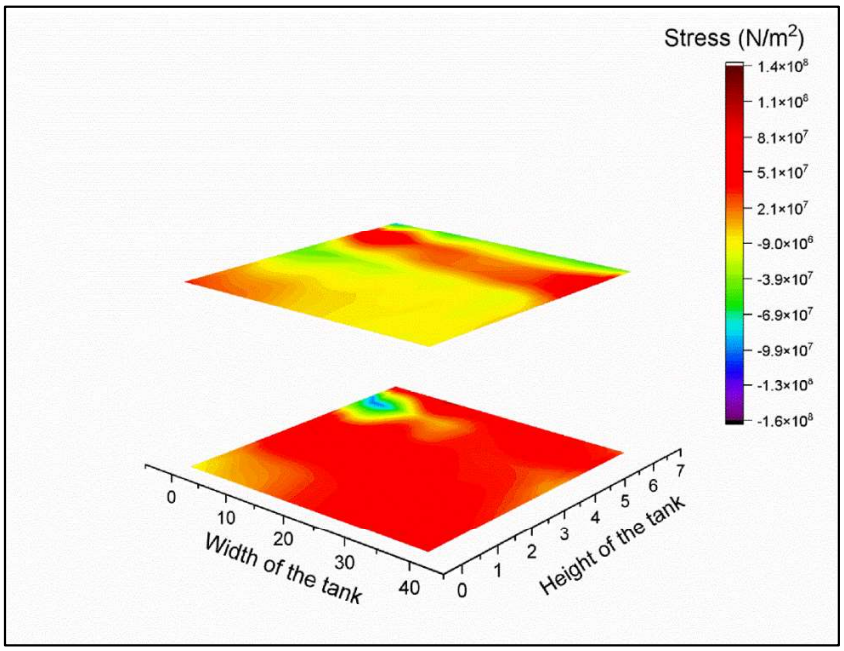

Fig. 4.97 Variation of inplane shear stress of the left tank wall (CCCC) with fundamental frequency as the forcing frequency for various layers (45/-45 laminations)

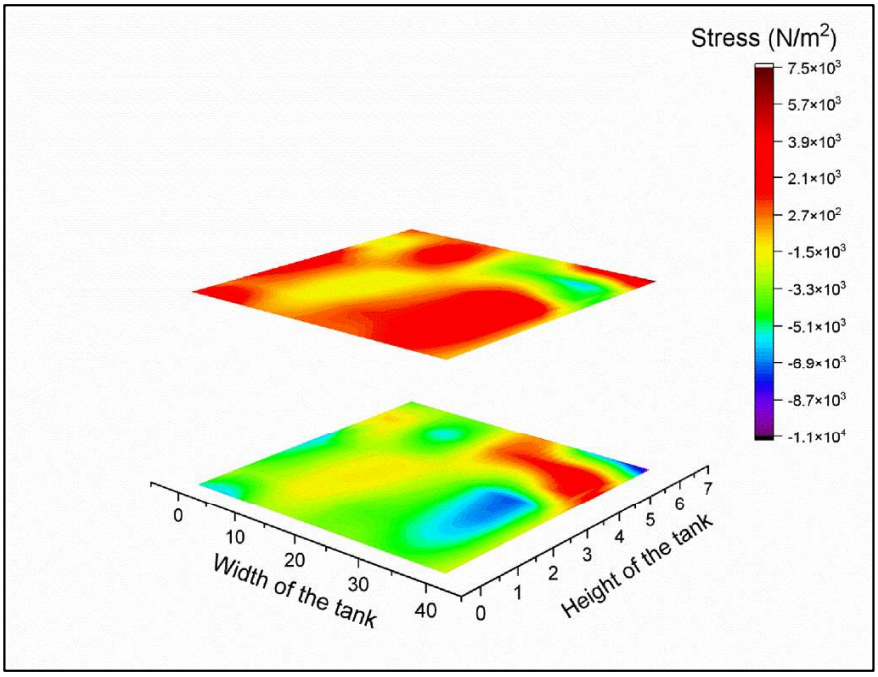

Fig. 4.98 Variation of inplane shear stress of the left tank wall (CCCC) with fundamental frequency as the forcing frequency for various layers (45/45 laminations)

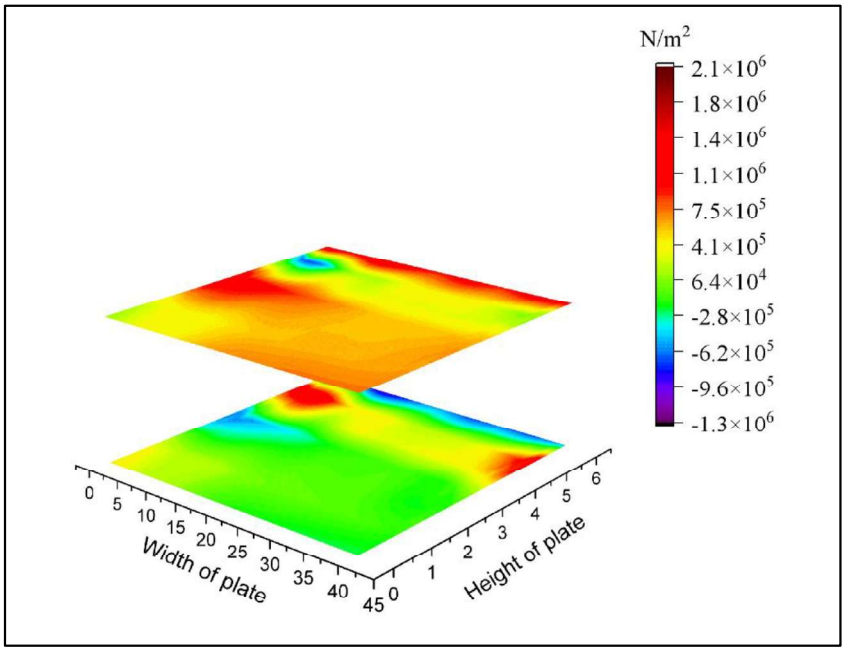

Fig. 4.99 Variation of inplane shear stress of the left tank wall (CCCC) with fundamental frequency as the forcing frequency for various layers (0/90 laminations)

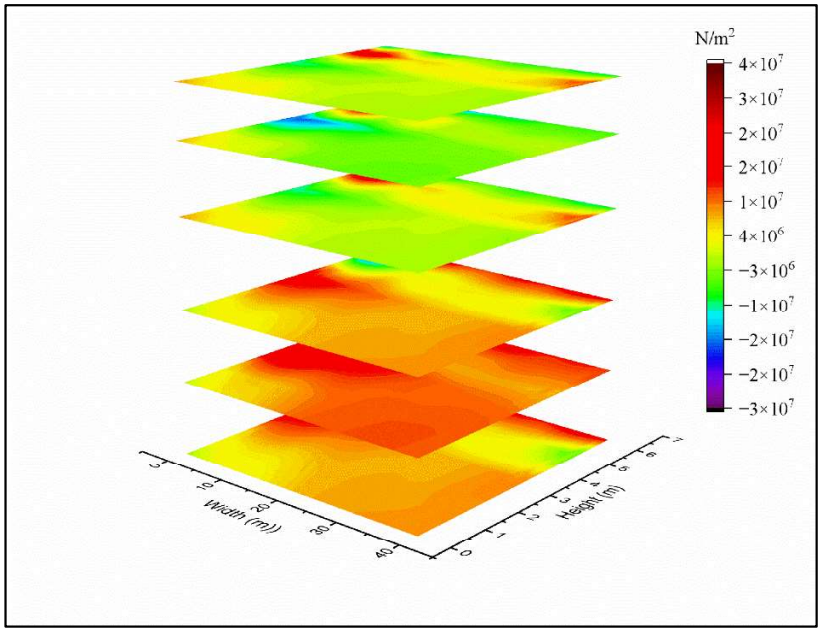

Fig. 4.100 Variation of inplane shear stress of the left tank wall (CCCC) with fundamental frequency as the forcing frequency for various layers (45/-45/45/45/-45/45 laminations)

Finally, the variation of transverse shear stress across various layers in the left wall is presented from Fig. 4.101 to 4.108. Stress contour for different layers is identical for transverse shear deformation except for 45° anti symmetric lamination. Alternate layers show similar pattern. In this case, top right corner shows higher stress values. 45° symmetric variation shows higher stress band in the diagonal direction throughout all the layer. 0°/90° lamination shows higher stress band parallel to its base near the top surface but at the top surface stress value is less than the maximum value. 2-layer 45° laminated plate shows higher stress at the left of the top and bottom corner of the plate for 45° and top right corner for -45° layer. Rest of the stress contours for 2-layer plate is same as the 4-layer plate. 6-layer 45° symmetric lamination also shows similar contour for 4-layer plate.

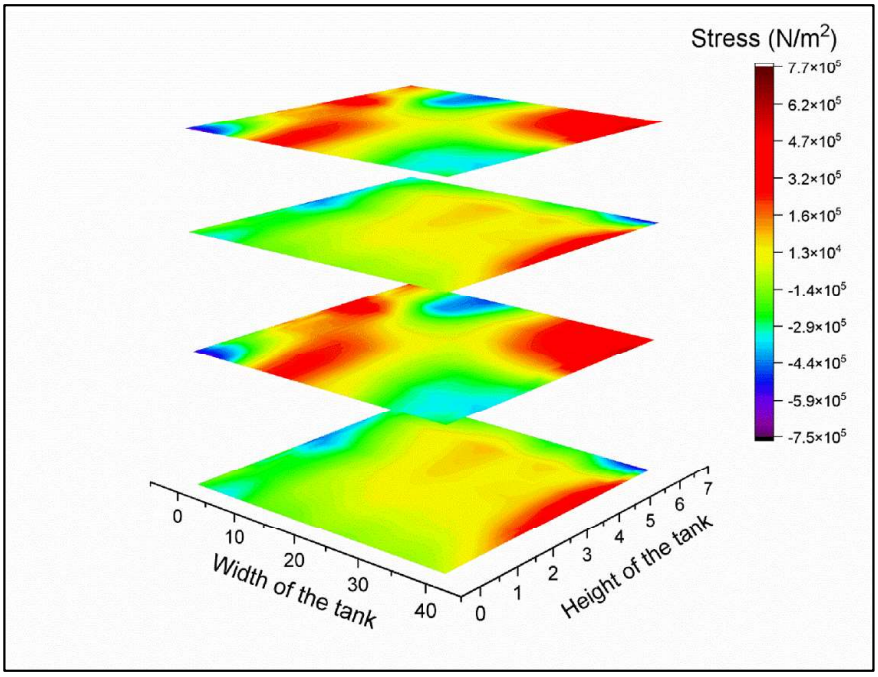

Fig. 4.101 Variation of transverse shear stress of the left tank wall (CCCC) with fundamental frequency as the forcing frequency for various layers (45/-45/45/-45 laminations)

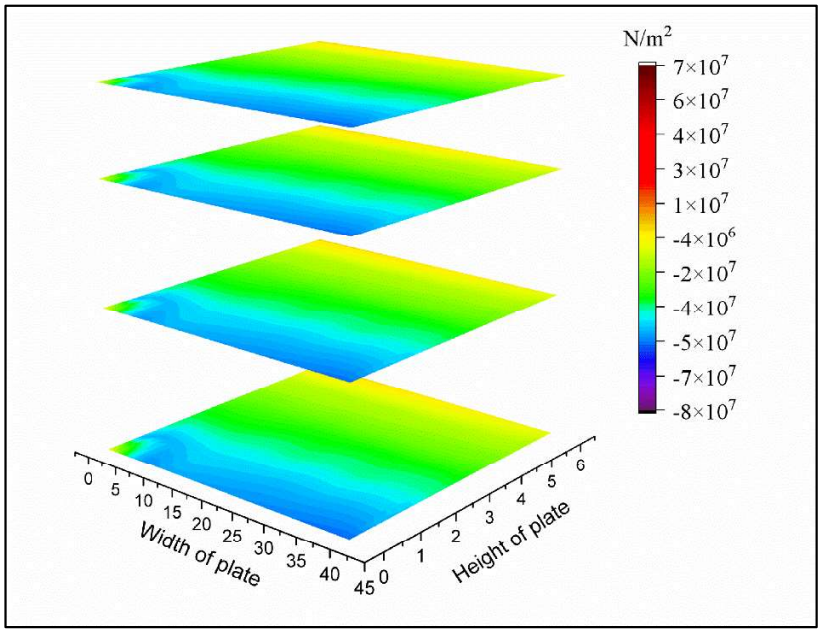

Fig. 4.102 Variation of transverse shear stress of the left tank wall (CCCC) with fundamental frequency as the forcing frequency for various layers (45/-45/-45/45 laminations)

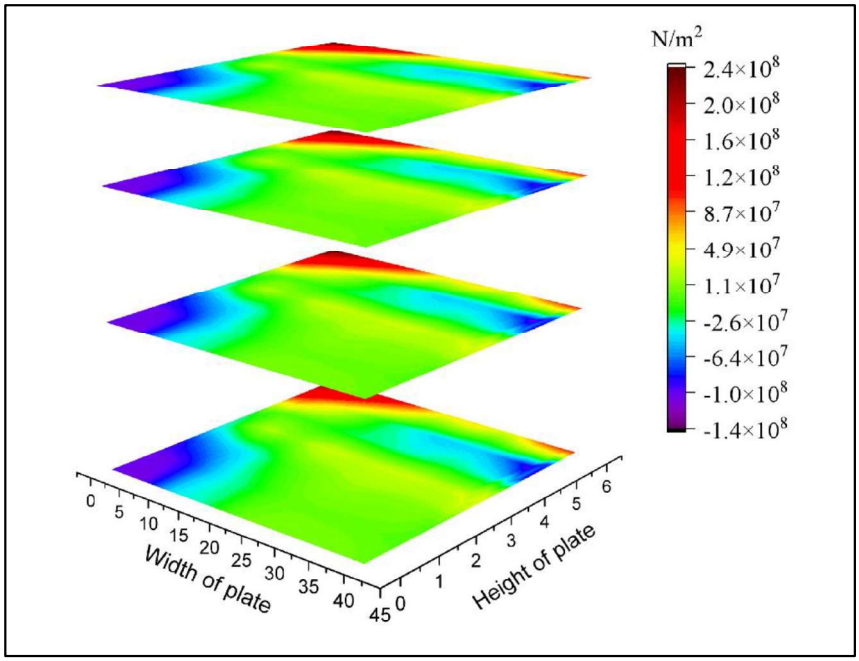

Fig. 4.103 Variation of transverse shear stress of the left tank wall (CCCC) with fundamental frequency as the forcing frequency for various layers (0/90/0/90 laminations)

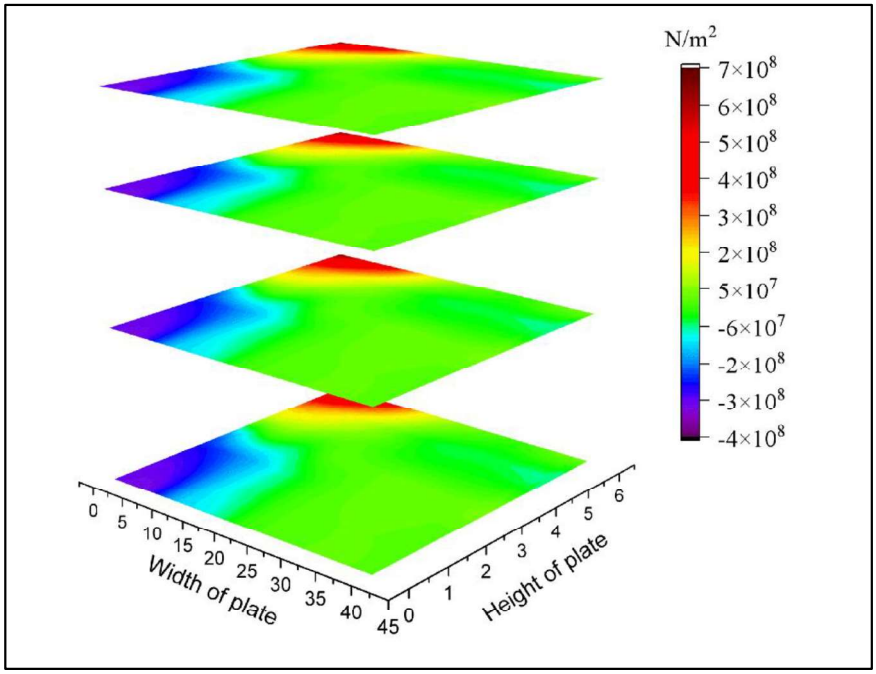

Fig. 4.104 Variation of transverse shear stress of the left tank wall (CCCC) with fundamental frequency as the forcing frequency for various layers (0/90/90/0 laminations)

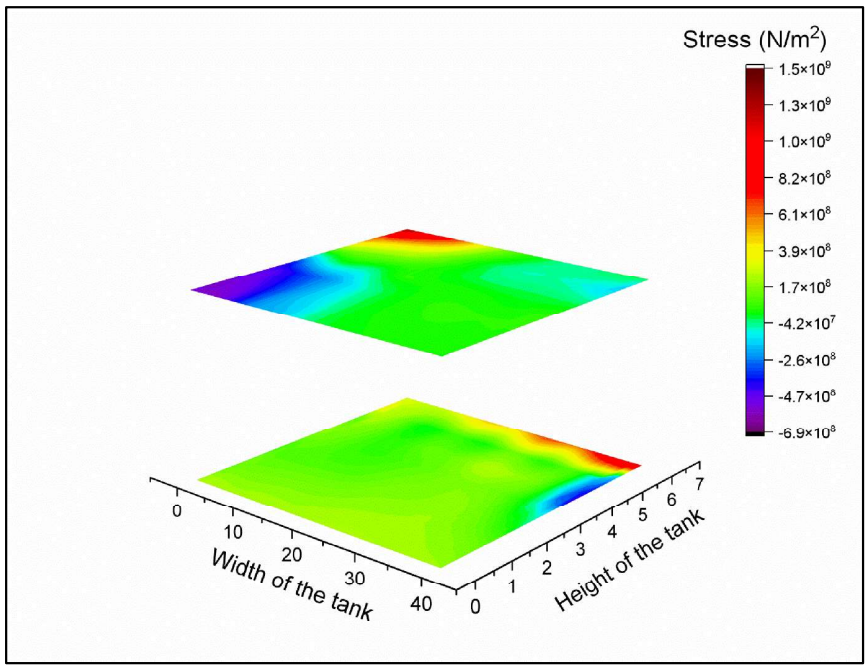

Fig. 4.105 Variation of transverse shear stress of the left tank wall (CCCC) with fundamental frequency as the forcing frequency for various layers (45/-45 laminations)

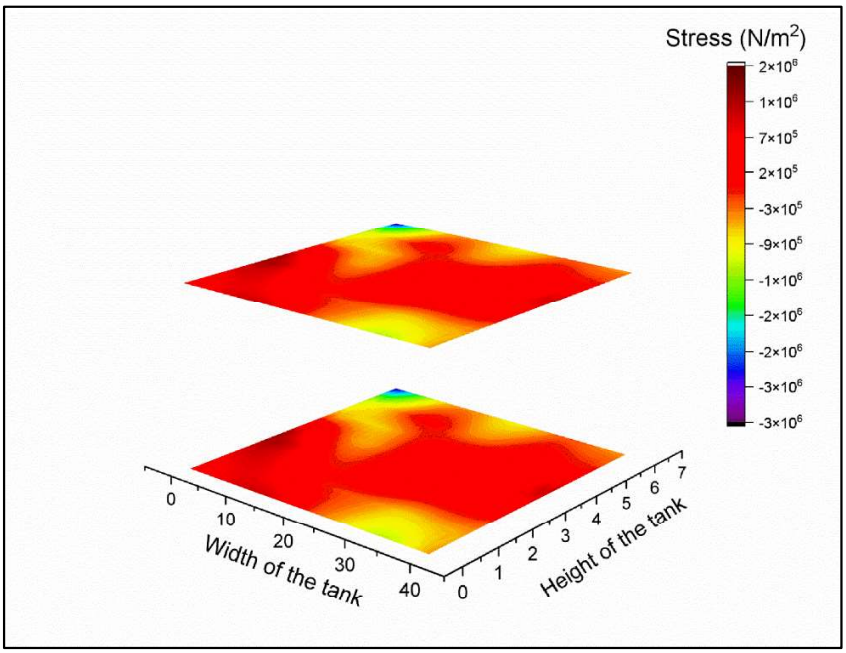

Fig. 4.106 Variation of transverse shear stress of the left tank wall (CCCC) with fundamental frequency as the forcing frequency for various layers (45/45 laminations)

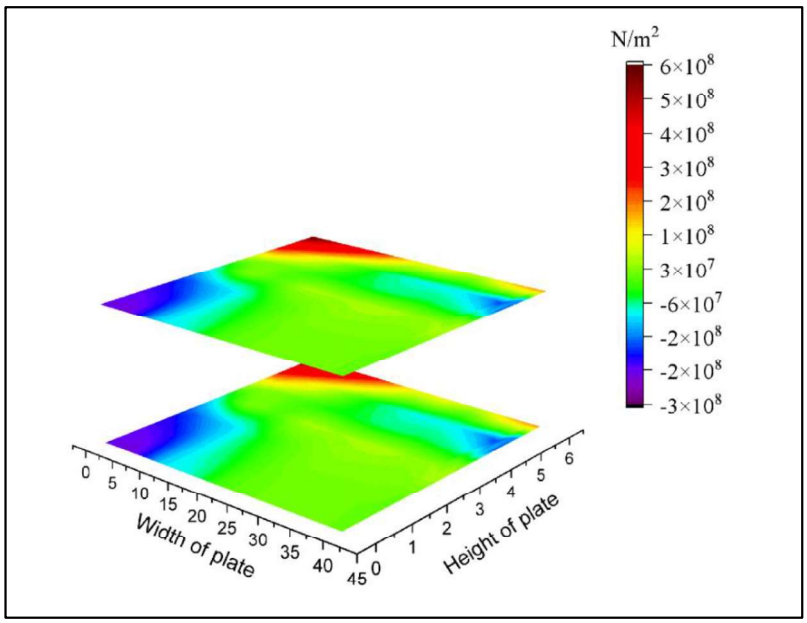

Fig. 4.107 Variation of transverse shear stress of the left tank wall (CCCC) with fundamental frequency as the forcing frequency for various layers (0/90 laminations)

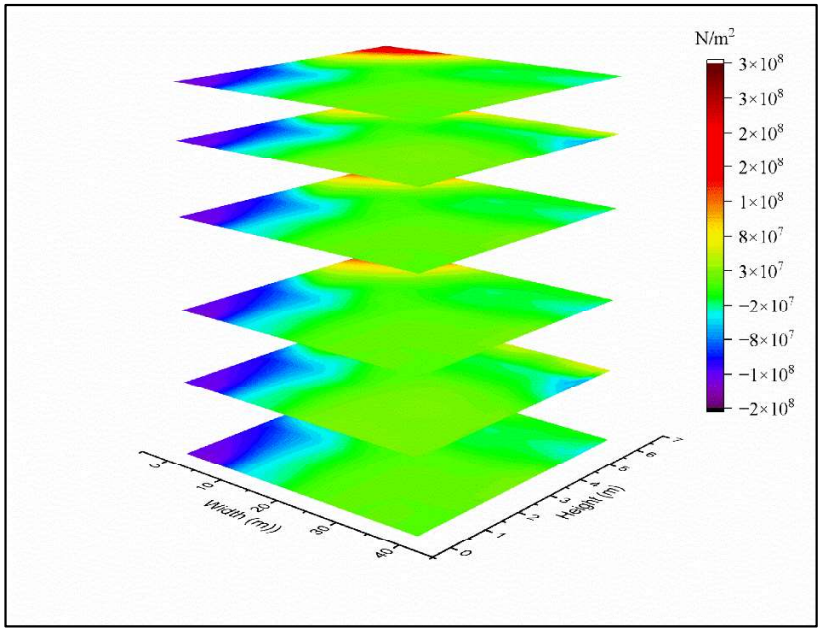

Fig. 4.108 Variation of transverse shear stress of the left tank wall (CCCC) with fundamental frequency as the forcing frequency for various layers (45/-45/45/45/-45/45 laminations)

Comparative study of 4 layer cross and angle ply laminated plate with four different boundary conditions are presented for normal stress contour as shown in Fig. 4.109. SSSS and CCCF plate has maximum stress values in the top two layers. Plate with SCSF edge shows highest normal stress values with stress variation along the edge perpendicular to the base. The comparison of stress for 45° symmetric lamination shows (Fig. 4.110) perpendicular dual maximum stress band for SSSS and SCSF edge plate. Fig. 4.111 shows variation of normal stress for 45° anti symmetric ply lay-ups. 45° anti symmetric lamination shows almost all boundary conditions except CCCC, having perpendicular stress band, only in case of CCCC edge, it has got horizontal stress band. Cross ply lamination in Fig. 4.112 shows horizontal stress band in all the support conditions except in CCCF case, where it is perpendicular to the base. Mostly in all the cases of cross ply lamination, stresses are in the form of a stress band horizontal or vertical.

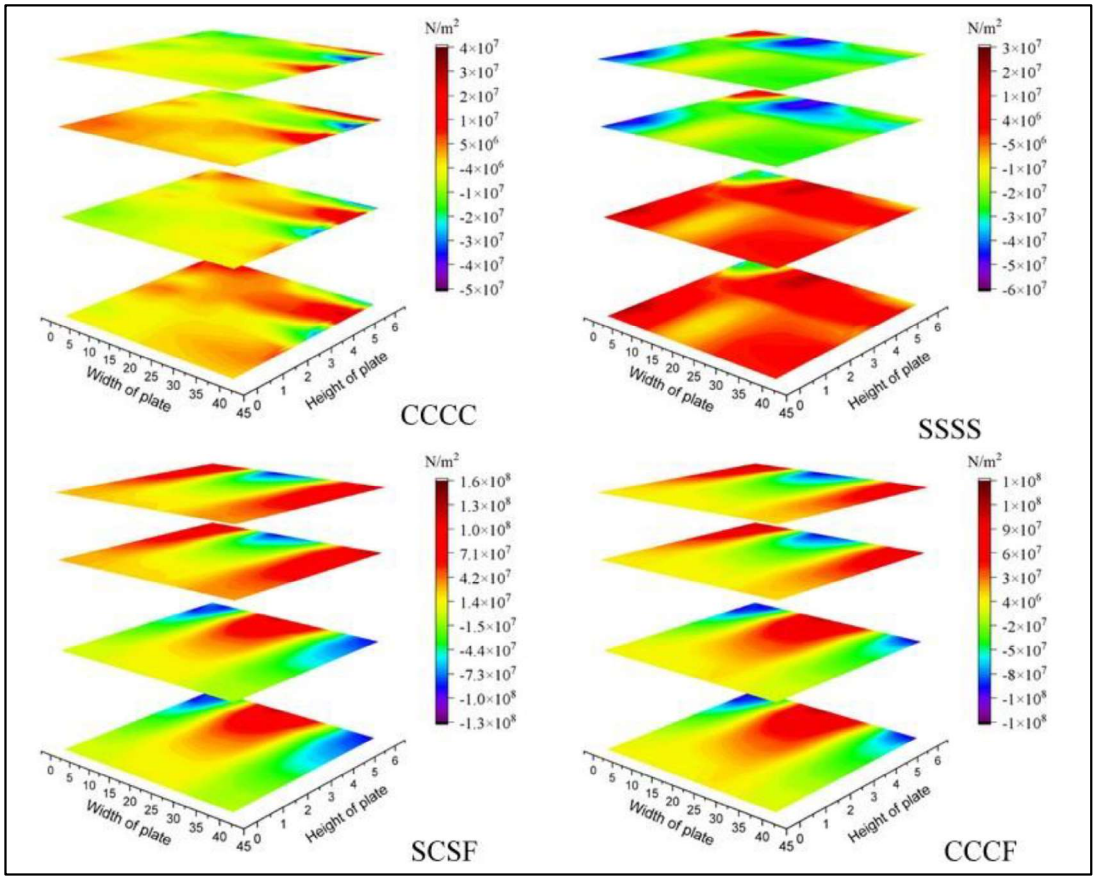

Fig. 4.109 Comparison of normal stress for various boundary conditions with fundamental frequency as the forcing frequency (0/90/90/0 laminations)

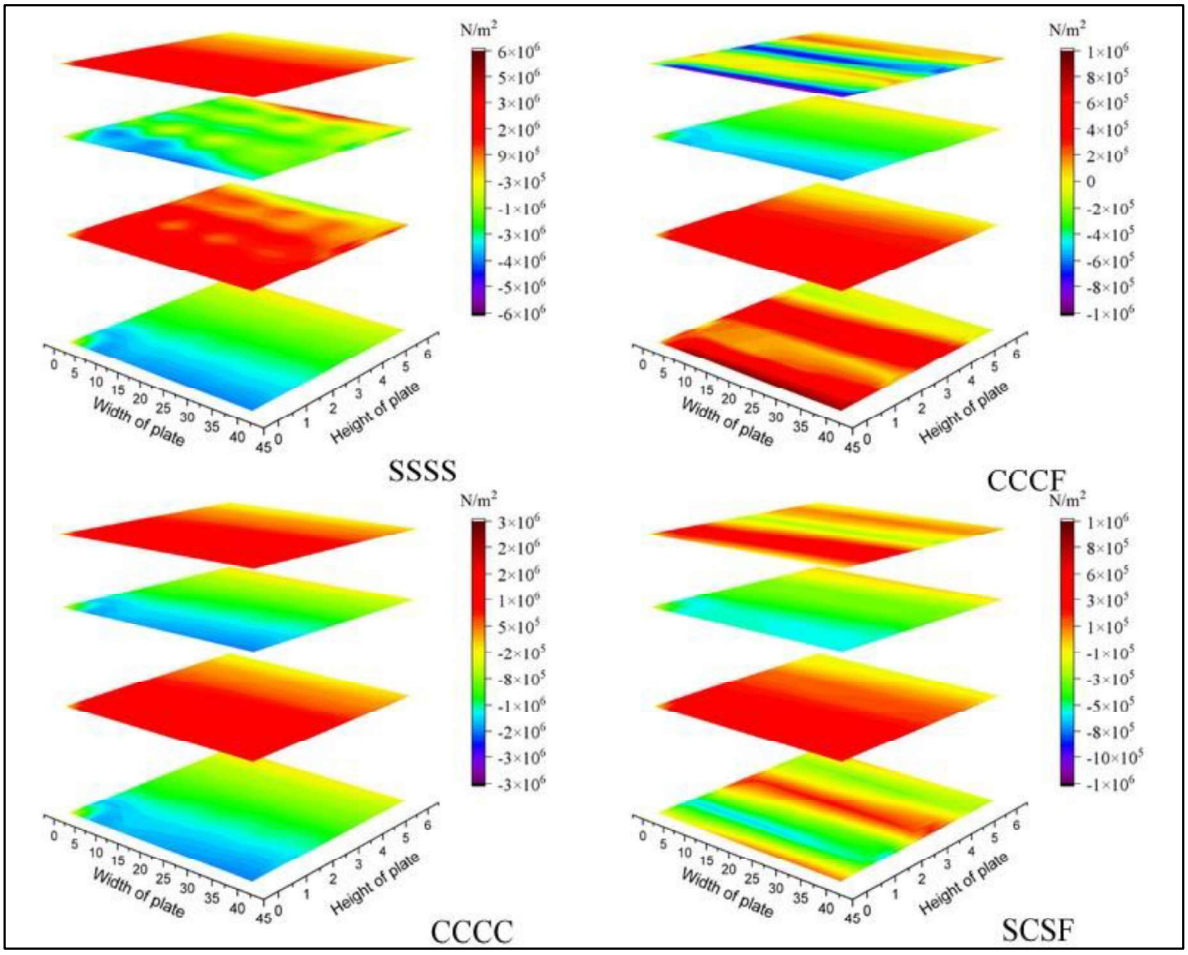

Fig. 4.110 Comparison of normal stress for various boundary conditions with fundamental frequency as the forcing frequency (45/-45/-45/45 laminations)

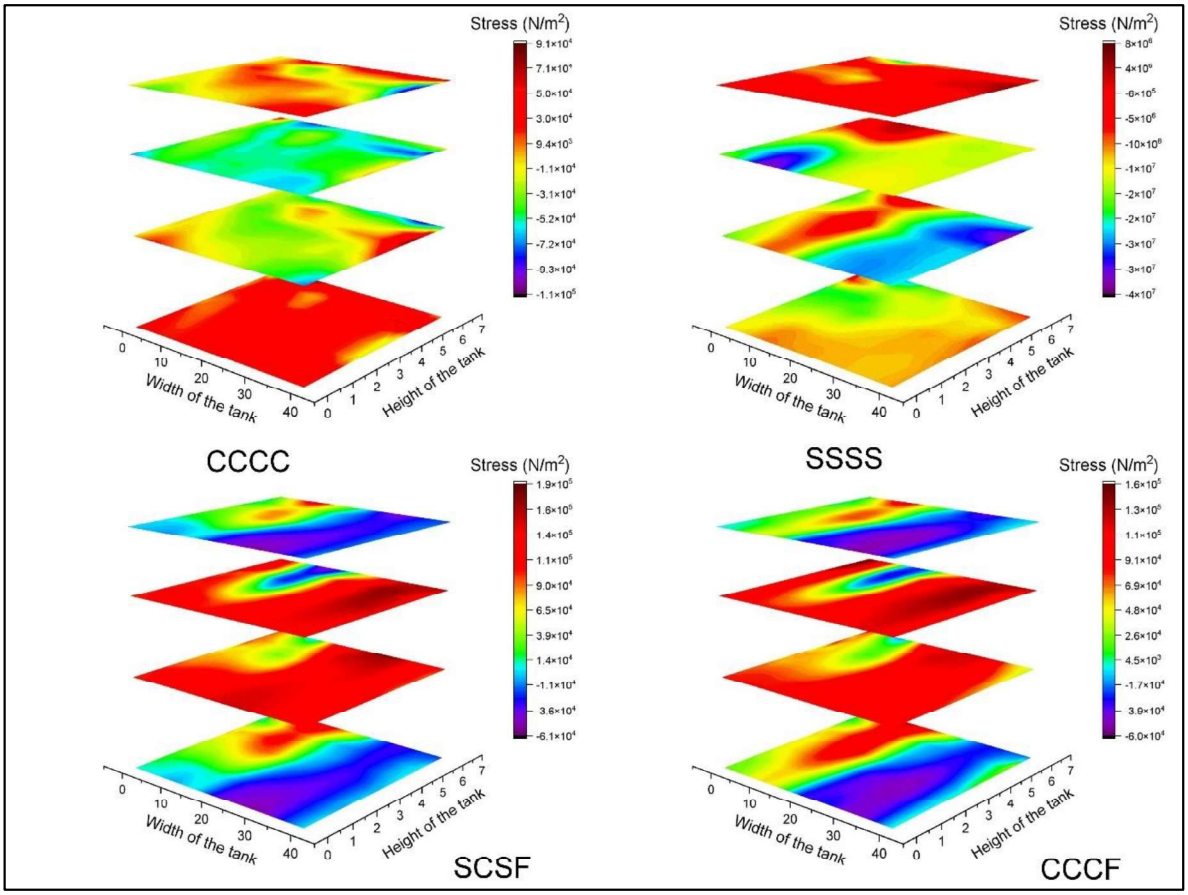

Fig. 4.111 Comparison of normal stress for various boundary conditions with fundamental frequency as the forcing frequency (45/-45/45/-45 laminations)

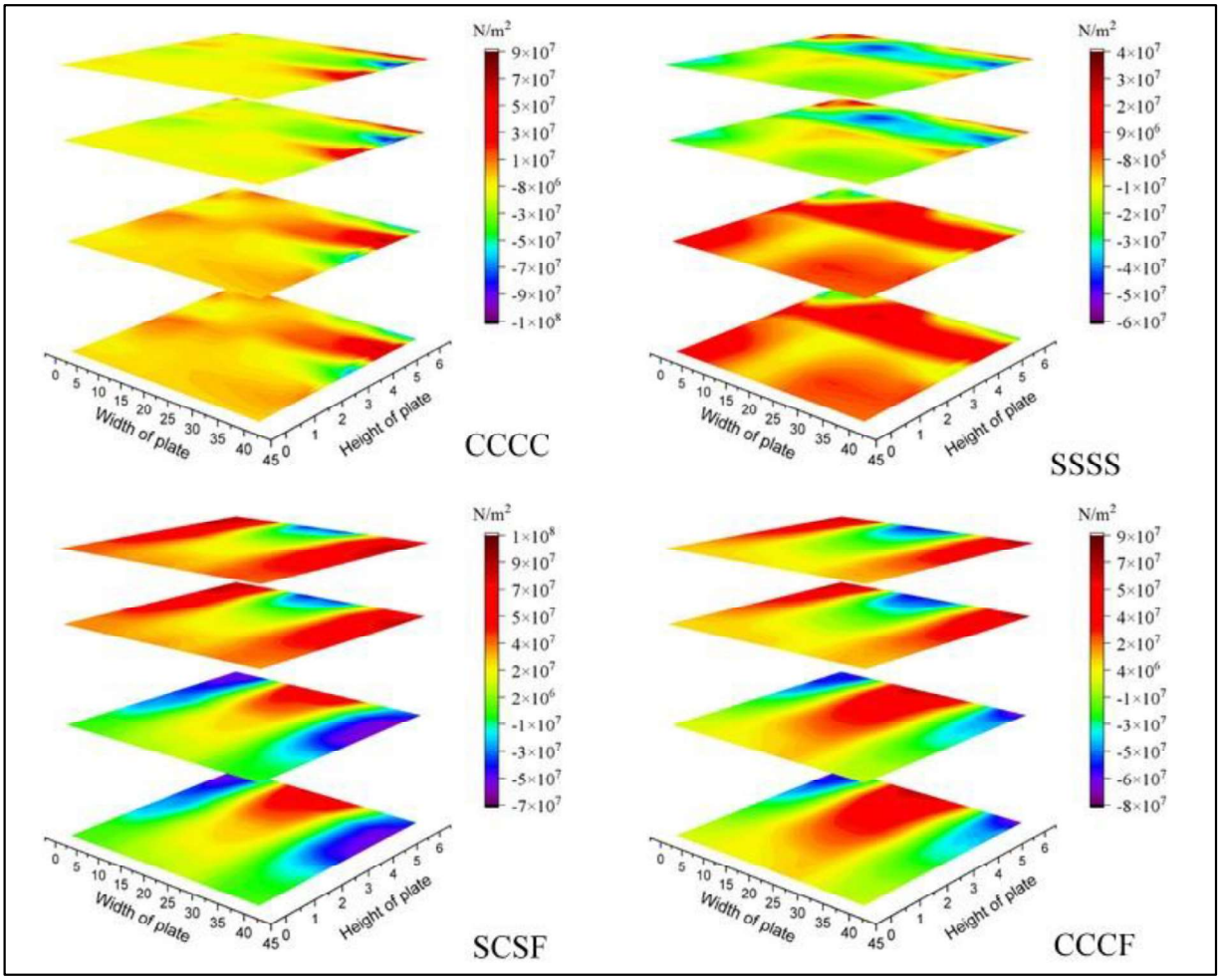

Fig. 4.112 Comparison of normal stress for various boundary conditions with fundamental frequency as the forcing frequency (0/90/0/90 laminations)

Variation of inplane shear stress for different boundary conditions are shown in Fig. 4.113 to 4.116. For 45° lamination shows lower perpendicular stress band for SSSS and CCCF boundary condition, whereas in case of CCCC and SCSF it shows inclined stress band. 45° anti symmetric lamination shows (Fig. 4.115) higher stress band along the right edge of the plate in all layers for SSSS, SCSF and CCCF boundary condition. Only in case of CCCC boundary condition, the stress band is parallel to the baseline. Cross ply lamination shows horizontal or vertical stress bands in almost all boundary conditions

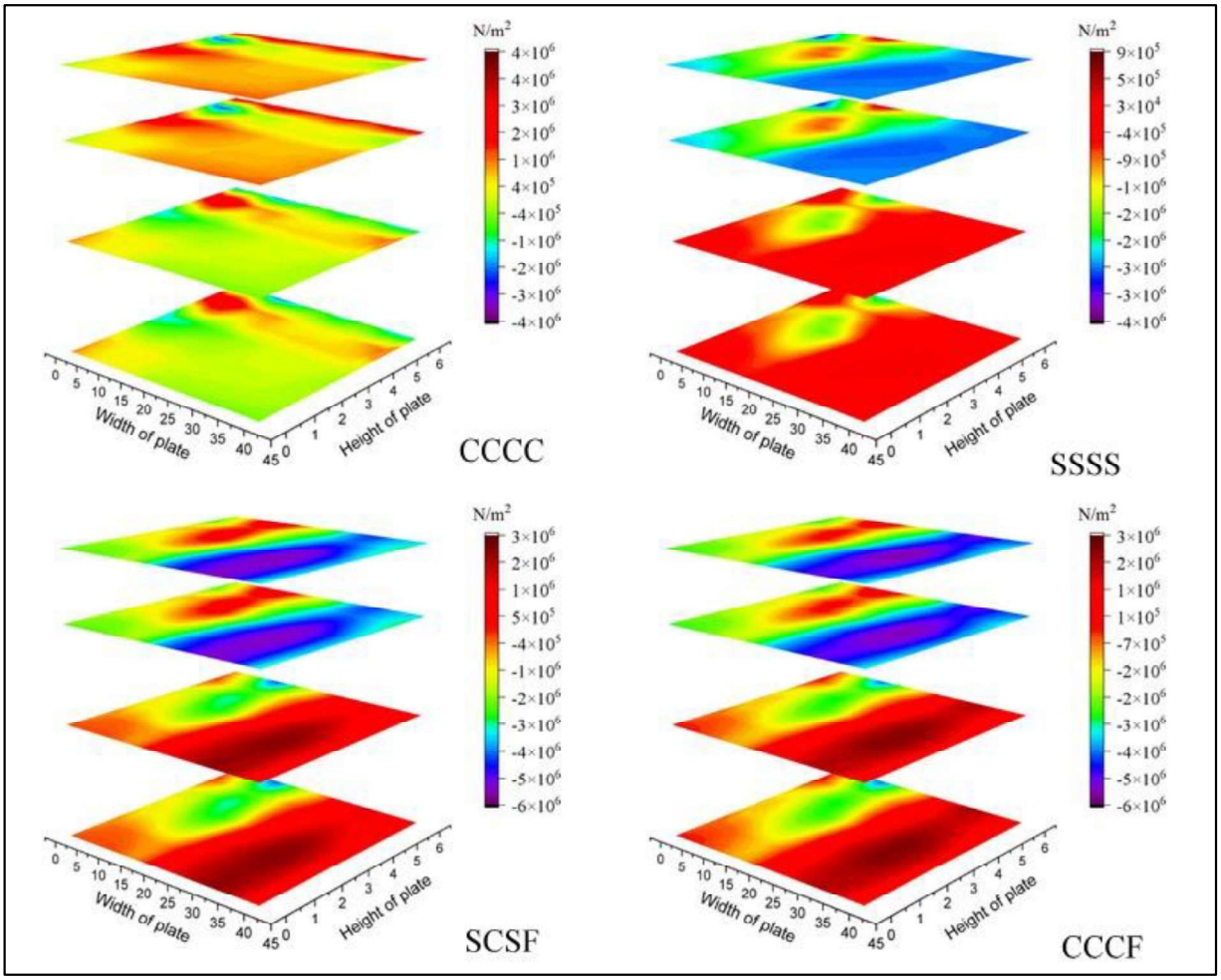

Fig. 4.113 Comparison of inplane shear stress for various boundary conditions with fundamental frequency as the forcing frequency (0/90/90/0 laminations)

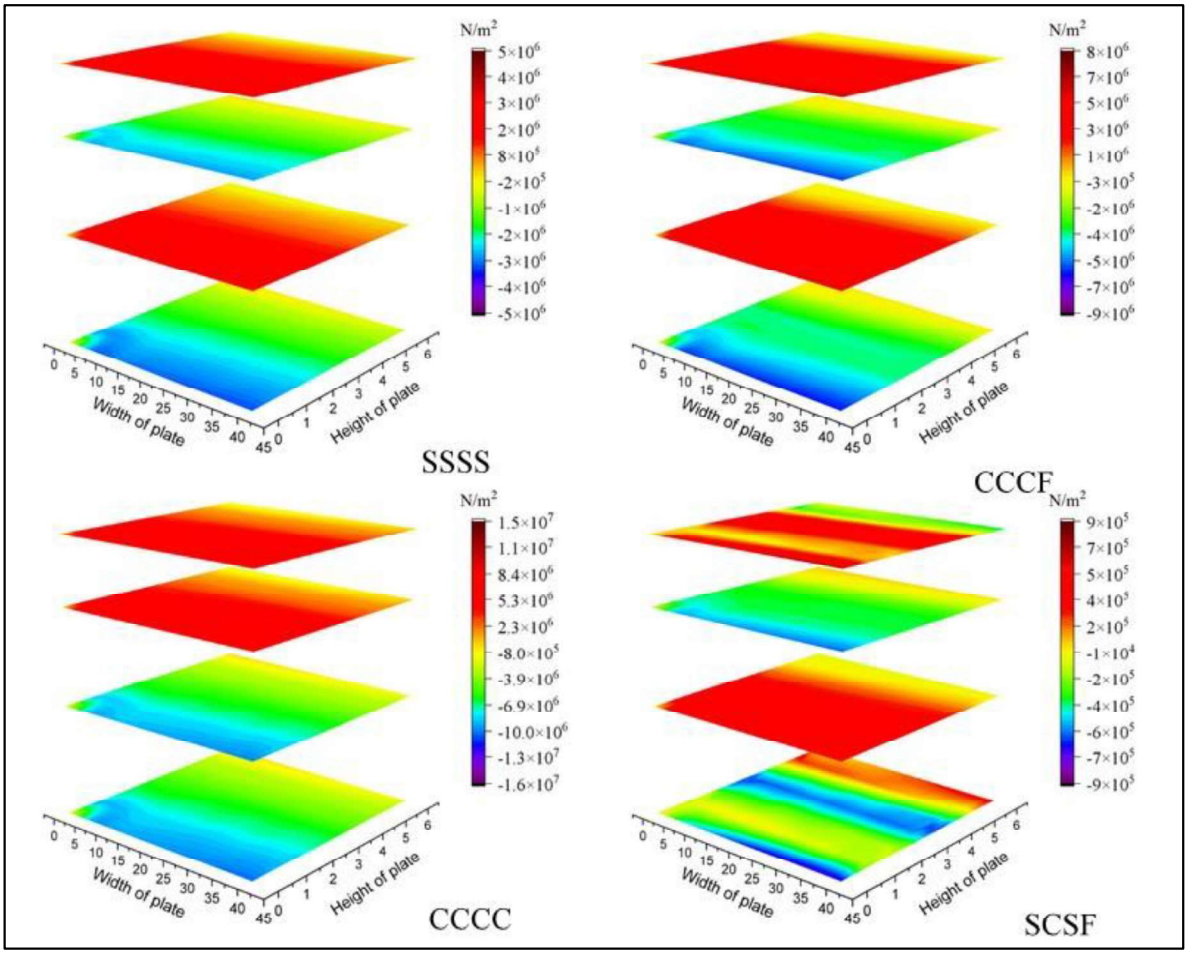

Fig. 4.114 Comparison of inplane shear stress for various boundary conditions with fundamental frequency as the forcing frequency (45/-45/-45/45 laminations)

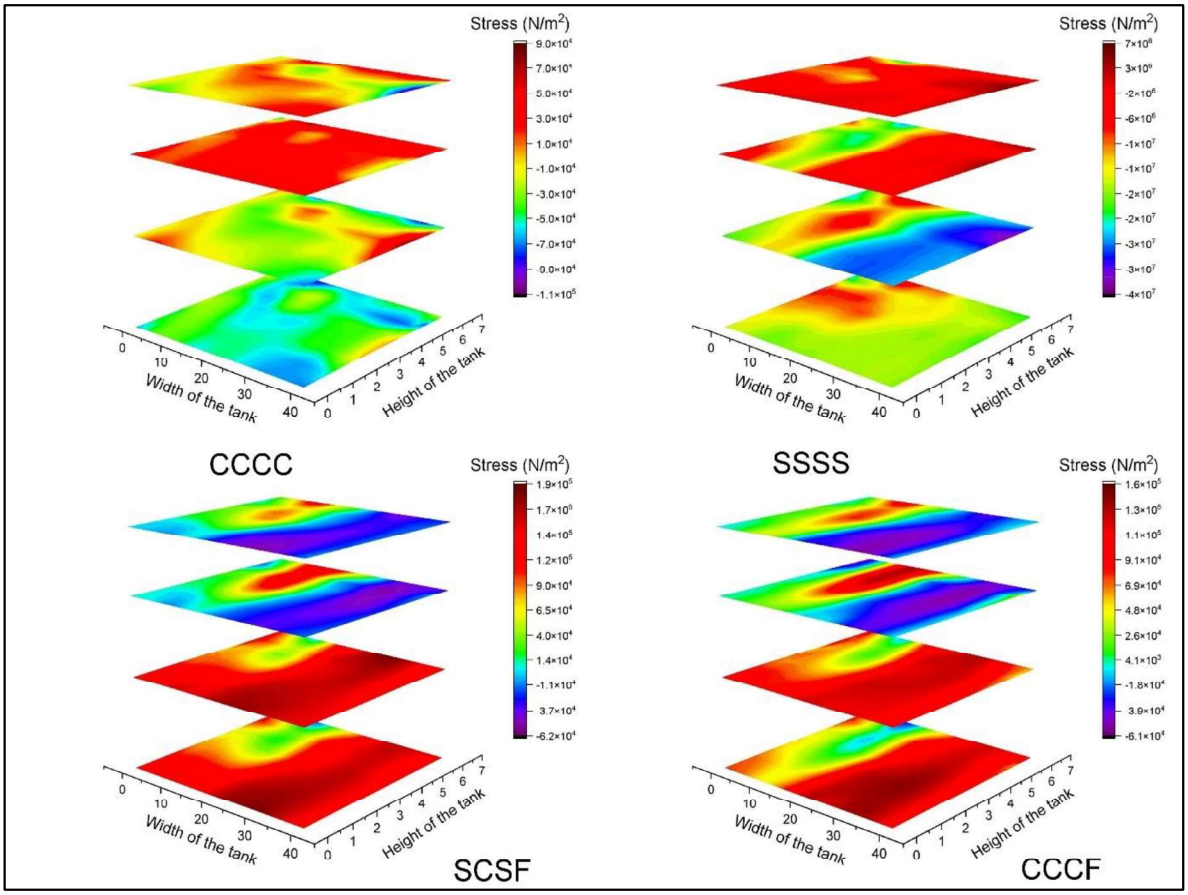

Fig. 4.115 Comparison of inplane shear stress for various boundary conditions with fundamental frequency as the forcing frequency (45/-45/45/-45 laminations)

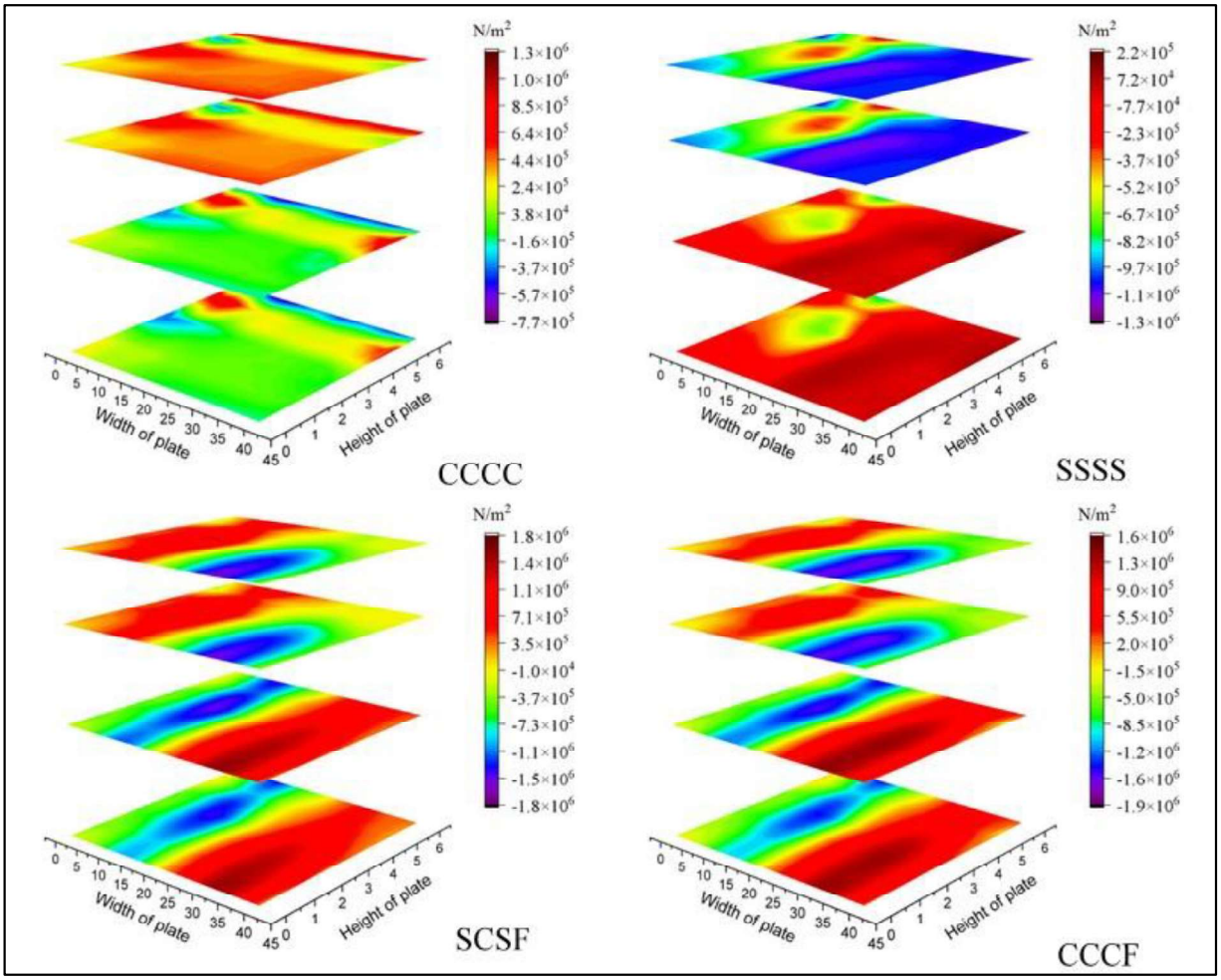

Fig. 4.116 Comparison of inplane shear stress for various boundary conditions with fundamental frequency as the forcing frequency (0/90/0/90 laminations)

Transverse shear stress contour (as shown in Fig. 4.117 to 4.120) is shown for cross ply laminations where maximum stress is concentrated at the top and bottom corners for all boundary conditions. 45° symmetric lamination shows (Fig. 4.118) stress bands perpendicular to the base for SCSF and CCCF edge. SSSS and CCCC edge plates shows lower and higher stress along the diagonals respectively. 45° anti symmetric lamination shows (Fig. 4.119) higher stress values along the edges for SCSF, CCCF and SSSS conditions. Higher stress values are seen at the opposite corners for CCCC boundary conditions. Lower stress concentration is present for SSSS edge plate and for CCCC clamped plate, higher stress can be seen parallel to the baseline.

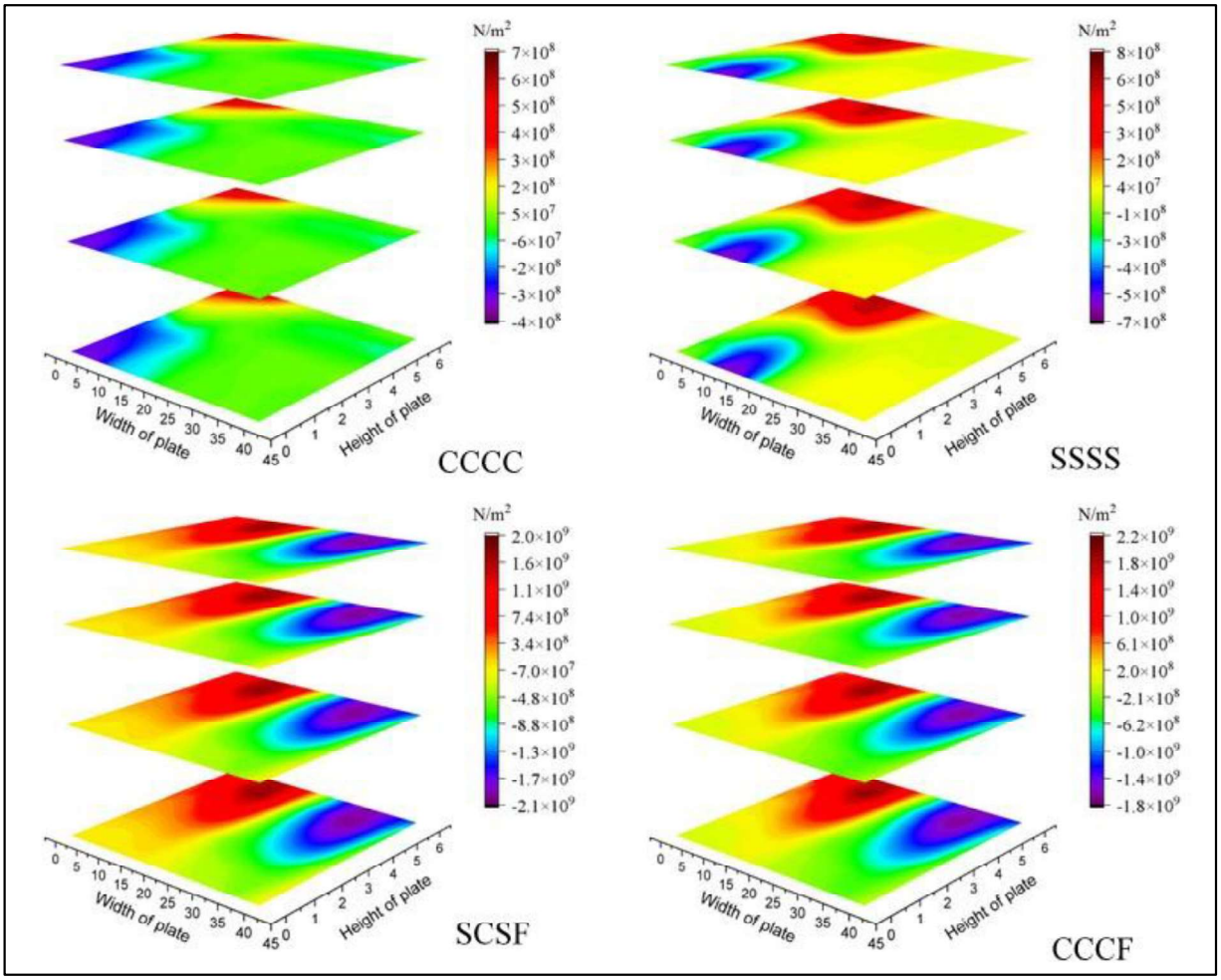

Fig. 4.117 Comparison of transverse shear stress for various boundary conditions with fundamental frequency as the forcing frequency (0/90/90/0 laminations)

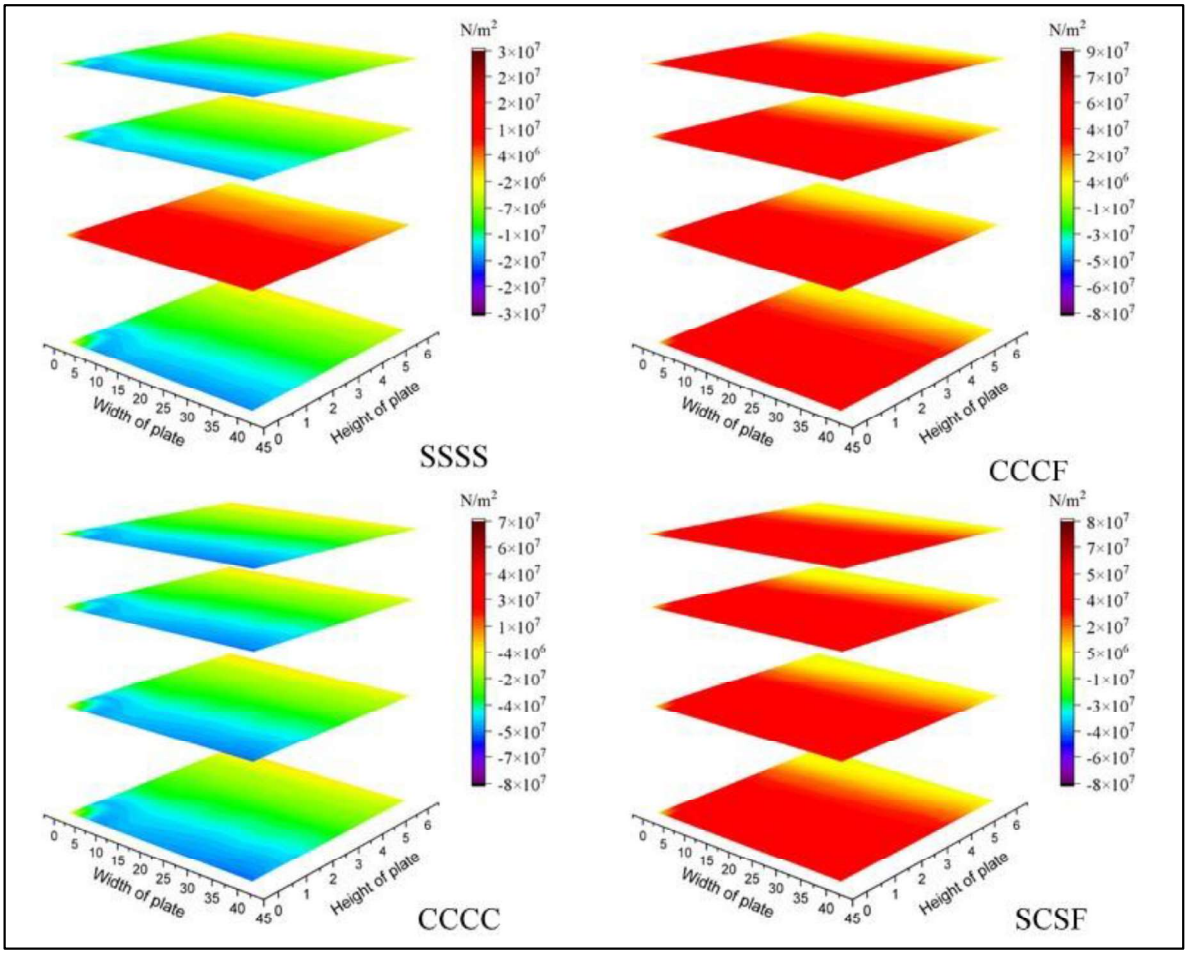

Fig. 4.118 Comparison of transverse shear stress for various boundary conditions with fundamental frequency as the forcing frequency (45/-45/-45/45 laminations)

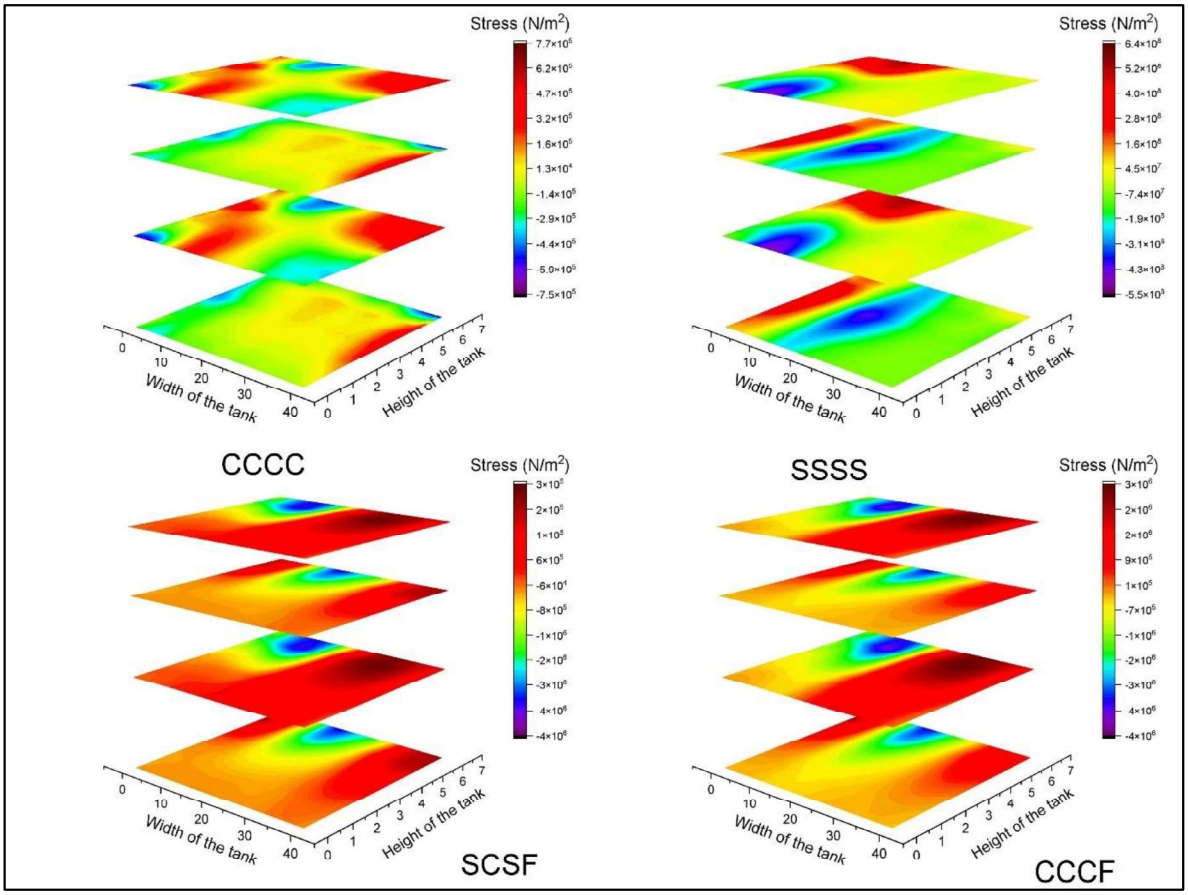

Fig. 4.119 Comparison of transverse shear stress for various boundary conditions with fundamental frequency as the forcing frequency (45/-45/45/-45 laminations)

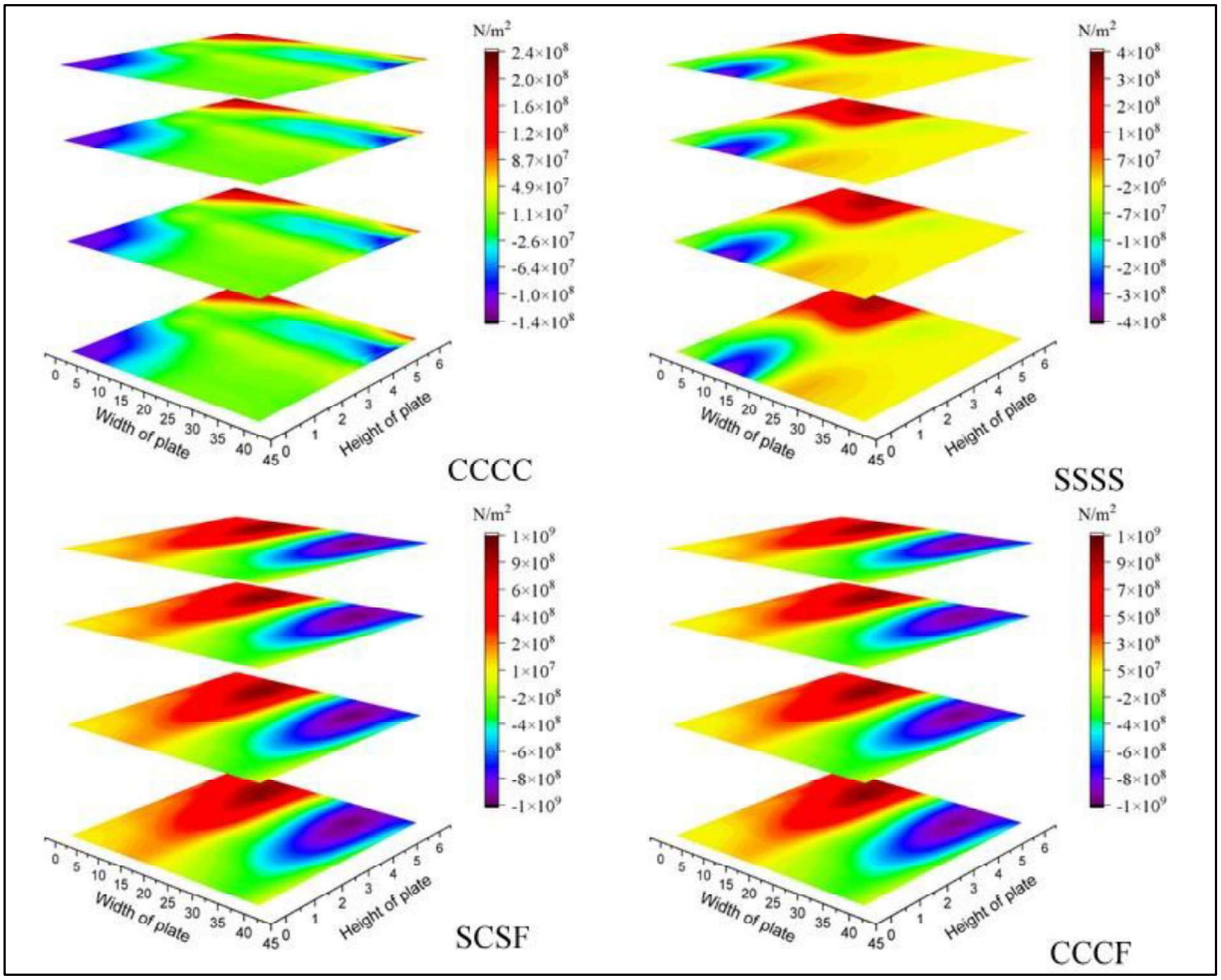

Fig. 4.120 Comparison of transverse shear stress for various boundary conditions with fundamental frequency as the forcing frequency (0/90/0/90 laminations)

Comparative study of three stresses (normal stress, inplane shear stress and transverse stress) for a particular boundary condition and ply lay-ups are presented in the next section (in Fig. 4.121 to 4.122). For cross ply lamination, normal stress is showing highest value among the set for SSSS lamination. On the other hand, plate is showing higher stress values across diagonals for clamped edged plate.

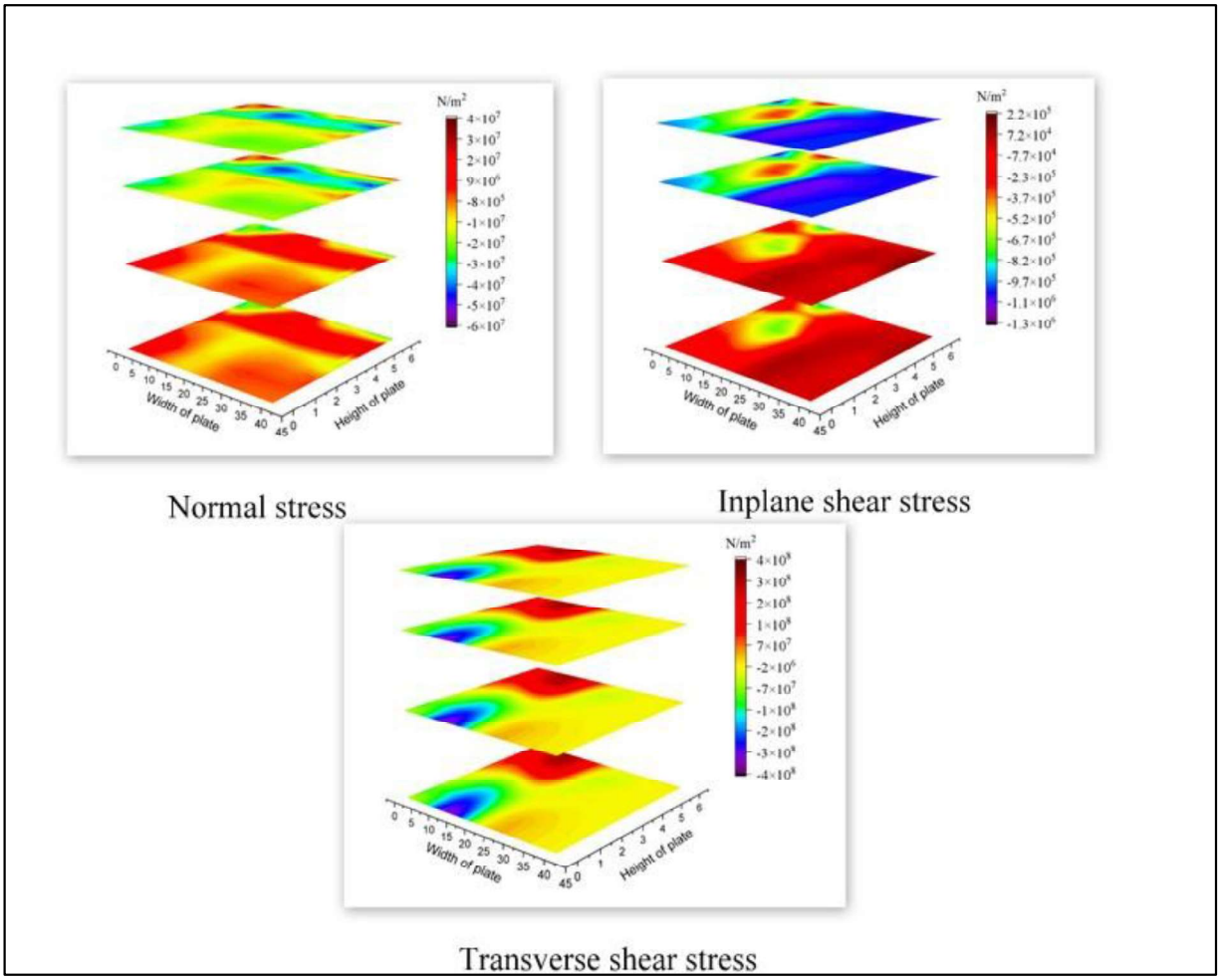

Fig. 4.121 Comparison of normal stress, inplane shear stress and transverse shear stress for SSSS boundary condition (0/90/0/90 laminations)

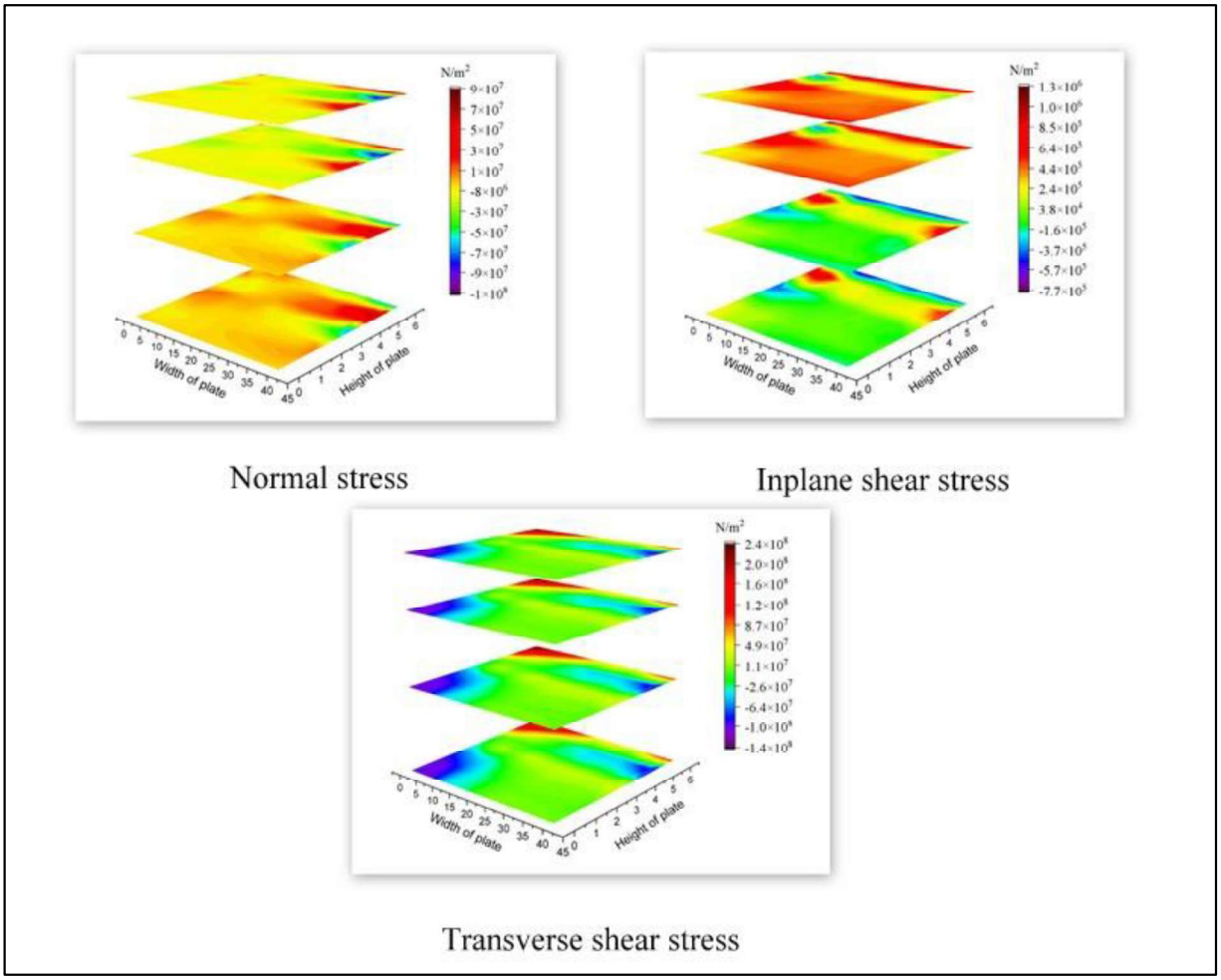

Fig. 4.122 Comparison of normal stress, inplane shear stress and transverse shear stress for CCCC boundary condition (0/90/0/90 laminations)

In case of angle ply laminations (Fig. 4.123 to 4.124), vertical stress band is observed for SSSS boundary condition and scattered higher stress patches can be seen in CCCC boundary condition. So, it's very prominent that with change in boundary and ply orientations, stress generations across various layers differs largely. Hence careful selection of ply angles and boundary conditions may lead to better stress carrying capacity of the tank walls.

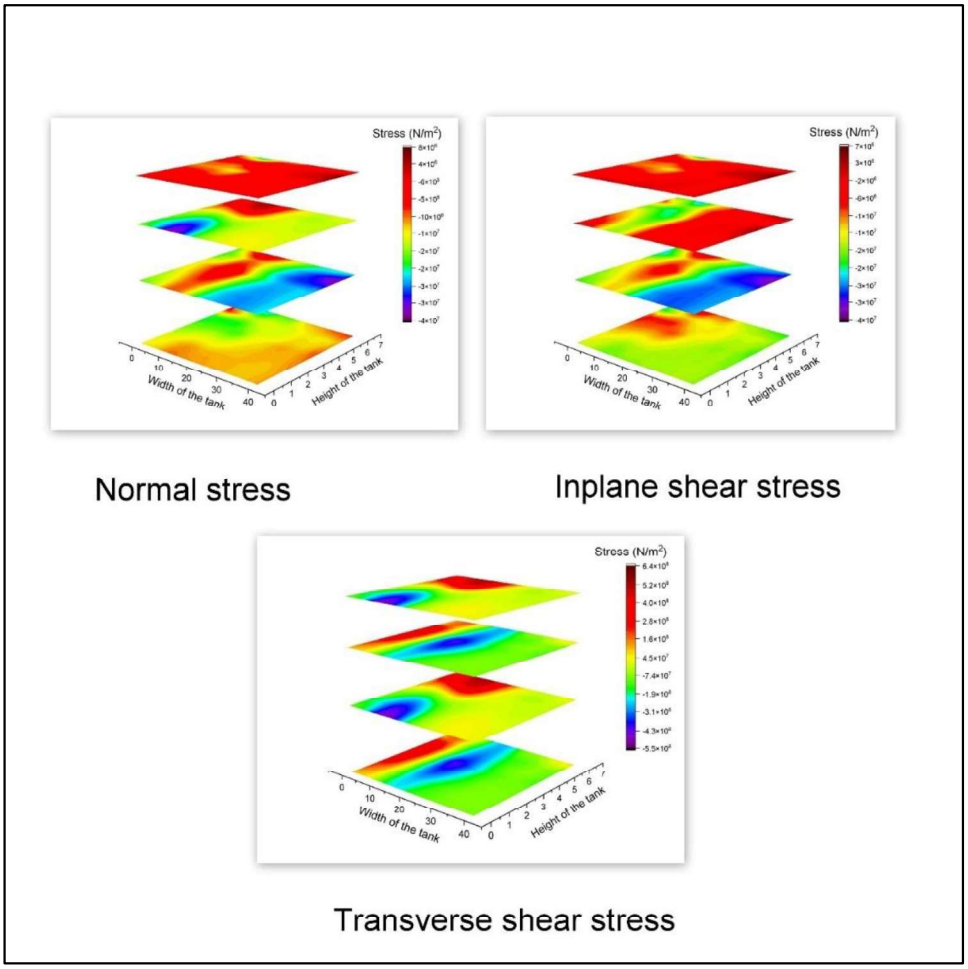

Fig. 4.123 Comparison of normal stress, inplane shear stress and transverse shear stress for SSSS boundary condition (45/-45/45/-45 laminations)

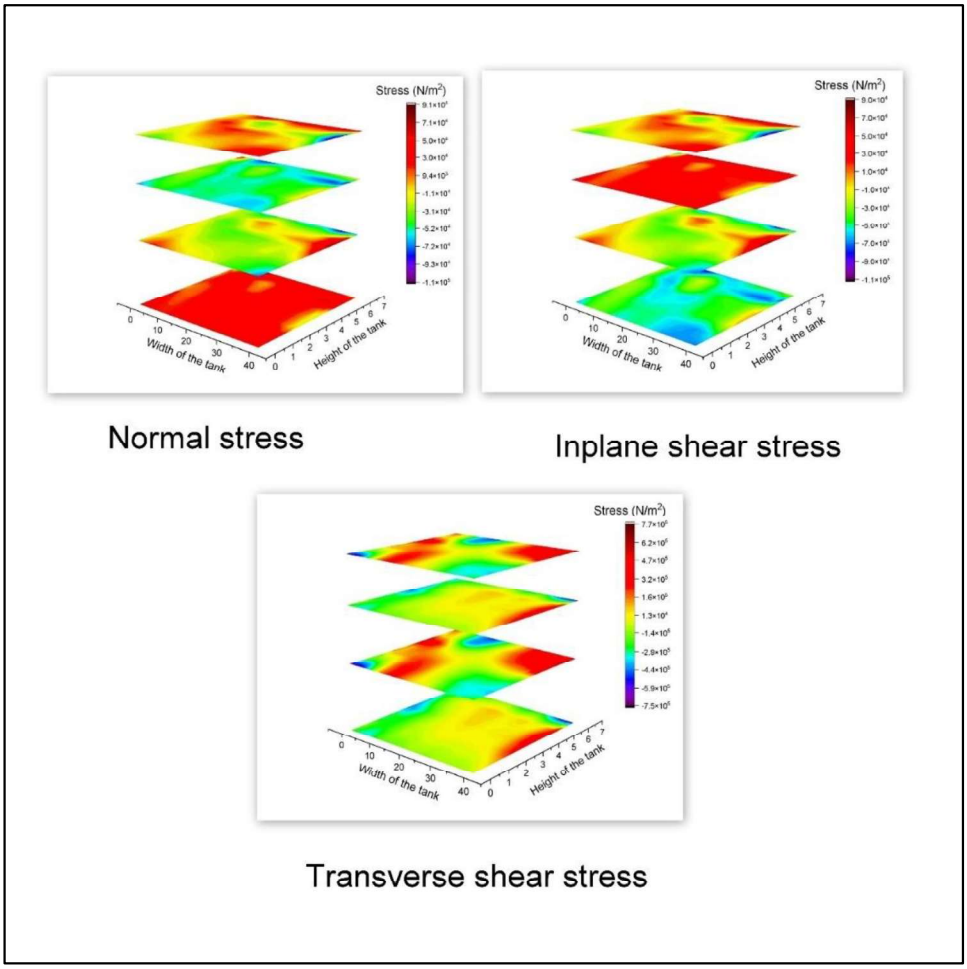

Fig. 4.124 Comparison of normal stress, inplane shear stress and transverse shear stress for CCCC boundary condition (45/-45/45/-45 laminations)

4.3.6 Analysis of tank wall-fluid coupled system under El-Centro ground motion

Central displacement of the left wall for two layered cross and angle ply laminated plate is presented in the next section under ground motion. El Centro ground motion (recorded on 19th May 1940) is considered for present study and the acceleration magnitude is shown in Fig. 4.125.

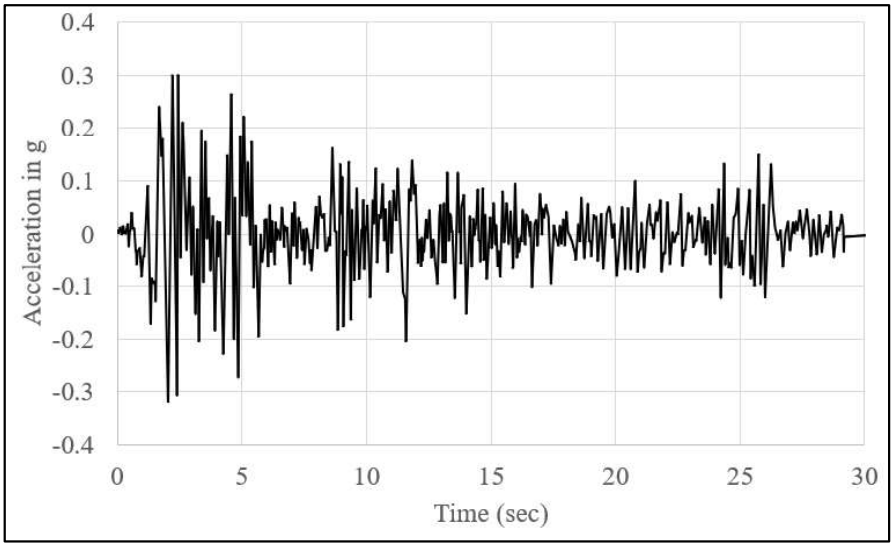

Fig. 4.125 Horizontal component of El Centro earthquake acceleration recorded on 19th May 1940

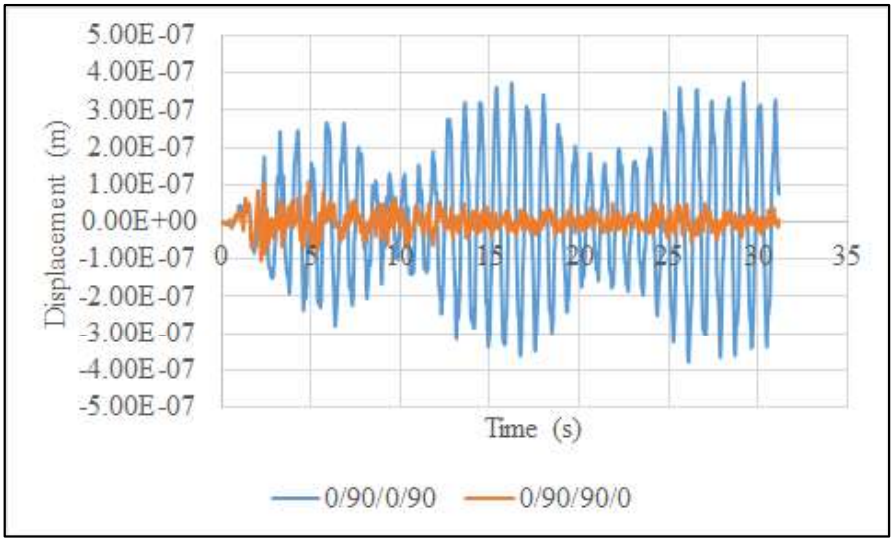

Fig. 4.126 Variation of central displacement for 4 layered cross-ply laminated side wall under El Centro earthquake acceleration

Variation of central displacement for 4 layered cross-ply laminated side wall is analysed under El centro ground motion presented in Figs. 4.126 – 4.127. Anti-symmetric cross-ply lamination shows much higher central displacement compared to symmetric one. Similarly for angle ply

lamination also symmetric ply lay-ups show much lesser displacement values comp`ared to the anti-symmetric ones.

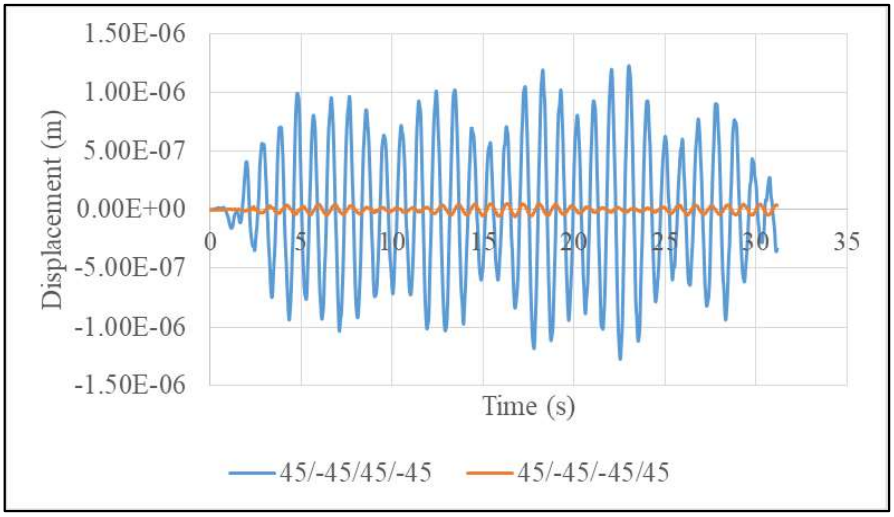

Fig. 4.127 Variation of central displacement for 4 layered angle-ply laminated side wall under El Centro earthquake acceleration

Normal stress developed at the side wall due to ground motion is presented in Figs. 4.128 – 4.129. It is observed that anti-symmetric lamination shows much higher normal stress values compared to synnetric ones. Same trend is maintained for angle ply lamination also. Variation of inplane shear stress for cross and angle ply is presented in the next part as shown in Figs. 4.130 – 4.131. It is observed that anti-symmetric angle ply lamination gives much higher stress values compared to symmetric one. Cross ply lamination on the other hand shows higher stress value for symmetric lamination in the first 10-12 second of the application of the ground motion, then the anti-symmetric lamination becomes pre-dominant for the rest of the time. Transverse shear variation is presented in the next section in Figs. 4.132 – 4.133, where it is observed that in case of cross ply lamination symmetric lamination always carry higher stress values and in case of angle ply lamination anti-symmetric lamination carries higher stresses.

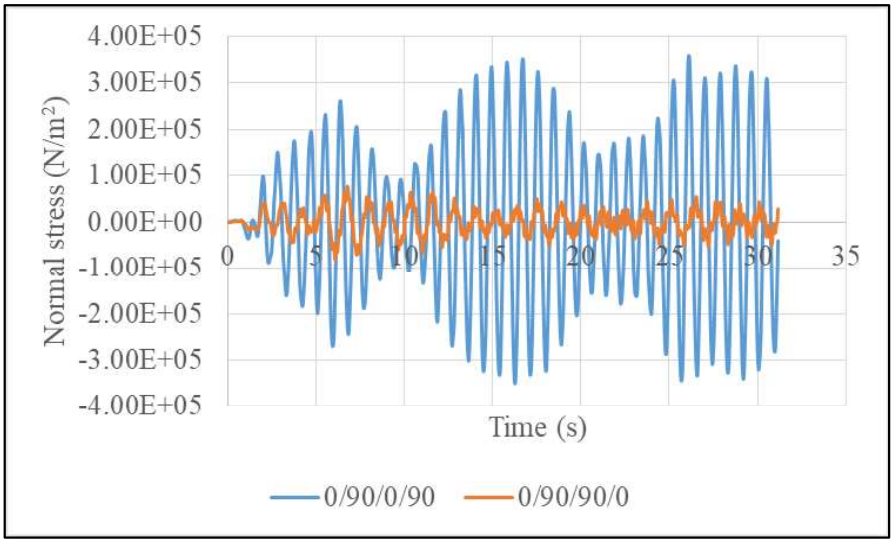

Fig. 4.128 Variation of normal stress in 4 layered cross-ply laminated side wall under El Centro earthquake acceleration

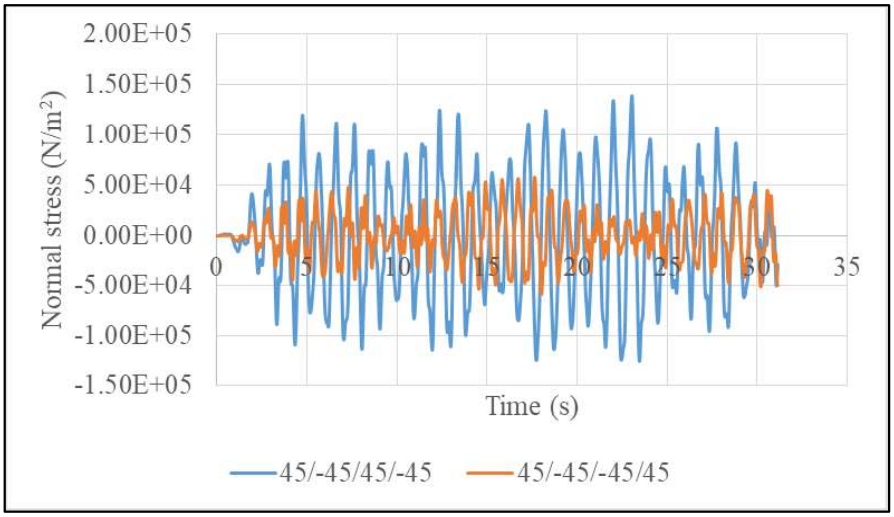

Fig. 4.129 Variation of normal stress for in 4 layered angle-ply laminated side wall under El Centro earthquake acceleration

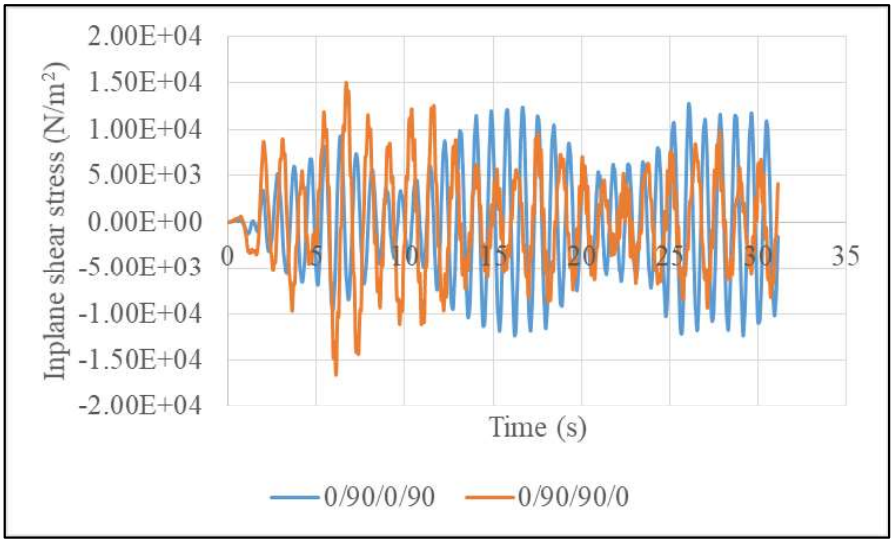

Fig. 4.130 Variation of inplane shear stress for 4 layered cross-ply laminated side wall under El Centro earthquake acceleration

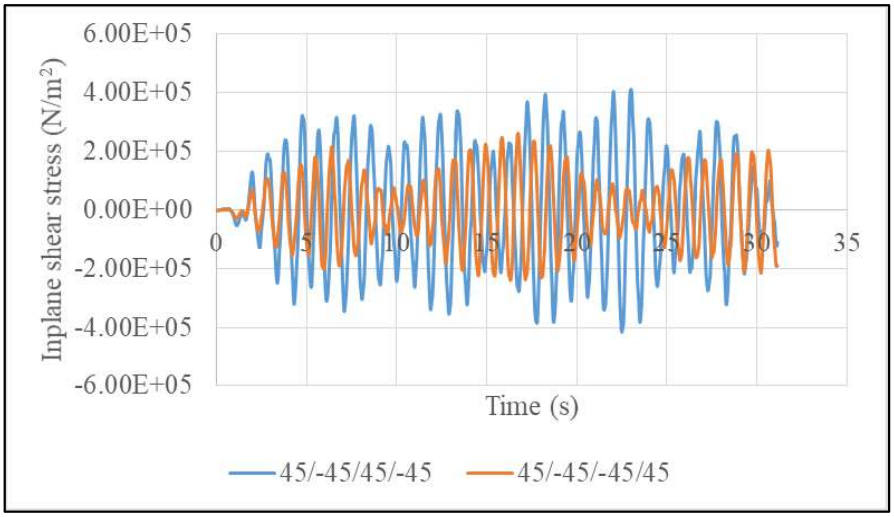

Fig. 4.131 Variation of inplane shear stress for 4 layered angle-ply laminated side wall under El Centro earthquake acceleration

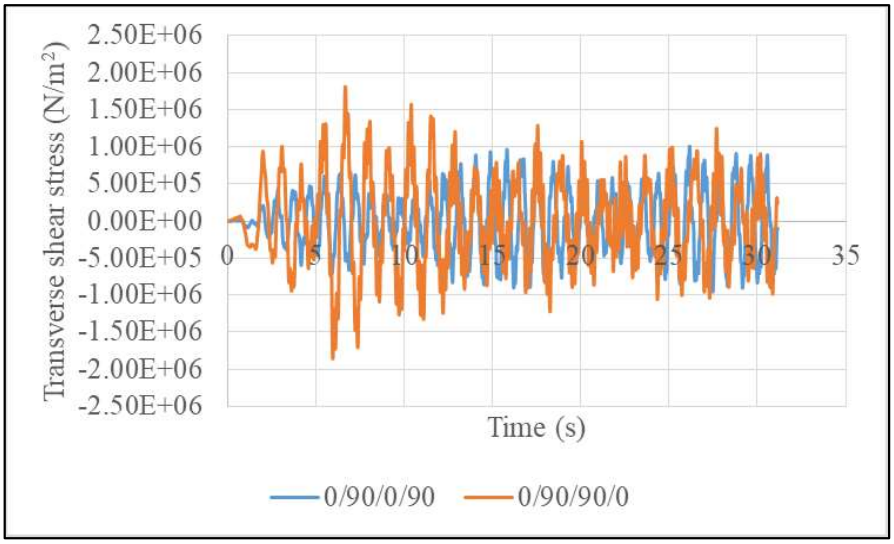

Fig. 4.132 Variation of transverse shear stress for 4 layered cross-ply laminated side wall under El Centro earthquake acceleration

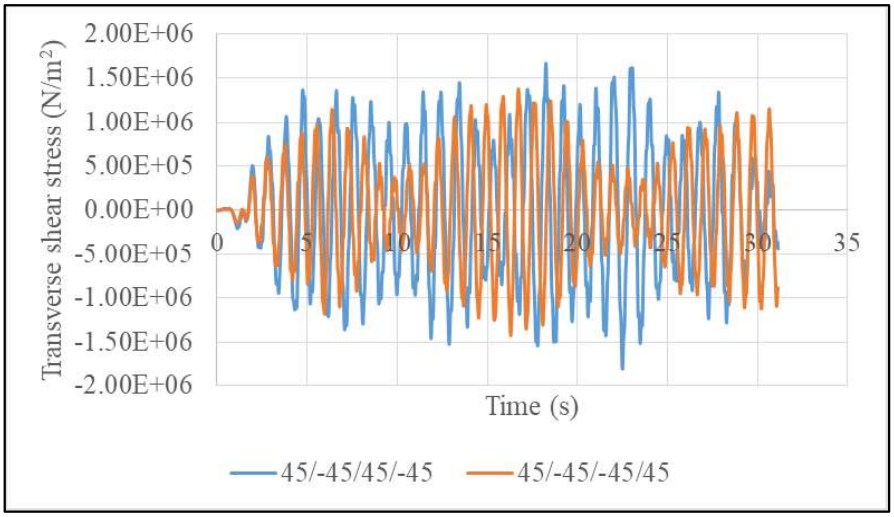

Fig. 4.133 Variation of transverse shear stress for 4 layered angle-ply laminated side wall under El Centro earthquake acceleration

As the next step the stress contour plot for different layers of anti-symmetric cross (0/90/0/90) and angle ply (45/-45/45/-45) lamination is presented in Figs.4.134- 4.139. In case of cross ply lamination, horizontal stress band at the upper portion of the plate is observed for all the layers in case of normal stress and inplane shear stress. The value of stresses developed are more in case of

normal stress compared to inplane shear stress. Transverse shear stress on the other hand generates higher and lower stress values at the corner portions of the ply layers in the plate. Stress parallel is also not much prominent in this case.

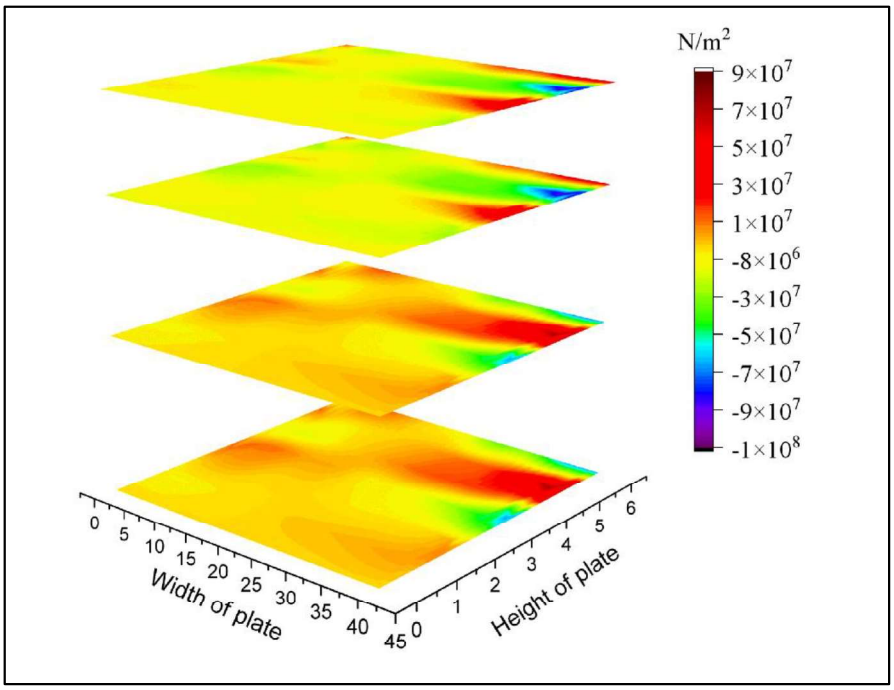

Fig. 4.134 Contour plot of normal stress for 4 layered cross-ply (0/90/0/90) laminated side wall under El Centro earthquake acceleration

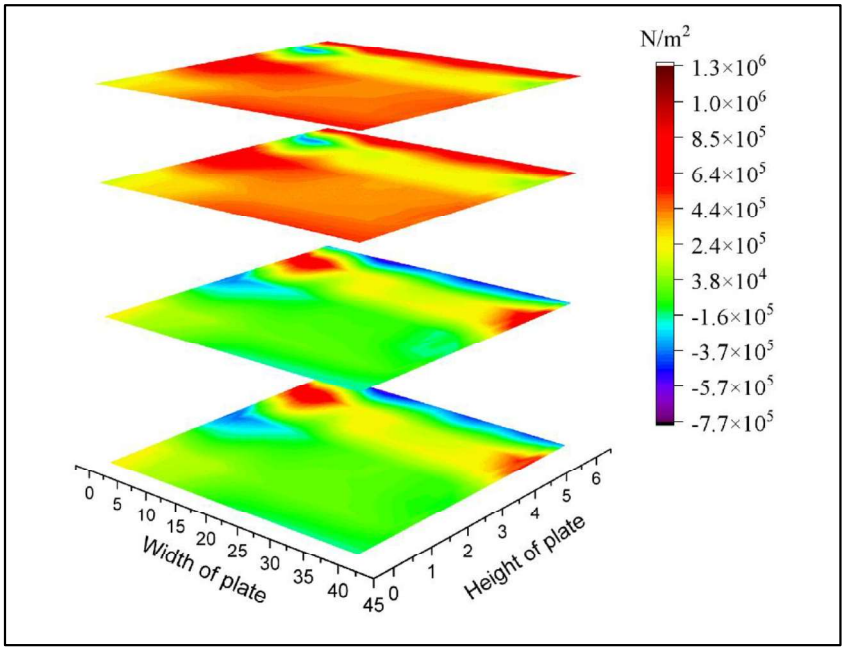

Fig. 4.135 Contour plot of inplane shear stress for 4 layered cross-ply (0/90/0/90) laminated side wall under El Centro earthquake acceleration

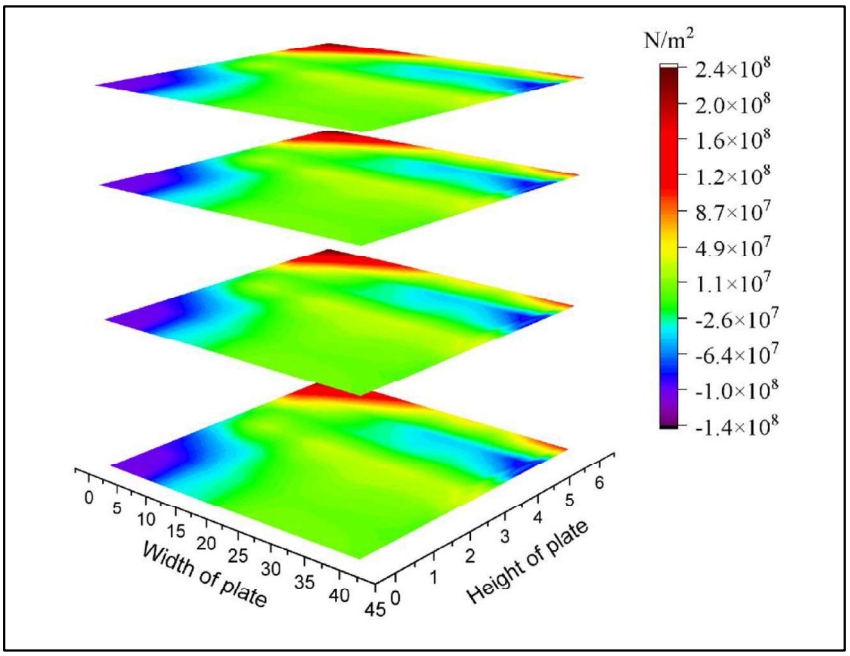

Fig. 4.136 Contour plot of transverse shear stress for 4 layered cross-ply (0/90/0/90) laminated side wall under El Centro earthquake acceleration

Variation of stress contour for angle ply lamination is presented and found to have stress band at different layers along different directions. In case of normal stress, a diagonal stress band is observed for 45 lamination, whereas horizontal band is observed for -45 lamination. Higher stress concentrations can be observed at top portions at two sides. Similar stress variation is present for inplane shear stress also, but in this case higher stress concentration is observed at top portion but along one side of the plate only. More over in this lamination horizontal stress band is present in all the layers. In transverse shear stress diagonal stress band can be observed with higher stress concentrations at the corners of the plate. Bottom left corners are more susceptible to transverse shear stress for all the layers.

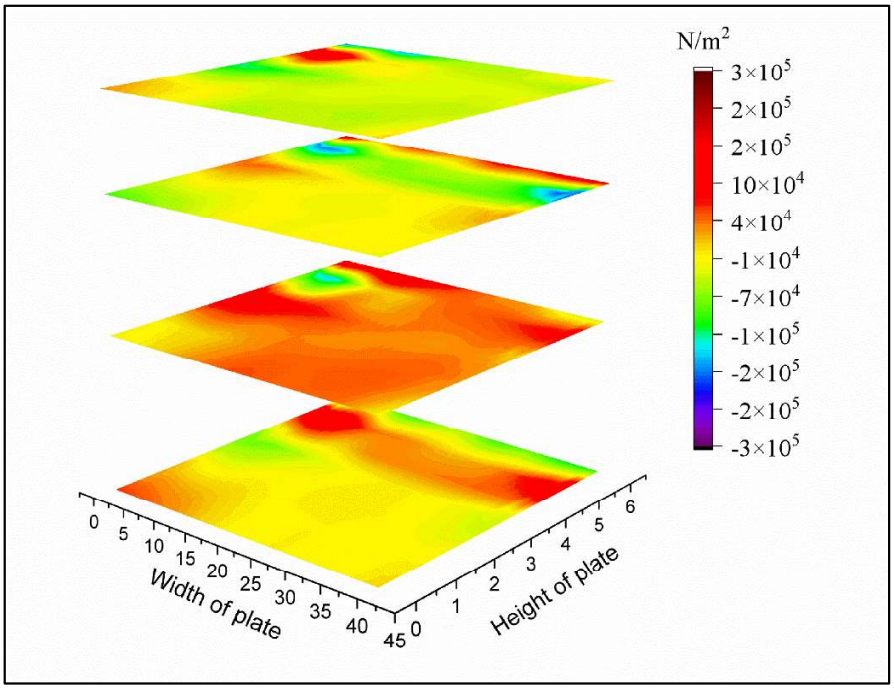

Fig. 4.137 Contour plot of normal stress for 4 layered angle-ply (45/-45/45/-45) laminated side wall under El Centro earthquake acceleration

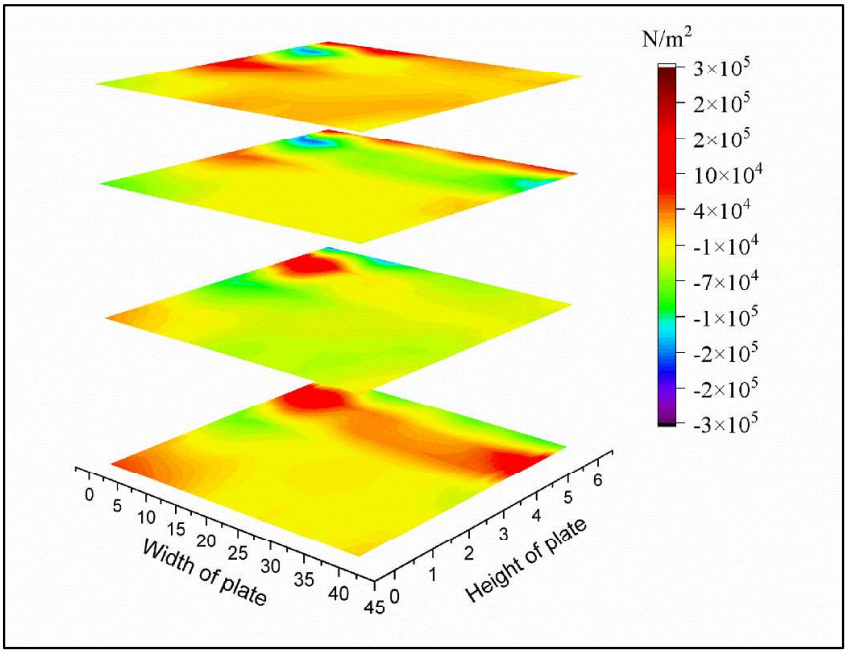

Fig. 4.138 Contour plot of inplane shear stress for 4 layered angle-ply (45/-45/45/-45) laminated side wall under El Centro earthquake acceleration

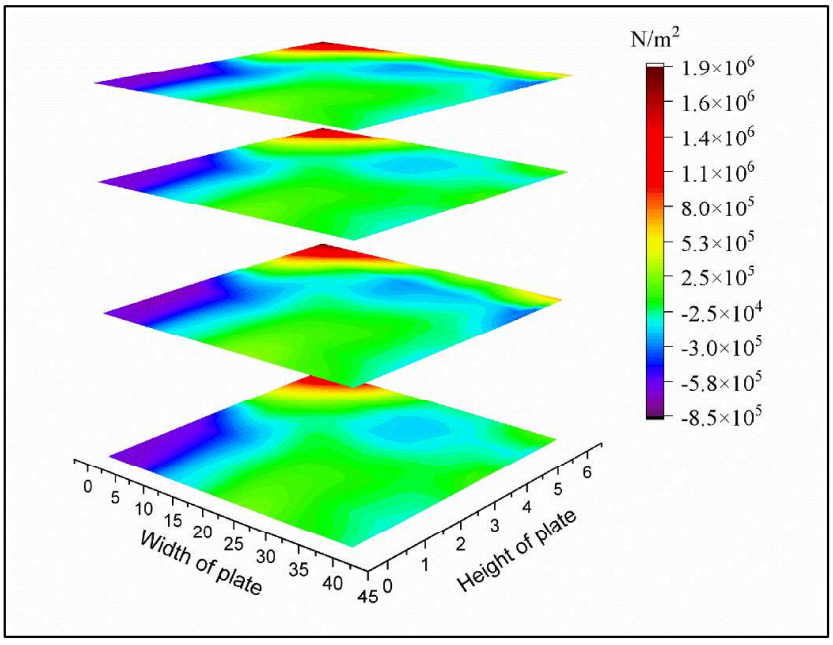

Fig. 4.139 Contour plot of transverse shear stress for 4 layered angle-ply (45/-45/45/-45) laminated side wall under El Centro earthquake acceleration

CHAPTER 5

SUMMARY AND CONCLUSIONS

5.1 SUMMARY

In section 4.2 response of uncoupled composite plate is studied. Free vibration response of such thin plates shows variation in fundamental frequency with increase in ply angle upto 45°. Central displacement of the plate under transient loading shows that 45° lamination having highest value that too with the symmetric ply lay ups. Displacement values decreases with increment in number of layers. Variation in plan dimension as well as thickness is also studied and reported at subsequent sections. Effect of four different boundary conditions was studied and found to have maximum displacement for the plate with all four edges simply supported. As the next step, the variation of stress values are studied under transient load. Normal stress, inplane shear stress and transverse shear stress in the plate is studied. in order to obtain the position of highest developed stress at any time instant within the plate, a study is carried out. Stress contours were plotted at different layers within the plate for the stresses. Response of the plate under Koyna ground motion is also presented.

In section 4.3 the response of direct coupling between composite plate and fluid is studied. The fluid is considered as compressible and inviscid. The study started with natural frequency of the coupled system. Variation of frequency with varying ply layup schemes are studied and some different observations were found. Especially in case of anti-symmetric 45° laminations, the different is most prominent as this lamination shows highest displacement values. Variation of central displacement is maximum in case of the tank with two opposite edges simply supported, bottom edge fixed and top edge free. Increment in number of layers shows that only angle ply lamination is significant as the value remains unchanged in case of cross ply laminations. Variation of displacement with change in geometry of the tank with totally filled with liquid is presented. A comparative response of two opposite side walls is studied on central displacement of the walls. It was observed that as the progression of time, there appears a time lag between the response of the two side walls. Stress time history and stress contour for three different stresses are studied. The tank is also studied for El-Centro ground motion. Development of stresses at

different layers are represented as contour plots. A guiding parameter of stress is also mentioned for the practicing engineers from the contour plot that which stress will show maximum value for same loading and same time step. This may also lead to understand the initiation of failure location in the plate.

5.2 CONCLUSIONS

- **Free vibration response of uncoupled composite plate:**
  - Frequency of a simply supported plate is mostly independent of Cross-ply lamination and it increases up to ply angle of 45° and then again decreases for angle-ply lamination.
  - Response for multilayered lamination is studied and obtained similar results.
  - Fundamental frequency varies for both cross and angle-ply lamination in clamped plates.
- **Transient response of uncoupled composite plate under sinusoidal loading**
  - 45° lamination shows higher central displacement compared to cross ply lamination.
  - Symmetric laminations show higher displacements compared to anti-symmetric laminations. In case of symmetric lamination [B] matrix is cancelled out so there is no bending stretching coupling. So the displacement is solely due normal elongation. But in case of anti-symmetric lamination, this displacement values are affected by the coupling effect of ply layers. The coupling effect can handle better the displacement values as it resists direct elongation as well by bending of the plate. So direct stiffness as well as bending stiffness can resist the displacement value. Hence, the displacement is less in case of anti-symmetric laminations.
  - Increment of number of layers in a plate with constant plate thickness reduces displacement value. As the number of layers increased transverse shear stiffness is better distributed, hence transverse displacement is reduced. Thinner layers also distribute stiffness more evenly through the thickness, hence the plate resists bending more efficiently, which also reduces transverse displacement.

- ❖ Effect of geometry of the plate (SSSS) is studied for cross and angle ply lamination. In both the cases, displacement values decreases with increase in a/b ratio.
- ❖ Effect of geometry for CSCS plate is studied for cross ply lamination. As *a/b* ratio increases, displacement values decreases. When *a/b = 0.75* then the plate is longer in the simply supported direction showing larger deflection. On the other hand, when *a/b = 1.5* then longer span is oriented along clamped direction and hence deflection value is minimum.
- ❖ Normal stress in the plate is studied for various ply angles and found to have maximum stress developed at the 45˚/-45˚ lamination. This lamination is primarily designed for shear so they deflects easily in bending which give rise to normal stress due to bending-stretching coupling effect. The bending-twisting coupling under transverse loading give rise to normal stress. 0/90 lamination under transient loading dampens the response due to its orthogonal directional laminates. On the other hand 45/-45 lamination may amplify localized stress components which will ultimately give rise to normal stress.
- ❖ Increase in number of layers decreases stress value in the plate.
- ❖ Stress contour for 4 and 8 layers are presented. 0˚ lamination away from the middle layer carries highest stress values. 45˚ lamination creates diagonal stress bands in the ply layers.
- ❖ Inplane shear stress contour for various layers is plotted. Cross ply laminated layer shows very less stress value and 45˚ laminations show higher stress values.
- ❖ Transverse shear stress values across layers are studied and found to have similar distribution in different layers. Variations in contour plots are predominant in angle ply laminations.

➢ **Response of uncoupled composite plate under ground motion**

- ❖ Symmetric laminations show higher displacements than anti-symmetric ones. Symmetric lamination does not have bending-stretching coupling effect as [B] is zero hence they deflect more easily. In case of anti-symmetric lamination, due to non zero [B] matrix, the plate offers a resistance in transverse deflection due to the

coupling effect. It is like in order to occur transverse displacement, it needs to axially stretch also. So it shows lesser deformation.

- ❖ Inplane shear stress value is compared between 45˚ symmetric and anti-symmetric laminations. Anti-symmetric laminations carry much higher stress almost 20 times that of symmetric ones.
- ❖ Inplane shear stress in case of 4-layer plate, 45˚ symmetric lamination does not have much effect on increment in number of layers. On the other hand with increase in number of layers in anti-symmetric lamination, [B] matrix tends to zero which reduces ply coupling effects. As this bending-stretching effect is reduced, hence it shows lower shear stress values.
- ❖ Contour plot for normal stress, inplane shear stress and transverse shear stress is presented for 2, 4 and 8 layer plate with various boundary conditions.

- ➢ **3D tank wall-fluid coupled response under sinusoidal loading**

  - ❖ Anti-symmetric 45˚ lamination shows maximum displacement. Due to the presence of non-zero [B] matrix transverse deflection gets modified.
  - ❖ Central displacement increases with decrease in plate thickness.
  - ❖ Forcing frequency is varied and response under three different coupled natural frequency ranges are used for same study (10% of fundamental frequency, fundamental frequency and 3 times fundamental frequency). In all the cases of 45/-45 lamination transverse deflection is maximum for different frequency ranges.
  - ❖ Various boundary conditions are used and SCSF boundary shows highest transverse deflection for cross as well as angle ply laminations.
  - ❖ Effect of layer increment on central displacement of side wall is studied for cross and angle ply laminations. Cross ply laminations do not show any variation of results whereas displacements value decreases drastically with increase in number of layers. As the number of layers increase with constant thickness, [B] matrix approaches zero. Hence the transverse deflection is reduced due to absence of bending-stretching coupling.

- ❖ Central displacement of side wall for variation in geometry is studied. Central displacement increases with increase in height and length of the tank, but it decreases with increase in tank width.
- ❖ Comparative study of central displacement of left and right tank (both cross and angle ply laminations) wall is presented. It was found that initially both the wall responded in the same manner but as time progresses there is a phase difference between the two walls.
- ❖ Stresses in the plate is studied for coupled system under transient loading. Cross ply lamination shows highest normal stress and 45˚ laminations show maximum inplane and transverse shear stresses. This is obvious because in case of cross ply lamination one layer is always in the direction of normal stress direction (X axis). In case of anti-symmetric lamination due to the non-zero [B] matrix, it shows higher inplane shear stress due to bending –stretching coupling effect. Transverse loading is converted to inplane stresses. On the other hand, in case of symmetric angle ply lamination, as [B] matrix is zero, hence it can not convert much of the transverse loading into inplane stresses. As a result a larger amount of loading is responsible for generation of transverse shear stress. So symmetric angle ply lamination shows higher transverse shear stress.
- ❖ Stress values for different boundary conditions are studied and results found are shown in tabular form below. [AP=Angle ply, CP=Cross ply]

Table 5.1. Stress values for different boundary conditions

Type of stress	**Boundary condition**	**SSSS**	**CCCC**	**SCSF**	**CCCF**
Normal stress		Min (AP)	-	Max (CP and AP)	Min (CP)
Inplane shear stress		Min (CP and AP)	Max (CP)	Max (AP)	-
Transverse shear stress		-	Min (AP)Max (CP)	Max (AP) Min (CP)	-

- Increase in number of layers decreases normal and transverse shear values but increases inplane shear value in the side walls.
- Value of all the three stresses increase with increase in wall height and length of the tank for both cross and angle ply laminations.
- Normal stress and inplane shear stress value increase with increase in tank width. Only transverse shear stress value decreases with increase in tank width.
- Contour plot for normal stress, inplane shear stress and transverse shear stress is studied for 2, 4 and 6 layers. Various ply angles and boundary conditions are varied and corresponding stress variations are reported.
- **3D tank wall-fluid coupled response under ground motion**

  Most important observation under ground motion for tank displacement or stress is that the pattern of response is absolutely different from that of the acceleration spectrum. It shows throughout the vibration period, the displacement or stress parameters are much prominent and larger in magnitude.

- In case of coupling, the overall response of the structure is increased. The reason is in the final equation of coupling, a term "E" is added in the overall mass matrix. Now under ground motion, as the mass increased, so the response due to ground acceleration is also automatically increased. So the structure shows amplified throughout displacement response under seismic load.
- A comparison of transverse displacement for four layer cross as well as angle ply lamination for symmetric as well as anti-symmetric lamination is presented. It is observed that in both the cases anti-symmetric lamination shows higher displacements. In case of anti-symmetric lamination, the [B] matrix is non-zero. At the same time in the final coupled equation, a "G" term is added in the stiffness matrix component. This term is similar to the [B] matrix of the structure. Hence the effect of overall [B] matrix is amplified. As a result under ground motion, axial stretching component is converted to transverse deflection term due to the bending-stretching coupling matrix. This leads to higher transverse displacement for anti-symmetric lamination.

- The comparison of normal stress shows similar result where anti-symmetric lamination shows higher values than symmetric ones. Due to the non-zero [B] matrix transverse loading generates some inplane stress components which increases the normal stress values.
- Comparative observation of inplane shear stress for angle ply lamination shows anti-symmetric lamination to have much higher stress values due to presence of bending –stretching coupling effect. This increases shear stress values. On the other hand, same study for cross ply lamination show a different observation. Initially symmetric lamination show higher stress values but later anti-symmetric lamination show higher values. Cross-ply lamination being orthogonal ply lay-ups having varying stiffness in two directions. Initially at the beginning of the ground motion, the side walls experience only impulsive pressure due to the fluid and the fluid pressure due to sloshing is also very low at the beginning. Hence, the symmetric cross ply laminates show higher bending stiffness (with zero [B] matrix) and generates higher inplane shear stress in the initial stage. Later on with passes of time, the fluid starts to interact more due to coupling. In this case impulsive as well as convective pressure terms become more active and higher fluid pressure acts on plate which further increases bending and ultimately it increases inplane shear stress via [B] matrix. Thus later on anti-symmetric laminates catches up and then overtakes the values of stress for symmetric laminations.
- Observation on transverse shear stress reveals that for both cross and angle ply lamination, symmetric lamination shows much higher stress compared to its anti-symmetric part. Symmetric laminated due to its zero [B] matrix component cannot convert transfer bending deformation to in plane deformations. So when the plate reacts with fluid, dynamic fluid pressure under ground motion results in pure bending. This increases transverse shear stress.
- Contour plot for normal stress and inplane shear stress shows stress band near the top edge of the plate. Higher stresses are also concentrated at this location. Due to the coupling effect of fluid on plate specially the sloshing effect of fluid on the

upper surface creates the higher stress band and also increases the stress values in the upper parts.

- ❖ Transverse shear stress on the other hand shows higher stress concentrations along the corners of the plate at different layers. Transverse shear flow occurs through different ply layers which has different orientation and shear stiffness. Shear stress needs to spread from one layer to other through the layer interface and this spreading becomes non-uniform at the corners due to discontinuity of a specific ply layer. Hence, stress concentration generates at those locations. Moreover when fluid interacts with side plate under ground motion, fluid pressure forces outer layers to deform more compared to inner layers as the inner layers are squeezed in between other layers. This may create a lag in relative deformation which results in transverse shear stress concentration at corners.

5.3 SCOPE OF FUTURE RESEARCH

Present study of liquid retaining structure considering composite plate as side wall has huge future scope of work. The work can be extended for the analysis of different liquid retaining structure or structural components such as

1. Composite plates have very limited application as structural unit in liquid retaining structures as of now. Various parts in a dam, side walls of large liquid retaining tanks can be modelled and analyzed for different excitation frequencies considering the effect of fluid-structure interaction (FSI).
2. In the present study the tank is always considered as full with liquid. Effect of liquid depth on various parameters can be studied.
3. In all cases all the fluid parameters are assumed constant throughout the study. Effect of fluid parameters on direct coupling is an important topic of research.
4. Present study is confined within the linear range of the material properties. Non-linear study of the same tank can be performed as an extension of the present work.
5. A comparative study of direct and indirect coupling on the same structure can be considered for future study.

6. Structural failure in terms of plate buckling can be performed and effect of fluid-structure coupling on plate buckling can be an important topic of research.
7. Liquid retaining tanks can obviously have cut-outs in the side walls. So, the vibration response of such walls considering cut-outs (Stiffener can be used) along with FSI is another extension of the present work.
8. An important topic of research on composite plate is the prediction of ply failure. How the coupling between fluid and structure modifies the failure stress or pattern, can be performed as an extension of the present study.

REFERENCES

- Abrate S. (2014) Impact on composite plates in contact with water. *Procedia Engineering.* 88:2-9.
- Abdelbaki B.M., Ahmed M.E.S. and Kaisy A.M.A. (2022) A parametric study on the free vibration of a functionally graded material circular plate with non-uniform thickness resting on a variable Pasternak foundation by differential quadrature method. *Coupled Systems Mechanics*. 11(4): 357-371.
- Adhikary R and Mandal K. K. (2018) Dynamic analysis of water storage tank with rigid block at bottom. *Oceans Systems Engineering*. 8(1): 57-77.
- Alavi S and Eipakchi H. (2019) Analytical method for free-damped vibration analysis of viscoelastic shear deformable annular plates made of functionally graded materials. *Mechanics Based Design of Structures and Machines*. 47(4): 497-519.
- Ali A.Q., D. P. Telang (2017) "A survey on dynamic analysis of elevated water tank for different staging configuration", *International Journal of Computer Science and Mobile Computing*. 6(5): 194-201
- Algreane G. A. I., Osman S.A., Karim O.A. and Kasa A. (2011) Study the fluid structure interaction due to dynamic response of elevated concrete water tank. *Australian Journal of Basic and Applied sciences*. 5(9): 1084-1087
- Alibeigloo A, Shakeri M and kari M.R. (2008) Free vibration analysis of antisymmetric laminated rectangular plates with distributed patch mass using third-order shear deformation theory. *Ocean Engineering*. 35: 183-190.
- Amabili M and Paidoussis M. (2003) Review of studies on geometrically nonlinear vibrations and dynamics of circular cylindrical shells and panels, with and without fluid-structure interaction. *American Society of Mechanical Engineers*. 56(4): 349-381.
- Anghileri M, Castelletti L and Tirelli M. (2005) Fluid-structure interaction of water filled tanks during the impact with the ground. *International Journal of impact Engineering*. 31: 235-254.
- Ansari, R., Shojaei, M. F., Mohammadi, V., Gholami, R. & Sadeghi, F. (2014) Nonlinear forced vibration analysis of functionally graded carbon nanotube-reinforced composite

Timoshenko beams. *Composite Structures*, https://doi.org/10.1016/j.compstruct.2014.03.015

- Arani A.G., Kiani F and Afsari H. (2019) Free and forced vibration analysis of laminated functionally graded CNT-reinforced composite cylindrical panels. *Journal of Sandwich Structures and Materials*. 23(1): 255-278
- Aregawi B., A. Kassahun (2017) Dynamic Response of ground supported rectangular water tanks to earthquake excitation, *Momona Ethiopian Journal of Science* 9(1): 66-75
- Arumugam A.B and Rajamohan V. (2017) Vibration analysis of rotating delaminated non-uniform composite plates. *Aerospace Science and Technology*. 60: 172-182
- Ayoub A (2007) Seismic analysis of wood building structures. *Engineering structures* 29:213-223. https://doi.org/10.1016/j.engstruct.2006.04.011
- Bathe K. J, Zhang H, and Ji S (1999) Finite element analysis of fluid flows fully coupled with structural interactions. *Computers and structures* 72:1-16.
- Balamurugan V. and Narayanan S. (2001) Shell finite element for smart piezoelectric composite plate/shell structures and its application to the study of active vibration control. *Finite Elements in Analysis and Design*. 37: 713-738
- Bayraktar A, Turker T and Akkose M (2010) The effect of reservoir length on seismic performance of gravity dams to near- and far-fault ground motions. *Natural Hazards* 52:257-275. https://doi.org/10.1007/s11069-009-9368-1
- Bazilevs Y, Hsu M, Kiendel J, Wuchner R and Bletzigner K. U. (2010). 3D simulation of wind turbine rotors at full scale. Part II: Fluid-structure interaction modeling with composite blades. *International Journal for Numerical Methods in Fluids*. 65:236-253
- Belytschko T, Flnagn D. P and Kennedy J.M. (1982) Finite element methods with user-controlled meshes for fluid-structure interaction. *Computer methods in applied mechanics and engineering.* 33: 669-688
- Bendahmane A, Hamza-Cherif S and Ouissi M. (2019) Free vibration analysis of variable stiffness composite laminate (VSCL) plates coupled with fluid. *Mechanics of Advanced Materials and Structures.* 28(2): 167-181.
- Bikri K.E., Benamar R and Bennouna M. (2003) Geometrically non-linear free vibrations of clamped simply supported rectangular plates. Part I: the effects of large vibration amplitudes on the fundamental mode shape. *Computers and Structures*. 81: 2029-2043.

- Bermudez A, Duran R and Rodriguez R. (1997) Finite element solution of incompressible fluid-structure vibration problems. *International Journal for Numerical Methods in Engineering.* 40:1435-1448.
- Bhowmick AK, Grondin GY and Driver RG (2014) Nonlinear seismic analysis of perforated steel plate shear walls. *Journal of constructional steel research* 94:103-113. http://dx.doi.org/10.1016/j.jcsr.2013.11.006
- Bozorgmehrnia S., Ranjbar M.M and Madandoust R (2013). Seismic behaviour assessment of concrete elevated water tank, *Rehabilitation in Civil Engineering* 1(2) (2013) 69-79
- Canales F.G. and Mantari J.L. (2017) Laminated composite plates in contact with a bounded fluid: Free vibration analysis via unified formulation. *Composite Structures*. 162: 374-387.
- Chang T. P. (2013) On the natural frequency of transversely isotropic magneto-electro-elastic plates in contact with fluid. *Appl. Math. Model*. 37(4):2503-2015.
- Chattopadhyay B, Sinha P. K, and Mukhopadhyay M. (1992) Finite element free vibration analysis of eccentrically stiffened composite plates. *Journal of Reinforced Plastics and Composite*, 11:1003-1034.
- Chakrabarti A, Topdar P and Sheikh A. H. (2006) Vibration and Buckling of laminated sandwich plates having interfacial imperfections. *European Journal of mechanics*. 25: 981-995
- Chen C-S. (2007) The nonlinear vibration of an initially stressed laminated plate. *Composites Part B: Engineering*. 38: 437-447
- Chen J. Z., M. R. Kianoush (2004) Response of concrete liquid containing structures in different seismic zones, *13th World Conference on Earthquake Engineering Paper No. 1441*
- Chopra A K and Chakrabarti P (1972) The earthquake experience at Koyna dam and stresses in concrete gravity dams. *Earthquake engineering and structural dynamics* 1(2):151-164. https://doi.org/10.1002/eqe.4290010204
- Chu C, Wu Y, Wu T and Wang C. (2018) Slosh-induced hydrodynamic force in a water tank with multiple baffles, *Ocean Engineering*. 167: 282-292.
- Civalek O. (2017) Vibration of laminated composite panels and curved plates with different types of FGM composite constituent. *Composites Part B.* 122: 89-108.

- Craig K.J., Kingsley T.C., Dieterich R, Haarhoff L. J and Stander N. (2003) Design optimisation of the fluid-structure interaction in a fuel tank. *Proceedings of 16th AIAA Computational Fluid Dynamics Conference.*
- Daricik F, Canbolat G and Koru M. (2022) Investigation of a fiber reinforced polymer composite tube by two way coupling fluid-structure interaction. *Coupled Systems Mechanics.* 11(4): 315-333.
- Davi G and Milazzo A. (2003) A meshfree method for transverse vibrations of anisotropic plates. *International journal of Solids and Structures*. 40: 5229-5249.
- Draoui A, Zidour M, Tounsi A and Adim B. (2019) Static and dynamic behaviour of nanotubes-reinforced sandwich plates using FSDT. *Journal of Nano Science*. 57: 117-135.
- Dudhatra K., V. Desani (2016) "Parametric study of hydrodynamic pressure for ground rested rectangular RC tank, *International Journal of Scientific Development and Research* 1(5): 259-264
- Ebrahimi F and Dabbagh A. (2018) On thermos-mechanical vibration analysis of multi-scale hybrid composite beams. *Journal of Vibration and Control*. 25(4): 1-13
- Elansary A and Damatty A El (2018) Seismic analysis of liquid storage composite conical tanks. *Engineering Structures* 159:128-140. https://doi.org/10.1016/j.engstruct.2017.12.030
- Fatt M. S. H, and Sirivolu D (2017) Marine composite sandwich plates under air and water blasts. *Marine structures,* 56:163-185.
- Ferreira A.J.M, Roque C.M.C and Jorge R.M.N (2005) Free vibration analysis of symmetric laminated composite plates by FSDT and radial basis functions. *Computer methods in Applied Mechanics and Engineering.* 194: 4265-4278.
- Ganesh S, Kumar K.S. and Mahato P.K. (2016) Free vibration analysis of delaminated composite plates using finite element method. *Procedia Engineering*. 144: 1067-1075.
- Ghafoori E and Asghari M (2010) Dynamic analysis of laminated composite plates traversed by a moving mass based on a first-order theory. *Composite Structures*. 92: 1865-1876
- Ghaheri A, Keshmiri A, and Taheri-Behrooz F. (2014) Buckling and Vibration of Symmetrically Laminated Composite Elliptical Plates on an Elastic Foundation Subjected to Uniform In-Plane Force. *Journal of Engineering Mechanics*, 140(7):2014.

- Ghallab A (2020) Simulation of cracking in high concrete gravity dam using the extended finite elements by ABAQUS. *American journal of mechanics and applications* 8(1):7-15. https://doi.org/10.11648/j.ajma.20200801.12
- Gong S. W, and Lam K. Y. (1998) Transient response of stiffened composite submersible hull subjected to underwater explosive shock. *Composite Structures*, 41:27-37.
- Gong M and Andreopoulos Y. (2009) Coupled fluid-structure solver: The case of shock wave impact on monolithic and composite material plates. *Journal of Computational Physics.* 228: 4400-4434.
- Hajimehrabi H. (2019) Fragility curves for baffled concrete cylindrical liquid-storage tanks, *Soil Dynamics and Earthquake Engineering*. 119: 187-195
- Han D, Gao X, Zhang H, Zhang S, Yu G and Song Y. (2020) Dynamic and fluid-structure interaction simulations of a ceramic matrix composite plate. *Composite Structures*. 243: 112177
- Haroun MA and Tayel MA (1985) Response of tanks to vertical seismic excitations. *Earthquake engineering and structural dynamics* 13: 583-595. https://doi.org/10.1002/eqe.4290130503
- Hejazi S. A., and Mohammadi M. K. (2019) Investigation on sloshing response of water rectangular tanks under horizontal and vertical near fault seismic excitations, *Soil Dynamics and Earthquake Engineering*. 116: 637-653
- Hemalatha P., K. V. N. M. Rao (2018) Analytical interpretation of hydrodynamic pressure causing slosh effect on overhead water tank, *International Journal of Recent Research Aspects* 5(1): 328-332
- Hinton E and Campbell J.S. (1974) Local and global smoothing of discontinuous finite element functions using a least square method. *International Journal for Numerical Methods in Engineering*. 8: 461-480
- Hirwani C.K, Panda S.K. and Mahapatra T.R. (2017) Nonlinear finite element analysis of transient behavior of delaminated composite plate. *Journal of Vibration and Acoustics.* 140(2): 021001
- Hosseini M., P. Farshadmanesh (2011) Simplified dynamic analysis of sloshing phenomenon in tanks with multiple baffles subjected to earthquake, *III ECCOMAS Thematic Conference on Computational Methods in Structural Dynamics and Earthquake*

Engineering

- Huang X, Kwon OS, Bentz E and Tcherner J (2018) Method for evaluation of concrete containment structure subjected to earthquake excitation and internal pressure increase. *Earthquake engineering and structural dynamics* 47(6):1544-1565. https://doi.org/10.1002/eqe.3029
- Huang W, Zhang W, Chen T, Jiang X and Liu J. (2018) Dynamic response of circular composite laminates subjected to underwater impulsive loading. *Composites part A.* 109: 63-74.
- Jain S. K., and Jaiswal O. R. (2005) Modified proposed provisions for aseismic design of liquid storage tanks: Part I – codal provisions. *Journal of Structural Engineering*, 32(3):195-206.
- Jeong K. (2013) Free vibration of two identical circular plates coupled with bounded fluid. *Journal of Sound and Vibration*. 260: 653-670.
- Jones R. M. (2018) Mechanics of Composite Materials. *CRC press*.
- Kant T, Ravichandran RV, Pandya BN and Mallikarjuna (1988) Finite element transient dynamic analysis of isotropic and fibre reinforced composite plates using a higher-order theory. *Composite Structures* 9(4):319–342. https://doi.org/10.1016/0263-8223(88)90051-7
- Kerboua Y, Lakis A. A. , Thomas M and Marcouiller L. (2008) Vibration analysis of rectangular plates coupled with fluid. *Applied Mathematical Modelling*. 32: 2570-2586.
- Khan A.H. and Patel B.P. (2014) Nonlinear forced vibration response of bimodular laminated composite plates. *Composite Structures*. 108: 524-537.
- Khorshidi K., Akbari F. and Ghadirian H. (2017) Experimental and analytical modal studies of vibrating rectangular plates in contact with a bounded fluid. *Ocean Engineering*. 140:146-154.
- Kim D and Kim S. (2019) Evaluation of bird strike induced damages of helicopter composite fuel tank assembly based on fluid-structure interaction analysis. *Composite Structures.* 210: 676-686.
- Kim J.K, Koh H.M. and Kwahk I.J. (1996) Dynamic response of rectangular flexible fluid container. *Journal of Engineering Mechanics*. 122(9): 807-817

- Koh H.M., Kim J.K. and Park J.H. (1998) Fluid structure interaction analysis of 3-D rectangular tanks by a variationally coupled BEM-FEM and comparison with test results. Earthquake Engineering and Structural Dynamics. 27: 109-124.
- Kormanikova E and Kotrasova K (2018) Multiscale modeling of liquid storage laminated composite cylindrical tank under seismic load. *Composites Part B* 146:189-197. https://doi.org/10.1016/j.compositesb.2018.03.011
- K. Kotrasova, E. Kormanikova (2018) Frequency analysis of partially-filled rectangular water tank, *International Journal of Mechanics*. 12: 59-66
- Kumar S.K., Cinefra M, Carrera E, Ganguli R and Harursampath D (2014) Finite element analysis of free vibrtion of the delaminated composite plate with variable kinematic multilayered plate elements. *Composites Part B*. 66: 453-465.
- Kwon Y. W., Bolstad S. H., Didoszak J. M., and Rodriguez J. A. (2016). Study of composite plate traveling in water containing Ice Equivalent Objects. *Composite Structures*, 135:38-48.
- LeBlanc J., and Shukla A. (2010) Dynamic response and damage evolution in composite materials subjected to underwater explosive loading: An experimental and computational study. *Composite Structures*, 92:2421-2430.
- LeBlanc J., and Shukla A. (2015) Underwater explosion response of curved composite plates. *Composite Structures*. 134:716-725.
- Lee, W. H., & Han, S. C. (2006) Free and forced vibration analysis of laminated composite plates and shells using a 9-node assumed strain shell element. *Computational Mechanics*, 39(1), 41-58.
- Liao C, and Ma C, (2016) Vibration characteristics of rectangular plate in compressible inviscid fluid. *Journal of Sound and Vibration*, 362:228-251.
- Liang C, Liao C, Tai Y and Lai W. (2001) The free vibration analysis of submerged cantilever plates. *Ocean Engineering*. 28:1225-1245.
- Liew K.M., He X.Q, Tan M.J. and Lim H.K. (2004) Dynamic analysis of laminated composite plates with piezoelectric sensor/actuator patches using the FSDT mesh-free method. *International Journal of Mechanical Sciences*. 46: 411-431

- Liu G.R, Zhao X, Dai K.Y., Zhong Z.H, LI G.Y. and Han X (2008) Static and free vibration analysis of laminated composite plates using the conforming radial point interpolation method. *Composites Science and Technology*. 68: 354-366
- Liu W. K., (1981). Finite element procedures for fluid-structure interactions and application to liquid storage tanks, *Nuclear Engineering and Design*, 65, 221-238. https://doi.org/10.1016/0029-5493(81)90091-1
- Liu H., Qu Y., Xie F. and Meng G. (2023) Fluid-structure interaction analysis of nonlinear flapping dynamic behaviors of variable stiffness composite laminated plates in viscous flows. *Composite Structures*. 315:116987, 1:15.
- Liu G.R., Zhao X, Dai K.Y., Zhong Z.H., Li G.Y. and Han X. (2008) Static and free vibration analysis of laminated composite plates using the conforming radial point interpolation method. *Composites Science and Technology*. 68: 354-366.
- Ma S and Mahfuz H. (2012) Finite element simulation of composite ship structures with fluid-structure interaction. *Ocean Engineering*. 52:52-59.
- Ma Y, Li H, Wu W, Cheng T and Fang D. (2017) A symplectic analytical wave propagation model for damping and steady state forced vibration of orthotropic composite plate structure. *Applied Mathematical Modelling*. 47: 318-339
- Madenci E, Ozkihc Y. O. and Gemi L. (2020) Buckling and free vibration analysis of pultruded GFRP laminated composites: Experimental, numerical and analytical investigasions. *Composite Structures*. 254: 112806
- Maity D and Bhattacharyya S. K. (1999) Time-domain analysis of infinite reservoir by finite element method using a novel far boundary condition. *Finite Elements in Analysis and Design.* 32: 85-96
- Mandal, A., Ray, C. & Haldar, S. (2019) Experimental and Numerical Free Vibration Analysis of Laminated Composite Plates with Arbitrary Cut-Outs. *Journal of The Institution of Engineers (India): Series C,* https://doi.org/10.1007/s40032-019-00537-7.
- Mandal KK and Maity D (2015) 2D finite element analysis of rectangular water tank with separator wall using direct coupling. *Coupled Systems Mechanics*. 4(4): 317-336.
- Mandal KK and Maity D (2016) Seismic response of aged concrete dam considering interaction of dam and reservoir in coupled way. *Asian Journal of Civil Engineering*, 17(5):571–592.

- Mandal K. K., Maity D. (2016) Nonlinear finite element analysis of water in rectangular tank, *Ocean Engineering*. 121: 592-601
- Mandal K. K, Maity D. (2016) Pressure based Eulerian approach for investigation of sloshing in rectangular water tank, *Procedia Engineering* 144: 1187-1194
- Maity D and Bhattacharyya S. K. (2003) A parametric study on fluid-structure interaction problems. *Journal of Sound and Vibration*. 263:917-935.
- Malekzadeh P. (2009) Three dimensional free vibration analysis of thick functionally graded plates on elastic foundation. *Composite Structures*. 89: 367-373.
- Moslemi M, Kianoush MR and Pogorzelski W (2011) Seismic response of liquid-filled elevated tanks. *Engineering structures* 33:2074-2084. https://doi.org/10.1016/j.engstruct.2011.02.048
- Mendes P. A, and Branco F. A. (1999) Analysis of fluid-structure interaction by an arbitrary Lagrangian-Eulerian finite element formulation. *International journal for numerical methods in fluids,* 30:897-919.
- Mitra S. and Sinhamahapatra K. P (2008) 2D simulation of fluid-structure interaction using finite element method. *Finite Elements in Analysis and Design*, 45(1):52-59.
- Motley M. R, Kramer M. R, and Young Y. L. (2013) Free surface and solid boundary effects on the free vibration of cantilevered composite plates. *Composite Structures*, 96:365-375.
- Mukhopadhyay M. (2004) Mechanics of Composite Materials and Structures. *Universities Press*.
- Murugesan N and Rajamohan V (2017) Prediction of Progressive Ply Failure of Laminated Composite Structures: A Review. *Archives of Computational Methods in Engineering. Springer Netherlands,* 24(4):841–853. https://doi.org/10.1007/s11831-016-9191-2
- Naghsh A and Azhari M. (2015) Non-linear free vibration analysis of point supported laminated composite skew plates. *International Journal of Non-linear Mechanics*. 76: 64-76.
- Nayak A.K., Shenoi R.A. and Moy S.S.J (2004) Transient response of composite sandwich plates. *Composite Structures*. 64: 249-267.
- Nikkhakian B, Alembagheri M and Shayan RS (2020) Parametric investigation of canyon shape effects on the seismic response of 3D concrete gravity dam model. *Geotechnical and geological engineering* 38:6755-6771. https://doi.org/10.1007/s10706-020-01467-3

- Nitti A, Kiendl J, Reali A and Tullio M. (2020) An immersed boundary/isogeometric method for fluid-structure interaction involving thin shells. *Computer Methods in Applied Mechanics and Engineering.* 364: 112977
- Niyogi A. G, Laha M.K. and Sinha P.K. (1999) Finite element vibration analysis of laminated composite folded plate structures. *Shock and Vibration*. 6: 273-283.
- Numayr K.S., Haddad R. H. and Haddad M.A. (2004) Free vibration of composite plates using the finite difference method. *Thin walled structures*. 42:399-414.
- Oh J, Cho M and Kim J. (2005) Dynamic analysis of composite plate with multiple delaminations based on higher order zigzag theory. *International Journal of Solids and Structures.* 42: 6122-6140
- Oke W. A, and Khulief Y. A. (2020) Dynamic Response Analysis of Composite Pipes Conveying Fluid in the Presence of Internal Wall Thinning. *Journal of Engineering Mechanics*, 146(10).
- Olson L. G. and Bathe K-J. (1983) A study of displacement-based fluid finite elements for calculating frequencies of fluid and fluid-structure systems. *Nuclear Engineering and Design.* 76:137-151.
- Olson L. G. and Bathe K-J. (1985) An infinite element for for analysis of transient fluid-structure interactions. *Engineering Computations*. 2(4):319-329
- Onkar A.K. and Yadav D (2005) Forced nonlinear vibration of laminated composite plates with random material properties. *Composite Structures*. 70: 334-342
- Pal N. C, Bhattacharyya S. K, and Sinha P. K (1999) Coupled slosh dynamics of liquid-filled, composite cylindrical tanks. *Journal of Engineering Mechanics*, 125:491-495.
- Pal N. C, Bhattacharyya S. K, and Sinha P. K (2001) Experimental investigation of slosh dynamics of liquid-filled containers. *Experimental Mechanics*. 41:63-69.
- Palmer R and Smith F. T. (2021) A body in non-linear near-wall shear flow: numerical results for a flat plate. *Journal of Fluid Mechanics*. 915: 1-28
- Pandit M.K, Haldar S and Mukhopadhyay M (2007) Free vibration analysis of laminated composite rectangular plate using finite element method. *Journal of reinforced plastics and composites* 26(1):69-80. https://doi.org/10.1177/0731684407069955
- Pani P. K, and Bhattacharyya S. K. (2007) Fluid–structure interaction effects on dynamic pressure of a rectangular lock-gate. *Finite elements in analysis and design*, 43:739-748.

- Parhi PK, Bhattacharyya SK and Sinha PK (2001) Hygrothermal effects on the dynamic behavior of multiple delaminated composite plates and shells. *Journal of Sound and Vibration* 248(2):195–214. https://doi.org/10.1006/jsvi.2000.3506
- Phung-Van P, Lieu Q X, Ferreira A J M, Thai C H. (2021) A refined nonlocal isogeometric model for multilayer functionally graded graphene platelet-reinforced composite nanoplates. *Thin-Walled Structures*, 164:107862.
- Prusty, B. G. and Ray C. (2004) Free vibration analysis of composite hat-stiffened panels by method of finite element. *Journal of Reinforced Plastics and Composites*. 23(5): 533-547.
- Pradyumna S and Bandyopadhyay J.N. (2008) Static and free vibration analysis of laminated shells using a higher order theory. *Journal of Reinforced Plastics and Composites.* 27: 197-186.
- Radnic J, Grgic N, Kusic M.S. and Harapin A. (2018) Shake table testing of an open rectangular water tank with water sloshing, *Fluids and Structures* 81 (2018) 97-115
- Rajamani A and Prabhakaran R. (1977) Dynamic response of composite plates with cut-outs Part I: simply supported plates. *Journal of sound and vibration*. 54(4): 549-564
- Rawat A, Mittal V, Chakraborty T and Matsagar V. (2019) Earthquake induced sloshing and hydrodynamic pressures in rigid liquid storage tanks analyzed by coupled acoustic-structural and Euler-Lagrange methods, *Thin-Walled structures*. 134: 333-346
- Rebouillat S and Liksonov D. (2010) Fluid-structure interaction in partially filled liquid containers: A comparative review of numerical approaches. *Computers and Fluids*. 39: 739-746.
- Reddy J. N. (2003) Mechanics of Laminated Composite Plates and Shells. *CRC press*.
- Reddy JN (1979) Free vibration of antisymmetric, angle-ply laminated plates including transverse shear deformation by the finite element method. *Journal of Sound and Vibration* 66(4):565-576. https://doi.org/10.1016/0022-460X(79)90700-4
- Reddy J and Pandey A (1987) A first-ply failure analysis of composite laminates. *Computers & Structures* 25(3):371-393. https://doi.org/10.1016/0045-7949(87)90130-1
- Reddy JN and Khdeir A (1989) Buckling and vibration of laminated composite plates using various plate theories. *AIAA Journal* 27(12):1808–1817. https://doi.org/10.2514/3.10338

- Reddy, J. N. (1983) Geometrically nonlinear transient analysis of laminated composite plates. *AIAA Journal*, 21(4), 621-629.
- Reddy, J. N. (2004) *Mechanics of laminated composite plates and shells-Theory and Analysis*. Washington, DC: CRC Press.
- Sadeghi MH and Moradloo J (2020) Seismic analysis of damaged concrete gravity dams subjected to mainshock-aftershock sequences. *European journal of environmental and civil engineering* https://doi.org/10.1080/19648189.2020.1763475
- Saghi H. (2016) The pressure distribution on the rectangular and trapezoidal storage tanks' perimeters due to liquid sloshing phenomenon, *International Journal of Naval Architecture and Ocean Engineering.* 8: 153-168
- Sanapala V.S., Sajish S.D., Velusamy K., Ravisankar A and Patnaik B.S.V. (2019) An experimental investigation on the dynamics of liquid sloshing in a rectangular tank and its interaction with an internal vertical pole. *Journal of Sound and Vibration*. 449: 43-63.
- Schiffer A, and Tagarielli V. L. (2014) The dynamic response of composite plates to underwater blast: *Theoretical and numerical modeling. International Journal of Impact Engineering.* 70:1-13.
- Setoodeh A.R. and Karami G. (2003) A solution for the vibration and buckling of composite laminates with elastically restrained edges. *Composite Structures*. 60: 245-253.
- Serdoun SMN and Cherif SM. H (2016) Free vibration analysis of composite and sandwich plates by alternative hierarchical finite element method based on Reddy's C' HSDT. *Journal of Sandwich structures and Materials*. 18(4): 501-528.
- Shekari M.R., Hekmatzadeh A.A. and Amiri S.M. (2019) On the nonlinear dynamic analysis of base-isolated three-dimensional rectangular thin-walled steel tanks equipped with vertical baffle, *Thin-Walled Structures*. 138: 79-94
- Sharma N, Swain P. K, Maiti D. K and Singh B. N. (2022) Static and free vibration analyses and dynamic control of smart variable stiffness laminated composite plate with delamination. *Composite Structures*. 280:114793, 1:17.
- Shankara C. A. and Iyengar N.G.R. (1996) A C^0 element for the free vibration analysis of laminated composite plates. *Journal of Sound and Vibration*. 191(5): 721-738.

- Shukla K.K., Chen J and Huang J. (2004) Nonlinear dynamic analysis of composite laminated plates containing spatially oriented short fibers. *International Journal of Solids and structures.* 41: 365-384
- Sinha M.K. and Daripa R (2009) Nonlinear vibration and dynamic stability analysis of composite plates. *Journal of Sound and Vibration*. 328: 541-554
- Sinha L, Das D, Nayak A. N and Sahu S.K. (2021) Experimental and numerical study on free vibration characteristics of laminated composite plate with/without cut-out. *Composite structures*. 256: 113051
- Soni S, Jain N. K, and Joshi P. V. (2018) Vibration analysis of partially cracked plate submerged in fluid. *Journal of Sound and Vibration*. 412:28-57.
- Souli M, Ouahsine A and Lewin L. (2000) ALE formulation for fluid-structure interaction problems. *Computer Methods in Applied Mechanics and Engineering*. 190:659-675.
- Talookolaei R and Lasemi-Imani S. (2015) Free vibration analysis of a delaminated beam-fluid interaction system. *Ocean Engineering*. 107: 186-192.
- Teixeira P.R.F, and Awruch A.M. (2005) Numerical simulation of fluid-structure interaction using the finite element method. *Computers and Fluids*. 34:249-273.
- Thinh T.I and Quoc T. H. (2010) Finite element modelling and experimental study on bending and vibration of laminated stiffened glass fiber/polyester composite plates. *Computational Materials Science*. 49: 5383-5389.
- Thinh T.I and Ngoc L.K (2010) Static behaviors and vibration control of piezoelectric cantilever composite plates and comparison with experiments. *Computational Materials Science*. 49: 276-280
- Tho N. C., Thom D. V., Cong P. H., Zenkour A. M. and Doan D. H. (2023) Finite element modelling of the bending and vibration behaviour of three-layer composite plates with a crack in the core layer. *Composite Structures*. 305:116529, 1:14.
- Tiwari P., Maiti D. K. and Maity D. (2023) 3D sloshing frequency analysis of partially filled cylindrical laminated composite containers. *International Journal of Advances in Engineering Sciences and Applied Mathematics*. https://doi.org/10.1007/s12572-023-00341-8
- Tran P, Ngo T. D., and Mendis P. (2014). Bio-inspired composite structures subjected to underwater impulsive loading. *Computational Materials Science*. 82, 134-139.

- Uckan E, Akbas B, Shen J, Wen R, Turandar K and erdik M (2014) Seismic performance of elevated steel silos during Van earthquake, October 23, 2011. *Natural Hazards* 75:265-287. https://doi.org/10.1007/s11069-014-1319-9
- Valdani A. J. and Adamian A. (2021) Numerical simulation and optimization of a reinforced steel plant against underwear explosions. *Progress in Computational Fluid Dynamics. 21(3): 170-185.*
- Virella J.C., Suarez L.E. and Godoy L.A (2005) Effect of pre-stress states on the impulsive modes of vibration of cylindrical tank-liquid systems under horizontal motions. *Vibration and Control* 11(9) (2005) 1195-1220
- Vidal P, Gallimard L. and Polit O. (2019) Free vibration analysis of composite plates based on a variable separation method. *Composite Structures*. 230:111493, 1:11.
- Watkins R.J., Santillan S , Radice J and Barton O Jr. (2010) Vibration response of an elastically point-supported plate with attached masses. *Thin Walled Structures.* 48:519-527.
- Wakchaure M. R., Besekar S. S. (2014) Behavior of elevated water tank under sloshing effect, *International Journal of Engineering Research & Technology* Vol. 3 Issue 2 ISSN: 2278-0181
- Woo J, Meguid S.A. and Ong L.S. (2006) Nonlinear free vibration behaviour of functionally graded plates. *Journal of Sound and Vibration.* 289: 595-611
- Wu H, Li Y, Li L, Kitipornchai S, Wang L and Yang J. (2022) Free vibration analysis of functionally graded graphene nanocmposite beams partially in contact with fluid. *Composite Structures.* 291: 115609
- Xue Y, Jin G, Ma X, Chen H, Ye T, Chen M and Zhang Y. (2019) Free vibration analysis of porous plates with porosity distributions in the thickness and in-plane directions using isogeometric approach. *International Journal of Mechanical Sciences.* 152: 346-362.
- You J. H., and Inaba K. (2013) Fluid–structure interaction in water-filled thin pipes of anisotropic composite materials. *Journal of Fluids and Structures*, 36:162-173.
- Yousefzadeh S, and Jafari A. A., Mohammadzadeh. (2017) Effect of hydrostatic pressure on vibrating functionally graded circular plate coupled with bounded fluid. *Applied Mathematical Modeling,* 60:435-446.
- Youzera H and Meftah S.A (2017) Nonlinear damping and forced vibration behaviour of sandwich beams with transverse normal stress. *Composite Structures.* 179: 258-268

- Yu Ching and Whittaker A. (2021) Review of analytical studies on seismic fluid-structure interaction of base supported cylindrical tanks. *Engineering Structutres*. 233: 111589.
- Yazdanian M, Razavi S.V. and Mashal M, (2016) Seismic analysis of rectangular concrete tanks by considering fluid and tank interaction, *Solid Mechanics*. 8(2) 435-445
- Zhu M, and Scott M H. (2016) Direct differentiation of the particle finite-element method for fluid-structure interaction. *Journal of Structural Engineering*, 142 (3):04015159-1-04015159-14.
- Zhang W, Wang A, Vlahopoulos N and Wu K. (2003) High-frequency vibration analysis of thin elastic plates under heavy fluid loading by an energy finite element formulation. *Journal of Sound and Vibration.*
- Zhao D, Hu Z, Chen G, Lim S and Wang S (2018) Nonlinear sloshing in rectangular tanks under forced excitation, *International Journal of Naval Architecture and Ocean Engineering*.. 10: 545-565.
- Zienkiewicz O. C., and Newton R. E., (1969) Coupled Vibrations of a Structure Submerged in a Compressible Fluid, *Symposium on Finite Element Techniques, Stuttgart, 1-15 May 1969: 360-378.*
- Zienkiewicz OC, Paul DK and Hinton E (1983) Cavitation in fluid-structure response (with particular reference to dams under earthquake loading). *Earthquake engineering and structural dynamics* 11:463-481. https://doi.org/10.1002/eqe.4290110403
- Zienkiewicz, O.C. and Taylor, R.L. (2000) *The Finite Element Method*, 5th Edition, Butterworth-Heinemann, Oxford, U.K.
- Zou C and Wang D. (2015) A simplified mechanical model with fluid structure interaction for rectangular tank sloshing under horizontal excitation. *Advances in Mechanical Engineering*. 7(5): 1-16.

Prithwish Sahu
12/08/2024

Kalyan kr. Mandal
12/08/2024

Associate Professor
Department of Civil Engineering
Jadavpur University